VOLUME 75 APRIL 1, 1971 NUMBER 7

JPCHAx

THE JOURNAL OF PHYSICAL CHEMISTRY

PUBLISHED BIWEEKLY BY THE AMERICAN CHEMICAL SOCIETY

THE JOURNAL OF

PHYSICAL CHEMISTRY

 Published biweekly by the American Chemical Society at 20th and Northampton Sts., Easton, Pa. 18042. Second-class postage paid at Easton, Pa.

All manuscripts should be sent to *The Journal of Physical Chemistry*, Department of Chemistry, University of Minnesota, Minneapolis, Minn. 55455.

Additions and Corrections are published once yearly in the final issue. See Volume 74, Number 26 for the proper form.

Extensive or unusual alterations in an article after it has been set in type are made at the author's expense, and it is understood that by requesting such alterations the author agrees to defray the cost thereof.

The American Chemical Society and the Editor of *The Journal of Physical Chemistry* assume no responsibility for the statements and opinions advanced by contributors.

Correspondence regarding accepted copy, proofs, and reprints should be directed to Editorial Production Office, American Chemical Society, 20th and Northampton Sts., Easton, Pa. 18042. Manager: CHARLES R. BERTSCH. Assistant Editor: EDWARD A. BORGER. Editorial Assistant: EVELYN J. UHLER.

Advertising Office: Century Communications Corporation, 142 East Avenue, Norwalk, Conn. 06851.

Business and Subscription Information

Remittances and orders for subscriptions and for single copies, notices of changes of address and new professional connections, and claims for missing numbers should be sent to the Subscription Service Department, American Chemical Society, 1155 Sixteenth St., N.W., Washington, D. C. 20036. Allow 4 weeks for changes of address. Please include an old address label with the notification.

Claims for missing numbers will not be allowed (1) if received more than sixty days from date of issue, (2) if loss was due to failure of notice of change of address to be received before the date specified in the preceding paragraph, or (3) if the reason for the claim is "missing from files."

Subscription rates (1971): members of the American Chemical Society, $20.00 for 1 year; to nonmembers, $40.00 for 1 year. Those interested in becoming members should write to the Admissions Department, American Chemical Society, 1155 Sixteenth St., N.W., Washington, D. C. 20036. Postage to Canada and countries in the Pan-American Union, $4.00; all other countries, $5.00. Single copies for current year: $2.00. Rates for back issues from Volume 56 to date are available from the Special Issues Sales Department, 1155 Sixteenth St., N.W., Washington, D. C. 20036.

This publication and the other ACS periodical publications are now available on microfilm. For information write to: MICROFILM, Special Issues Sales Department, 1155 Sixteenth St., N.W., Washington, D. C. 20036.

Notice to Authors last printed in the issue of December 24, 1970

THE JOURNAL OF

PHYSICAL CHEMISTRY

Volume 75, Number 7 April 1, 1971

NOTES

COMMUNICATIONS TO THE EDITOR

AUTHOR INDEX

THE JOURNAL OF
PHYSICAL CHEMISTRY

VOLUME 75, NUMBER 7 APRIL 1, 1971

The Continuous Photolysis at 253.7 nm of Acetone in Aqueous Solution in the Presence of Nitromethane

by Tran-Dinh-Son and Jack Sutton*

Centre d'Etudes Nucleaires de Saclay, 91 Gif-sur-Yvette, France *(Received September 3, 1970)*

Publication costs assisted by Centre d'Etudes Nucleaires de Saclay

Methyl radicals produced from the photolysis of aqueous acetone at 253.7 nm are efficiently scavenged by nitromethane. From the resulting decrease in the methane and ethane yields at 22° a value of 140 ± 15 is deduced for the rate constant ratio, k_7/k_4, of the reactions $CH_3 + CH_3COCH_3 \rightarrow CH_4 + CH_2COCH_3$ (reaction 4) and $CH_3 + CH_3NO_2 \rightarrow CH_3NO_2CH_3$ (reaction 7).

Introduction

Photolysis of nitromethane in the solid state[1,2] and flash photolysis in the gaseous phase[3,4] have indicated that the primary decomposition reaction is rupture of the C–N bond. In an esr study of the radiolysis of this compound at 77°K Chachaty[5] observed the formation of important quantities of the radicals NO_2 and CH_2NO_2 together with a small amount of the methyl radical. On warming gently this last radical disappeared and the concentrations of the other two radicals became effectively equal. On the basis of these results the author concluded that the major reactions involved were the breakage of the C–N bond followed by the disappearance of the CH_3 by hydrogen atom abstraction from nitromethane

$$CH_3 + CH_3NO_2 \longrightarrow CH_4 + CH_2NO_2 \qquad (1)$$

Equation 1 is a reaction previously invoked[6,7] to explain the formation of large methane yields in the gas phase pyrolysis of nitromethane.

On the other hand, recent studies[8-11] of both the radiolysis and the photolysis of liquid nitromethane at room temperature have shown that the methane yield represents only a small fraction of the total products. As a result the possible role of a reaction between CH_3 and nitromethane has been largely neglected in the mechanisms proposed to account for the observed products.

During a study of the photolysis of aqueous solutions

(1) B. H. J. Bielski and R. B. Timmons, *J. Phys. Chem.*, **68**, 347 (1964).

(2) C. Chachaty and A. Forchioni, *C. R. Acad. Sci., Ser. C*, **268**, 300 (1969).

(3) J. J. McGarvey and W. D. McGrath, *Trans. Faraday Soc.*, **60**, 2196 (1964).

(4) I. M. Napier and R. G. W. Norrish, *Proc. Roy. Soc.*, **299**, 317 (1967).

(5) C. Chachaty, *J. Chim. Phys.*, **62**, 728 (1965).

(6) T. L. Cottrell and T. J. Reid, *J. Chem. Phys.*, **18**, 1306 (1950).

(7) T. L. Cottrell, T. E. Graham, and T. J. Reid, *Trans. Faraday Soc.*, **47**, 584 (1951).

(8) S. Paszyc, *Photochem. Photobiol.*, **4**, 841 (1965).

(9) R. B. Cundall, A. W. Locke, and G. C. Street, "The Chemistry of Ionisation and Excitation," G. R. A. Johnson and G. Scholes, Ed., Taylor and Francis, London, 1967, p 131.

(10) Tran-Dinh-Son, 3rd Cycle Thesis, Faculty of Science, Paris, Dec 1967.

(11) J. L. Corey and R. F. Firestone, *J. Phys. Chem.*, **74**, 1425 (1970).

of nitromethane it was observed that the concentration of methane produced was about 50 times less than that of the nitrite ion.[12] However, the addition of ethanol or isopropyl alcohol prior to photolysis caused the methane yield to increase strongly suggesting a competition between the alcohol and a second compound, probably nitromethane, for methyl radicals.

In order to obtain more information about this latter reaction the effect of nitromethane on the yields of methane and ethane produced in the photolysis of aqueous solutions of acetone has been investigated and the results are now presented.

Experimental Section

Products. Nitromethane (Serlabo, analytical grade) was purified by distillation under a reduced pressure of helium (*ca.* 380 mm) on a spinning-band column. This treatment led to the complete disappearance of the impurities initially detected by gas chromatography.

Acetone (Merck "extra pure") was employed without further purification.

Water was the conventional triply distilled product employed for radiolysis experiments. Solutions were prepared by successive dilutions and degassed according to previously described techniques.[10] The final oxygen concentration in the degassed solutions did not exceed 3×10^{-7} M as measured by gas chromatographic analysis carried out on selected samples.

Photolysis Apparatus. The solution to be photolyzed was contained in a cylindrical cell 15 mm in diameter and 60 mm long, having two capillary arms for filling and degassing. This cell was constructed in silica (Germisil, Quartz et Silice) having a transmission of about 80% at 253.7 nm falling to 0% at about 230 nm. A helicoidal, low-pressure, mercury-vapor lamp (manufactured by Claude) having its principal emission at 253.7 nm was used. The cell was mounted axially inside the lamp.

The solutions employed contained 5×10^{-2} M acetone and a variable concentration of nitromethane. The temperature of the solution remained at 22.0 ± 0.5° during photolysis and the degree of conversion of the acetone was kept below 1%. In most cases a single photolysis time of 60 sec was employed, but a few runs were made at shorter times to verify the linear dependence of the product yield on the energy absorbed. Under the experimental conditions described the concentration of radicals produced by the photolysis of acetone was practically uniform throughout the volume of the solution.

Actinometry was carried out using 10^{-2} M uranyl oxalate solutions containing 5×10^{-2} M oxalic acid. The light intensity, I, in the wavelength range of interest was calculated from measurements of the CO_2 obtained from the actinometer solution corrected for the contribution of light of wavelength 300 nm. Taking

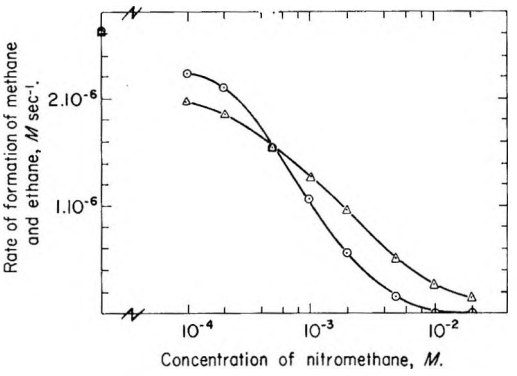

Figure 1. Rates of formation of methane (△) and ethane (⊙) in the photolysis of 5×10^{-2} M, deaerated, aqueous acetone as a function of the concentration of nitromethane.

$\phi_{CO_2} = 0.68$[13] the value $I = 5.95 \times 10^{-6}$ einstein mn^{-1} cm^{-3} was obtained.

Gaseous products were analyzed by gc[10] and the nitrite ion by the modified Shinn's method.[14]

Results

The photolysis of acetone in aqueous solution gives rise to the formation of methane, ethane, and carbon monoxide, the latter being a very minor constituent, just detectable by gas chromatography for a 60-sec irradiation. The quantum yields of these products were constant for irradiation times between 20 and 60 sec. The present values, $\phi_{CH_4} = (2.9 \pm 0.1) \times 10^{-2}$, $\phi_{C_2H_6} = (2.6 \pm 0.1) \times 10^{-2}$, and $\phi_{CO} = (0.2 \pm 0.05) \times 10^{-2}$, are in reasonable agreement with the extrapolated results of Volman and Swanson,[15] bearing in mind the differences in intensity and degree of conversion used in the two studies.

Figure 1 shows the rates of formation of methane and ethane, R_{CH_4} and $R_{C_2H_6}$, expressed in M sec^{-1} obtained from the photolysis of the 5×10^{-2} M acetone solution as a function of the concentration of added nitromethane.

Only traces of nitrite were found, its maximum concentration attaining about 10^{-6} M for $[CH_3NO_2] \geqslant 10^{-2}$ M. In this case it was probably formed by direct photolysis of nitromethane.[12]

Discussion

The results of previous studies of the photolysis of acetone in the vapor phase,[16] in aqueous solution,[15] and in perfluorodimethylcyclobutane[17] have been explained in terms of the following mechanism

(12) Tran-Dinh-Son, F. Barat, and J. Sutton, unpublished work.

(13) D. H. Volman and J. R. Seed, *J. Amer. Chem. Soc.*, **86**, 5095 (1964).

(14) B. F. Rider and M. G. Mellon, *Ind. Eng. Chem., Anal. Ed.*, **18**, 96 (1946).

(15) D. H. Volman and L. W. Swanson, *J. Amer. Chem. Soc.*, **82**, 4141 (1960).

(16) R. Pieck and E. W. R. Steacie, *Can. J. Chem.*, **33**, 1304 (1955).

(17) R. Doepker and G. J. Mains, *J. Amer. Chem. Soc.*, **83**, 294 (1961).

$$CH_3COCH_3 \xrightarrow{h\nu} CH_3 + CH_3CO \quad (2)$$

$$CH_3CO \xrightarrow{k_3} CH_3 + CO \quad (3)$$

$$CH_3 + CH_3COCH_3 \xrightarrow{k_4} CH_4 + CH_2COCH_3 \quad (4)$$

$$CH_3 + CH_3CO \xrightarrow{k_5} CH_4 + CH_2CO \quad (5)$$

$$2CH_3 \xrightarrow{k_6} C_2H_6 \quad (6)$$

In the presence of low concentrations of nitromethane the yields of methane and ethane diminish, and the low yields of nitrite simultaneously observed strongly suggest that energy transfer from excited acetone to nitromethane is not responsible for this decrease. The most obvious explanation for it and one which is borne out by the results of the photolysis of nitromethane in aqueous solutions containing alcohol already mentioned is that the nitromethane captures methyl radicals without giving methane or ethane. The fact that the

$$CH_3 + CH_3NO_2 \xrightarrow{k_7} CH_3CO_2CH_3 \quad (7)$$

$$CH_3CO_2CH_3 \longrightarrow \text{products}$$

methane yield diminishes constantly with increasing nitromethane concentration indicates that it is chiefly formed by a radical reaction (from methyl radicals) and that a molecular process, if it exists, is of negligible importance.

(*a*) *Determination of the Ratio* k_4^2/k_6. In their study of the photolysis of the system acetone–water Volman and Swanson[15] have shown that an expression of the following form derived from the above mechanism represents their overall results

$$\frac{R_{CH_4}}{R_{C_2H_6}^{1/2}R_{CO}} = \frac{k_4}{k_6^{1/2}}\frac{[CH_3COCH_3]}{R_{CO}} + \frac{k_5}{k_3k_6^{1/2}} \quad (I)$$

These authors also showed that the value of the term $k_5/k_3k_6^{1/2}$ is small between 2 and 27°. Furthermore, in the presence of a low concentration of nitromethane and with the acetone concentration employed, it may be shown from the results of Figure 1 that the ratio $R_{CH_4}^2/R_{C_2H_6}$ remains practically constant (Table I). This result suggests that for this range of nitromethane concentration the reactions 3 and 5 are suppressed,

Table I

(CH_3NO_2), M	$R_{CH_4}^2/R_{C_2H_6}$, M sec^{-1} × 10^6
0	2.32
10^{-4}	1.77
2×10^{-4}	1.62
5×10^{-4}	1.54
10^{-3}	1.57
2×10^{-3}	1.60
5×10^{-3}	1.70
Average value = 1.62 ± 0.16	

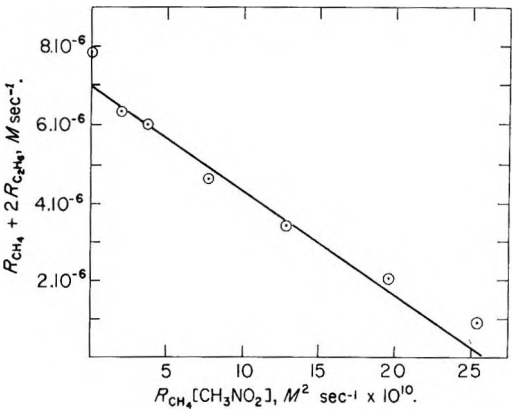

Figure 2. Plot derived from eq IV to obtain k_7/k_4.

probably due to capture of the CH_3CO radical by this solute.

Under these conditions the expression I may be simplified to

$$\frac{R_{CH_4}^2}{R_{C_2H_6}} = \frac{k_4^2}{k_6}[CH_3 \cdot CO \cdot CH_3]^2 \quad (II)$$

and, from the average value of $R_{CH_4}^2/R_{C_2H_6}$ found in Table I, the value

$$\frac{k_4^2}{k_6} = (6.5 \pm 0.6) \times 10^{-4}\ M^{-1}\ \text{sec}^{-1} \text{ at } 22°$$

may be derived, in good agreement with that interpolated for the same temperature from the results of Volman and Swanson,[15] namely $6.1 \times 10^{-4}\ M^{-1}\ \text{sec}^{-1}$.

(*b*) *Determination of the Ratio* k_7/k_4. At the acetone concentration employed (5×10^{-2} M) the incident light at 253.7 nm is completely absorbed. Moreover the concentrations of nitromethane added are sufficiently low that the direct photolysis of this compound may be neglected (for example at the two highest concentrations of nitromethane employed, 5×10^{-3} and 10^{-2} M, only 7 and 15%, respectively, of the total energy at 253.7 nm is absorbed by the nitromethane). The low concentrations of nitrite ion found after photolysis provide further proof of this point. One has, then, excellent reasons to suppose that the total rate of formation of the methyl radical, $R°_{CH_3}$, remains constant and independent of the nitromethane concentration for all the solutions where $[CH_3NO_2] \leqslant 10^{-2}$ M.

Since the methyl radicals disappear only by the reactions 4, 6, and 7 for any given concentration of nitromethane, one may write

$$R_{CH_3NO_2CH_3} = R°_{CH_3} - (R_{CH_4} + 2R_{C_2H_6}) \quad (III)$$

where R represents the rate of formation of the species indicated by the subscript. From a kinetic consideration of reaction 4 and 7 and taking into account relation III, one may write

$$R°_{CH_3} - (R_{CH_4} + 2R_{C_2H_6}) = \frac{k_7}{k_4}\frac{R_{CH_4}[CH_3NO_2]}{[CH_3COCH_3]} \quad (IV)$$

In Figure 2 the experimental values of $R_{CH_4}[CH_3NO_2]$ are plotted as abscissas and the corresponding values of $(R_{CH_4} + 2R_{C_2H_6})$ as ordinates. One sees that all the points except those corresponding to the two highest concentrations of nitromethane fall on a good straight line.

The intercept obtained by extrapolating the line to cut the ordinate axis gives a value for $R^\circ_{CH_4}$ in the absence of nitromethane. This value is about 10% lower than the experimental value, probably due to a reduced participation of reactions 3 and 5 in the presence of nitromethane.

The ratio k_7/k_4 obtained from the slope of the straight line of Figure 2 is $k_7/k_4 = 140 \pm 15$ from which one may derive

$$\frac{k_7^2}{k_6} = 12.7 \pm 4.0\ M^{-1}\ \text{sec}^{-1}$$

This high value of k_7/k_4 shows that nitromethane, in addition to being an efficient scavenger of solvated electrons and hydrogen atoms,[18] is also a good scavenger of methyl radicals.

(18) J. Sutton and Tran-Dinh-Son, *J. Chim. Phys.*, **64**, 688 (1967).

The Photooxidation of Carbon Disulfide

by William P. Wood[1] and Julian Heicklen*

Department of Chemistry and Center for Air Environment Studies, The Pennsylvania State University, University Park, Pennsylvania 16802 *(Received November 18, 1970)*

Publication costs borne completely by The Journal of Physical Chemistry

The photooxidation of CS_2 was studied with radiation at 3130 Å in a conventional static photochemical system at room temperature. The reactant pressures varied from 2 to 70 Torr of CS_2 and 1 to 745 Torr of O_2. The absorbed light intensity, I_a, varied from 2.0 to 111 μ/min. The products of the reaction were CO, OCS, SO_2, and a polymer. CO_2 and SO_3 were not produced. In the absence of O_2, only the polymer was formed, but in smaller amounts. The quantum yields of the gaseous products were small and typically ranged from 3×10^{-4} to 10^{-1}. In spite of significant variations in the quantum yields, the ratios of products were invariant for all the runs with $\Phi\{OCS\}/\Phi\{CO\} \simeq 1.2$ and $\Phi\{SO_2\} \simeq \Phi\{OCS\} + 2\Phi\{CO\}$. The latter expression indicates a carbon–sulfur mass balance among the gaseous products. The product quantum yields depended only on $[O_2]/[CS_2]$; otherwise they were invariant to changes in $[O_2]$, $[CS_2]$, or I_a. The mechanism which best explains the results is illustrated in reactions 1–8. Furthermore, our findings are consistent with an earlier report[2] that $k_2/k_3 = 7.6$. Our results also indicate that $k_{4a}/k_{4b} \simeq 1.2$, $k_{2a}/k_2 = 0.8 \times 10^{-4}$, and $k_{3b}/k_3 = 0.062$.

Introduction

During the oxidation of CS_2, the intermediates CS and SO have been observed in the cold flame,[3a,b] in the explosion,[3c] and in photochemical oxidation.[4,5] An examination of the oxidation of these species will aid our understanding, not only of CS_2 oxidation, but also of the oxidation of other compounds which can produce these intermediates. For example, CS has been reported in the photolysis of thiophene[6] and should be produced in the photolysis of thioketones and thioaldehydes. We have evidence in our laboratory[7] that SO can be produced in the photolysis of SO_2 at 3130 Å in the presence of CO or C_2F_4.

We have initiated a comprehensive program for studying the oxidation of CS and SO. In this paper we present our results on the room temperature studies of the photooxidation of CS_2 at 3130 Å.

Experimental Section

Most of the gases used were from the Matheson Co. These included extra dry grade O_2 and CP grade CO which were used without further purification. Anhydrous SO_2 showed no impurities and was used after degassing at −196°. Commercial grade CO_2 showed one

(1) U. S. Public Health Service Air Pollution Trainee.

(2) M. de Sorgo, A. J. Yarwood, O. P. Strausz, and H. E. Gunning, *Can. J. Chem.*, **43**, 1886 (1965).

(3) (a) V. N. Kondratiev, *Zh. Fiz. Khim.*, **13**, 1260 (1939), as reported in *Chem. Abstr.*, **35**, 3544 (1941); (b) V. N. Kondratiev, *Zh. Fiz. Khim.*, **14**, 287 (1940), as reported in *Chem. Abstr.*, **36**, 4011[6] (1942); (c) A. L. Myerson, F. R. Taylor, and P. L. Hanst, *J. Chem. Phys.*, **26**, 1309 (1957).

(4) V. N. Kondratiev and A. Yakovleva, *Zh. Eksp. Teor. Fiz.*, **10**, 1038 (1940).

(5) F. J. Wright, *J. Phys. Chem.*, **64**, 1648 (1960).

(6) H. A. Wiebe and J. Heicklen, *Can. J. Chem.*, **47**, 2965 (1969).

(7) E. Cehelnik and C. Spicer, unpublished results (1969).

unidentified impurity (~3%), but was used without purification except degassing at −196°. Both Fisher Scientific Co. spectral grade and Matheson Coleman and Bell reagent grade CS_2 were used after degassing at −196°. No impurities were present. The CF_3I, which was used for actinometer studies, was from Peninsular ChemResearch Inc. The CF_3I was used after degassing at −160° to remove CO_2.

Gas pressures were measured by Wallace–Tiernan absolute pressure indicators, mercury manometers, or a McLeod gauge. The gases were introduced into the cell, and the reaction was monitored continually by ultraviolet absorption spectroscopy utilizing low intensities so that photochemical reactions were not induced by the monitoring lamp.

The reaction vessel was a quartz cell 10 cm long by 5 cm in diameter. The monitoring source was an Osram 150-W high-pressure xenon lamp. Its radiation was passed through a Jarrell-Ash 82-410 0.25-m Ebert monochrometer with 500-μ slits and an 1180 groove/mm grating blazed at 3000 Å. After passing through the windows of the reaction cell, the radiation was focused on a RCA 9-35 phototube.

The photochemical source was a Hanovia Model 30620 150-W medium-pressure U-shaped lamp. The radiation passed through a Corning 0-54 filter to remove radiation below 3050 Å before entering the side of the reaction vessel. The effective radiation was at 3130 Å. Actinometer runs were done by measuring the CF_2O produced in the photooxidation of CF_3I using matched absorbances of the CF_3I and CS_2 at 3130 Å. In this way all geometrical corrections are eliminated. The CF_2O produced, assumed to have a quantum yield of 1.0,[8] was converted into CO_2 which was measured on a gas chromatograph.

In each experiment, after the reaction was terminated, the products were collected and analyzed by gas chromatography. The products noncondensable at −196° were collected with a Toepler pump and passed through a 15-ft, 5-Å molecular sieve column operating at 50° and a He flow rate of 150 cc/min. The condensable products were collected and analyzed on a 10-ft Porapak Q column at 70° with a He flow rate of 250 cc/min. In both cases a Gow Mac Model 40-05D voltage regulator with a thermistor detector was used in conjunction with a 1-mV recorder.

An analysis was attempted for SO_3 by passing the products condensable at −160° through either oxalic acid or an oxalate salt immediately after the reaction. It has been reported[9] that oxalic acid quantitatively reacts with SO_3 to produce CO_2. We have verified this result for samples of SO_3 corresponding to about 50 μ or more SO_3 in our reaction vessel. In none of our experiments did we find evidence of SO_3 formation using this technique. However, SO_3 may have been produced, but in an insufficient quantity to be detected.

Results

Four products were found when mixtures of CS_2 and O_2 were photolyzed with 3130-Å radiation at room temperature. These were CO, OCS, SO_2, and a polymer which deposited on the walls. The polymer could be removed after the run by flaming the cell or by prolonged pumping. No other products were found though repeated attempts were made to find CO_2, SO_3, S_2O, and O_3. It is certain that CO_2 was not produced, but the other products might have been produced in small amounts below the detection limit of our analytical scheme. Typically the final pressures of gaseous products were 3–60 μ. Our analytical scheme should have detected 60 μ of SO_3, but might be inadequate to detect less than 10 μ. However, there was no evidence to suggest SO_3, except possibly at the very highest $[O_2]/[CS_2]$ ratios. Consequently we assume it to be negligible, if produced at all. Analyses for S_2O and O_3 were attempted by absorption spectroscopy at 2500 and 2700 Å. Both molecules absorb in this region, and the extinction coefficients for both molecules were determined.[10] If more than 10 μ of either gas were produced, they would have been detected. During the photolysis, absorption at both wavelengths grew, that at 2700 Å being stronger than at 2500 Å. The ratio of absorbance at the two wavelengths did not correspond to either that of O_3 or S_2O, though it could have been due to both gases being present. However, it seems unlikely to us that both gases would have been produced in the same ratio under all conditions, and we have discarded this possibility. Furthermore, the ratio of absorbance at the two wavelengths was exactly identical with that found when CS_2 was photolyzed in the absence of O_2, where the only product is polymer. Thus we attribute the absorbance exclusively to the polymer. Nevertheless, undetectable amounts of O_3 and/or S_2O might have been produced.

If the photolysis was performed in a cell cleaned either by prolonged evacuation (~2 weeks) or by nitric acid solution, then the reproducibility of the results was poor and the product quantum yields were as much as three times greater than for a cell conditioned by several previous photolyses. Furthermore, even in conditioned cells, the product quantum yields dropped as the exposure time was lengthened. In order to obtain initial quantum yields, very low conversions were required; it was often necessary to keep the final pressure of some of the gases to less than 5 μ.

Thus all the data reported here were obtained in conditioned cells at very short conversions. As a result, the accuracy is poor and the data show considerable scatter.

(8) J. Heicklen, *Advan. Photochem.*, 7, 57 (1969).

(9) R. Bent, W. R. Ladner, and W. J. Mullin, *Chem. Ind. (London)*, 461 (1967).

(10) The extinction coefficients for S_2O were determined by E. Cehelnik of our laboratory.

Table I: Photolysis of CS_2–O_2 Mixtures at 3130 Å and Room Temperature

$[O_2]$, Torr	Exposure time, min	$\Phi\{CO\}$	$\Phi\{OCS\}$	$\Phi\{SO_2\}$	$10^6\Phi\{P\}$, absorbance/μ	$\frac{\Phi\{CO\}}{\Phi\{OCS\}}$
		$[CS_2]$ = 2.0 Torr, I_a = 2.0 μ/min				
740	120.0	0.054	0.069	0.100		0.79
		$[CS_2]$ = 5.0 Torr, I_a = 5.0 μ/min				
1.0	240.0		0.0025	0.0047		
2.5	120.0	0.0060	0.0055	0.0163		1.09
9.2	60.0	0.0166	0.0160	0.045		1.04
405	120.0	0.060	0.056			1.07
740	120.0	0.053	0.046	0.098		1.15
745	120.0	0.048	0.044	0.093		1.09
		$[CS_2]$ = 10.0 Torr, I_a = 9.7 μ/min				
1.4	240.0	0.0034	0.0034	0.0068		0.98
4.8	90.0	0.0060	0.0078	0.0154	0.84	0.77
10.0	45.0	0.0109	0.0125	0.028	1.54	0.87
		$[CS_2]$ = 10.0 Torr, I_a = 20.5 μ/min				
50	10.0	0.029	0.039	0.112		0.74
54	10.0		0.029	0.049	2.5	
82	10.0	0.023	0.034	0.093	2.3	0.68
100	10.0		0.039	0.100	2.7	
159	10.0	0.024	0.042	0.078	5.3	0.59
200	10.0		0.037	0.083		
740	10.0		0.0195	0.024		
		$[CS_2]$ = 20.0 Torr, I_a = 2.05 μ/min				
42	90.0		0.021	0.029	1.45	
100	110.0	0.033	0.035	0.086	5.3	0.94
200	90.0	0.021	0.036	0.058	1.47	0.60
		$[CS_2]$ = 20 Torr, I_a = 38 μ/min				
2.0[a]	120.0	0.00119	0.00113	0.0025		1.05
10	10.0				1.21	
40	10.0	0.0081	0.0135	0.029		0.60
46	10.0	0.0081	0.0170	0.051	1.41	0.48
100	10.0	0.0184	0.032	0.096	2.9	0.57
100	10.0		0.028	0.068		
200	10.0	0.021	0.032	0.088	2.2	0.66
400	10.0	0.025	0.026	0.071	3.2	0.95
600	10.0	0.0137	0.022	0.055	6.8	0.63
		$[CS_2]$ = 40 Torr, I_a = 6.0 μ/min				
90	60.0	0.024	0.024	0.065	2.7	1.00
200	45.0	0.026	0.033	0.052	3.3	0.78
300	60.0	0.0153	0.024	0.050	2.9	0.65
400	45.0	0.021	0.033	0.072	1.92	0.62
720	60.0	0.0153	0.024	0.050	2.9	0.65
		$[CS_2]$ = 40 Torr, I_a = 70 μ/min				
20	10.0		0.0057	0.0107	1.26	
80	10.0		0.0143	0.033	1.52	
209	10.0	0.0192	0.021	0.043	2.2	0.92
410	10.0		0.021	0.049	3.8	
770	10.0	0.0179	0.0192	0.047	2.8	0.93
		$[CS_2]$ = 70 Torr, I_a = 11 μ/min				
30	520.0	0.0039	0.0043	0.0113	0.25	0.92
40	60.0	0.0030	0.0043	0.0093	0.68	0.70
70	100.0	0.0059	0.0057	0.0152		1.05
140	60.0	0.0086	0.0121	0.031	1.06	0.71
140	100.0	0.0080	0.0099	0.024	0.94	0.81
350	60.0	0.0100	0.0192	0.033	1.44	0.52
350	100.0	0.0144	0.0167	0.045	1.85	0.87
700	60.0		0.0161	0.046	2.1	

Table I (*Continued*)

$[O_2]$, Torr	Exposure time, min	$\Phi\{CO\}$	$\Phi\{OCS\}$	$\Phi\{SO_2\}$	$10^3\Phi\{P\}$, absorbance/μ	$\frac{\Phi\{CO\}}{\Phi\{OCS\}}$
		$[CS_2] = 70$ Torr, $I_a = 111$ μ/min				
1.2	213.0	0.00034	0.00040	0.00030	0.022	0.84
3.0	150.0	0.00042	0.00054	0.00048	0.044	0.78
6.0	60.0	0.00083	0.00075	0.0014	0.072	1.10
10.0	25.0	0.0022	0.0022	0.0052	0.187	1.00
20	30.0	0.0032	0.0033	0.0066	0.22	0.96
33	15.0	0.0048	0.0057	0.0138	0.44	0.84
70	10.0		0.0075	0.0197		
70	25.0	0.0070	0.0076	0.0178	0.85	0.93
141	10.0	0.0112	0.0136	0.0314	2.1	0.82
350	10.0	0.0162	0.0195	0.050	2.6	0.83

[a] $I_a = 28$ μ/min.

Experiments were done at various absorbed intensities, I_a, and reactant pressures. The absorbed intensity was varied by a factor of 56; $[CS_2]$, by a factor of 35; $[O_2]$, by a factor of 620; and $[O_2]/[CS_2]$, by a factor of 2.2×10^4. The results are listed in Table I. For the polymer only relative yields, $\Phi\{P\}$, were found, and they are reported in units of absorbance per micron. The product quantum yields were independent of I_a, but increased about 100-fold as $[O_2]/[CS_2]$ increased by a factor of 2.2×10^4. However, for a given ratio of reactants, the yields were independent of total pressure, and the ratios of yields were even nearly independent of $[O_2]/[CS_2]$. The quantum yields of the gaseous products were small and varied between 3×10^{-4} and 0.11.

The ratio $\Phi\{CO\}/\Phi\{OCS\}$ is listed for each of the runs in Table I, and it is seen to be invariant at 0.83 with a mean deviation of 0.15 with all changes in experimental variables. The variation of $\Phi\{SO_2\}/\Phi\{OCS\}$ with $[O_2]/[CS_2]$ is shown in Figure 1. The data points are quite scattered, but the solid line representing the average value of the ordinate at each value of $[O_2]/[CS_2]$ indicates that $\Phi\{SO_2\}/\Phi\{OCS\}$ is essentially constant at about 2.4 for $[O_2]/[CS_2]$ between 0.3 and 30. If a carbon–sulfur mass balance exists among the gas phase products, then

$$\Phi\{SO_2\} = \Phi\{OCS\} + 2\Phi\{CO\} \quad \text{(I)}$$

Since $\Phi\{CO\}/\Phi\{OCS\} = 0.83$, then $\Phi\{SO_2\} = 2.66\Phi\{OCS\}$. Within the experimental uncertainty, this relationship is obeyed; the polymer C–S ratio must be similar to that of CS_2 itself.

Discussion

The initial steps in the photolysis of CS_2 have been shown to be[2,11]

$$CS_2 + h\nu \longrightarrow CS_2^* \quad (1)$$

$$CS_2^* + CS_2 \longrightarrow 2CS + S_2 \quad (2a)$$

$$\longrightarrow 2CS_2 \quad (2b)$$

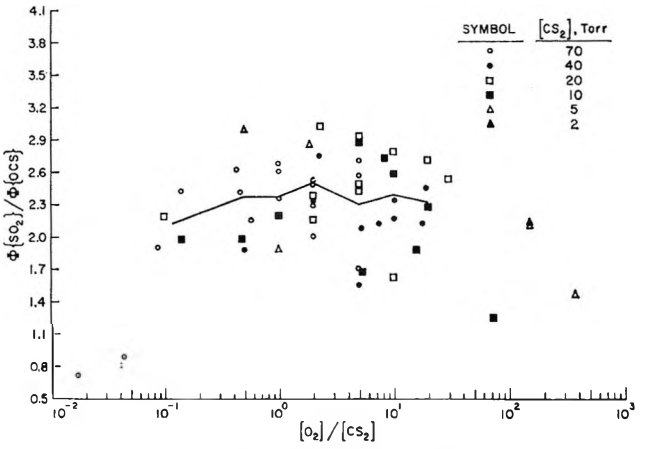

Figure 1. Plot of $\Phi[SO_2]/\Phi[OCS]$ *vs.* $[O_2]/[CS_2]$ in the photolysis of CS_2–O_2 mixtures at 3130 Å and room temperature.

where the asterisk denotes electronic excitation. The excited electronic state is quenched by oxygen.[2] If nonchemical quenching was the only step, then the oxidation would ultimately diminish as O_2 completely quenched CS_2^*, contrary to our results. Furthermore polymer production is also enhanced, and the polymer has the same C–S ratio as CS_2. Thus we add the following steps

$$CS_2^* + O_2 \longrightarrow CS_2 + O_2 \quad (3a)$$

$$\longrightarrow CS + SO_2 \quad (3b)$$

$$\longrightarrow \text{polymer} \quad (3c)$$

The precursor to SO_2 formation may be the unstable species SOO as proposed by de Sorgo, *et al.*[2] Myerson, *et al.*,[3c] believed that this species was responsible for the transient absorption they observed prior to SO_2 formation in the explosive oxidation of CS_2.

The invariance of the ratio $\Phi\{CO\}/\Phi\{OCS\}$ with all of our experimental parameters suggests that CO and

(11) J. Heicklen, *J. Amer. Chem. Soc.*, 85, 3562 (1963).

OCS are produced in parallel processes. We suggest the oxidation of CS

$$CS + O_2 \longrightarrow OCS + O \quad (4a)$$

$$\longrightarrow CO + SO \quad (4b)$$

That CS can be oxidized under our conditions conflicts with at least three earlier studies;[2,4,5,12] this discrepancy will be discussed later.

The steps necessary to complete the mechanism are

$$SO + O_2 \rightleftarrows OSOO \quad (5)$$

$$CS \xrightarrow{\text{wall}} \text{polymer} \quad (6)$$

$$O + CS_2 \longrightarrow CS + SO \quad (7)$$

$$OSOO + SO \longrightarrow 2SO_2 \quad (8)$$

The reaction step 5 has been discussed by Myerson, *et al.*,[3c] who even suggested SOOO as a possibility. In our system it must be followed by reaction 8 or a comparable step if SO_3 is not a product. In our system there is no evidence for reaction 6 as will be shown. However, since others[5] have included it, and since it must occur at sufficiently low $[O_2]$, we have included it for generality. Reaction 7 has now been firmly established,[13] and alternate product possibilities need not be considered. Another step which could be included without changing the mechanistic conclusions is

$$SO + O_2 \longrightarrow SO_2 + O$$

This reaction proceeds with an activation energy and has been measured at higher temperatures.[14,15] However, there is no compelling evidence from our results to include this step so it has been omitted for simplicity.

The above mechanism predicts that

$$\Phi\{CO\}/\Phi\{OCS\} = k_{4b}/k_{4a} \quad (II)$$

The results show that $\Phi\{CO\}/\Phi\{OCS\}$ is invariant to all changes in experimental parameters and k_{4b}/k_{4a} is found to be 0.83 ± 0.15 based on 44 experiments. Another prediction is that at low $[O_2]/[CS_2]$ where CS is produced primarily by reaction 2a, then

$$\Phi\{SO_2\} = \Phi\{OCS\} + \Phi\{CO\} = 1.83\Phi\{OCS\} \quad (III)$$

On the other hand, at high $[O_2]/[CS_2]$ where CS is produced primarily by reaction 3b, then eq I should hold. The results in Figure 1 indicate that reaction 3b is the primary source of CS for $[O_2]/[CS_2] \geq 0.3$. There is no clear indication that eq III ever applies.

Another prediction of the mechanism is

$$\Phi\{OCS\} = \frac{k_{4a}[O_2]}{(k_{4b}[O_2] + k_6)} \frac{(2k_{2a}[CS_2] + k_{3b}[O_2])}{(k_2[CS_2] + k_3[O_2])} \quad (IV)$$

where $k_2 \equiv k_{2a} + k_{2b}$ and $k_3 \equiv k_{3a} + k_{3b} + k_{3c}$. $\Phi\{OCS\}$ is plotted *vs.* $[O_2]/[CS_2]$ in Figure 2. The log–log plot initially rises, reaches unit slope, and then levels off at $\Phi\{OCS\} = 0.050$ at high $[O_2]/[CS_2]$. The surprising feature is the invariance of $\Phi\{OCS\}$ to $[CS_2]$ for a given $[O_2]/[CS_2]$. This result can only be consistent with eq IV if reaction 6 is negligible under all conditions. Furthermore if reaction 6 is omitted, then eq IV requires that $\Phi\{OCS\}$ reach some lower limit equal to $2k_{2a}k_{4a}/k_2k_{4b}$. This value is just being approached at our lowest values of $[O_2]/[CS_2]$ and is about 2×10^{-4}. The linear portion of the curve gives $k_{3b}k_{4a}/k_2k_{4b} = 0.90 \times 10^{-2}$, whereas the upper limit gives $k_{3b}k_{4a}/k_3k_{4b} = 0.050$. The theoretical curve based on these values is shown by the solid line in Figure 2. The appropriate rate constant ratios are listed in Table II. Our value of 0.18 for k_3/k_2 agrees reasonably well with the value of 0.13 obtained by de Sorgo, *et al.*[2]

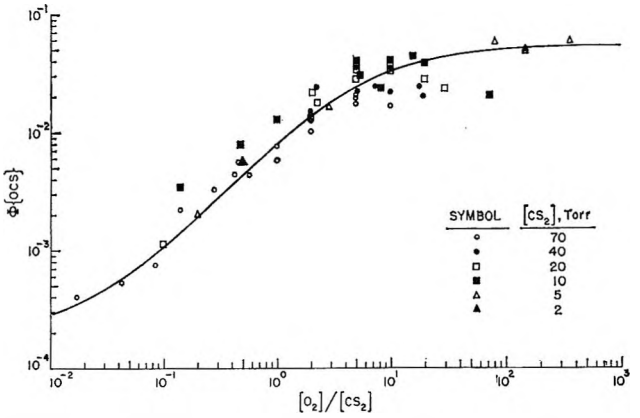

Figure 2. Plot of $\Phi[OCS]$ *vs.* $[O_2]/[OCS]$ in the photolysis of CS_2–O_2 mixtures at 3130 Å and room temperature.

With reaction 6 omitted, and S_2 absorption assumed negligible, the quantum yield of polymer formation $\Phi\{P\}$ is given by

$$\Phi\{P\} = k_{3c}[O_2]/(k_2[CS_2] + k_3[O_2]) \quad (V)$$

Table II: Summary of Rate Constant Data

Rate constant	Value	Units	Source
k_{4b}/k_{4a}	0.83 ± 0.15	None	Eq II
k_{2a}/k_2	0.8×10^{-4}	None	Eq IV, Figure 2
k_{3b}/k_3	0.042	None	Eq IV, Figure 2
k_{3b}/k_3	0.062	None	Eq IV, Figure 2 + reaction 10
k_3/k_2	0.18	None	Eq IV, Figure 2
k_3/k_2	0.17	None	Eq V, Figure 3
k_3/k_2	0.12	None	Eq IV, Figure 2 + reaction 10
k_3/k_2	0.13	None	de Sorgo, *et al.*[2]
k_{3c}/k_3	~0.027	None	See text
k_6^2/k_{11}	3.9×10^{-4}	M^{-1} sec^{-1}	Figure 1

(12) V. N. Kondratiev and E. Magaziner, *Zh. Fiz. Khim.*, **14**, 6 (1940); as reported in *Chem. Abstr.*, **35**, 979[6] (1941).

(13) N. Cohen and J. Heicklen, *Compr. Chem. Kinet.*, **6**, XX (1971).

(14) K. H. Homann, G. Krome, and H. G. Wagner, *Ber. Bunsenges. Phys. Chem.*, **72**, 998 (1968).

(15) D. J. Williams, *Combust. Flame*, **12**, 165 (1968).

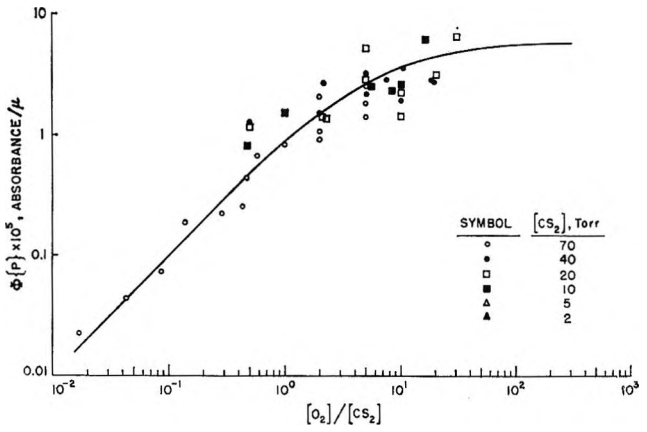

Figure 3. Plot of relative quantum yield of polymer formation *vs.* $[O_2]/[CS_2]$ in the photolysis of CS_2–O_2 mixtures at 3130 Å and room temperature.

Figure 3 is a plot of $\Phi\{P\}$ *vs.* $[O_2]/[CS_2]$. At low values of $[O_2]/[CS_2]$ the log–log plot has unit slope giving a relative value of $k_{3c}/k_2 = 1.0 \times 10^{-6}$. If we take the upper limit of $\Phi\{P\} = 6.0 \times 10^{-6}$, then this value corresponds to the relative ratio for k_{3c}/k_3. The resulting value for k_3/k_2 becomes 0.17 in good agreement with the result deduced from eq IV and Figure 2. The theoretical curve based on the above relative rate constants is shown in Figure 3, and it adequately represents the data points. A run was done with 80 Torr CS_2 at an intensity of about 120 μ/min in the absence of O_2. Polymer absorption corresponding to $\Phi\{P\} = 0.035 \times 10^{-5}$ was observed after 17 hr of exposure. This value is slightly higher than at our lowest ratios of $[O_2]/[CS_2]$, and corresponds to CS and S_2 deposition rather than polymer formation *via* reaction 3c. If the extinction coefficients of the polymers formed by the two processes are the same, then the absolute value $k_{3c}/k_3 = 0.027$. Furthermore since $\Phi\{P\}$ is lower at $[O_2]/[CS_2] = 0.017$ than in the absence of O_2, at least some of the CS must have been scavenged by O_2.

A final piece of evidence in support of the mechanism comes from the work of de Sorgo, *et al.*,[2] on the flash photolysis of CS_2. In the absence of O_2, the spectrum of S_2 was observed, but it was completely suppressed in the presence of O_2.

A reexamination of Figure 1 suggests that other reactions might play some role at very high or very low $[O_2]/[CS_2]$. For example at very high $[O_2]/[CS_2]$, the ratio $\Phi\{SO_2\}/\Phi\{OCS\}$ may be reduced. This would be expected if the SO were removed sufficiently rapidly by O_2 so that it could not react with OSOO which would then rearrange to SO_3. Under the conditions at which

$$OSOO \longrightarrow SO_3 \qquad (9)$$

our experiments were performed, the SO_3 would have been too small for us to detect. The ratio $\Phi\{SO_2\}/\Phi\{OCS\}$ should drop, which is compatible with our findings.

Furthermore at very high $[O_2]/[CS_2]$ the ozone producing reaction could be important

$$O + 2O_2 \longrightarrow O_3 + O_2 \qquad (10)$$

The rate constant $k_{10} = 2.5 \times 10^8\ M^{-2}\ sec^{-1}$,[16] whereas that for reaction 7 is $2.5 \times 10^9\ M^{-1}\ sec^{-1}$.[17-19] Thus at our highest $[O_2]/[CS_2]$, reaction 10 consumes 58% of the oxygen atoms. Of course if the O_3 produced reacts with CS_2 to produce CS and SO, there is no net difference in the two reactions. However, if the O_3 does not further react then reaction 10 would reduce $\Phi\{OCS\}$ by one-third; the value of k_3/k_2 would drop to 0.12 in even better agreement with de Sorgo, *et al.*,[2] while k_{3b}/k_3 would become 0.062.

At the lowest values of $[O_2]/[CS_2]$, $\Phi\{SO_2\}/\Phi\{OCS\}$ is markedly reduced which indicates that all the SO species are not oxidized. The indicated competing overall reaction is[20]

$$3SO \longrightarrow SO_2 + S_2O$$

The S_2O produced would have been below our detection limits. The reaction is a composite reaction which presumably proceeds *via* the second-order step

$$2SO \longrightarrow \text{products} \qquad (11)$$

The details of this reaction have not been ascertained but SO_2 and S_2O are produced,[13,20] presumably in equal amounts; the ratio $\Phi\{SO_2\}/\Phi\{OCS\}$ would drop to one-third its value at higher O_2 pressures in conformance with the results indicated in Figure 1. These results suggest that reactions 5 and 11 are of equal importance when $I_a = 111$ μ/min, $[O_2] \sim 5.6$ Torr, and $[CS_2] = 70$ Torr. The ratio k_5^2/k_{11} is estimated to be $3.9 \times 10^{-4}\ M^{-1}\ sec^{-1}$. Reaction 11 could also be the route to SO_2 production if the initially formed SO dimer reacted with O_2. Thus reactions 5 and 8 might not be needed.

The above mechanism explains all of our observations. Nevertheless all investigations from other laboratories have concluded that CS does not react with O_2, even at elevated temperatures.[13] Thus we must consider other possible mechanisms. Apparently the only other mechanism which produces a constant ratio of OCS and CO without oxidizing CS includes the additional steps

$$CS_2^* + O_2 \longrightarrow OCS + SO \qquad (3d)$$

$$SO + CS \longrightarrow CO + S_2 \qquad (12)$$

This mechanism will give a constant value for $\Phi\{OCS\}/\Phi\{CO\}$ under all conditions if the SO undergoes no

(16) F. Kaufman and J. R. Kelso, *J. Chem. Phys.*, **40**, 1162 (1964).
(17) A. B. Callear and I. W. M. Smith, *Nature*, **213**, 382 (1967).
(18) I. W. M. Smith, *Trans. Faraday Soc.*, **64**, 378 (1968).
(19) A. A. Westenberg and N. de Haas, *J. Chem. Phys.*, **50**, 707 (1969).
(20) P. W. Schenk and R. Steudel, *Angew. Chem., Int. Ed. Engl.*, **4**, 402 (1965).

other reactions. Thus the mechanism would consist of reactions 1–3d, 6, and 12. This mechanism predicts that

$$\Phi\{OCS\}/\Phi\{CO\} = 1.0 \qquad (VI)$$

and

$$\Phi\{SO_2\}/\Phi\{OCS\} = k_{3b}/k_{3d} > 1.0 \qquad (VII)$$

Equation VI might be consistent with our results. For most of our conditions eq VII is obeyed, but it fails to explain the low values obtained for $\Phi\{SO_2\}/\Phi\{OCS\}$ at low $[O_2]/[CS_2]$. However this mechanism also predicts that the steady-state pressures of both CS and S_2 should be markedly greater in the presence of O_2 than in its absence. Both predictions are contrary to the findings of de Sorgo, *et al.*,[2] who observed not much change in [CS] and complete quenching of $[S_2]$ when O_2 was present. Therefore we discard this mechanism.

The question still remains concerning CS oxidation. Two earlier studies of the low-intensity photooxidation of CS_2 with energy above 2300 Å (where no photodissociation occurs) were reported by Thompson and Kearton[21] and de Sorgo, *et al.*[2] In neither study was OCS found, but this can be attributed to insufficient analytical sensitivity for the low quantum yields produced. However, de Sorgo, *et al.*,[2] monitored [CS] in the flash photolysis and found that it was only slightly different in the absence or presence of O_2, even at large O_2 pressures (90 Torr O_2, 22 Torr CS_2, and 280 Torr N_2). From this they concluded that CS does not react with O_2. Nevertheless this result can be consistent with our mechanism. In the absence of O_2, the steady-state pressure of CS is given by

$$[CS] = 2k_{2a}I_a/k_2k_6 \qquad (VIII)$$

while under their conditions with O_2 present, our rate constant ratios give

$$[CS] \sim \frac{k_{3b}}{k_{4b}} \frac{I_a}{(k_2[CS_2] + k_{13}[N_2])} \qquad (IX)$$

where reaction 13 is

$$CS_2^* + N_2 \longrightarrow CS_2 + N_2 \qquad (13)$$

Consequently [CS] is nearly independent of $[O_2]$ and would be similar in the absence and presence of O_2 if $2k_{2a}/k_2k_6 \simeq k_{3b}/k_{4b}(k_2[CS_2] + k_{13}[N_2])$.

The flash photolysis of CS was examined by Wright[5] both in the absence of O_2 and in the presence 0.2 and 5 Torr of O_2. He also monitored [CS] and found that [CS] decreased as $[O_2]$ increased, but that the rate of CS disappearance was independent of O_2. The latter result led him to conclude also that CS did not react with O_2. In fact his observation can also be consistent with our mechanism for appropriate CS_2 pressures. Unfortunately he did not list the pressure of either CS_2 or the diluent gas. However, reasonable values of these parameters do exist such that our mechanism predicts [CS] varying inversely with $[O_2]$ in which case $d[CS]/dt$ is independent of $[O_2]$, if CS is removed only by reaction 4.

Kondratiev and his coworkers[4,12] also report that CS does not react with O_2 below 100°. This conclusion is particularly surprising from the results of Kondratiev and Yakovleva[4] who photolyzed CS_2 with effective radiation essentially at 2000 Å where the primary process is

$$CS_2 + h\nu\ (<2300\ \text{Å}) \longrightarrow CS + S \qquad (14)$$

They found OCS as a principal product of the photooxidation. Furthermore they monitored the CS absorption bands and found that they were completely suppressed in the presence of O_2.

Finally, Wiebe and Heicklen[6] found both OCS and CO in the photooxidation of thiophene, where the only reasonable precursor could have been CS, though it might have been excited.

Acknowledgment. The authors wish to thank Dr. H. A. Wiebe for his many useful contributions. This work was supported by the National Air Pollution Control Administration through Grant No. AP00022 for which we are grateful.

(21) H. W. Thompson and C. F. Kearton, *Z. Phys. Chem. Abt. B*, **14**, 359 (1931).

Kinetics and Mechanism of the Carbon Disulfide–Oxygen Explosion[1a]

by William P. Wood[1b] and Julian Heicklen*

Department of Chemistry and Center for Air Environment Studies, The Pennsylvania State University, University Park, Pennsylvania 16802 *(Received November 18, 1970)*

Publication costs borne completely by The Journal of Physical Chemistry

Explosion limits for the CS_2–O_2 reaction were obtained at 341 and 415°K. For a given set of conditions a plot of O_2 pressure *vs.* CS_2 pressure at the explosion limits gave an explosion peninsula. For O_2–CS_2 compositions within the peninsula a spontaneous explosion occurred, while outside the peninsula no reaction occurred. At 341°K the nature of the wall and the addition of 100 Torr of N_2 were also investigated. The lower explosion limit was reduced by conditioning the surface or adding N_2, whereas the upper limit was reduced only by the addition of N_2. The mechanism which explains the results is given by reactions 1–8. The mechanism leads to an expression relating $[O_2]$, $[CS_2]$, and $[N_2]$ at the explosion limits through five rate constant ratios. Computer computations for these ratios to give a best fit to the data showed that the mechanism was consistent with all the observations.

Introduction

The oxidation of carbon disulfide exhibits limit phenomena which can be interpreted in terms of branching reaction chains and has been the object of study for over 40 years.[2–9] These previous investigations have been concerned primarily with the determination of the explosion limits as a function of temperature as well as the effects upon these limits with the addition of an inert gas or change in vessel diameter. In addition, Myerson and Taylor[10] have spectroscopically identified the unstable intermediates present during the explosion. However, owing to difficulties of reproducibility, knowledge of the nature of the reaction mechanism has been limited.

Until recently not enough was known about the oxidation of carbon disulfide to allow a quantitative interpretation of the explosion limits of CS_2–O_2 mixtures. However, recent photochemical studies[11,12] have elucidated the oxidation mechanism which now allows the possibility of rendering a quantitative interpretation of the explosion kinetics.

In the present study, explosion limits were obtained at temperatures of 341 and 415°K as a function of oxygen and carbon disulfide pressure. Based upon the mechanism developed from photochemical studies,[12] a computer program was utilized in a least-squares fitting of the experimentally obtained explosion limits at the two temperatures. In addition, the data representing the inert gas effect and the change in surface conditioning upon the explosion limits at 341°K were also fitted.

Experimental Section

Extra dry grade O_2 and N_2 obtained from the Matheson Co. were used without further purification. The only impurities found were 80 ppm of O_2 in the N_2 and 300 ppm of N_2 in the O_2. Fisher Scientific Co. spectral grade CS_2 was used after degassing at −196°. No impurities (<12 ppm) were detected in the CS_2. Gas pressures were measured by a Wallace-Tiernan absolute pressure indicator, a mercury manometer, or a McLeod gauge.

The reaction mixtures were premixed in a 1-l. bulb before admission into the evacuated reaction cell which was contained in a wire-wound aluminum furnace maintained at the desired temperature. The furnace was equipped with quartz windows at both ends. The reaction cell was a cylindrical quartz cell 10 cm in length and 5 cm in diameter.

The occurrence of an explosion was detected spectrophotometrically by a sudden increase in absorption at 2700 Å. The monitoring source was an Osram 150-W high-pressure xenon lamp. Its radiation passed through a Jarrell-Ash 82-410 0.25-m Ebert monochromator with 500-μ slits and a 1180-groove/mm grating blazed at 3000 Å. After passing through the windows

(1) (a) CAES Report No. 181-70; (b) U. S. Public Health Service Air Pollution Trainee.

(2) (a) A. B. Sagulin, *Z. Phys. Chem. Abt. B*, 1, 275 (1928); (b) H. W. Thompson, *ibid.*, 10, 273 (1930).

(3) H. W. Thompson and C. F. Kearton, *ibid.*, 14, 359 (1931).

(4) A. Ritchie, R. R. H. Brown, and J. J. Muir, *Proc. Roy. Soc., Ser. A*, 137, 511 (1932).

(5) H. W. Thompson, F. L. Hovde, and A. C. H. Cairns, *J. Chem. Soc.*, 208 (1933).

(6) V. G. Voronkov and N. N. Semenov, *Zh. Fiz. Khim.*, 13, 1695 (1939).

(7) N. N. Semenov and V. G. Voronkov, *Acta Physicochim. URSS*, 12, 831 (1940).

(8) A. L. Myerson and F. R. Taylor, *J. Amer. Chem. Soc.*, 75, 4348 (1953).

(9) F. R. Taylor and A. L. Myerson, *Symp. Int. Combust., Proc. 7th*, 72 (1959).

(10) A. L. Myerson, F. R. Taylor, and P. L. Hanst, *J. Chem. Phys.*, 26, 1309 (1957).

(11) M. de Sorgo, A. J. Yarwood, O. P. Strausz, and H. E. Gunning, *Can. J. Chem.*, 43, 1886 (1965).

(12) W. P. Wood and J. Heicklen, *J. Phys. Chem.*, 75, 854 (1971).

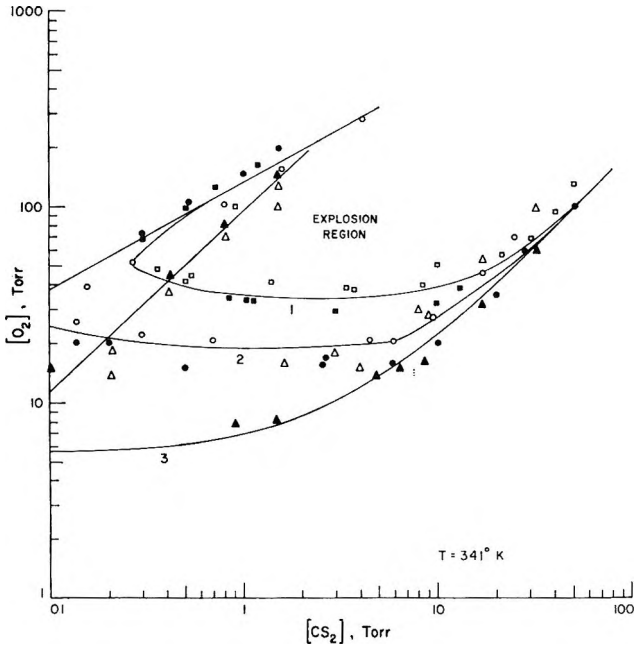

Figure 1. Log–log plots of the O_2 pressure *vs.* the CS_2 pressure at 341 ± 2°K. Three series of experiments are represented: (1) reaction vessel partially conditioned by polymer deposition from photochemical runs, squares; (2) reaction vessel fully conditioned by polymer deposition from numerous previous explosions, circles; (3) reaction vessel fully conditioned by polymer deposition from numerous previous explosions; 100 Torr of N_2 also present, triangles. The empty symbols indicate explosion, whereas the filled symbols indicate no explosion. The curves give the theoretical explosion limits computed from the rate constant ratios in Table II.

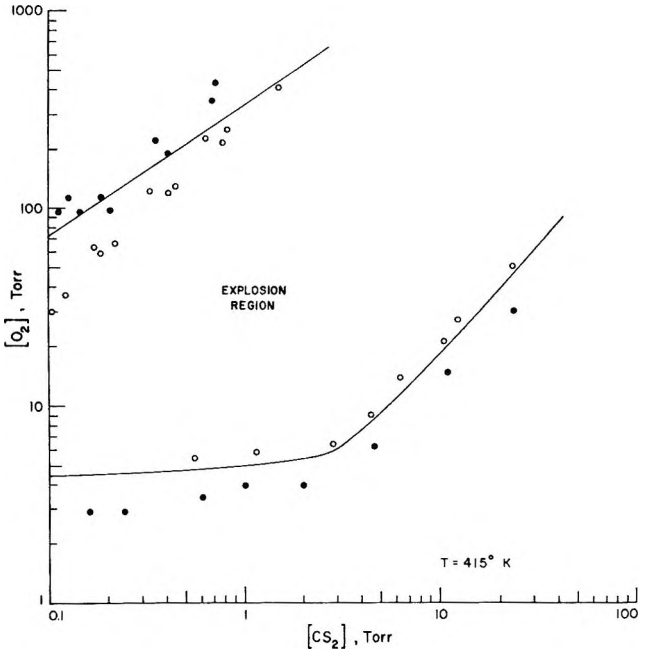

Figure 2. Log–log plot of the O_2 pressure *vs.* the CS_2 pressure at 415 ± 2°K for a reaction vessel fully conditioned by polymer deposition from numerous previous explosions. The empty circles indicate explosion, whereas the filled circles indicate no explosion. The curve gives the theoretical explosion limits computed from the rate constant ratios in Table II.

of the furnace and the reaction cell, the radiation was focused onto a RCA 9-35 phototube.

The products of the explosion were collected and analyzed by gas chromatography. The products noncondensable at −196° were collected with a Toepler pump and passed through a 15-ft, 5-Å molecular sieve column operating at 50° and a He flow rate of 150 cc/min. The condensable products were collected and analyzed on a 10-ft Porapak Q column at 70° with a He flow rate of 250 cc/min.

Results

Explosion limits were obtained at 341 and 415°K for $[O_2]$ to $[CS_2]$ ratios between 2 and 400. An explosion was considered to occur if a sudden absorption at 2700 Å occurred within less than 1 min after introducing the mixture into the reaction vessel. The 1-min time interval was to ensure that the reaction mixture had reached the temperature of the cell. Usually, if explosion did not occur within 1-min, it did not occur at all. Except very near the explosion limits, the explosion was almost immediate. The data show a critical region of pressure and composition within which a spontaneous explosion will occur and outside of which no noticeable reaction will take place. These limits were found to be reproducible as long as the walls of the reaction vessel had been previously conditioned by coating them with the polymer of several explosions.

Figures 1 and 2 are log–log plots of oxygen *vs.* carbon disulfide pressure at the two respective temperatures. The data points included in both figures are only the points obtained closest to the explosion limits. The empty symbols on the graphs indicate that an explosion took place, while the filled symbols indicate no reaction in less than 1 min. Additional data were also obtained over the entire range of pressure and composition covered by the graph. However these points were omitted in order to present the pertinent data as clearly as possible.

Curves 1 and 2 of Figure 1 demonstrate the effect of the wall upon the lower explosion limit. Curve 1 is the explosion peninsula obtained in a cell partially conditioned by polymer deposition from previous photochemical studies, while curve 2 represents the explosion peninsula obtained in the same cell which had been additionally conditioned by the deposition of polymer from numerous previous explosions. For the two curves the lower explosion limit is shifted, but there is no difference at high O_2 pressures.

Curve 3 of Figure 1 illustrates the reduction of the lower and upper limits of curve 2 upon the addition of 100 Torr of N_2 to the reaction mixtures. As can be seen from Figure 1, there is a lowering of the lower limit as had been described in previous investigations.[4,5] However, in addition there is a lowering of the upper

limit for very lean mixtures of CS_2 in O_2 (<1:100). Previous studies had not covered such an extensive mixture composition ratio so that this effect was not seen.

Analysis of the products of the explosion was done by gas chromatography for mixtures with $[O_2]/[CS_2]$ of 2.8 and 4.9 at 341°K and 2.0 at 415°K. At the lower temperature the CS_2 pressure ranged from 9.3 to 62.0 Torr, whereas at the higher temperature the CS_2 pressure ranged from 11.0 to 40 Torr. From the figures, it can be seen that these mixtures correspond to the lower explosion limit. Under these conditions no flash of light accompanied the explosion.

The products found were SO_2, OCS, CO, and polymer. No attempt was made to analyze for either SO_3 or O_3. The observed product ratios are listed in Table I. They do not vary markedly with changes in reactant pressures or temperature. The average values are $[CO]/[OCS] = 0.84 \pm 0.07$ and $[SO_2]/[OCS] = 6.6 \pm 0.9$ where the uncertainties are mean deviations. The value of 0.84 ± 0.07 agrees with that of 0.83 ± 0.15 found for $[CO]/[OCS]$ at room temperature in the photooxidation studies.[12] CO_2 was absent for these mild explosions, but was found for the more violent explosions which occurred for CS_2–O_2 compositions well-within the explosion peninsula.

Table I: Product Ratios from the CS_2–O_2 Reaction near the Explosion Limit

$[CS_2]$, Torr	$[O_2]$, Torr	$[CO]/[OCS]$	$[SO_2]/[OCS]$
Temp = 341°K, $[O_2]/[CS_2] \simeq 4.92$			
61.8	303.2	0.58	4.9
32.1	158.9	0.64	6.4
16.4	80.6	0.70	7.0
9.3	45.7	0.79	6.2
Temp = 341°K, $[O_2]/[CS_2] \simeq 2.80$			
62.0	174.0	0.84	4.6
31.8	89.2	0.98	6.1
25.4	71.6	1.07	6.2
16.3	45.7	1.04	6.8
9.5	26.5	0.96	7.0
Temp = 415°K, $[O_2]/[CS_2] \simeq 2.03$			
40.0	80.0	0.84	7.1
29.0	59.7	0.87	8.3
20.0	40.6	0.78	8.7
11.0	22.0	0.86	5.0
		Av 0.84 ± 0.07	Av 6.6 ± 0.9

Discussion

Essential to the theory of explosions as developed by Semenov[13] is the occurrence of an exponential increase in the rate of the reaction with time. This is explained by the existence of a branching chain reaction. The well-known rapid reaction[14]

$$O + CS_2 \longrightarrow CS + SO \qquad (1)$$

will satisfy the criteria for a branching chain reaction if the destruction of one unstable species "O" leads to the production of two unstable intermediates "CS" and "SO." This requires that CS as well as SO must then enter into some further reactions to regenerate the chain.

In some studies[11,15–17] the investigators have concluded that CS does not enter into oxidation reactions and disappears at the wall. However, in our photochemical studies,[12] we have shown that CS is removed by O_2 exclusively in the gas phase *via*

$$CS + O_2 \longrightarrow OCS + O \qquad (2a)$$

$$\longrightarrow CO + SO \qquad (2b)$$

Also it was shown[12] that the earlier observations are consistent with reactions 2a and 2b. Other studies give further support for these reactions. McGarvey and McGrath[18] found that O_2 removed the CS absorption spectrum in the flash photolysis of CS_2–O_2 mixtures. Sheen[19] has also argued in favor of these reactions in the shock tube oxidation of CS_2. Wiebe and Heicklen[20] found both OCS and CO as products in the photooxidation of thiophene, where the only reasonable precursor was CS (though it might have been excited). Finally it should be noted that the $[CO]/[OCS]$ ratio was the same in both the photochemical studies at room temperature and for the mild explosions reported in Table I. In addition, CO_2 was not found as an initial product in either system. Thus it can be concluded that reactions 2a and 2b are the main routes to OCS and CO production, respectively. The invariance of the $[CO]/[OCS]$ ratio with temperature further suggests that the products of the two reactions originate from the same activated complex.

SO can enter into the following reactions

$$SO + O_2 \longrightarrow SO_2 + O \qquad (3)$$

$$SO + O_2 \longrightarrow SO_3 \qquad (4)$$

$$SO \xrightarrow{\text{wall}} \text{removal} \qquad (5)$$

Reaction 3 is a simple chain reaction (the destruction of one unstable species produces only one unstable species) and has an activation energy.[14] Reaction 4 has been postulated in at least two studies,[10,12] but the evidence

(13) N. N. Semenov, "Some Problems in Chemical Kinetics and Reactivity," English Translation by M. Boudart, Vol. 2, Princeton University Press, Princeton, N. J., 1959.

(14) N. Cohen and J. Heicklen, *Compr. Chem. Kinet.*, in press.

(15) V. N. Kondratiev and A. Yakovleva, *Zh. Eksp. Teor. Fiz.*, **10**, 1038 (1940).

(16) V. N. Kondratiev and E. Magaziner, *Zh. Fiz. Khim.*, **14**, 6 (1940); as reported in *Chem. Abstr.*, **35**, 979[6] (1941).

(17) F. J. Wright, *J. Phys. Chem.*, **64**, 1648 (1960).

(18) J. J. McGarvey and W. D. McGrath, *Proc. Roy. Soc., Ser. A*, **278**, 490 (1964).

(19) D. B. Sheen, *J. Chem. Phys.*, **52**, 648 (1970).

(20) H. A. Wiebe and J. Heicklen, *Can. J. Chem.*, **47**, 2965 (1969).

Table II: Rate Constant Ratios

Temp, °K	k_6/k_1, Torr^{-1}	k_{2b}/k_2	k_3/k_3	k_5/k_3, Torr^2	k_4/k_3	Source
341 ± 2	2.78×10^{-6}	0.48	0.79	465	1.66	Figure 1, curve 1
341 ± 2	2.80×10^{-6}	0.48	0.80	164	1.67	Figure 1, curves 2 and 3
415 ± 2	1.0×10^{-7}	0.49	0.15	1.86	1.92	Figure 2

for its existence is not conclusive. Undoubtedly the initial adduct is not the normal form of symmetric SO_3, but is the species OSOO (Myerson, *et al.*,[10] even considered SOOO). This species could then rearrange to symmetric SO_3 or react with another SO to produce two molecules of SO_2. (In the latter case our rate constant reported for k_4 in Table II should be reduced by a factor of 2, since two SO are removed.) The latter possibility was preferred by us in our photochemical studies at room temperatures[12] where the data indicated that SO was removed in a nonchain process to produce SO_2. Because of the uncertainty of the existence of reaction 4, we first attempted to fit our data by omitting this reaction but with no success. Likewise, including a chaperone gas in reaction 4 was unsuccessful.

The lower explosion limit has generally been attributed to a diffusion-controlled wall-termination step involving an active species.[13] In the CS_2–O_2 system the only active species at the lower limit are O, CS, and SO (O_3 is only important near the upper limit). As previously discussed, both O and CS are removed exclusively in the gas phase. Therefore, by the method of Holmes,[21] it can be concluded that reaction 5 must occur if there is a wall-termination step. In the absence of O_2, SO is known to be a semistable molecule which disappears slowly by a wall reaction[14] to produce S_2O and SO_2 as products.[22] Probably it is S_2O (which has an intense absorption at 2700 Å) which accounts for at least part of the absorption used by us as a test of explosion.

If there is a wall reaction, the addition of an inert gas or an increase in vessel diameter should result in the reduction of the lower explosion limit. This is due to the fact that the time which it takes the active intermediate to reach the wall and be destroyed is increased either due to a slower diffusion to the wall because of the presence of the inert gas or, in the case of an increased vessel diameter, the active intermediate must travel a further distance before destruction. In either case the probability that the intermediate can enter into some chain reaction is augmented. Several prior studies[2b-5] have examined the effect on the lower limit of the addition of an inert gas or by the increase in vessel diameter. In these instances the presence of a wall reaction was indicated by the reduction of the lower explosion limit.

In this study the existence of a wall reaction was further corroborated in two ways. First, the nature of the surface was changed by different conditioning procedures. Curves 1 and 2 of Figure 1 clearly show that the lower limit is different for the two wall conditions used. Furthermore, some runs were done with 100 Torr of N_2 added. In Figure 1, curve 2 represents the explosion limits of various mixtures of CS_2 and O_2 as a function of pressure of the two constituents. Curve 3 represents the explosion limits of these same mixtures with the addition of 100 Torr of N_2. It can be seen that the lower limit is indeed reduced with greatest effect in the region of CS_2 pressure from 0.1 to 6.0 Torr.

A reduction in the upper limit upon the addition of the inert gas can be seen as well, although this effect had not been reported previously. The effect of 100 Torr of N_2 on the upper limit would be most dominant at low $[O_2]$ and decrease in importance as $[O_2]$ increases. This effect can be seen in Figure 1. At low $[O_2]$ the upper limit is reduced by a factor of 3, while at higher $[O_2]$ where $[O_2]$ and $[N_2]$ are comparable the upper limit is reduced by only 20%. This would explain why in the previous investigations of the inert gas effect no note was made of an effect upon the upper limit. In all those previous studies the amount of N_2 added was either less or comparable to the amount of O_2 in the mixture.

The reduction in the upper limit can be explained if we assume that the important termination reaction at the upper limit is

$$O + O_2 + M \longrightarrow O_3 + M \qquad (6)$$

The O_3 produced in reaction 6 might be removed by reaction with either SO, O, or CS. With SO the reaction is

$$O_3 + SO \longrightarrow SO_2 + O_2 \qquad (7)$$

Halstead and Thrush[23] have shown this to be a rapid bimolecular reaction which produces almost exclusively electronic ground state molecules and has a rate constant of $k_7 = 1.5 \times 10^9 \exp(-2100/RT)\ M^{-1}\ \text{sec}^{-1}$. The rate constant for the reaction of oxygen atoms with O_3 is[24] $8.4 \times 10^8 \exp(-3000/RT)\ M^{-1}\ \text{sec}^{-1}$, which is

(21) S. Holmes has successfully demonstrated the power of the intriguing argument that if only one possibility exists, it must be true no matter how implausible it may seem.

(22) P. W. Schenk and R. Steudel, *Angew. Chem., Int. Ed. Engl.*, **4**, 402 (1965).

(23) C. J. Halstead and B. A. Thrush, *Proc. Roy. Soc., Ser. A*, **295**, 380 (1966).

(24) DASA Reaction Rate Handbook #1948 (1967).

comparable in magnitude to that for reaction 7. The reaction of CS with O_3 is also known,[25] but its rate constant is not. However, it cannot be much larger than that of reaction 7. Since both O and CS are removed efficiently in the gas phase by other reactions, whereas SO is removed with difficulty, it can be concluded that the steady-state concentrations of SO must be orders-of-magnitude greater than those of CS and O. Thus the removal of O_3 by either O or CS is unimportant compared to the removal by SO and can be neglected.

Previous researchers[5] have described the inhibiting effect of CS_2 itself upon the explosion. In addition Semenov and Voronkov[7] have investigated the lowering of the glow limit and glow temperature upon the reduction of the CS_2 content in their flame studies. This effect is also evident in Figures 1 and 2. At both temperatures the lower explosion limit is raised at high CS_2 concentrations. This indicates that CS_2 must enter into some termination reaction of the type

$$CS_2 + SO \longrightarrow \text{removal}$$

Thompson, *et al.*,[5] proposed

$$CS_2 + SO \longrightarrow CO + 3S$$

but this reaction is hopelessly endothermic. A more likely reaction is

$$CS_2 + SO \longrightarrow OCS + S_2 \qquad (8)$$

which is exothermic by 30 kcal/mol. An apparent difficulty with reaction 8 is that it provides another source of OCS production and should lead to a change in [CO]/[OCS] as a function of CS_2 pressure. In the photochemical oxidation of CS_2 with 3130-Å radiation[12] the ratio [CO]/[OCS] was invariant to all experimental parameters of total pressure, mixture composition, and absorbed intensity. Thus this reaction cannot be important at room temperature. However, it might proceed with an activation energy and be significant at higher temperatures. In fact our subsequent determinations of rate constant ratios shows that the temperature dependence of k_8/k_3 is less than expected from the activation energy of k_3 alone, and that k_8 must also have an activation energy. Analysis was done of the products formed for mild explosions (Table I), and [CO]/[OCS] was still found to be invariant to reaction conditions, but the scatter in the data was large. If reaction 8 is included, the rate constants obtained on the following pages lead to the expectation that under the conditions where [CO]/[OCS] was measured the largest spread in the ratio should be 30% which is smaller than the experimentally observed spread.

At the explosion limits, the rate of chain branching equals the rate of termination. When the steady-state assumption is applied to [O], [CS], [SO], and [O_3], the mechanism consisting of reactions 1–8 leads to the following expression

$$[O_2] = (k_6/k_1)(2 + k_4/k_3)[O_2]^2[M]/[CS_2] + (k_5k_6/k_1k_3)[O_2]/[CS_2] + (k_6k_8/k_1k_3)[M][O_2] + (k_{2b}k_4/k_2k_3)[O_2] + k_{2b}k_5/k_2k_3[M] + (k_{2b}k_8/k_2k_3)[CS_2] \qquad (I)$$

which applies at the explosion limits. Since reaction 5 is a diffusion-controlled wall reaction, its rate, $R\{5\}$, was assumed to be

$$R\{5\} = k_5[SO]/[M] \qquad (II)$$

in deriving eq I. Also $k_2 \equiv k_{2a} + k_{2b}$.

Equation I relates $[O_2]$, $[CS_2]$, and [M] at the explosion limits through the five rate constant ratios k_6/k_1, k_{2b}/k_2, k_8/k_3, k_5/k_3, and k_4/k_3. Therefore from the experimentally determined values of $[O_2]$, $[CS_2]$, and [M] corresponding to the explosion limits, a least-square fitting of the data will produce the values of these five ratios of rate constants. However, first it is necessary to determine the functional form of [M].

The inert gas effect appears in both reactions 5 and 6, but for different reasons. In the former reaction, the inert gas effect controls diffusion to the walls, whereas in the latter reaction it is a chaperone effect. Diffusion through N_2 and O_2 occurs at about the same rate. However for CO_2, diffusion through air is slightly greater than twice that through CS_2 at room temperature.[26] Thus for reaction 5, we have adopted the following form for [M]

$$[M] = [O_2] + [N_2] + 2[CS_2] \qquad (III)$$

In reaction 6, O_2 and N_2 are nearly equally efficient chaperone gases.[24] The relative efficiency of CS_2 is not known, but it should be more efficient than either N_2 or O_2, perhaps by a factor of 2–5. Fortunately reaction 6 is only important at high ratios of $[O_2]$ to $[CS_2]$, so that CS_2 plays almost no role as a chaperone. Equation III is also adopted for [M] in reaction 6.

The experimentally obtained explosion limits were then subjected to a least-squares fitting of eq I by computer calculation using the IBM Nonlinear Parameter Estimation Program #360D 13.6.003. The results gave the rate constant ratios listed in Table II. With these rate constant ratios, the theoretical explosion-limit curves based on eq I can be computed, and they are shown in Figures 1 and 2. These curves adequately fit all the data.

In fitting the data the following procedure was used. First the explosion limits for the fully conditioned cell at 341°K were fitted to obtain one set of rate constants for the data with both N_2 absent and present. In this way curves 2 and 3 of Figure 1 were obtained. The ratios k_8/k_3, k_5/k_3, and k_4/k_3 were allowed to assume any positive value necessary to improve the fit, but k_6/k_1 and k_{2b}/k_2 were restrained between fairly narrow limits

(25) K. J. Olszyna and J. Heicklen, *J. Phys. Chem.*, **74**, 4188 (1970).
(26) "International Critical Tables," Vol. V, 1929, p 62.

because values for these ratios are reasonably well known. The best values for k_6 and k_1 are, respectively, $2.0 \times 10^8(T/300)^{-2.6}\ M^{-2}\ \text{sec}^{-1}$[24] and $2.2 \times 10^{10} \exp(-1500/RT)\ M^{-1}\ \text{sec}^{-1}$.[14] At 341°K, these values give $k_6/k_1 = 2.80 \times 10^{-6}\ \text{Torr}^{-1}$. From this work as well as the previous photochemical studies,[12] $k_{2b}/k_2 = 0.46 \pm 0.04$. The values which are consistent with these known ratios and best fit the explosion limit data are listed in Table II.

Next, the data for the partially conditioned cell were fitted. In order for the mechanism to be valid, the only ratio which should change is k_5/k_3. Therefore the other four ratios were only permitted to vary slightly about their values for the fully conditioned cell. Again a good fit could be obtained easily, the value for k_5/k_3 being about 2.8 times larger. This increase is in the expected direction, since for the freshly cleaned cell, the wall reaction is even more important.

Finally an attempt was made to fit the explosion limits at 415°K in the same manner as used to obtain curves 2 and 3 of Figure 1. At this temperature $k_6/k_1 = 8.8 \times 10^{-7}\ \text{Torr}^{-1}$. With this value it was not possible to fit the upper explosion limit, so that the value for k_6/k_1 was lowered until a good fit could be obtained. This was accomplished with $k_6/k_1 = 1.0 \times 10^{-7}\ \text{Torr}^{-1}$ which is a factor of 8.8 lower than expected. Of course there is some uncertainty in the known value for both k_6 and k_1. Yet it seems impossible that their ratio could be this much in error. Another (or several) reaction must be important at 415°K near the upper explosion limit.

The obvious reaction to consider is the reverse of reaction 6

$$O_3 + M \longrightarrow O_2 + O + M \qquad (-6)$$

The effect of reaction −6 is to reduce the apparent value of k_6. If reaction −6 is responsible for the discrepancy, then reaction −6 must be 7.8 times as fast as reaction 7 at the upper explosion limit. The rate constant expression for k_{-6} is about[27] $4.6 \times 10^{12} \exp(-24{,}000/RT)\ M^{-1}\ \text{sec}^{-1}$. At 415°K this corresponds to a value of $1.0\ M^{-1}\ \text{sec}^{-1}$. At the same temperature $k_7 = 1.15 \times 10^8\ M^{-1}\ \text{sec}^{-1}$. If reaction −6 is responsible for the apparent lowering of k_6, then $[SO]/[M] \simeq 10^{-9}$, a ratio which is not impossible.

Acknowledgment. The authors are deeply indebted to R. L. Divany for his assistance with the computer computations. This research was supported by the National Air Pollution Control Administration through Grant No. AP00022 for which we are grateful.

(27) S. W. Benson, "The Foundations of Chemical Kinetics," McGraw-Hill, New York, N. Y., 1960, p 402.

The Explosion Limits of Chlorine–Fluorine Mixtures[1]

by Steve J. Wiersma and Edward A. Fletcher*

Department of Mechanical Engineering, University of Minnesota, Minneapolis, Minnesota 55455
(Received November 25, 1970)

Publication costs borne completely by The Journal of Physical Chemistry

The spontaneous explosion limits, the pressure and temperature conditions dividing the explosion region from the nonexplosion region for a gaseous mixture in a closed vessel, were found for mixtures of chlorine and fluorine in the 130–200° temperature range. The results showed that the Semenov thermal explosion theory is applicable to the chlorine–fluorine system. Deductions based on two kinds of experiments, isothermal measurements of the slow, low-temperature reaction rates and those of the present study, suggest that the rate is best expressed by

$$\frac{d[ClF]}{dt} = \frac{10^{11}[F_2][Cl_2]^{1/2}\exp(-21{,}200/RT)}{\left(0.2 + 0.4\frac{[Cl_2]}{[F_2]} + \frac{[ClF]}{[F_2]}\right)^{1/2}} \frac{\text{mol}}{\text{cm}^3\ \text{sec}}$$

in which the terms in the denominator which dominate depend on the kind of experiment to which the expression is to be applied. A mechanism is proposed.

Introduction

Mixtures of chlorine and fluorine burn to form chlorine fluoride.[2,3] The flame is unusually simple. Only five different molecular species, Cl_2, F_2, ClF, Cl, and F are anticipated in the flame. Of these, only three, Cl_2, F_2, and ClF are present in appreciable amounts. The low-temperature kinetics[4] of the reaction and spatial flame speeds[3] in tubes have been studied. Predictions of the kinetic behavior of the system from theoretical considerations[5,6] were not borne out in the isothermal study or by the flame speeds.

In this study, we have measured the spontaneous ignition limits. The Semenov thermal explosion theory is used to analyze the results. The kinetics and mechanism of the reaction are deduced from the combined data of two studies, one previously reported[4] in which the low-temperature reaction rate was measured and the present one.

Experimental Section

Chlorine and fluorine were obtained from Air Products and Chemicals, Inc. The manufacturer claimed a purity of 99.5% for chlorine and 98% for fluorine. Hydrogen fluoride was removed from the fluorine by means of a standard Matheson Co. sodium fluoride trap. The fluorine purity was checked by allowing it to react with mercury which does not react with the most probable impurity, oxygen. The gas was found to contain at least 97% fluorine.

We found the explosion limits by mixing the reactants, expanding a portion of the mixture into a thermostated reaction vessel, and observing which mixtures exploded. The mixing vessel, the reaction vessel, a Heise Bourdon Tube Co. Model H43545C pressure gauge, reactant bottles, a nitrogen purge bottle, a vacuum pump, and a vent line were all connected to a common manifold.

The stainless steel mixing vessel of approximately 43 l. was maintained at room temperature. The heavier gas, Cl_2, was first introduced; then F_2 was introduced. The gases were mixed by jet mixing which accompanied the introduction of the second gas. Mixing was considered adequate because the results were reproducible.

Two reaction vessels were used. The larger was 6.34 l. in volume, the smaller, 0.394 l. The larger reaction vessel was constructed from a 35-cm length of 15-cm i.d. Monel 400 pipe with a 6-mm thick Monel 400 cap welded to each end. A single 0.25-in. Gyrolock tube fitting was welded into one of the end caps. From this fitting a 10-cm length of Monel 400 tubing connected the reaction vessel to a Hoke 413HT Monel 400 packless valve which was silver soldered to the tubing. The smaller vessel was similarly constructed. The reaction vessel, valve, and connecting tubing were submerged in a thermostated oil bath whose temperature was maintained to within 1°.

The gaseous mixture was expanded into the evacuated reaction vessel to a predetermined pressure. Filling the reaction vessel took 10–15 sec. The temperature of the gaseous mixture then rose due to the exothermic reaction. If the pressure of the mixture was

(1) The paper is taken in part from Dr. Wiersma's Ph.D. Thesis, 1970. The financial support given to Dr. Wiersma by a NDEA Fellowship was gratefully appreciated.

(2) O. Ruff and E. Ascher, *Z. Anorg. Allg. Chem.*, 176, 258 (1928).

(3) E. A. Fletcher and L. L. Ambs, *Combust. Flame*, 12(2), 115 (1968).

(4) E. A. Fletcher and B. E. Dahneke, *J. Amer. Chem. Soc.*, 91, 1603 (1969).

(5) S. W. Benson and G. R. Haugen, *ibid.*, 87, 4036 (1965).

(6) R. M. Noyes, *ibid.*, 88, 4311 (1966).

high enough for an explosion to occur, a pressure spike was observed on the pressure gauge, and the temperature, measured by a thermocouple in the reaction vessel, rose rapidly. If the pressure of the mixture was not high enough for an explosion to occur, the temperature eventually equilibrated with that of the vessel wall. The experiment was done at several pressures with each mixture at a series of preset bath temperatures. The pressures at which explosions occurred, or did not occur, defined the limits. The explosion limit was found over a wide range of compositions in the temperature range 130–200°.

Results

Figures 1–6 show the spontaneous explosion limits at various pressures, temperatures, compositions, surface area to volume ratios, and inert gas dilutions. Figure 1 shows the variation of explosion limit pressure with the vessel wall temperature for eight different fluorine–chlorine mixtures in the large reaction vessel, which had a surface area to volume ratio of 0.321 cm^{-1}. Figure 2 is a convenient cross plot of the information contained in Figure 1. Figures 3–5 are plots of data from tests in which nitrogen, argon, and helium were added to stoichiometric chlorine–fluorine mixtures as diluents. The data in Figure 6 are from tests in which the surface area to volume ratio has been increased to 0.762 cm^{-1}. Comparison of this figure with Figure 1 shows that increasing the surface to volume ratio raises the pressure limits as it should.

It is noteworthy that the spontaneous explosion limit curves are approximately parallel. Thus, all pressure–concentration curves in which temperature is the parameter are shaped like those shown in Figure 2. It is interesting that although the reaction looks symmetrical from a stoichiometric standpoint, the ease of spontaneous explosion is far from being symmetrical; fluorine makes the mixture much more ignitable than chlorine. The curves have the same general characteristics whether the mixtures contain diluents or not.

Thermal Explosion Theory

The thermal explosion theory of Semenov[7,8] predicts the combination of pressure and temperature necessary to ignite a gaseous mixture enclosed in a given volume. Temperature gradients exist within a reacting system because in practice heat generated by the chemical reaction is transferred and lost to the surrounding medium at a finite rate. The temperature differences cause differences in reaction rate at various points in space. The system is nonuniform. The general solution of the set of nonlinear equations describing such a system involves many mathematical difficulties.

Semenov's thermal theory disregards the temperature and concentration gradients. It examines the course of a homogeneous reaction with time. The reactants are enclosed in a vessel, the wall temperature

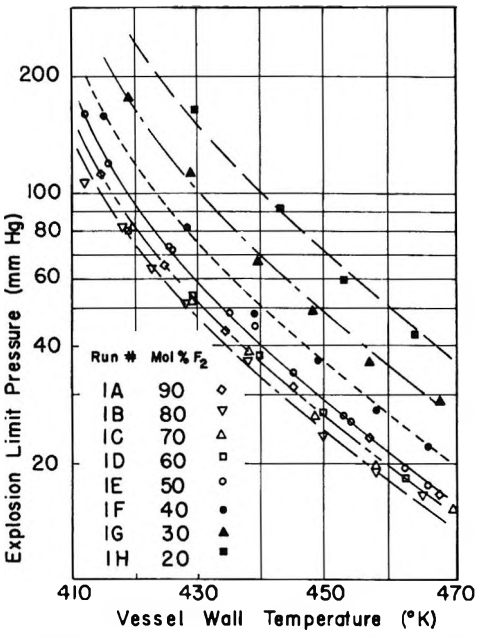

Figure 1. Variation of explosion limit pressure with vessel wall temperature for various chlorine–fluorine mixtures. The data points are the maximum pressures at which the mixture did not explode.

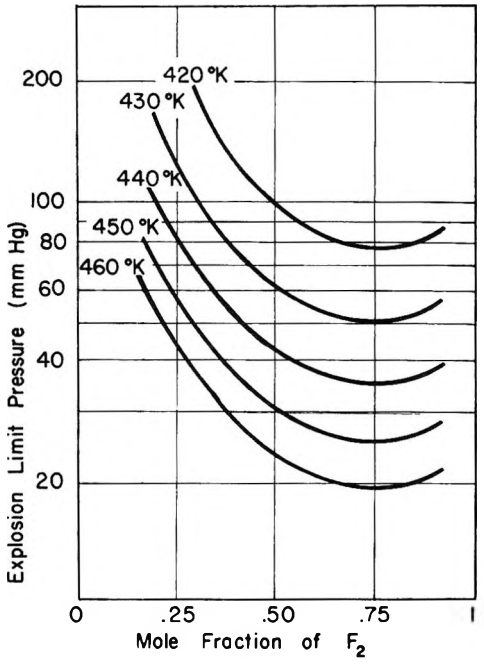

Figure 2. Variation of explosion limit pressure with composition at various temperatures. The plots show that fluorine is more effective than chlorine at all temperatures in increasing ignitability.

of which is constant. The reactant temperature is the same everywhere, but it is higher than the wall temperature if the reaction is exothermic.

(7) L. N. Khitrin, "Physics of Combustion and Explosion," translated for National Science Foundation, Washington, D. C., by the Israel Program for Scientific Translations, Jerusalem, 1962.

(8) L. A. Vulis, "Thermal Regimes of Combustion," translated by M. D. Friedman, McGraw-Hill, New York, N. Y., 1961.

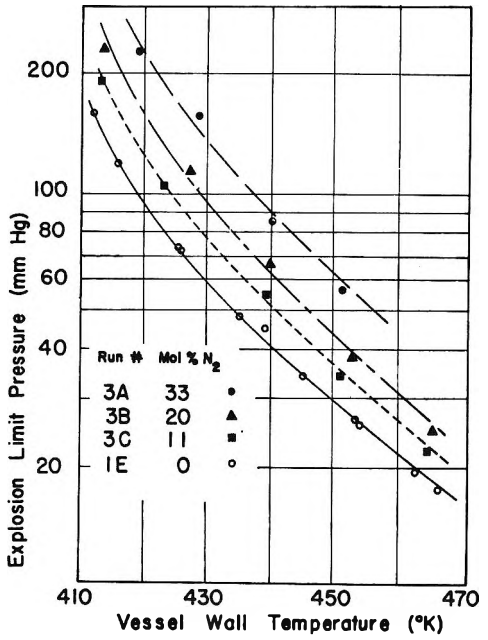

Figure 3. Explosion limits of stoichiometric Cl_2–F_2 mixtures diluted with nitrogen. The data points are the maximum pressures for which the mixtures did not explode.

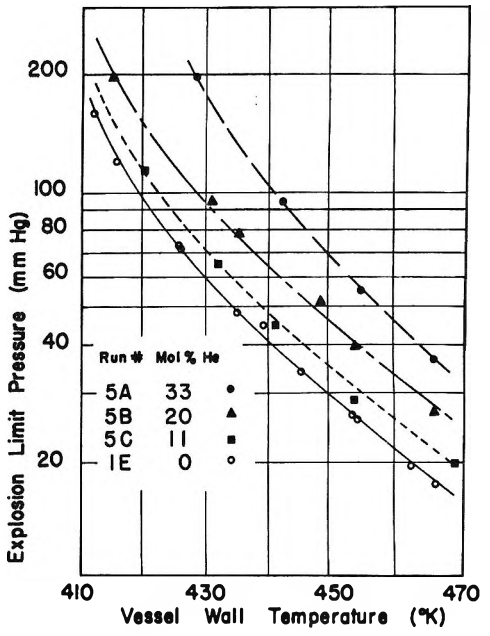

Figure 5. Explosion limits of stoichiometric Cl_2–F_2 mixtures diluted with helium. The data points are the maximum pressures for which the mixtures did not explode.

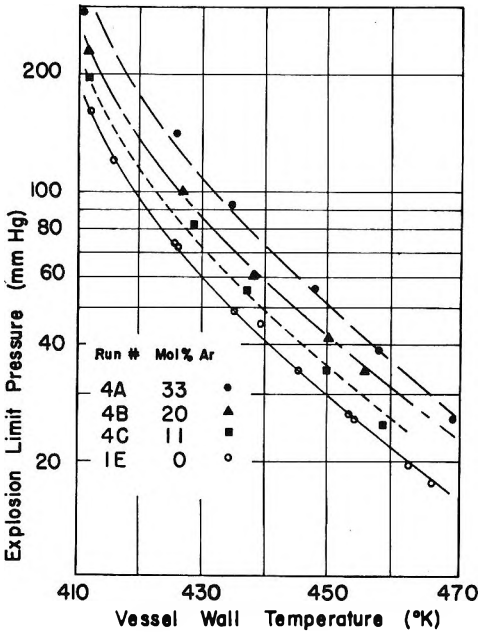

Figure 4. Explosion limits of stoichiometric Cl_2–F_2 mixtures diluted with argon. The data points are the maximum pressures for which the mixtures did not explode.

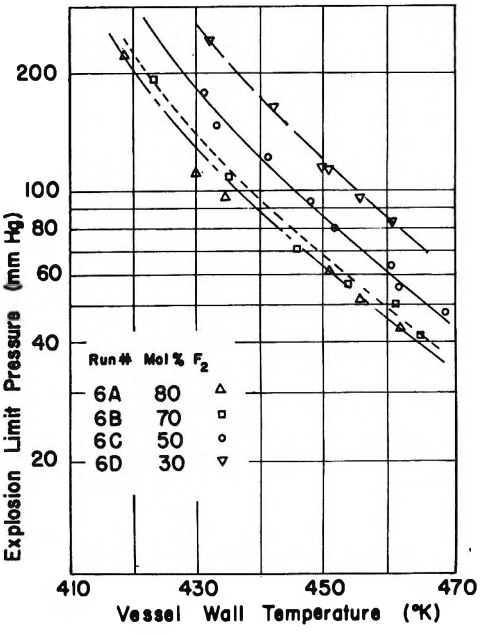

Figure 6. Explosion limits of Cl_2–F_2 mixtures in the smaller reaction vessel. The data points are the maximum pressures for which the mixtures did not explode.

In such a reacting mixture of gases of which ΔU is the constant volume heat of reaction and W is the reaction rate per unit volume, the rate at which heat is generated in a volume V is $r = WV\Delta U$. Heat is simultaneously lost through the walls of the vessel. The rate of heat loss is $q = hS(T - T_w)$ where h is the coefficient of heat transfer, S is the surface area of the vessel, and $(T - T_w)$ is the temperature difference between the reacting gas and the vessel walls.

The graphical representation of heat generated and heat lost, Figure 7, helps one visualize the conditions necessary for explosion. The curves r_1, r_2, and r_3 represent the rate of heat generation at three reaction rates corresponding to three different reactant concentrations as a function of the gas temperature. The straight line q represents the rate of heat loss as a function of the gas temperature when the wall temperature is T_w.

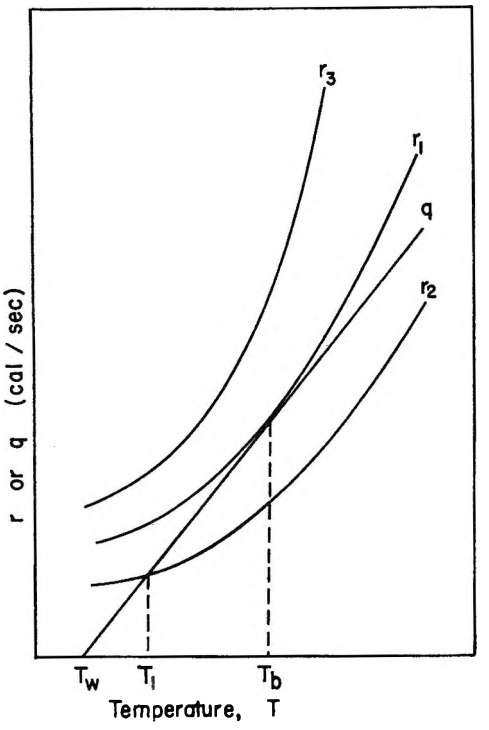

Figure 7. A plot of heat generated and heat lost *vs.* temperature. A mixture following the r_2 curve will have a steady-state temperature T_1. A mixture following the r_3 curve will explode as more heat is always being generated than is being lost. The r_1 curve which is tangent to the line q separates the mixtures that will explode from the mixtures that will not explode.

When the reaction proceeds according to curve r_2, the gaseous mixture achieves (approaches) a temperature T_1, since, until this temperature is achieved, the rate of heat generation exceeds the rate of heat loss. If, for any reason, the gas temperature should momentarily exceed T_1, the rate of heat loss will exceed the rate of heat generation and the temperature will drop. When the reaction proceeds according to curve r_3 (if the reactant concentration is increased, for example), the rate of heat generated always exceeds the rate of heat loss and the mixture explodes.

The curve r_1 is for a reactant concentration which characterizes the transition from the case of limited temperature increase to unlimited increase. The limit condition is that for which the heat loss curve is tangent to the heat generation curve. At the explosion temperature T_b, where r_1 and q are tangent, the rates of heat generated and heat lost are equal and their rates of change with temperature are equal; *i.e.*, $r_1 = q$ and $dr_1/dT = dq/dT$.

Reaction Mechanism

We considered as possible, seven bimolecular and three recombination reactions

$$F_2 + M \xrightarrow{k_1} 2F + M \quad \text{(I)}$$

$$F + Cl_2 \xrightarrow{k_2} ClF + Cl \quad \text{(II)}$$

$$Cl + F_2 \xrightarrow{k_3} ClF + F \quad \text{(III)}$$

$$Cl + F + M \xrightarrow{k_4} ClF + M \quad \text{(IV)}$$

$$F + F + M \xrightarrow{k_5} F_2 + M \quad \text{(V)}$$

$$Cl + Cl + M \xrightarrow{k_6} Cl_2 + M \quad \text{(VI)}$$

$$Cl + ClF \xrightarrow{k_7} Cl_2 + F \quad \text{(VII)}$$

$$F + ClF \xrightarrow{k_8} F_2 + Cl \quad \text{(VIII)}$$

$$Cl_2 + M \xrightarrow{k_9} 2Cl + M \quad \text{(IX)}$$

$$ClF + M \xrightarrow{k_{10}} Cl + F + M \quad \text{(X)}$$

The rate of formation of chlorine–fluoride according to this scheme is

$$W = \frac{d[ClF]}{dt} = k_2[F][Cl_2] + k_3[Cl][F_2] + k_4[Cl][F][M] - k_7[Cl][ClF] - k_8[F][ClF] - k_{10}[ClF][M] \quad (1)$$

where concentrations are in mol/cm^3 and time is in sec.

The steady-state approximation applied to [F] and [Cl] gives

$$\frac{d[F]}{dt} = 0 = 2k_1[F_2][M] - k_2[F][Cl_2] + k_3[Cl][F_2] - k_4[Cl][F][M] - 2k_5[F]^2[M] + k_7[Cl][ClF] - k_8[F][ClF] + k_{10}[ClF][M] \quad (2)$$

and

$$\frac{d[Cl]}{dt} = 0 = k_2[F][Cl_2] - k_3[Cl][F_2] - k_4[Cl][F][M] - 2k_6[Cl]^2[M] - k_7[Cl][ClF] + k_8[F][ClF] + 2k_9[Cl_2][M] + k_{10}[ClF][M] \quad (3)$$

Equations 2 and 3 are solved simultaneously for [F] and [Cl] which are then substituted into eq 1. Elimination of unimportant terms by order of magnitude estimates (Table I) gives

$$W = \frac{d[ClF]}{dt} = \frac{2\left(\frac{k_1k_2k_3}{k_4}\right)^{1/2}[F_2][Cl_2]^{1/2}}{\left\{1 + \frac{k_2k_6[Cl_2]}{k_3k_4[F_2]} + \frac{k_7[ClF]}{k_3[F_2]} + \frac{k_3k_5[F_2]}{k_2k_4[Cl_2]} + \frac{2k_5k_7[ClF]}{k_2k_4[Cl_2]} + \frac{k_5k_7^2[ClF]^2}{k_2k_3k_4[Cl_2][F_2]}\right\}^{1/2}} \quad (4)$$

Table I: Estimates of Reaction Rate Constants and Gas Concentrations

Quantity	Estimate	E_{act}, cal/mol	Source of estimate
k_1	10^{-4} cm³/mol sec	27,300	[a,b]
k_2	10^{14} cm³/mol sec	500	[a,c]
k_3	10^{14} cm³/mol sec	300	[a,c]
k_4	10^{15} (cm³/mol)² l./sec	0	Comparison with k_5 and k_6
k_5	10^{15} (cm³/mol)² l./sec	0	[a,d]
k_6	10^{15} (cm³/mol)² l./sec	0	[a,e]
k_7	10^{14} cm³/mol sec	400	Comparison with k_2 and k_3
k_8	$<10^{13}$ cm³/mol sec	400	Comparison with k_7
k_9	10^{-14} cm³/mol sec	48,300	[a,f]
k_{10}	10^{-14} cm³/mol sec	48,000	Comparison with k_9
[M]	10^{-5} mol/cm³		Perfect gas law
[F_2]	10^{-5} mol/cm³		Perfect gas law
[Cl_2]	10^{-5} mol/cm³		Perfect gas law
[ClF]	10^{-7} to 10^{-5} mol/cm³		Perfect gas law

[a] *Pyrodynamics*, **4**, 371 (1966). [b] D. J. Seery and D. Britton, *J. Phys. Chem.*, **70**, 4074 (1966). [c] S. W. Mayer and L. Schieler, L. Aerospace Corp. Report TDR-669 (9210-02)-1 (Jan 1966) (SSD-TR-66-26). [d] W. G. Burwell, V. J. Sarli, and T. R. Zupnik, *Chem. Eng. Progr. Symp. Ser.*, **61**, 125 (1966). [e] L. W. Bader and E. A. Ogryzlo, *Nature*, **201**, 491 (1964). [f] T. R. Jacobs and R. R. Giedt, *J. Chem. Phys.*, **39**, 749 (1963).

Only the first seven reactions have been retained in eq 4; the last three have been eliminated as a result of order of magnitude estimates. As will be seen below, the terms in the denominator which must be retained depend on the observation which is to be described.

Explosion Kinetics

It is shown later that at the explosion point the extent of reaction is less than 0.01. Therefore [ClF] is several orders of magnitude less than [F_2] or [Cl_2] and, in the description of spontaneous explosions, the third, fifth, and sixth terms in the denominator of eq 4 are unimportant.

The activation energies of reactions II–VII are very small; only reaction I has an appreciable dependence on temperature over the experimental temperature range. If we let $k_1 = k_{01}\exp(-E_1/RT)$, the rate of formation of chlorine fluoride before ignition is

$$W = \frac{d[ClF]}{dt} = \frac{2\left(\frac{k_{01}k_2k_3}{k_4}\right)^{1/2}[F_2][Cl_2]^{1/2}\exp(-E_1/2RT)}{\left\{1 + \frac{k_2k_6}{k_3k_4}\frac{[Cl_2]}{[F_2]} + \frac{k_3k_5[F_2]}{k_2k_4[Cl_2]}\right\}^{1/2}} \quad (5)$$

Substitution for r_1 and q in the two conditions for transition to explosion, *i.e.*, that the heat generation and heat loss rates be equal and that their derivatives with respect to temperature be equal, and letting $k'_0 = 2(k_{01}k_2k_3/k_4)^{1/2}$, $E = E_1/2$, $c_1 = k_2k_6/k_3k_4$, and $c_2 = k_3k_5/k_2k_4$ yields

$$\Delta UV\frac{k'_0[F_2][Cl_2]^{1/2}\exp(-E/RT_b)}{\left(1 + c_1\frac{[Cl_2]}{[F_2]} + c_2\frac{[F_2]}{[Cl_2]}\right)^{1/2}} = hS(T_b - T_w) \quad (6)$$

and

$$\Delta UV\frac{k'_0[F_2][Cl_2]^{1/2}\exp(-E/RT_b)}{\left(1 + c_1\frac{[Cl_2]}{[F_2]} + c_2\frac{[F_2]}{[Cl_2]}\right)^{1/2}}\frac{E}{RT_b^2} = hS \quad (7)$$

Equations 6 and 7 can be solved to eliminate T_b. Let a be the mole fraction of F_2 in the mixture, b the mole fraction of Cl_2, and p the total pressure of the mixture. Then $[F_2] = ap/RT_w$ and $[Cl_2] = bp/RT_w$. The heat transfer coefficient for laminar flow over a wall in terms of the thermal conductivity of the mixture, λ, the viscosity, μ, and the density at 1 atm pressure, ρ_1, is $h = c\lambda\sqrt{\rho_1/\mu}$, where c is a constant. The flow characteristics of the gas in the reaction vessel are not known, but it is not likely to be turbulent and, in any case, the laminar flow approximation explains some of the experimental results. The vessel wall temperature and explosion limits pressure are then related by the equation

$$\frac{E}{RT_w} = \ln\left(\frac{p}{T_w^{7/2}}\frac{V\mu^{1/2}}{S\lambda\rho_1^{1/2}}\frac{ab^{1/2}}{(1 + c_1b/a + c_2a/b)^{1/2}}\right) + \ln\left(\frac{k'_0\Delta UE}{cR^{5/2}}\right) \quad (8)$$

For a given mixture and reaction vessel, a plot of $1/T_w$ *vs.* ln $(p/T_w^{7/2})$ should yield a straight line with a slope of R/E. Figure 8 plots $1/T_w$ *vs.* ln $(p/T_w^{7/2})$ for test 1E, the 50% F_2 and 50% Cl_2 mixture in the large reaction vessel. Plots of tests in which the mixture composition or the vessel size was changed yield parallel straight lines. The average activation energy, E, obtained by the method of least squares, is 18,500 cal/mol °K. Since the ratio k'_0/c appears in eq 8, only this ratio can be obtained from the ignition limits. Neither the values of k'_0 nor c can be determined independently.

To find constants c_1 and c_2 in eq 8 and to verify that assumptions made in the explosion theory are valid, plots of temperature *vs.* pressure for the various mixture compositions and vessel sizes were compared to the plot for the 50% F_2 and 50% Cl_2 mixture in the large reaction vessel. From eq 8 it can be seen that

$$\frac{p}{p'} = \frac{S}{S'}\frac{V'}{V}\frac{\lambda}{\lambda'}\left(\frac{\mu'}{\mu}\frac{\rho_1}{\rho_1'}\right)^{1/2}\frac{0.5^{3/2}}{ab^{1/2}} \times \frac{(1 + c_1b/a + c_2a/b)^{1/2}}{(1 + c_1 + c_2)^{1/2}} \quad (9)$$

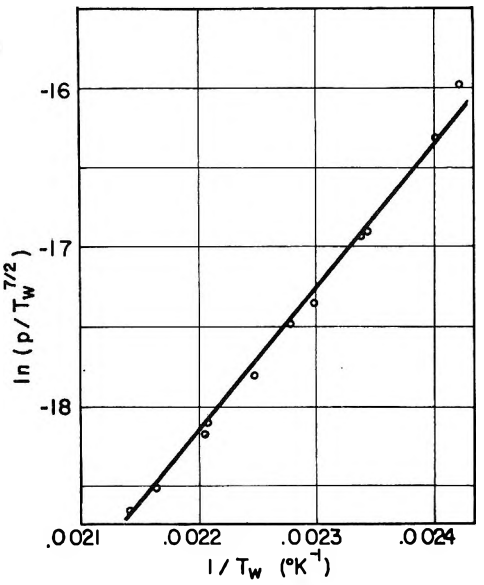

Figure 8. A plot of $1/T_w$ *vs.* ln $(p/T_w^{7/2})$ for the 50% F_2 and 50% Cl_2 mixture in the large reaction vessel. The Semenov thermal explosion theory predicts that the plot will be a straight line.

where the primed quantities are the values for the 50% F_2 and 50% Cl_2 mixture in the large reaction vessel.

Equation 9 shows that the pressure ratio p/p' does not depend on the temperature T_w. The best least-squares fit of the explosion limits data occurs when $c_1 = 2$ and $c_2 = 0$. Therefore, the explosion limit pressures are much more responsive to changes in F_2 concentration than Cl_2 concentration, and the rate expression which best describes the spontaneous explosion limits is

$$\frac{d[ClF]}{dt} = \frac{2.24 \times 10^{11}[F_2][Cl_2]^{1/2} \exp(-18{,}500/RT)}{\left(1 + 2\frac{[Cl_2]}{[F_2]}\right)^{1/2}} \frac{\text{mol}}{\text{cm}^3 \text{ sec}}$$

or

$$\frac{d[ClF]}{dt} = \frac{10^{11}[F_2][Cl_2]^{1/2} \exp(-18{,}500/RT)}{\left(0.2 + 0.4\frac{[Cl_2]}{[F_2]}\right)^{1/2}} \frac{\text{mol}}{\text{cm}^3 \text{ sec}} \quad (10)$$

Low-Temperature Isothermal Kinetics

We have reanalyzed the low-temperature data of a previous study[4,9] to explore further the possibility that other terms in the denominator of eq 4 should be included. They had been previously rejected as a result of order-of-magnitude estimates, but the behavior of the explosion limits suggested that the data should be reexamined.

As the isothermal reaction proceeds, the ClF concentration grows until it is of the same order of magnitude as the F_2 and Cl_2 concentrations, suggesting that the third, fifth, and sixth terms in the denominator of eq 4 for the reaction rate should not be disregarded in this case. The test expression, $d[ClF]/dt = k''[F_2][Cl_2]^{1/2}/(0.2 + 0.4[Cl_2]/[F_2] + [ClF]/[F_2])^{1/2}$ fits the experimental data quite well. The third term in the denominator of eq 4 is apparently the most important term when [ClF] is of the same order of magnitude as $[F_2]$ or $[Cl_2]$. This rate expression was solved by separation of variables and was integrated, giving on the right-hand side, $k''t$, and on the left-hand side a known function of the initial concentrations of Cl_2 and F_2 and the instantaneous concentration of ClF. A plot of $k''t$, as determined by substituting the measured value of the concentration of ClF into the appropriate expression, *vs.* time yields a straight line with a slope of k''. Similar plots for other tests at the same temperature but with varying initial concentrations superimpose well. The straight-line correlation with the new expression is slightly better than the older one; the correlation coefficients being about 0.99 and 0.97, respectively. The variation of the rate constants with temperature is well accounted for by the more general equation

$$\frac{d[ClF]}{dt} = \frac{6 \times 10^{11}[F_2][Cl_2]^{1/2} \exp(-22{,}500/RT)}{\left(0.2 + 0.4\frac{[Cl_2]}{[F_2]} + \frac{[ClF]}{[F_2]}\right)^{1/2}} \frac{\text{mol}}{\text{cm}^3 \text{ sec}} \quad (11)$$

which is to be compared with the rate expression obtained from the Semenov analysis of the spontaneous ignition limits, eq 10. The differences in the infinite temperature reaction rate constants (preexponential terms) and in the activation energies in these two equations should be reconciled. To suggest how the reconciliation should be made, we used the ignition delays and a computer simulation of the behavior of this system.

Ignition Delays

Examination of eq 6 and 7 shows that only the ratio k'_0/h can be determined from ignition limits. Our value for the rate constant depends on an independent estimate of the heat transfer coefficient. If we had chosen a higher heat transfer coefficient, the rate constant we deduced from the ignition limit would have been higher, but consistent with our experimentally determined pressure limits. The accuracy of the rate constant thus depends on the accuracy with which we can estimate the heat transfer coefficient, and we have no *a priori* reason for believing we can estimate the

(9) B. E. Dahneke, Ph.D. Thesis, University of Minnesota, 1967.

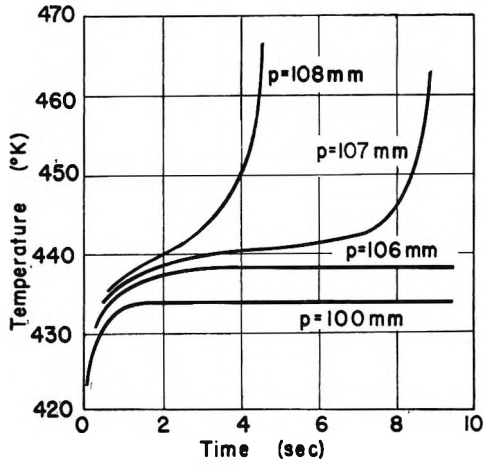

Figure 9. Mixture temperature *vs.* time for a vessel wall temperature of 420°K. A computer solution to the differential equation describing the temperature of a 50% F_2 and 50% Cl_2 mixture in the large reaction vessel is shown for several reactant pressures. The pressures for which the mixture explodes can be seen.

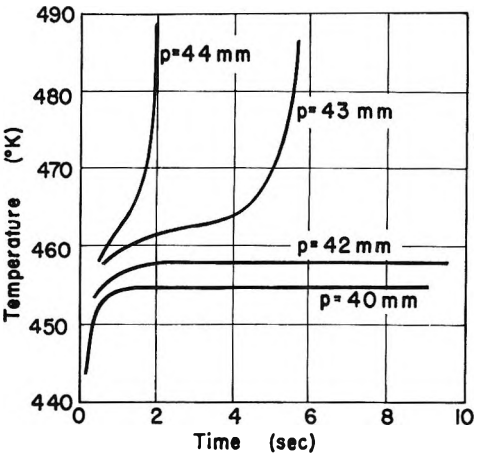

Figure 10. Mixture temperature *vs.* time for a vessel wall temperature of 440°K. A computer solution to the differential equation describing the temperature of a 50% F_2 and 50% Cl_2 mixture in the large reaction vessel is shown for several reactant pressures. The pressures for which the mixture explodes can be seen.

heat transfer coefficient with great accuracy. The ignition delay, however, provides us with an independent means of estimating the preexponential term in the rate expression. A simple computer experiment describes the temporal behavior of this system nicely.

The variation of the internal energy of the reacting mixture with time is given by

$$\frac{dU}{dt} = hS(T - T_w) = \sum_i u_i \, dn_i/dt + \sum_i n_i \, du_i/dt \quad (12)$$

where n is the number of moles and u is the molar internal energy, h is the heat transfer coefficient, S the vessel surface area, and $(T - T_w)$ the temperature difference between the reacting gas and the vessel wall.

If the constant volume heat capacities of all gases are assumed constant and equal and $n = \Sigma_i n_i$, then

$$-hS(T - T_w) = u_{Cl_2}\frac{dn_{Cl_2}}{dt} + u_{F_2}\frac{dn_{F_2}}{dt} + u_{ClF}\frac{dn_{ClF}}{dt} + nc_V\frac{dT}{dt} \quad (13)$$

For the reaction $Cl_2 + F_2 \rightarrow 2ClF$, $dn_{ClF}/dt = -{}^1/_2 dn_{Cl_2}/dt = -{}^1/_2 dn_{F_2}/dt = V d[ClF]/dt$. The reaction rate $d[ClF]/dt$ is known implicitly from eq 10. We now assume that if an explosion is going to occur, it will occur when the extent of reaction is very small, that is, when $[Cl_2] = [Cl_2]_0$ and $[F_2] = [F_2]_0$. Then eq 13 becomes

$$\frac{dT}{dt} = -\frac{hS(T - T_w)}{nc_V} - \frac{Vk'_0(2u_{ClF} - u_{Cl_2} - u_{F_2})[F_2]_0[Cl_2]_0^{1/2}\exp(-E/RT)}{2nc_V\left(0.2 + 0.4\frac{[Cl_2]_0}{[F_2]_0}\right)^{1/2}} \quad (14)$$

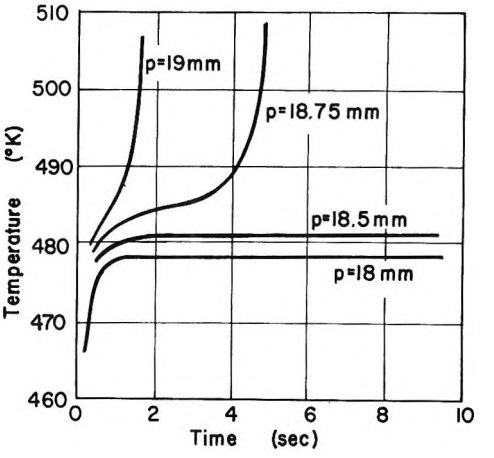

Figure 11. Mixture temperature *vs.* time for a vessel wall temperature of 460°K. A computer solution to the differential equation describing the temperature of a 50% F_2 and 50% Cl_2 mixture in the large reaction vessel is shown for several reactant pressures. The pressures for which the mixture explodes can be seen.

The differential equation was solved numerically for several pressures at each vessel wall temperature for a stoichiometric mixture in the large reaction vessel. The values of the constants are $V = 6340$ cm^3; $S = 2020$ cm^3; $c_V = 5.17$ cal/mol °K; $2u_{ClF} - u_{Cl_2} - u_{F_2} = -26{,}000$ cal/mol; $k_0 = 10^{11}$ (cm^3/mol)$^{1/2}$ sec^{-1}; $E = 18{,}500$ cal/mol; $h = 9.1 \times 10^{-5}p^{1/2}$ cal/°K cm^2 sec, where p is the mixture pressure in mm; $[Cl_2]_0 = 5.87 \times 10^{-8}\,bp$ mol/cm^3, where b is the mole fraction of Cl_2; and $[F_2]_0 = 5.87 \times 10^{-8}\,ap$ mol/cm^3, where a is the mole fraction of F_2. Figures 9–11 show how the gas temperature varies with time for several pressures at the vessel wall temperatures 420, 440, and 460°K.

The explosion time for the lowest pressure for which an explosion occurs, is between 5 and 10 sec, approxi-

mately the same length of time observed in the experiments. An increase in pressure of the gaseous mixture of only 1 to 2% above the highest pressure at which no explosion occurs produces an explosion in 5 to 10 sec. The pressure limit is thus quite sharp. The extent of reaction of mixtures reacting at a temperature 20° above the vessel wall temperature, the approximate temperature of the mixture during most of the induction period, is less than 0.01 in the induction period justifying the approximation of using the initial values $[Cl_2]_0$ and $[F_2]_0$.

The ignition delay depends strongly on the pressure once the pressure limit has been exceeded and the delay is of the proper magnitude when the preexponential term in the rate expression is 10^{11}, thus justifying our initial estimate of the magnitude of h.

Reconciliation of the Rate Constants

Spontaneous ignition limits and ignition delays suggest that the proper rate expression for this reaction should be

$$\frac{d[ClF]}{dt} = \frac{10^{11}[F_2][Cl_2]^{1/2}\exp(-18{,}500/RT)}{\left(0.2 + 0.4\frac{[Cl_2]}{[F_2]}\right)^{1/2}} \frac{\text{mol}}{\text{cm}^3\ \text{sec}} \quad (15)$$

Low-temperature isothermal studies suggest that the rate expression should be

$$\frac{d[ClF]}{dt} = \frac{6 \times 10^{11}[F_2][Cl_2]^{1/2}\exp(-22{,}500/RT)}{\left(0.2 + 0.4\frac{[Cl_2]}{[F_2]} + \frac{[ClF]}{[F_2]}\right)^{1/2}} \frac{\text{mol}}{\text{cm}^3\ \text{sec}} \quad (16)$$

It is necessary that we rationalize the difference in the preexponential terms and in the activation energies. If we take the preexponential term of the ignition limit result as the infinite temperature rate constant with the four isothermally determined rate constants in a conventional least-squares log k *vs.* $1/T$ treatment, the result is the expression

$$\frac{d[ClF]}{dt} = \frac{10^{11}[F_2][Cl_2]^{1/2}\exp(-21{,}200/RT)}{\left(0.2 + 0.4\frac{[Cl_2]}{[F_2]} + \frac{[ClF]}{[F_2]}\right)^{1/2}} \frac{\text{mol}}{\text{cm}^3\ \text{sec}} \quad (17)$$

which reconciles all the rates observed quite well as can be seen in Table II. The systematic variation of the rate constants as measured in the isothermal experiment is evident, but the agreement between them and the spontaneous ignition result is surprisingly good. The "activation energy" observed in the ignition energy experiment alone, 18,500 kcal, is more attractive than the reconciled value of eq 17 because it most nearly represents one-half the dissociation energy of F_2, which, according to the mechanism, it should.

Table II: Variation of the Rate Constant with Temperature

Temp, °K	$k_{calcd(17)}$, $(cm^3/mol)^{1/2}$ sec^{-1}	k_{obsd}, $(cm^3/mol)^{1/2}$ sec^{-1}
353.8	0.007477	0.008339
373.6	0.03769	0.04118
388.8	0.1379	0.1257
401.0	0.3248	0.2894
∞	10^{11}	10^{11} (from ign. limit)

Studies of Surface Reactions of NO by Isotope Labeling. II. Deuterium Kinetic Isotope Effect in the Ammonia–Nitric Oxide Reaction on a Supported Platinum Catalyst

by K. Otto,* M. Shelef, and J. T. Kummer

Scientific Research Staff, Ford Motor Company, Dearborn, Michigan 48121 *(Received September 16, 1970)*

Publication costs assisted by the Ford Motor Company

The existence of a kinetic isotope effect was established when substituting ND_3 for NH_3 in the reaction between ammonia and nitric oxide over a supported Pt catalyst at 202.5°. The ratio of the overall reaction rates at this temperature is $r_{NH_3}/r_{ND_3} \simeq 1.4$. The reaction of NH_3 (or ND_3) with NO is of zero order indicating that the rate-determining step occurs in the adsorbed layer. This step is interpreted as the surface dissociation of ammonia, $(NH_3)_{ads} \rightarrow (NH_2)_{ads} + (H)_{ads}$.

Introduction

In a previous communication,[1] the overall mechanism of the catalytic reaction between NO and NH_3 on a supported Pt catalyst was found to proceed with the formation and consumption of chemisorbed hydrogen atoms. The experimental results indicated that the formation of these chemisorbed hydrogen atoms is slow in relation to their consumption. The formation of $(H)_{ads}$ must include the rupture of at least one NH bond in the NH_3 molecule, most probably during the dissociative chemisorption of NH_3. If this event is associated with the rate-limiting step of the overall process, a kinetic isotopic effect (KIE) should be observed when substituting NH_3 by ND_3.

The recorded facts on a KIE in catalytic reactions involving ammonia are surprisingly meager considering the vast amount of research on the synthesis, decomposition, and oxidation of this molecule. Thus, a KIE was observed only in two instances[2,3] at high temperatures (900–1100°K) in the NH_3 decomposition over W filaments. In the synthesis of NH_3 the absence of a KIE was shown by Ozaki, Taylor, and Boudart[4] on promoted iron oxide catalysts indicating that in this case the NH bond formation is not involved in the rate-determining step. This conclusion has been extended by Aika and Ozaki to other catalysts.[5] The rate-determining step generally involves adsorption of the N atoms; conversely, the ammonia decomposition (in most cases but not in those given in ref 2 and 3) is rate limited by the desorption of N_2 molecules.

This conclusion that the breaking (or formation) of NH bonds in the low-temperature decomposition (or synthesis) of NH_3 is not rate limiting is strongly contested.[6] Furthermore, the data of Ozaki, Taylor, and Boudart[4] have been reinterpreted by Logan and Philp[7] as showing a considerable KIE.

The comparison of the reaction of ammonia oxidation, such as studied in ref 1, with the synthesis or decomposition reaction suggests intuitively that the possible involvement of NH bond rupture (or formation) in the rate-determining step will be less ambiguous in the oxidation reaction. The synthesis and decomposition take place on reduced metallic surfaces where the chemisorption of N atoms is pronounced. On the other hand, in the oxidation the surface is at least partially oxidized which makes the adsorption of nitrogen very unlikely.

The work described below justifies the search for the KIE in the reactions of ammonia oxidation. The observed KIE, in turn, narrows the choice of the rate-determining step.

Experimental Procedure

Catalyst. Most of the particulars concerning the catalyst, the reactants, and the vacuum equipment have been described before.[1] Therefore, experimental details will be kept concise, while stressing those conditions which deviate from the previous setup. The platinum catalyst, containing alumina as support material, was taken from the same batch which had been prepared for the previous studies. The total BET sur-

(1) K. Otto, M. Shelef, and J. T. Kummer, *J. Phys. Chem.*, **74**, 2690 (1970).

(2) J. C. Jungers and H. S. Taylor, *J. Amer. Chem. Soc.*, **57**, 679 (1935).

(3) R. M. Barrer, *Trans. Faraday Soc.*, **32**, 490 (1936).

(4) A. Ozaki, H. S. Taylor, and M. Boudart, *Proc. Roy. Soc., Ser. A*, **258**, 47 (1960).

(5) (a) K. Aika and A. Ozaki, *J. Catal.*, **13**, 232 (1969); (b) K. Aika and A. Ozaki, *ibid.*, **14**, 311 (1969); (c) K. Aika and A. Ozaki, *ibid.*, **16**, 97 (1970).

(6) R. E. Mardaleishvili, H. C. Hu, and Zh. Ya. Smordinskaya, *Kinet. Katal.*, **8**, 786 (1967).

(7) S. R. Logan and J. Philp, *J. Catal.*, **11**, 1 (1968).

face area of the supported catalyst was 194 m^2/g. It included 4.07×10^{18} platinum atoms per gram of catalyst, as determined from the adsorption of hydrogen and oxygen at room temperature, under the assumption that one oxygen atom is adsorbed per surface atom of platinum.[8]

Diffusional limitations of the reaction which had been suspected before[1] were eliminated by grinding the catalyst granules to a powder. This powder was screened, and only the fraction ranging in particle size from 74–105 μ was used, in order to keep the flow resistance of the catalyst low. Even so, the amount of catalyst had to be restricted to 0.13 g to maintain a flow rate of 300–400 cm^3/min, thus permitting a complete recirculation of the gas mixture in the closed reaction loop at least once every minute.

The catalyst was reduced before every run. The standard procedure consisted of a reduction by 300 Torr of hydrogen (or deuterium) at 400° for 30 min, followed by a 1-hr evacuation. Reduction and evacuation were repeated, and the catalyst was then cooled to the reaction temperature of 202.5 (±0.2)°, while pumping with a gettering pump. The conditions for all the runs were kept as identical as possible to permit a meaningful comparison between reaction rates for NH_3 and ND_3. The necessity for maintaining a constant temperature from run to run required a separate furnace controller for the reaction temperature, kept at a constant setting through the whole course of the study, and another one for the reduction and outgassing of the catalyst.

In a few instances the catalyst was reduced by ammonia. This had a definite influence on the reaction rate as discussed below.

Gas Reactants and Analysis of Gases. The reaction mixture consisted of 60 Torr of ammonia and 60 Torr of nitric oxide. Krypton at a pressure of 200 Torr, rather than argon, was used as a diluent here because of the coincidence of the doubly charged argon ions, and the ordinary ND_3^+ ions at the same peak, m/e 20.

Deuterated ammonia, purchased from Merck, Sharp and Dohme of Canada Ltd., was not subjected to further purification. An accurate mass spectrometric analysis for the amount of H atoms in the ND_3 was not possible, as a fast exchange occurred between the deuterium atoms and species containing hydrogen, such as water, which were present on the surfaces of the mass spectrometer. Thus a fresh sample of ND_3 injected directly from the original container into the mass spectrometer resulted in a hydrogen impurity of 15–20 atom % H. This result was obtained from a comparison of mass peaks m/e 19 (ND_2H) and m/e 20 (ND_3). After the mass spectrometer had been purged several times with deuterated ammonia, the isotope impurity decreased to 5 atom % H or less. The last analysis is in agreement with the degree of purity claimed by the manufacturer. However, the percentage of H increased considerably when the sample was left in the mass spectrometer for a longer time. The gas samples were scanned from m/e 11–90, in order to monitor impurities, but only the peaks at m/e 28, 30, 44, and 84, pertaining to N_2, NO, N_2O, and Kr, were actually used for the determination of the gas-mixture composition. The contributions of N_2O fragments at m/e 28 and 30 were, of course, taken into account, and the amounts of N_2 and N_2O present in the zero mixture were subtracted from the reaction products. The absolute amounts in the gas mixture were calculated by referring to the composition of the gas phase before the reaction (zero mixture). The analysis of this mixture was accurately known from the admitted pressures of ammonia, nitric oxide, and krypton. In order to minimize errors introduced by changes in the sensitivity of the mass spectrometer for the different compounds and by fluctuations in the fragmentation patterns, calibration measurements for Kr, NO, N_2O, N_2, and NH_3 (or ND_3) were executed before each series of analyses. Changes in the absolute number of moles in the gas phase (*e.g.*, by losses of water and ammonia by adsorption on the support material or on the walls of the mass spectrometer) were taken into account by using the constant amount of krypton as a reference. The analyses were checked by performing a material balance for nitrogen. For this purpose the amount of disappearing NO was compared with the amounts of N_2 and N_2O formed. The latter two were multiplied by 1.2 and 1.6, respectively, according to the stoichiometry of the two overall paths for NO reduction

$$4NH_3 + 6NO = 5N_2 + 6H_2O$$

and

$$2NH_3 + 8NO = 5N_2O + 3H_2O$$

The balance between the decrease of NO and the increase of nitrogen-containing products agreed, well within 10%.

Experimental Results and Discussion

The decrease of the reactant NO and the increase of the products N_2O and N_2 are given on Figure 1 as a function of time for a typical pair of reactions. The reaction with NH_3 is marked by open symbols, that with ND_3 by filled symbols. The two most prominent features of this graph are the linear course of the reaction isotherms, at least for $t \geq 50$ min, and the obviously

(8) The assumption of D. E. Mears and R. C. Hansford, *J. Catal.*, **9**, 125 (1967), has been recently questioned by Wilson and Hall.[9] They point out that while the ratio for (O atoms on bare Pt surface:H atoms on bare Pt surface:H atoms on oxidized Pt surface) of (1:2:4) holds (under certain circumstances), the surface stoichiometry of the oxidized surface can be Pt_2O instead of PtO. Then the number of surface Pt atoms is doubled. The controversies associated with counting Pt surface atoms by H chemisorption require a precise statement of the stoichiometry assumed in arriving at the stated figure.

(9) G. R. Wilson and W. K. Hall, *ibid.*, **17**, 190 (1970).

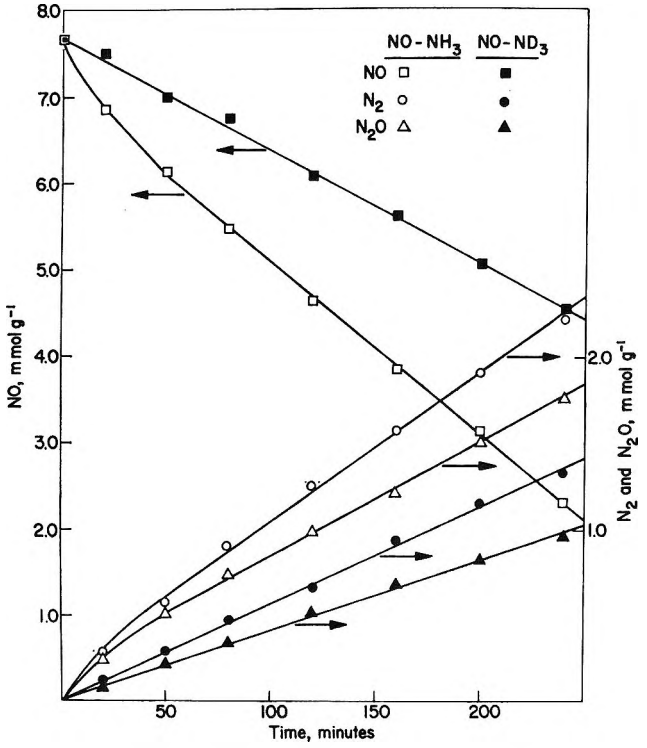

Figure 1. Decrease of NO and increase of N_2 and N_2O as a function of time for NO–NH_3 and NO–ND_3 reactions at 202.5°.

faster reaction for NH_3, as shown by the steeper slope of the curves defined by the open symbols.

One can compare the rates obtained with the finer catalyst grains used here with those measured with the coarser grains used in ref 1. The average reaction rate between 50 and 225 min as read from Figure 3 of that reference is ~12–13 (μg NO/g of catalyst)/min. On the ground catalyst it is, at $t \geq 50$ min, 19–22 (μg NO/g)/min as seen from Table I for the NO–NH_3 reaction. The comparison confirms a degree of diffusion control when using the coarser grains, as mentioned in ref 1. The interference of diffusion is also the most probable reason for the fact that a decrease of the NO pressure linear with $t^{1/2}$ has been observed before,[1] while a decrease linear with t is found here with the finer grains.

The deviations from straight lines below 50 min on Figure 1 in case of NH_3 are considered as being associated with the establishment of steady-state conditions, while the surface is changed from a reduced state to a surface covered by nitric oxide and ammonia. In part the deviation may be due to a transient temperature increase of the active area caused by the heat released during the initial massive adsorption. The course of the reaction during this preliminary period was not satisfactorily reproducible. In the case of ND_3 an initial deviation from a straight line did not show up sometimes, as shown in Figure 1, but was observed in other cases (*cf.* Figure 2). Therefore, the best measure of the steady-state rate is the slope of the linear portion of the plots such as shown on Figures 1 or 2. The linear time dependence as shown on Figures 1 and 2 describes a zero-order process both with respect to the reactants and the products. This in turn implies that the rate-determining step occurs in the adsorbed layer.

The summary of the results for various runs is given in Table I. The runs are arranged in the succession in which they have been measured. We are disregarding at this time runs 1 and 6 which have been obtained after reduction of the catalyst by ND_3. Comparing runs 3, 5, 7, and 10, for which ND_3 has been used as a reactant, does not reveal any differences for a surface pre-reduced by H_2 (runs 3 and 5) or by D_2 (runs 7 and 10).

The magnitude of the KIE is evaluated in Table II.

Table I: Summary of the Reaction Rates at 202.5° per Gram of Catalyst

Run no.	Surface pre-reduced by	Ammonia reactant	$\lvert\Delta n/\Delta t\rvert$, μmol/min NO	N_2	N_2O	N_2/N_2O
1	ND_3	ND_3	12.0	4.55	3.50	1.30
2	H_2	NH_3	20.1	7.82	6.65	1.18
3	H_2	ND_3	16.0	5.95	4.90	1.21
4	H_2	NH_3	21.9	8.40	7.12	1.18
5	H_2	ND_3	13.7	5.84	4.43	1.32
6	ND_3	ND_3	5.25	2.10	1.63	1.29
7	D_2	ND_3	13.7	5.72	4.32	1.32
8	H_2	NH_3	20.1	8.40	6.88	1.22
9	H_2	NH_3	18.7	6.65	5.84	1.14
10	D_2	ND_3	14.6	5.25	4.55	1.15

Table II: Isotope Effect in Adjacent Pairs of Experiments

Pairs of runs compared	n =	$(\Delta n/\Delta t)_{NH_3}/(\Delta n/\Delta t)_{ND_3}$ NO	N_2	N_2O
2–3		1.25	1.31	1.36
3–4		1.37	1.41	1.45
4–5		1.59	1.44	1.61
5–8		1.47	1.44	1.55
7–8		1.47	1.47	1.59
9–10		1.28	1.27	1.31
	Av	1.40	1.39	1.48

The runs from Table I which have been measured on a Pt surface, reduced by H_2 or D_2, are arranged in adjacent pairs of reactions with NH_3 and ND_3. The rate ratios for these pairs of reactions in reference to NO, N_2, and N_2O are listed in Table II. The average values for the consumption of NO and the appearance of N_2 show that the reaction with NH_3 is 1.40 times as fast as that with ND_3. The ratio derived for the formation of N_2O is somewhat larger.

Within the framework of the mechanism proposed in the previous publication[1] it is expected that the isotope

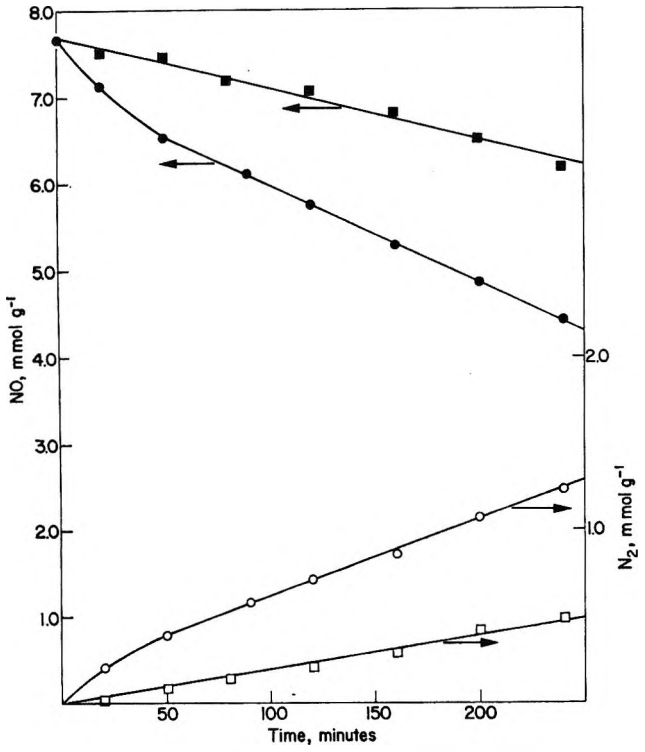

Figure 2. Retarding effect of prereduction of catalyst surface by ND_3. For runs 1 (round symbols) and 6 (square symbols). Open symbols designate the formation of N_2, filled symbols the consumption of NO.

effect as measured by the N_2O formation will be somewhat larger than that measured by the formation of N_2. This is because the nitrogen and nitrous oxide are produced (in the main) by different routes.[1] The nitrogen is produced by splitting of complex I [NH_2NO] and the nitrous oxide by the reduction of NO by chemisorbed hydrogen (deuterium) atoms. These, in turn, are created by (a) dissociative chemisorption of ammonia, and (b) splitting of complex I. The rate of formation of complex I is in turn dependent on the rate of dissociation of ammonia. Taking these relationships into account and assuming that each D atom is split-off by a factor of 1.4 more slowly than an H atom, while D_2O is always split-off at the same rate as is H_2O, the isotope effect for the formation of N_2O is calculated (with the data from ref 1) as 1.57. This figure is somewhat larger than that obtained from averaging the experimental results (1.48 *cf.* Table II). Owing to the assumptions involved and considering the experimental error, one cannot expect a better numerical agreement. However, the trend is in accord with our proposed mechanism.[1] Table II shows for all runs that the KIE as measured in the case of N_2O was somewhat larger than in the case of N_2. Correspondingly, the N_2/N_2O ratios are on the average higher for ND_3 than for NH_3 (Table I, last column).

In runs involving the NO–ND_3 reaction, the reduction was initially performed, in some instances by ND_3, in order to clean the surface from any residual surface hydrogen. The main sources of this hydrogen are the exchangeable OH groups still covering a large part of the support (γ-Al_2O_3) surface, after pumping at 400°.[10] As seen from the data of Table I and Figure 2 the use of ND_3 as the prereducing agent (runs 1 and 6) causes an additional retardation effect. The only difference between runs 1 and 6 was the duration of the pump-out at 400°, which was overnight for run 1 and 1 hr for run 6. The substitution of ND_3 by D_2 as the reducing agent gave rates in the subsequent NO–ND_3 reaction close to those obtained when H_2 was used as the reducing agent. There was no appreciable distortion of the KIE due to the OH groups on the support surface. This is understandable if one considers that the amount of D atoms in the ND_3 introduced in the gas phase is ~3000 μg-atom, while H left in the OH groups on the 0.13 g of the catalyst support is only ~200 μg-atom. On the other hand, the hampering of the reaction by prereducing with NH_3 or ND_3 was strong. We attribute the poisoning to the excessive coverage of the surface by the NH_2 (ND_2) groups formed during the prereduction.[11–13] These could either block the access of NO molecules to the surface or block the free site-pairs needed for the surface dissociation of ammonia at the reaction temperature. It can be argued that in the course of the reaction at 200°, the surface coverage should gradually revert to the same state observed when it is prereduced with H_2. This is, however, not observed experimentally and the above explanation is not necessarily the only one that could be put forward for the observed poisoning. The experimental fact of the poisoning of the surface by ammonia pretreatment remains, and it can seriously vitiate the investigation of the isotopic effect, if it is not avoided carefully.

The magnitude of the primary KIE has been worked out within the framework of the absolute rate theory and presented in several monographs and reviews.[14–17] The main contribution comes from the difference in the zero-point vibrational energy of the reactant molecules. In polyatomic molecules such as NH_3 or ND_3 the difference in this energy associated with the bond undergoing scission along the reaction coordinate is the main contributing factor. In the absolute rate theory the stretching vibration becomes, in the activated complex, a complete translational degree of freedom. If no other

(10) J. B. Peri, *J. Phys. Chem.*, 69, 211 (1965).

(11) J. W. May, R. J. Szostak, and L. H. Germer, *Surface Sci.*, 15, 37 (1969).

(12) P. J. Estrup and J. Anderson, *J. Chem. Phys.*, 43, 523 (1968).

(13) C. E. Melton and P. H. Emmett, *J. Phys. Chem.*, 68, 3318 (1964).

(14) K. Wiberg, *Chem. Rev.*, 55, 713 (1955).

(15) S. Z. Roginskii, "Theoretical Principles of Isotope Methods for Investigating Chemical Reactions," A. N. USSR Press, Moscow, 1956, pp 251–259.

(16) L. Melander, "Isotope Effects on Reaction Rates," Ronald Press, New York, N. Y., 1960.

(17) F. H. Westheimer, *Chem. Rev.*, 61, 265 (1961).

energy differences are involved in the respective structures of the activated complex the full KIE attributable to the zero-point energy difference between one N–H and one N–D bond vibration in NH_3 (ND_3) will be manifested, thus determining the upper limit of KIE. This picture assumes equality in the coverages of the surface when NH_3 is substituted by ND_3 and all other possible effects on the preexponential factor of the rate equation to be negligible.

If, on the other hand, the activated complex is energetically different when the light (H) or heavy (D) isotope atom forms a part of it, then deviations from the maximum isotope effect are the rule. The KIE being lower than the maximum value is the usually observed phenomenon in heterogeneous reactions.[15,17] The simplistic supposition of an incomplete conversion of the stretch along the reaction coordinate into a translation is at odds with the basic assumptions of the absolute rate theory and the energetic differences in the transition state are attributable to subtler causes.[16,17] The above-mentioned references present theoretical treatments of varying rigor; in general, however, the exact magnitude of the KIE cannot be predicted as the properties or even the shape of the transition state are unknown.

The maximum KIE expressed as the reaction rate ratio at 473°K for the N–H (N–D) bond is given by Wiberg[14] as 3.9, which corresponds to a zero-point energy difference (ΔE) of 1270 cal/mol. Another measure is given by Jungers and Taylor.[2] These authors, by assuming that the maximum possible KIE was realized in their high-temperature decomposition of NH_3, give ΔE_0 = 900 cal/mol which is equivalent to KIE (max, 473°K) = 2.6. Our measured values of Table II are substantially lower than either of these maximum values, and the obvious conclusion is that the transition states incorporating the different isotopic species of hydrogen are also energetically different.

Based on the mechanism proposed in ref 1, the rate-determining step in which the scission of the H (D) atom manifests itself in the observed KIE is most likely the surface dissociation of NH_3

$$(NH_3)_{ads} \longrightarrow (NH_2)_{ads} + (H)_{ads}$$

The shape of the transition state for this step is not known. If the assumption is made, which may be farfetched, that it can be approximated by a linear, three-center picture such as

$$(S)NH_2\overset{k_1}{\cdots\cdots}H\overset{k_2}{\cdots\cdots}(S)$$

[where (S) is the designation for a surface site and k_1, k_2 are force constants], the derivation of Westheimer[17] can be used to check whether the measured isotope effect gives a reasonable value for the zero-point vibration frequency of the "symmetric" vibration associated with the transition state. This, of course, involves another implicit assumption that the zero-point energy difference in the transition state is due only to the "symmetric" vibration and not to the bending vibrations.

Equation 17 of ref 15 reads as follows

$$4\pi^2\nu^{\pm}{}_{H,D}{}^2 = \frac{k_1}{m_A} + \frac{k_2}{m_B} + \frac{k_1 + k_2 - 2\sqrt{k_1k_2}}{m_{H,D}} \quad (1)$$

where $\nu^{\pm}{}_{H,D}$ frequency of the "symmetric" vibration in the TS, m_A and m_B masses of the terminal centers, $m_{H,D}$, mass of the proton (deuteron), and k_1,k_2, force constants. Taking the masses of the almost rigid surface sites as infinite with respect to m_H (m_D) the ratio of the zero-point frequencies must be in the limit equal to $\sqrt{m_D}/\sqrt{m_H}$ = 1.41. (The measured value of KIE is only fortuitously the same.)

From the observed value of the KIE (1.4) the $\Delta E_0^{\pm}$, the zero-point energy difference in the TS is determined

$$\frac{r_H}{r_D} = 1.4 = \exp[(1270 - \Delta E_0^{\pm})/(2 \times 475)] \quad (2)$$

where 475 is the temperature (in °K) during the measurements and 1270 cal/mol is the ΔE_0 in the reactants for one N–H (N–D) bond taken from Wiberg. From (2), $\Delta E_0^{\pm}$ = 950 cal/mol. Having

$$\Delta E_0^{\pm} = {}^1/_2\, h(\nu^{\pm}{}_{0(H)} - \nu^{\pm}{}_{0(D)})$$

the energy associated with the full difference between the zero-point vibrations is 1900 cal/mol or 665 cm^{-1}. Solving now for $\nu^{\pm}{}_{0(H)}$ and $\nu^{\pm}{}_{0(D)}$, of the "symmetric" vibration in the TS, from their ratio and difference we obtain, respectively, 2325 and 1660 cm^{-1}. These values appear reasonable when compared with the symmetric stretching frequencies of the gaseous NH_3 and ND_3 molecules, which are known to be 3336 and 2419 cm^{-1}, respectively.[18]

Acknowledgment. We thank A. G. Piken for the literature search.

(18) G. Herzberg, "Molecular Spectra and Molecular Structure. II. Infrared and Raman Spectra of Polyatomic Molecules," Tenth ed, Van Nostrand, New York, N. Y., 1962, p 294.

Pressure Jump and Isotope Replacement Studies of Acetylene Hydrogenation on Palladium Surface

by Yasunobu Inoue and Iwao Yasumori*

Department of Chemistry, Tokyo Institute of Technology, Ookayama, Meguro, Tokyo, Japan *(Received August 10, 1970)*

Publication costs borne completely by The Journal of Physical Chemistry

The catalytic activity of cold-worked palladium foil for acetylene hydrogenation was examined. From the change in the activity with annealing the presence of two kinds of active sites were predicted. One was characterized by a high activity of the foil annealed at 200° (Catalyst L) and another by the low activity of the foil annealed at 800° (Catalyst H). In order to investigate the kinetic behavior of the reaction on these catalysts, pressure jump and hydrogen–deuterium replacement techniques were applied in addition to the conventional kinetic study. When the hydrogen pressure was jumped up or down, during the hydrogenation on Catalyst H, a transition period of about 1 hr in the rate change appeared until the reaction attained a final steady state. Similar relaxation on the rate change due to isotopic effect was also found when hydrogen was replaced immediately by deuterium. On the other hand, no time lag for the reaction on Catalyst L was observed. Mechanisms for the reaction on these catalysts are developed and it was concluded that the reactive hydrogen in the acetylene hydrogenation was in an absorbed state on Catalyst H and in an adsorbed state on Catalyst L. This conclusion was also supported from the deuterium distributions in ethylene produced. The relaxation phenomenon of the rate can be interpreted on the basis of the role of Catalyst H as the reservoir of absorbed hydrogen.

Introduction

In the study of heterogeneous catalysis by metals it has frequently been attempted to ascertain the relationship between the fine structure of the surface and its catalytic activity. Apart from the influence of lattice spacing on the activity, several results have been offered to suggest that lattice imperfections such as point defects and dislocations play a significant role in catalysis. Eckell[1] observed that the catalytic activity of Ni wire for the hydrogenation of ethylene was increased by cold-rolling and fell off with annealing at a temperature range 200–300°. Uhara, *et al.*,[2] showed that the drastic decrease in catalytic activity of a twisted or rolled Ni wire occurred stepwise at two temperature ranges of annealing: 200–300° and 460–550° for the dehydrogenation of ethanol and 200–300° and 400–500° for the para–orthohydrogen conversion. They indicated that these ranges of temperature, respectively, correspond to that at which vacancies and dislocations can be annealed out.

It was found in the previous study[3] that the activity of cold-worked palladium foil decreased markedly in the hydrogenation of acetylene when the foil was annealed at a temperature range of 200–300° but thus reduced activity partly recovered by annealing above 600°. This recovery of activity with high-temperature annealing has not been reported hitherto. It is reasonable to suppose that the decrease in activity results from the disappearance of active sites and the recovery is due to the formation of a new kind of active sites. In the present study, therefore, the foil annealed at 200° (hereafter called Catalyst L) and that annealed at 800° (called Catalyst H) are taken as typical examples of the catalyst having a different nature, so the kinetic behavior of the reaction in the early stages was investigated. It seems to be difficult to obtain a definite mechanism from only a conventional kinetic study. Accordingly, we introduced new techniques of a pressure jump and an isotope replacement in addition to the traditional static measurement. The jump of reactant pressure caused a dynamic variation to the rate and the isotope replacement was performed by immediately displacing the hydrogen in gas phase by deuterium. Both techniques provided much information about the adsorption equilibria of hydrogen and acetylene and about the reactive states of hydrogen. Further, the deuterium distributions in products and reactants were investigated in order to determine the detailed mechanisms for the reaction on Catalysts L and H.

Experimental Section

A conventional closed system of about 400 cc incorporated with a circulating pump, and a catalyst vessel was used for the kinetic study. The pressure decrease during the course of the reaction was followed with a glass Bourdon gauge, and the products were analyzed by low-pressure type gas chromatography using a

(1) J. Eckell, *Z. Electrochem.*, **39**, 433 (1933).

(2) I. Uhara, T. Hikino, Y. Numata, H. Hamada, and Y. Kageyama, *J. Phys. Chem.*, **66**, 1374 (1962); I. Uhara, S. Kishimoto, T. Hikino, Y. Kageyama, H. Hamada, and Y. Numata, *ibid.*, **67**, 996 (1963).

(3) Y. Inoue and I. Yasumori, *ibid.*, **73**, 1618 (1969).

6-m column containing activated alumina with squalane. Cylinder hydrogen was used as carrier gas.

Palladium of 99.99% purity, obtained from Johnson Matthey and Co., Ltd., was subjected to successive rolling in one direction at room temperature and was used in the form of foil of 0.2-mm thickness and 20-mm width. After being washed with acetone and distilled water, the cold-worked foil of 1–2 g was put into the vessel and was reduced with 50 Torr of hydrogen at 150°. The annealing of this foil was performed by heating it in the vessel at various temperatures between 200 and 800° under vacuum below 10^{-6} Torr for 1 hr. Prior to each kinetic run, the annealed foil was reduced again with hydrogen at 150° for 1 hr. In some cases the cold-worked foil was etched slightly with concentrated nitric acid. The surface area of the foil was estimated by the BET method using xenon at 77°K. Values of 11.7, 10.0, and 9.2 cm^2/g within error of 10% were obtained for the foils annealed at 200, 300, and 800°, respectively.

The kinetics of acetylene hydrogenation was studied in the pressure ranges of hydrogen from 10 to 40 Torr and of acetylene from 5 to 20 Torr at temperatures of 27, 40, 50, and 60°. The pressure jump was performed in two ways: (a) hydrogen of high pressure in a reservoir was diffused quickly, without giving any change in the pressures of acetylene and ethylene, to the reaction system through a stopcock; (b) a small catalyst vessel was closed and the hydrocarbon mixture in the remaining part of the system was condensed in a trap with liquid nitrogen. A definite amount of hydrogen was transferred into the system (or removed by evacuation) and then the trapped mixture was evaporated. After mixing of the hydrocarbon with hydrogen for several minutes, the catalyst vessel was opened and the reaction was started again. In both cases the same result was obtained.

Hydrogen–deuterium replacement was carried out with the following procedure. When the reaction of the $C_2H_2 + H_2$ (or $C_2H_2 + D_2$) mixture proceeded at a steady rate, all gases in the reaction system were removed by evacuation and the $C_2H_2 + D_2$ (or $C_2H_2 + H_2$) mixture of the same molar ratio and total pressure was immediately introduced into the system. The change in the reaction rate after the replacement was followed as usual. The hydrocarbon mixture produced after the reaction of acetylene with deuterium was separated into the fractions of acetylene, ethylene, and ethane using a chromatographic column and then the distributions of deuterium in respective hydrocarbons were determined by mass spectrometry. High purity hydrogen, acetylene, and deuterium (HD less than 0.5%) from Takachiho Co., Ltd., were used without further purification.

Results

General Features of Acetylene Hydrogenation. General features of the reaction on palladium foil were similar to those on supported metal catalyst.[4-6] Both ethylene and ethane were observed as the initial products of the reaction under all conditions studied, ethylene being the major product. The selectivity, defined as the ratio of ethylene to ethane produced, was very high and was kept constant in the early stage of the reaction. This finding predicts that both ethylene and ethane are concurrently produced by direct hydrogenation of adsorbed acetylene on the surface and that desorbed ethylene in the gas phase hardly contributes to ethane formation until the gaseous acetylene is consumed. This prediction was confirmed from the fact that the initial yield of ethane-d_4 was within 20% of the total ethane when 13 Torr of ethylene-d_4 was added to 40 Torr of the reaction mixture of C_2H_2 and H_2 (1:2 in molar ratio) at 50°. The foils annealed at various temperatures, however, differed in the detailed behavior of the reaction. Figure 1 shows the change in the catalytic activity of ethylene and ethane formation with annealing. These activities fell precipitously in the temperature range between 200 and 300°. With the treatments above 600°, only the activity of ethylene formation recovered to some extent. The selectivity of the reaction on Catalyst H was about 30 and that on Catalyst L was less than 15 under usual conditions. A long induction period appeared on the

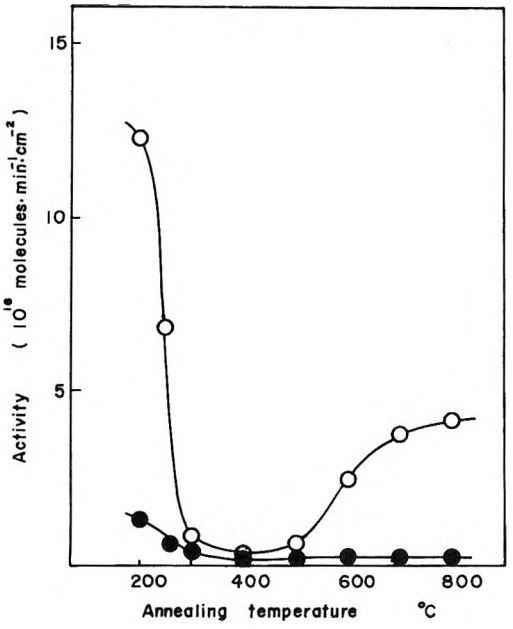

Figure 1. Change in the catalytic activity of cold-worked palladium foil with annealing: ○, ethylene formation; ●, ethane formation; reaction temperature, 50°; total pressure, 50 Torr; $P_H:P_a = 2:1$.

(4) J. Sheridan, *J. Chem. Soc.*, 470 (1945).

(5) G. C. Bond, D. A. Dowden, and N. Mackenzie, *Trans. Faraday Soc.*, **54**, 1537 (1958); G. C. Bond, "Catalysis by Metals," Academic Press, London and New York, N. Y., 1962, p 291.

(6) T. Kabe and I. Yasumori, *J. Chem. Soc. Jap.*, **85**, 410 (1964); **86**, 39 (1965).

Table I: Deuterium Distributions on Catalyst H

Reactions	t, °C	C, %	Acetylene, %			Ethylene, %					HD	H_2
			d_0	d_1	d_2	d_0	d_1	d_2	d_3	d_4		
$C_2H_2 + D_2$[a]	27	23				3	18	64	12	3.5		
	50	20				3	20	62	12	3		
$C_2H_2 + H_2 + D_2$[b]	50	27	100	0	0	43	43	13	1.5	0	0	0
$C_2H_2 + D_2 \rightarrow C_2H_2 + H_2$[c]	27	10				41	40	18	2	0		
H_2 preabs $\rightarrow C_2H_2 + D_2$[d]	27	37				95	5	0	0	0		

[a] The reaction of C_2H_2 with D_2. P_a = 10 Torr, P_D = 30 Torr. [b] The reaction of C_2H_2 with mixture of D_2 and H_2. P_a = 10 Torr, $P_D = P_H$ = 15 Torr. [c] The reaction after the replacement of deuterium by hydrogen. The analysis was taken at the end of the relaxation time which is represented by the arrow in Figure 4. [d] The reaction of C_2H_2 with D_2 on the surface in which hydrogen is preabsorbed. C, %, represents the conversion of acetylene. Correction was made for small amounts of HD and C_2HD present in the source hydrogen and acetylene, respectively.

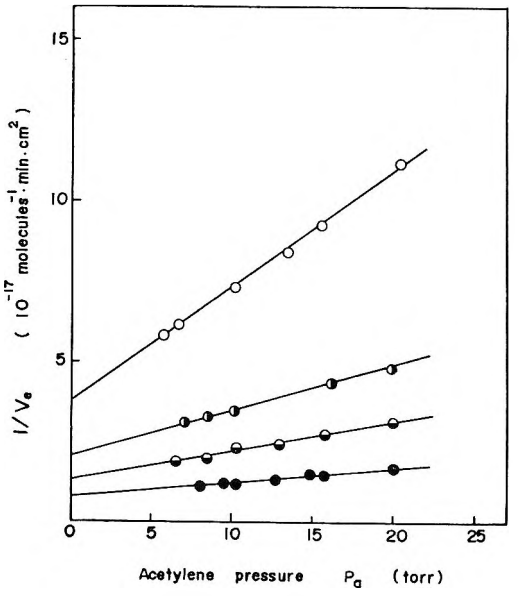

Figure 2. Dependence of the rate on acetylene pressure on Catalyst H: ○, 27°; ◑, 40°; ◒, 50°; ●, 60°.

former but not on the latter. The detailed kinetic behavior on these catalysts (Catalyst H and L) was investigated separately.

Behavior of the Reaction on Catalyst H. A long induction period on a fresh surface of this catalyst was observed. This induction period was not due to poisoning by oxide formed during annealing at high temperature because the catalyst was always reduced at 150° with hydrogen prior to each kinetic run. From a study on the behavior of preadsorbed acetylene labeled with ^{14}C during the reaction,[3] it was shown that the catalyst surface is first covered with strongly adsorbed acetylene and the induction period is that in which the reaction attained steady state, as these retained acetylene molecules are removed slowly from the active site.

The kinetics of ethylene formation showed that the rate V_e was almost proportional to the hydrogen pressure P_H over the temperatures studied. The dependence on the acetylene pressure P_a is shown in Figure 2. The reciprocal of the rate shows a good linear relation with P_a at respective temperatures. Accordingly, the rate equation is expressed as

$$V_e = k_1 P_H / 1 + K_1 P_a \quad (1)$$

where k_1 and K_1 are constants. From their dependences on temperature, k_1 and K_1 are formulated as $5.3 \times 10^{21} e^{-9250/RT}$ molecules cm^{-2} min^{-1} Torr^{-1} and $5.6 \times 10^{-4} e^{3000/RT}$ Torr^{-1}, respectively.

A kinetic isotopic effect was observed in the reaction of acetylene with deuterium. The rate of the reaction with hydrogen was faster than that with deuterium by a factor of 1.6. The distributions of deuterium in the produced ethylene were unchanged up to about 50% conversion of acetylene. As shown in Table I, neither C_2HD nor C_2D_2 was found in the gas phase, and the hydrogen exchange reaction, giving HD and H_2 in gas phase, did not occur under the present conditions.

The effect of the pressure jump on the reaction was examined. When the hydrogenation proceeded at the rate expressed by eq 1 at 27°, the hydrogen pressure was jumped up or down and the change of the rate which approached the reaction rate in a new steady state was followed. As shown in Figure 3, even after a sudden increase of the hydrogen pressure to two times the previous value, the reaction proceeded at a similar rate as before during a certain period. A corresponding new rate was achieved after about 1 hr. A similar time lag on the rate change was also observed in the cases of decreasing hydrogen and of increasing acetylene pressure.

Hydrogen–deuterium replacement was performed in order to give insight on the time lag observed in the pressure jump. It was found that after the replacement of deuterium by hydrogen the rate of the reaction with deuterium changed to that with hydrogen, having a time lag which was very similar in magnitude to that observed in the pressure jump (Figure 4). When the order of replacement was reversed, a similar time lag was also observed. Table I shows that the appreciable amounts of ethylene-d_1, -d_2, and -d_3 were produced in the early stage of the transition period in spite of the absence of deuterium in the gas phase. The

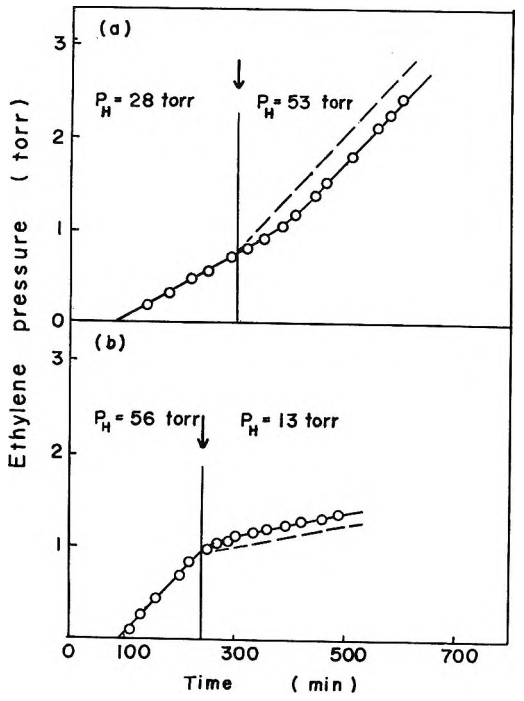

Figure 3. Effect of hydrogen jump on the reaction at 27° over Catalyst H. Hydrogen pressure was suddenly increased from 28 to 53 Torr (a) or decreased from 56 to 13 Torr (b). The dotted lines represent the expected ethylene formation obeying eq 1 in the absence of time lag.

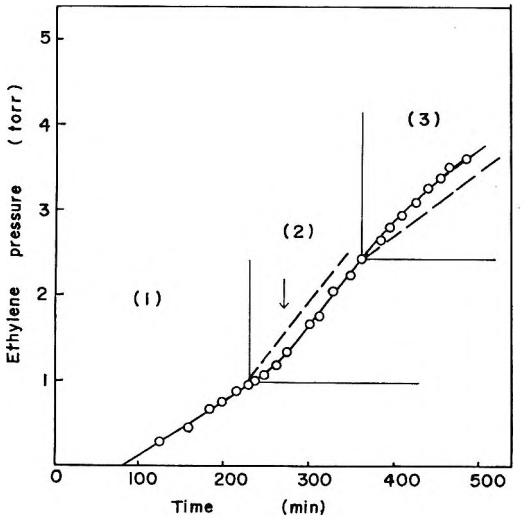

Figure 4. Effect of isotope replacement on the reaction at 27° over Catalyst H: (1) the reaction of C_2H_2 with D_2; (2) that with H_2; (3) that with D_2. The origins of parts 2 and 3 are elevated to the values of ethylene pressure before evacuation. The dotted lines represent the expected ethylene formation in the absence of time lag. The arrow shows the sampling time of the products after D_2–H_2 replacement.

amount of deuterium in ethylene produced was estimated to be more than 100 times the amount to be adsorbed as a monolayer. This suggests that dissolved hydrogen (deuterium) in metal plays an important role in the hydrogenation over this catalyst. It was found that on the catalyst preabsorbing hydrogen the reaction

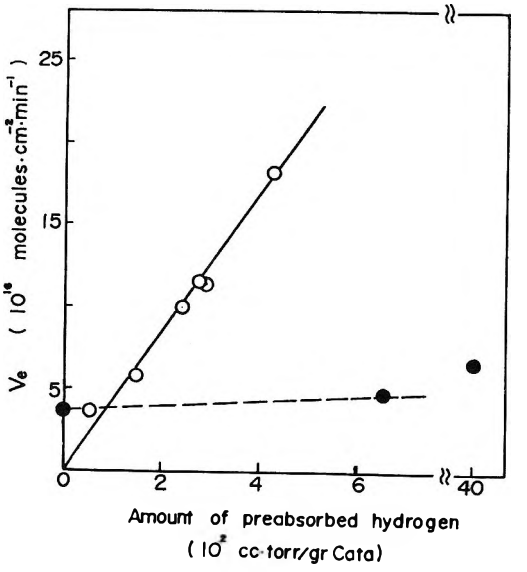

Figure 5. Effect of preabsorbed hydrogen on reaction rate: O, Catalyst H; ●, Catalyst L: P_a, 10 Torr; P_H, 30 Torr.

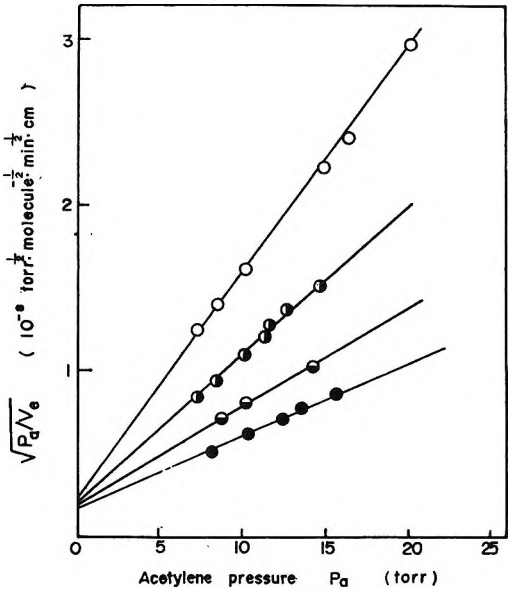

Figure 6. Dependence of the rate on acetylene pressure on Catalyst L: O, 27°; ◑, 40°; ◒, 50°; ●, 60°.

proceeded very rapidly without the induction period and its rate was proportional to the amount of absorbed hydrogen up to 0.002 atomic ratio of hydrogen to palladium (Figure 5). When the reaction of acetylene with deuterium was carried out on the surface in which hydrogen was preabsorbed with the ratio 0.002, no deuterioethylenes were formed as shown in Table I. The result evidently shows that the contribution of deuterium in the gas phase to the reaction is negligible on this surface.

Behavior of the Reaction on Catalyst L. The kinetics of ethylene formation showed that the order in hydrogen was almost unity and independent of the reaction tem-

Table II: Deuterium Distributions on Catalyst L

Reactions	t, °C	C, %	Acetylene, %			Ethylene, %					HD	H_2
			d_0	d_1	d_2	d_0	d_1	d_2	d_3	d_4		
$C_2H_2 + D_2$	27	20	100	0	0	3	25	54	14	4	0	0
$C_2H_2 + H_2 + D_2$	50	25				43	36	18	3	0		
$C_2H_2 + D_2 \rightarrow C_2H_2 + H_2$	27	10				93	7	0	0	0		
H_2 preabs $\rightarrow C_2H_2 + D_2$	27	10				69	24	7	0	0		

perature. The dependence on acetylene pressure was given by a linear relationship between $\sqrt{P_a/V_e}$ and P_a, as shown in Figure 6. Therefore, the rate equation of ethylene formation is expressed as

$$V_e = k_2 P_H P_a/(1 + K_2 P_a)^2 \quad (2)$$

where k_2 and K_2 are constants. By analyzing temperature dependences, k_2 and K_2 were expressed as $2.2 \times 10^{22} e^{-8700/RT}$ molecules min^{-1} cm^{-2} $Torr^{-1}$ and $6.5 \times 10^{-4} e^{3600/RT}$ $Torr^{-1}$, respectively.

A kinetic isotopic effect was also observed in the reaction over this catalyst and the rate of the reaction with hydrogen was faster than that with deuterium by a factor of 1.4 at 27°. The results of the reaction with deuterium are summarized in Table II. The yield of ethylene-d_2 reduced slightly compared with that on Catalyst H and this reduction was compensated by the increase in the yields of ethylene-d_1 and -d_3. Neither C_2D_2 nor C_2HD was observed in the gas phase and HD was produced to a negligibly small extent.

The effect of the pressure jump was also examined. When the hydrogen pressure was jumped, the rate value changed immediately to a new one obeying eq 2, and the time lag did not appear. Moreover, when the reaction mixture of C_2H_2 and D_2 was rapidly replaced by C_2H_2 and H_2, the reaction after the replacement proceeded immediately at the rate of the latter in contrast to the case of Catalyst H. The products were analyzed after the replacement and the results are also included in Table II. It is noted that there are no deuterioethylenes except a small amount of ethylene-d_1 and, further, that deuterioethylenes are mainly produced in the reaction of C_2H_2 and D_2 on the surface preabsorbing hydrogen. Figure 5 reveals also that the effect of preabsorbed hydrogen on the reaction is very small.

The kinetics of ethane formation showed that the reaction rate was proportional to the square of hydrogen pressure and the rate dependence on acetylene pressure was described in the form $P_a/(1 + K_3 P_a)^3$, where K_3 is a constant. The distribution of deuterium in ethane produced was hardly determined because of its small yield, but the presence of ethane deuterated more than d_4 was recognized.

Discussion

In the present study using the catalyst foil, the apparent orders of reaction which conform to eq 1 or 2 were estimated as 1.0 in hydrogen and $-0.4 \sim -0.6$ in acetylene pressure. The overall activation energies were found to be 10.9 kcal/mol for Catalyst L and 10.6 kcal/mol for Catalyst H. These values agree with those of the reaction order, 1.0 in hydrogen and $-0.5 \sim -0.67$ in acetylene pressure, and the activation energy, 11.0 kcal/mol, which were obtained by Bond and Wells[7] using a palladium supported on alumina. They reported a highly selective formation of ethylene in the reactions where acetylene pressures were above 50 Torr. Similar selective behavior was also observed under the conditions of the present study.

The Reaction Mechanism on Catalyst H. The experimental fact that neither deuterioacetylene nor HD was produced in the gas phase in the reaction of C_2H_2 with D_2 is understood either on the assumption that both the adsorption of acetylene and hydrogen is irreversible or that the formation of the half-hydrogenated state, vinyl radical on the surface, is a rate-determining step so that the reverse process to adsorbed acetylene and deuterium scarcely occurs. The pressure jump study revealed that no partial equilibrium is established between the gaseous and the adsorbed species of acetylene or hydrogen. Then the first alternative given above is probably valid. However, the adsorption of those gases cannot be the rate-determining step because the velocity of the rate change was very slow compared to the rate of the hydrogenation. The results in Figure 4 and Table I indicate that a large amount of absorbed hydrogen participates in the hydrogenation. Accordingly, the relaxation phenomena observed in the pressure jump and isotope replacement can be explained in terms of characteristics of absorbed hydrogen. It is suggested that the reacting hydrogen must dissolve into the bulk of metal once to reach the active site. The following scheme is proposed on the basis of the consideration given above.

$$H_2 \xrightarrow{k_3} 2H_{(s)} \quad (3)$$

$$C_2H_2 \xrightarrow{k_4} C_2H_{2(a)} \quad (4)$$

$$C_2H_{2(a)} + H_{(s)} \underset{k_{-5}}{\overset{k_5}{\rightleftarrows}} C_2H_{3(a)} \quad (5)$$

$$C_2H_{3(a)} + H_{(s)} \underset{k_{-6}}{\overset{k_6}{\rightleftarrows}} C_2H_{4(a)} \quad (6)$$

(7) G. C. Bond and P. B. Wells, *J. Catal.*, 5, 65 (1965).

$$C_2H_{4(a)} \xrightarrow{k_7} C_2H_4 \qquad (7)$$

where the symbols (a) and (s) denote, respectively, adsorbed and dissolved states, which are reactive.

The tracer study[3,8] using $C_2H_2C^{14}$ showed that the preadsorbed acetylene on a clean surface was classified into several species according to their reversibility on adsorption or reactivity with hydrogen. On the basis of this knowledge, the following picture is suggested for the reaction. A part of the surface is occupied by the irreversibly adsorbed species which play no part in the reaction. Then a fraction of the rest of the surface is covered by the reversible adsorption of acetylene that is not hydrogenated and simply blocks the surface, in accordance with the usual adsorption law. The remaining fraction of the surface is almost covered with irreversibly adsorbed acetylene which reacts by the dissolved hydrogen coming up from the inside of the catalyst. It is supposed that, in the steady state, the rate of ethylene formation is equal to that of hydrogen absorption. Then, the rate is given by

$$V_e = k_3 P_H N_s (1 - \theta_I) \qquad (8)$$

where N_s expresses the number of the site that enables the hydrogen to reach the inside of the catalyst and θ_I denotes the fraction of N_s covered with the reversible and inert species.

Since θ_I can be expressed as

$$\theta_I = K_a P_a / (1 + K_a P_a) \qquad (9)$$

by introducing an adsorption constant K_a, one can obtain the final expression

$$V_e = k_3 N_s P_H / (1 + K_a P_a) \qquad (10)$$

by substituting eq 9 into eq 8. This rate equation conforms to that established from the experiment.

The time lag observed in the jump or the replacement study is explained from the role of the catalyst as the reservoir for the dissolved hydrogen. Pressure-jumped hydrogen or replaced deuterium is at first adsorbed on the vacant site of N_s, rapidly changing the surface concentration or the isotopic ratio, and diffuses into the bulk of the catalyst. The value of the concentration or the deuterium fraction of the dissolved hydrogen changes to that in the new steady state, controlling the rate of hydrogenation or the deuterium content in the produced ethylene. The initial change in the fraction Φ of the dissolved hydrogen is expressed approximately as

$$-\frac{d\Phi}{dt} \approx \frac{V_e}{N_b} = \frac{V_e'}{N_b}\Phi = \frac{1}{\tau}\Phi \qquad (11)$$

where V_e' is the rate of the reaction per dissolved hydrogen and N_b is the maximum content of the dissolved hydrogen atoms per unit area of the catalyst foil. In the steady state V_e' is estimated to be 1.4×10^{19} molecules/min from the rate V_e and from the values of the fraction Φ which was obtained in the D_2–H_2 replacement. N_b is about $8 \times 10^{20}/cm^2$ in the present catalyst foil, estimated from the β phase of the Pd–H system at the reaction temperature. Therefore, the half-time

$$\tau = N_b / V_e' \qquad (12)$$

of the reaction is evaluated as about 60 min, which agrees well with the observed time in the experiments. This gives support to the reaction mechanism described above.

The distributions of deuterium in ethylene produced in the reaction of C_2H_2 with D_2 as shown in Table I can be interpreted in terms of the exchange in steps 5 and 6. It is provided, according to Keii,[9] Kemball,[10] and Bond,[11] that acetylene-d_i (i = 0, 1, 2) and vinyl-d_i (i = 0, 1, 2, 3) are formed on the surface in the steady concentrations and that these species each have the same probability S of taking a deuterium atom or $(1 - S)$ of taking a hydrogen atom. Each vinyl radical has the probability P of undergoing hydrogenation to ethylene. The process of the reverse in step 6 is neglected in this procedure because $C_2H_{4(a)}$ formed can desorb rapidly as expected from the negligible production of ethane. The optimum values of the parameters S and P are found to be 0.86 and 0.63, respectively. These values agree with that obtained by Bond in the case of a high deuterium pressure of 100 Torr.[11] The fact that HD and H_2 were not found in the gas phase suggests that $H_{(a)}$ and $D_{(a)}$ produced from the reverse reaction in steps 5 and 6 are absorbed immediately.

Rennard and Kokes observed the inverse isotopic effect in the ethylene hydrogenation on palladium hydride with H/Pd ratio 0.1–0.6.[12] This effect vanished on the hydride with H/Pd ratio below 0.05. In the present study the ratio of absorbed hydrogen to palladium atom was smaller than this value by a factor of 10^3. Accordingly, the present result of the normal isotopic effect does not contradict their results, while the value of 1.6 obtained in the hydrogenation coincides with that of 1.57 due to the normal isotopic effect found in the diffusion of hydrogen through the bulk of palladium at 27°.[13] This situation predicts that step 3 in the reaction scheme may be responsible for this isotopic effect.

The Reaction Mechanism on Catalyst L. The absence of time lag in the reaction on Catalyst L leads to the conclusion that the absorbed hydrogen does not play a significant role in the hydrogenation. This conclusion is also supported from the absence of deu-

(8) I. Yasumori, T. Kabe, and Y. Inoue, unpublished work.

(9) T. Keii, *J. Res. Inst. Catalysis, Hokkaido Univ.*, **3**, 36 (1953); *J. Chem. Phys.*, **22**, 144 (1954).

(10) C. Kemball, *J. Chem. Soc.*, 735 (1956).

(11) G. C. Bond and P. B. Wells, *J. Catal.*, **6**, 397 (1966).

(12) R. J. Rennard, Jr., and R. J. Kokes, *J. Phys. Chem.*, **70**, 2543 (1966).

(13) G. Toda, *Catalyst*, **5**, 11 (1963).

terated ethylene in the products after the replacement of deuterium by hydrogen (Table II). Besides, it is apparent from Figure 5 that the effect of preabsorbed hydrogen on the reaction is extremely small compared with that for Catalyst H. Accordingly, the following scheme seems plausible in this case in which the contribution of adsorbed hydrogen is taken into account.

$$H_2 \rightleftarrows H_{2(a)} \quad (13)$$

$$C_2H_2 \rightleftarrows C_2H_{2(a)} \quad (14)$$

$$C_2H_{2(a)} + H_{2(a)} \xrightarrow{k_{15}} C_2H_{3(a)} + H_{(a)} \quad (15)$$

$$C_2H_{3(a)} + H_{(a)} \rightleftarrows C_2H_{4(a)} \quad (16)$$

$$C_2H_{3(a)} \xrightarrow{k_{17}} C_2H_4 \quad (17)$$

$$C_2H_{4(a)} + H_{2(a)} \xrightarrow{k_{18}} C_2H_6 \quad (18)$$

The fact that neither C_2HD nor HD was produced in the gas phase predicts that step 15 is irreversible and that the adsorbed hydrogen atom is rapidly liberated with the vinyl radical and hence is scarcely recombined to hydrogen. The absence of time lag reveals that steps 13 and 14 are very fast processes. The rate equation of ethylene formation is, therefore, derived by assuming that the partial equilibrium is established between the adsorbed and the gaseous state of hydrogen or acetylene, respectively, and that the irreversible process of vinyl formation is very slow.

$$V_e = k_{17}\theta_{C_2H_4} \quad (19)$$

It is plausible to suppose that ethane is produced by the successive addition of the adsorbed hydrogen to $C_2H_{4(a)}$ formed. Its rate V_n is expressed as

$$V_n = k_{18}\theta_{C_2H_4}\theta_{H_2} \quad (20)$$

where θ_{H_2} denotes the fraction of coverage of the adsorbed hydrogen. From the condition of steady state, $\theta_{C_2H_4}$ is described as

$$\theta_{C_2H_4} = k_{15}\theta_H\theta_{C_2H_2}/k_{17} + k_{18}\theta_{H_2} \quad (21)$$

Then, eq 19 is rewritten in a form, by neglecting the coverage $\theta_{C_2H_3}$, $\theta_{C_2H_4}$, and θ_H

$$V_e = \frac{k_{15}K_3K_4P_aP_H}{\{1 + K_3P_a + (1 + k_{18}/k_{17})K_4P_H\}(1 + K_3P_a + K_4P_H)} \quad (22)$$

where K_3 and K_4 are the adsorption constants of acetylene and hydrogen, respectively. When hydrogen is weakly adsorbed compared with acetylene, eq 22 becomes

$$V_e = k_{15}K_3K_4P_aP_H/(1 + K_3P_a)^2 \quad (23)$$

by eliminating the term $(1 + k_{18}/k_{17})K_4P_H$ in the denominator. This equation has the same form obtained from the experiments. Using supported Pd which was prepared under similar conditions as Catalyst L, Bond and Wells[14] suggested that the adsorption of hydrogen was irreversible and that ethylene was produced by the reaction between two vinyl radicals. However, a sufficient explanation about the negative order in acetylene pressure was not given.

Equation 20 is also rewritten as, on the basis of similar consideration

$$V_n = k_{18}k_{15}K_3K_4^2P_aP_H^2/k_{17}(1 + K_3P_a)^3 \quad (24)$$

This equation can explain fairly well the kinetic results for ethane formation.

The distribution of deuterium in ethylene produced in the reaction of C_2H_2 with D_2 is explained in terms of the exchange in reaction 16 by performing a similar analysis in the case of Catalyst H. The probabilities of the vinyl species gaining a deuterium atom and of the adsorbed ethylene reverting to vinyl are found to be 0.80 and 0.50, respectively. The high value of the latter is probably responsible for the increase of ethane formation.

Properties of the Active Sites on Catalyst L and H. The great difference in the reaction mechanisms over Catalyst L and H is due to whether the major reactive intermediate is adsorbed hydrogen or absorbed one. The different behavior of reaction was also found in CO poisoning using tracer technique. The activity of Catalyst H decreased with the amount of adsorbed CO, whereas that of Catalyst L was not affected by CO up to 0.2 surface coverage.[3,8] In the previous study[15] the surface area of palladium foil was estimated using xenon BET technique and it was found that the change in the surface area by annealing was too small to account for that in catalytic activity. Accordingly, the differences in the catalytic activities, in the reaction mechanisms, and in the effects of CO poisoning are ascribed to a surface fine structure which is not detected by the adsorption of a molecule as large as xenon.

When the foil is subjected to cold-working, lattice imperfections involving point defects and dislocations are formed. A marked decrease of catalytic activity with annealing between 200 and 300° suggests that vacancies of various point defects work as the active sites for the hydrogenation because the defect disappears with annealing in this temperature range.[16] The surface structure including vacancy is probably effective in adsorbing hydrogen on positions accessible to the adsorbed acetylene. When the foil was annealed above 800°, on the other hand, the stable and smooth lattice plane was exposed to the surface after recrystallization.[3] It was found that the strongly adsorbed acetylene which remained unreacted during the hydro-

(14) G. C. Bond and P. B. Wells, *Advan. Catal.*, 15, 91 (1964).

(15) T. Kabe, T. Mizuno, and I. Yasumori, *Bull. Chem. Soc. Jap.*, 40, 2047 (1967).

(16) L. M. Clarebrough, M. E. Hargreaves, and G. W. West, *Proc. Roy. Soc. Ser. A*, 232, 252 (1955); *Phil. Mag.*, 1, 528 (1956).

genation occupied a large fraction of surface. This predicts that the interaction between the adsorbed acetylenes increases on this smooth surface and hence the mode of the adsorbed species becomes peculiar. These species may, therefore, destroy the sites for the reactive adsorption of hydrogen and the role of the absorbed hydrogen atom becomes important.

In conclusion, the dynamic treatments such as pressure jump and isotope replacement proved to be effective in revealing the behavior of the reactive intermediates during the reaction. It is possible to apply these methods extensively to the investigation of the behavior of adsorbed acetylene and CO poison during the hydrogenation by labeling with a radioactive isotope ^{14}C. Details of the study will be reported in the following paper of this series.

Reactions of Adsorbed Organic Molecules. II. Bromination of 4-Nitrobiphenyl on a Silica Surface

by M. J. Rosen* and J. Gandler

Department of Chemistry, Brooklyn College of The City University of New York, Brooklyn, New York 11210
(Received August 17, 1970)

Publication costs borne completely by The Journal of Physical Chemistry

The bromination of 4-nitrobiphenyl adsorbed onto Cab-O-Sil, a nonporous, hydroxylated silica, has been investigated. The reaction products, 2-bromo-4′-nitrobiphenyl and 4-bromo-4′-nitrobiphenyl, are obtained in a 20/80 ratio, similar to that obtained upon bromination in solution, irrespective of the coverage of the surface by the 4-nitrobiphenyl. The kinetics of the reaction indicate inhibition of the bromination by the organic adsorbates, implying strong competitive adsorption by these onto the catalytically active sites. As a consequence, the reaction is shown to have first-order dependency upon the 4-nitrobiphenyl on the surface and on the bromine adsorbed onto these active sites. A mechanism for the reaction is proposed.

In a previous investigation,[1] the bromination of an olefin, diethyl fumarate, adsorbed onto Cab-O-Sil,[2] a nonporous, hydroxylated silica, it was found that gaseous bromine, when adsorbed onto an active OH group on the Cab-O-Sil surface, formed a highly electrophilic complex capable of adding to strongly deactivated double bonds. It seemed reasonable that so electrophilic a reagent might be capable of brominating aromatic nuclei in the absence of any other catalyst. The current study is an investigation into the bromination of aromatic nuclei by this complex.

Initial work indicated that bromine adsorbed onto Cab-O-Sil did indeed brominate aromatic nuclei adsorbed onto that surface. In fact, the rate of bromination, as in the case of ordinary olefins,[1] was so rapid that valid data were difficult to obtain. (Studies on the adsorption of bromine by Cab-O-Sil in this and in our previous investigation have shown that 10–40 min is required to reach adsorption equilibrium and therefore only kinetic data taken after that period of time are valid.) Biphenyl, when impregnated onto the surface at a concentration equivalent to about half the monolayer value, was completely monobrominated at 25° in about 30 min when treated with gaseous bromine at a concentration of 5×10^{-3} M and almost completely dibrominated in about 2 hr. Comparable quantities of biphenyl and bromine, when mixed together in carbon tetrachloride solution, showed no perceptible reaction overnight in the dark. The less reactive 4-bromobiphenyl also gave too rapid a reaction; at a concentration equivalent to about half the monolayer value, about half of the material was monobrominated in 30 min by gaseous bromine at a concentration of 4×10^{-3} M. Eventually, the still less reactive 4-nitrobiphenyl was found suitable for our purpose.

Experimental Section

Materials and Apparatus. The 4-nitrobiphenyl (A) used was Eastman Kodak Co. White Label grade, recrystallized to a constant mp of 114.0–114.5°. The bromine (Baker Analyzed) was redistilled from NaBr and kept over P_2O_5.

(1) M. J. Rosen and C. Eden, *J. Phys. Chem.*, **74**, 2303 (1970).
(2) Cabot Corp., Boston, Mass.

The Cab-O-Sil was a sample of Type M-5, obtained through the courtesy of Dr. H. Cochrane of the Cabot Corp. It had a surface area of 210 m^2/g as determined by nitrogen adsorption and a surface OH concentration of 1.00 mequiv/g as measured by $LiAlH_4$.[3] It was dried for 3 days at 110° immediately before use.

The apparatus for determining adsorption isotherms and kinetic studies was similar to that used previously,[1] but was fitted with Teflon bore valves (Kontes Glass Co., Vineland, N. J.) instead of glass stopcocks to eliminate the use of vacuum grease and was somewhat modified in size and shape to permit the entire apparatus to fit into the cell compartment of a Cary 14 recording spectrophotometer maintained at 25 ± 0.05° by connection to a large water bath.

Preparation of the Surface. The desired quantities of 4-nitrobiphenyl in ACS Certified Reagent grade CCl_4 were added to the dried Cab-O-Sil, the solvent was removed, and the impregnated surface transferred to the reaction cell of the apparatus, with all operations conducted under dry argon as described previously.[1] As before, the reaction cell was covered with opaque material to exclude light.

Determination of Adsorption Isotherms of Bromine on Cab-O-Sil Covered with Brominated 4-Nitrobiphenyl and Kinetic Studies of the Reaction between Bromine and 4-Nitrobiphenyl on Cab-O-Sil. These were conducted in the same fashion as described previously[1] by measuring the change in bromine concentration of the gas phase at 416 mμ, using ε 170.

For the kinetic studies, the amount of adsorbed bromine, *Ba*, on the surface at any bromine vapor concentration, [*B*], was taken from the adsorption isotherm of bromine on a brominated 4-nitrobiphenyl-covered surface with the same coverage as the 4-nitrobiphenyl used. The amount of unreacted bromine, $B^0 - x$, in the system at any time, where x = the amount reacted at any time, was obtained as before by adding the amount of adsorbed bromine on the surface to that in the gas phase. Thus

$$B^0 - x = Ba + [B]V$$

where V = the total free volume of the gas phase in the apparatus.

Analysis of the reaction mixture by gas chromatography (see below) immediately upon the completion of a kinetic run confirmed this method of calculating the amount of reaction. In those cases where the reaction proceeded very rapidly (>50% reaction during the first hour) due to very high initial bromine concentration, however, the amount of reaction as indicated by gas chromatographic analysis differed considerably from that calculated from the bromine concentration in the gas phase, indicating that conditions close to adsorption or temperature equilibrium, or both, were not being maintained at these rates of reaction. Kinetic data from these runs were considered invalid and are not included in the reported results.

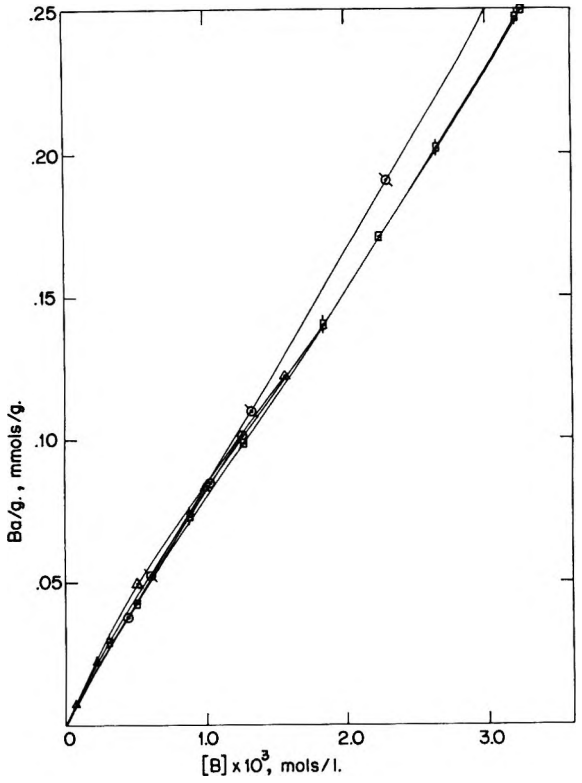

Figure 1. Adsorption isotherms of bromine on Cab-O-Sil at different coverages by brominated 4-nitrobiphenyl. Coverages in mmol/g: △, 0.0374; ⊕, 0.0570; ⊡, 0.0933; ⊙, 0.1347; ⊘, 0.2927.

Initial concentrations of 4-nitrobiphenyl (A^0/g) used in the kinetic studies varied from 0.035 mmol/g of Cab-O-Sil to 0.26 mmol/g; adsorbed bromine concentrations (Ba/g) varied from 0.04 to 0.16 mmol/g of Cab-O-Sil. Concentrations beyond these ranges could not be used because of limitations imposed by the size of the apparatus, the accuracy of optical density measurements, and the need to maintain conditions close to adsorption and temperature equilibrium during the reaction.

Gas Chromatograms of Reaction Mixtures. These were performed on a Hewlett-Packard 5754B research chromatograph with disk integrator (SE-30 column at 250°; a flame ionization detector at 320°; He carrier gas at 40 ml/min; reference substance, naphthalene). The organic materials were extracted directly from the surface with benzene and analyzed without further purification.

Results and Discussion

Nature of the Bromination Products. Analysis of the reaction mixture by gas chromatography showed that for the period during which the kinetic studies were made only two products were formed: 2-bromo-

(3) H. Cochrane, Cabot Corp., private communication.

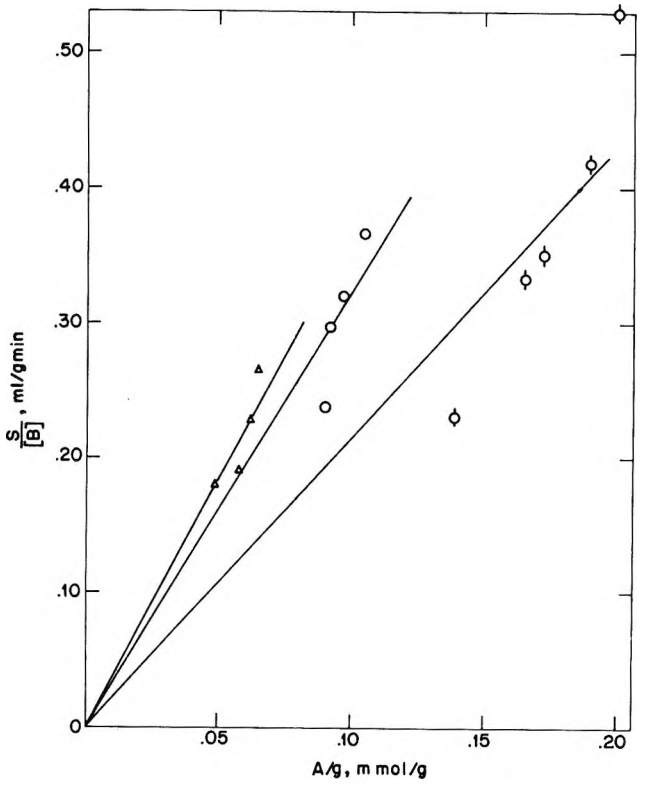

Figure 2. Kinetics of bromination of 4-nitrobiphenyl: △, A^0/g = 0.0855 mmol/g; ⊙, A^0/g = 0.1348 mmol/g; ⊕, A^0/g = 0.2625 mmol/g.

4′-nitrobiphenyl and 4-bromo-4′-nitrobiphenyl, the *o*- and *p*-monobromination products, respectively. No trace of the *m*-bromination isomer was found. The ortho/para ratio was 20/80 and did not vary with coverage of the surface by 4-nitrobiphenyl over the entire range studied (0.033–0.26 mmol/g). The invariance of this ratio with an eightfold increase in surface concentration of the 4-nitrobiphenyl and its similarity to that (25/75) reported for homogeneous bromination of 4-nitrobiphenyl in the presence of $FeCl_3$[4] indicate that the presence of the Cab-O-Sil surface introduces no steric or electronic factors into the 4-nitrobiphenyl molecule which affect the bromination reaction and that the catalytic effect of the surface is confined to the bromine molecule.

Adsorption Studies. Adsorption isotherms of bromine onto Cab-O-Sil covered with various amounts of brominated 4-nitrobiphenyl are illustrated in Figure 1. All of these isotherms were determined on surfaces on which the adsorbed 4-nitrobiphenyl had been treated with bromine overnight to ensure that none of the bromine uptake was due to a reaction with the organic adsorbate. After overnight bromination, the unreacted bromine was desorbed from the surface by immersing the spectral compartment of the apparatus in liquid N_2 until the surface appeared colorless and then by evacuation to 10^{-5} Torr until measurement showed no Br_2 in the gas phase. The isotherms show the two

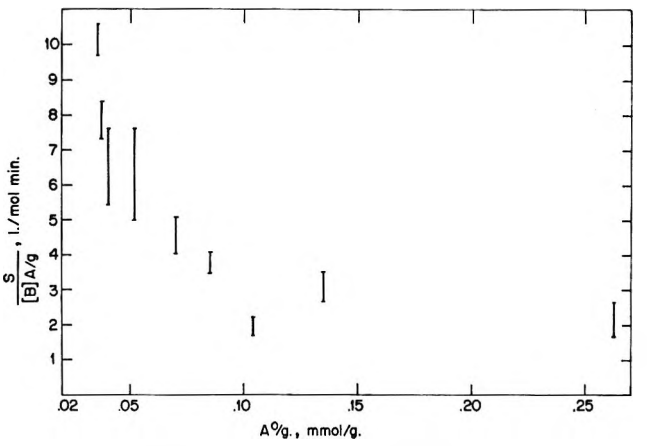

Figure 3. Kinetics of bromination of 4-nitrobiphenyl. Values plotted represent range of the function $S/([B]A/g)$ for a run at that particular initial concentration, A^0/g.

effects noted previously with brominated diethyl fumarate: (1) at low bromine pressures, the amount of bromine adsorbed per gram of Cab-O-Sil is almost linear with bromine pressure and is only slightly affected by change in surface concentration of the brominated adsorbate in the range studied; (2) at higher bromine pressures, there is increased bromine uptake by the surface, due to solubility in or adsorption on the material already on the surface.

Kinetics of the Bromination Reaction. The rate of bromination of 4-nitrobiphenyl at any instant, $d(B^0 - x/g)/dt \equiv S$, was determined from slopes of plots of $B_0 - x/g$ *vs.* time. Some plots of $S/[B]$ *vs.* A/g, where A/g is the concentration of unreacted 4-nitrobiphenyl at time t, are shown in Figure 2. It is apparent that there is considerable deviation from linearity, indicating that the reaction does *not* show simple second-order kinetics (first order in both the bromine in the gas phase and the unreacted 4-nitrobiphenyl). Figure 3 shows plots of the function for a reaction first order with respect to both the gaseous bromine and the 4-nitrobiphenyl on the surface, $(S)/([B]A/g)$ as a function of A^0/g, the initial 4-nitrobiphenyl concentration. The values plotted represent the range of values of the function $(S)/[B]A/g)$ for a run at that particular initial coverage. It is apparent that there is a steady decrease in the value of the function with increasing coverage of the surface by the organic adsorbate. This implies inhibition of the bromination reaction by the latter as a result of very strong, competitive adsorption onto the catalytic sites.[5] Inspection of the data also indicates greater than first-order dependency upon the bromine concentration.

The adsorption of bromine directly onto the Cab-O-Sil surface (in contrast to that adsorbed onto molecules

(4) L. Guglialmelli and M. R. Franco, *An. Asoc. Quim. Argent.*, **20**, 8 (1932).

(5) K. J. Laidler, "Chemical Kinetics," McGraw-Hill, New York, N. Y., 1965, p 278.

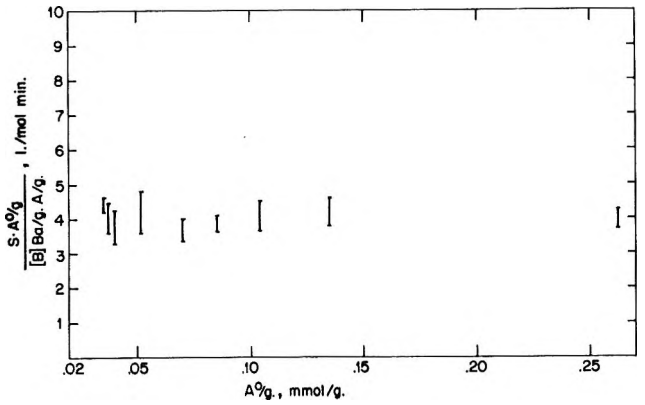

Figure 4. Kinetics of bromination of 4-nitrobiphenyl. Values plotted represent range of the function $(SA^0/g)/[B]Ba/gA/g$ for a run at that particular initial concentration, A^0/g.

already on the surface) and therefore capable of being activated by the surface, has been shown in our previous investigation to be a linear function of the bromine pressure in the gas phase, resulting from the fast adsorption equilibrium

$$\mathrm{SiOH^*} + \mathrm{Br_2(g)} \underset{k_{-1}}{\overset{k_1}{\rightleftharpoons}} \mathrm{SiOHBr_2^*}$$

where SiOH* represents an active OH group on the Cab-O-Sil surface. In the absence of another adsorbate, the expression for the concentration of bromine on active sites, Ba^*/g, is then

$$Ba^*/g = K[\mathrm{SiOH^*}][B]$$

In the presence of another adsorbate at a concentration of c/g, the fraction of adsorbed bromine on active sites is $(Ba/g)/(Ba/g + nc/g)$, where n is a constant measuring the tendency of that adsorbate molecule to adsorb onto an active site relative to that of a bromine molecule. The expression for the concentration of bromine on active sites is then

$$Ba^*/g = \frac{K[\mathrm{SiOH^*}][\mathrm{B}]Ba/g}{Ba/g + nc/g}$$

If $nc/g \gg Ba/g$, for example, when the adsorbate is very strongly adsorbed relative to bromine and n is consequently very large

$$Ba^*/g \cong \frac{K[\mathrm{SiOH^*}][\mathrm{B}][Ba/g]}{nc/g}$$

Under these conditions, the expression in the present case for the rate constant, k_2, for a reaction which is first order in both bromine adsorbed on *active sites* and 4-nitrophenyl on the surface is

$$k_2 = \frac{SnA^0/g}{K[\mathrm{SiOH^*}][\mathrm{B}](Ba/g)(A/g)} = \frac{K^1SA^0/g}{[\mathrm{B}](Ba/g)(A/g)}$$

Figure 4 is a plot of $(SA^0/g)/[\mathrm{B}](Ba/g)(A/g) = k_2/K^1$ *vs.* A^0/g. In the range covered by the experimental data, the function has a value of 4.0 ± 0.8 l./mol min indicating first-order dependency of the bromination reaction on both the bromine adsorbed *on active sites* and on the 4-nitrobiphenyl on the surface.

From the ortho/para ratio of 20/80, the value of the constant

$$\frac{SA^0/g}{[\mathrm{B}]Ba/g \cdot A/g} = \frac{k_2K[\mathrm{SiOH^*}]}{n}$$

is 0.80 ± 0.16 and 3.2 ± 0.64 l./mol min, for bromination in the ortho and para position, respectively.

The inhibition of the bromination reaction by the organic adsorbate is in sharp contrast to its almost negligible effect upon the physical adsorption of bromine onto the surface, as shown in Figure 1. The kinetic and adsorption data obtained imply the following: (1) Br_2 is weakly physisorbed onto the Cab-O-Sil surface, presumably primarily *via* van der Waals types of interactions; (2) only a small fraction of the physisorbed Br_2 is complexed with active sites; and (3) the probability of interaction between adsorbed 4-nitrobiphenyl or adsorbed brominated 4-nitrobiphenyl and active sites is relatively high.

A possible mechanism for the reaction is therefore

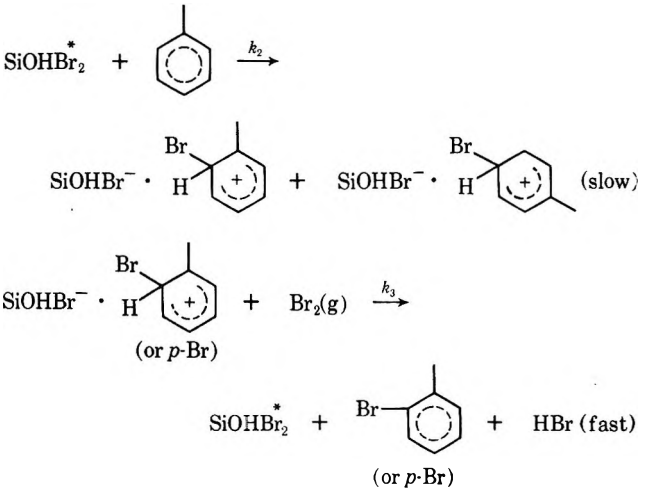

Acknowledgment. This investigation was supported in part by Undergraduate Science Education Program Grants GY-5723 and GY-7540, National Science Foundation. The authors gratefully acknowledge the assistance of Miss Sara Lustgarten and Messrs. Ira Michaels and Jack Emert in the preliminary stages of this investigation.

The Oxidation of Hypophosphorous Acid by Vanadium(V)[1]

by J. N. Cooper,* H. L. Hoyt, C. W. Buffington, and C. A. Holmes

Department of Chemistry, Bucknell University, Lewisburg, Pennsylvania 17837 *(Received October 19, 1970)*

Publication costs assisted by the Research Corporation

The oxidation of H_3PO_2 by vanadium(V) in perchlorate media was investigated. The formation quotient of the 1:1 VO_2^+–$H_2PO_2^-$ complex was measured. The rate law of the redox reaction indicates that several vanadium(V)–phosphorus(I) complexes are kinetically significant and a mechanism consistent with this is proposed.

Introduction

The oxidation of aqueous hypophosphorous acid by a variety of oxidizing agents, including the halogens, Cu(II), and Ag(I), proceeds by a common, acid-dependent rate law which is zero order in the oxidizing agent.[2] The accepted mechanism for these reactions involves a general-acid catalyzed tautomerization of the kinetically unreactive, four-coordinated hypophosphorous acid, $H_2PO(OH)$, to a reactive, three-coordinated species $HP(OH)_2$, in the rate-determining step. Recently, slower oxidations of hypophosphorous acid by Ce(IV) and Cr(VI) have been reported[3,4] in which the oxidant forms a complex with P(I). The rate laws of these reactions are also acid dependent and the mechanisms proposed involve the acid-catalyzed tautomerization of the complexed hypophosphite moiety followed by a rapid electron transfer. Thus a general mechanism can be expressed as

$$H_2PO(OX) + H^*A \longrightarrow HP(OH^*)(OX) + HA \quad (I)$$

where X may be either a complex-forming oxidant or hydrogen.

In the case of the Ce(IV) oxidation,[3a] the diminution of the rate relative to oxidation by the halogens was attributed to virtually complete complexation of the hypophosphorous acid by excess Ce(IV); it was not clear whether the reactivity of the free, tautomerized $HP(OH)_2$ with Ce(IV) was reduced. In the oxidation by Cr(VI)[3b,4] excess H_3PO_2 was present suggesting that the uncomplexed hypophosphorous acid is unreactive to Cr(VI) oxidation. In searching for a cationic oxidant for H_3PO_2 with a relatively uncomplicated aqueous chemistry, we examined the oxidation by V(V), which had been proposed as an analytical procedure for H_3PO_2,[5] and we observed that the rates of oxidation in perchloric acid were exceptionally slow. We report here an investigation of this oxidation in 1 *M* perchlorate media. The study was undertaken for the purpose of comparison with Ce(IV) and Cr(VI) oxidations. It appears to be a clear example of rapid complex formation prior to the oxidation step.

Experimental Section

Hypophosphorous acid was purified and handled as described previously.[4] All water was redistilled from alkaline permanganate. Vanadium(V) solutions were prepared by continuously stirring an excess of "Baker Analyzed" 100.0% V_2O_5 in *ca.* 0.7 *F* $HClO_4$ for a period of several days at room temperature and filtering the resulting solution. Total V(V) was determined titrimetrically with Fe(II).[6] Oxovanadium(IV) perchlorate was prepared from $Ba(ClO_4)_2$ and $VOSO_4$ and recrystallized from dilute perchloric acid. Otherwise, reagent grade chemicals were used without further purification. All solutions were purged with a stream of deoxygenated nitrogen before use.

A recent study[7] raised the question whether more highly charged, protonated forms of V(V) than VO_2^+ were of importance in strongly acid solutions. This prompted us to reexamine the nature of V(V) in acidic perchlorate media. The total charge-equivalent concentration was obtained by displacement of H^+ from a cation exchange column of large excess capacity. The free perchloric acid in the V(V) was estimated using a glass and a saturated NaCl–calomel electrode pair, calibrated against solutions of known hydrogen ion concentration, made up to the same ionic strength with $LiClO_4$. The charge per V obtained was 1.1 ± 0.1, pH 0.8–1.5. The absorption spectrum of V(V) solution in 1 *M* perchlorate media was essentially independent of hydrogen ion concentration, pH 0.0–1.0, for the wavelengths 230–400 nm. These results are in accord

(1) Presented at the 161st National Meeting of the American Chemical Society, Los Angeles, Calif., March 1971.

(2) (a) R. O. Griffith, A. McKeown, and R. P. Taylor, *Trans. Faraday Soc.*, **36**, 752 (1940); (b) W. A. Jenkins and D. M. Yost, *J. Inorg. Nucl. Chem.*, **11**, 297 (1959).

(3) (a) R. L. Carroll and L. B. Thomas, *J. Amer. Chem. Soc.*, **88**, 1376 (1966); (b) G. P. Haight, Jr., M. Rose, and J. Preer, *ibid.*, **90**, 4809 (1968).

(4) J. N. Cooper, *J. Phys. Chem.*, **74**, 955 (1970).

(5) G. G. Rao and H. S. Gowda, *Z. Anal. Chem.*, **146**, 167 (1955).

(6) A. Berka, J. Vulterin, and J. Zyka, *Chemist-Analyst*, **51**, 24 (1962).

(7) G. St. Nikolov and D. Mihailova, *J. Inorg. Nucl. Chem.*, **31**, 2499 (1969).

Table I: Absorbance of Solutions of V(V) and H_3PO_2 at 260 nm (temp, 25°; path length = 1.00 cm; ionic strength = 1.00 *M*; V(V) = 3.86×10^{-4} *F*)

			$[H^+] = 0.100$ *M*			
P(I), *F*	0.000	0.0282	0.0564	0.0845	0.141	0.198
$[H_2PO_2^-]$, *M*	0.000	0.0141	0.0282	0.0423	0.0704	0.0990
A_{260}, Obsd	0.339	0.376	0.400	0.417	0.438	0.450
Calcd		0.376	0.400	0.416	0.437	0.453
			$Q_f = 20.1 \pm 0.8$			
			$[H^+] = 0.200$ *M*			
P(I), *F*	0.000	0.0422	0.0846	0.1268	0.211	0.422
$[H_2PO_2^-]$, *M*	0.000	0.0141	0.0282	0.0423	0.0704	0.141
A_{260}, Obsd	0.336	0.370	0.395	0.412	0.433	0.470
Calcd		0.372	0.394	0.413	0.439	0.464
			$Q_f = 15.2 \pm 1.3$			
			$[H^+] = 0.300$ *M*			
P(I), *F*	0.000	0.0423	0.0846	0.1268	0.211	
$[H_2PO_2^-]$, *M*	0.000	0.0106	0.0211	0.0317	0.0527	
A_{260}, Obsd	0.335	0.362	0.383	0.400	0.423	
Calcd		0.363	0.384	0.400	0.424	
			$Q_f = 15.1 \pm 1.7$			
			$[H^+] = 0.400$ *M*			
P(I), *F*	0.000	0.0423	0.0846	0.1268	0.211	
$[H_2PO_2^-]$, *M*	0.000	0.00845	0.0169	0.0253	0.0422	
A_{260}, Obsd	0.334	0.357	0.375	0.389	0.412	
Calcd		0.357	0.375	0.390	0.411	
			$Q_f = 15.9 \pm 0.9$			

with other reports[8] that only one V(V) species, VO_2^+, is dominant in these solutions. It is of course possible that small equilibrium concentrations of protonated V(V) species are *kinetically* important.

The stoichiometry was confirmed, allowing VO_2^+ to react completely with excess H_3PO_2 in 0.5 *M* $HClO_4$. The cationic products were separated from neutral and anionic species using a cation column of large excess capacity in the H^+ form. P(I) and P(III) in the eluent were determined iodometrically.[9] The stoichiometric ratios found were: V/P(I) = 2.08 ± 0.10 and V/P(III) = 1.91 ± 0.13. The vanadium product was largely displaced from the column by 1 *M* $Ba(ClO_4)_2$ and its absorption spectrum was essentially identical with $VO(ClO_4)_2$, wavelength 400–750 nm. No evidence of a redox reaction was observed between H_3PO_3 and VO_2^+ in 1 *M* $HClO_4$. These results are consistent with the gross stoichiometry given in eq II.

$$2V(V) + P(I) \longrightarrow P(III) + 2V(IV) \qquad (II)$$

The formation quotient of the V(V)–P(I) complex was estimated photometrically at 260 nm, where the V(V) spectrum has a well defined shoulder. Ionic strength was maintained at 1 *M* with $LiClO_4$. P(I) concentrations were chosen to assure negligible V(V) reduction during the measurement, and hypophosphite anion concentrations, $[H_2PO_2^-]$, were calculated using the measured acid dissociation quotient[4] of hypophosphorous acid, $Q_A = 0.101 \pm 0.010$, in 1 *M* $LiClO_4$. Hydrogen ion concentration was adjusted with $HClO_4$, and the data taken over the range of $[H^+]$, 0.100–0.400 *M*, are presented in Table I. Formation quotients were obtained from the slopes of least-squares fits of the expression $[A_{260} - \epsilon_V V(V)]/[H_2PO_2^-]$ as a function of A_{260}. The average value over the range of $[H^+]$ is $Q_f(VO_2H_2PO_2) = 16.6 \pm 2.2$. A referee has suggested that H_3PO_2, as well as $H_2PO_2^-$, may form a complex with VO_2^+ that could be detected as an increase in the apparent formation quotient with increasing $[H^+]$. While we observed no systematic trend in the quotients, the uncertainty in the average value of Q_f permits us to estimate an upper bound for the formation quotient of a complex between VO_2^+ and H_3PO_2, $Q_f(VO_2H_3PO_2^+) < 1.4$.

Kinetics were followed at 350 nm on a Beckman DU spectrophotometer equipped with a thermostated cell holder; absorbances after 10 half-lives were about 4% of the initial absorbance. Individual runs, flooding with hypophosphorous and perchloric acids, were cleanly first order in V(V). The pseudo-first-order rate constants were essentially constant over the range of initial V(V) concentrations, 1.01–16.2 $\times 10^{-3}$ *F*, and were reproducible to ±4%. Addition of product H_3PO_3 or

(8) F. J. C. Rossotti and H. Rossotti, *Acta Chem. Scand.*, **10**, 957 (1956); C. F. Wells and L. V. Kurtisyn, *J. Chem. Soc. A*, 1372 (1970).

(9) R. T. Jones and E. H. Swift, *Anal. Chem.*, **25**, 1272 (1953).

Table II: Pseudo-First-Order Rate Constants (25°)

$[H^+]$, M	P(I), F	$[H_3PO_2]$, M	$k \times 10^4$, sec^{-1} Obsd	Calcd[a]
		$LiClO_4$ Medium		
0.501	0.140	0.117	0.618	0.618
0.501	0.281	0.234	1.26[b]	1.24
0.499	0.421	0.350	1.94	1.87
0.500	0.702	0.584	3.16[b]	3.31
0.501	0.702	0.584	3.23[b]	3.31
0.503	0.983	0.819	4.98	4.98
0.503	1.122	0.934	6.03	5.89
0.512	1.404	1.173	8.07[b]	8.07
0.251	0.702	0.501	1.84	1.71
0.376	0.702	0.553	2.59	2.56
0.626	0.702	0.604	3.93	3.98
0.750	0.702	0.619	4.53	4.57
1.00	0.702	0.638	5.72	5.56
0.301	0.281	0.210	0.908	0.871
0.751	0.281	0.248	1.53	1.54
0.998	0.281	0.255	1.79	1.75
0.300	0.562	0.420	1.59	1.64
0.309	0.562	0.423	1.62	1.69
0.301	0.842	0.630	2.44[b]	2.50
0.302	0.981	0.735	2.96	2.97
		$NaClO_4$ Medium		
0.489	0.1875	0.155	0.798	0.814
0.467	0.1875	0.154	0.811[b]	0.794
0.501	0.1875	0.156	0.858	0.824
0.489	0.1875	0.155	0.767[b]	0.814
0.506	0.1875	0.156	0.763	0.829
0.509	0.1875	0.157	0.752	0.831
0.501	0.375	0.312	1.64	1.66
0.509	0.500	0.417	2.43	2.29
0.208	0.301	0.203	0.710	0.681
0.272	0.301	0.220	0.865	0.854
0.342	0.301	0.232	1.07[b]	1.02
0.497	0.301	0.250	1.35	1.32
0.732	0.301	0.265	1.64[b]	1.65
0.966	0.301	0.273	2.09	1.88
0.483	0.101	0.0835	0.397	0.443

[a] Median deviation, 3.3%. [b] Average of two runs.

$VO(ClO_4)_2$ in excess of the stoichiometric limits had no effect on the rates.

Results and Discussion

Complexes of VO_2^+ with mononegative ions appear not to have been extensively studied. Evidence has been reported of chloro and bisulfato complexes[10] but quantitative data are lacking. Kinetic evidence of complex formation between organic reductants and VO_2^+ has been reported: formation quotients of about 1.6 for VO_2^+ complexes with *n*-butyraldehyde and propionaldehyde can be inferred[11] and a quotient of 84 has been reported[12] for the 1:1 complex of atrolactic acid, $C_6H_5C(CH_3)OHCOOH$, and VO_2^+; the formation quotient for the complex between the proton and hypophosphite anion is, of course, $Q_A^{-1} = 10$. Our value of $Q_f(VO_2H_2PO_2) = 16.6$ appears reasonable.

The rate law, obtained from 44 observed pseudo-first-order rate constants, $k(\text{sec}^{-1}) = -\text{d ln}(A - A_\infty)_{350}/\text{d}t$, is

$$\text{rate} = [VO_2^+][H_2PO_2^-][H^+] \times \{k_0 + k_1[H_3PO_2] + k_2[H_3PO_2]^2\}$$

where

$$\text{rate} = -\text{d}[V(V)]/\text{d}t$$

$$[VO_2^+] = [V(V)]/(1 + Q_f[H_2PO_2^-])$$

and

$$[H_2PO_2^-] = Q_A[P(I)]/(Q_A + [H^+])$$

The rate constants, $k_0 = 5.5 \pm 0.4 \times 10^{-3}$, $k_1 = 14.6 \pm 0.9 \times 10^{-3}$, and $k_2 = 7.5 \pm 0.7 \times 10^{-3}$, were obtained by computed least-squares fit of the expression, $k[V(V)]/[H_2PO_2^-][VO_2^+][H^+]$, equivalent to the factor in braces in the rate law, to a function of $[H_3PO_2]$ and $[H_3PO_2]^2$. The observed and calculated pseudo-first-order rate constants in perchlorate media, ionic strength 1 M, are presented in Table II. The data obtained in $NaClO_4$ are somewhat more scattered than those in $LiClO_4$ but there is no significant difference in the results.

The reaction of V(V) and P(I) rapidly induces the polymerization of acrylonitrile in 1 M $HClO_4$, whereas neither V(V) nor H_3PO_2 alone induces appreciable polymerization at this hydrogen ion concentration. Several other tests were performed to detect the influence of trace species on the kinetics; the results are summarized in Table III. Under an atmosphere of O_2, the reaction is slightly slower than under N_2: $k(O_2)/k(N_2) = 0.96$. In the presence of ethanol, 4% v/v, the reaction is accelerated: $k(\text{EtOH})/k(N_2) = 1.11$; in the absence of H_3PO_2, V(V) is not reduced. The polymerization of acrylonitrile is strongly indicative of free radical intermediates. Littler and Waters[13] have shown that oxidation of alcohols, diols, ketones, and phenols proceeds through acid-catalyzed mechanisms generating free radicals; in their study of the pinacol–V(V) reaction both acrylonitrile polymerization and a negligible effect of O_2 on the rate were found. However, the presence of free radical intermediates does not preclude the possibility of a two-electron reduction of V(V) as well. Such a step has been proposed[14] to explain the term, first order in mercaptosuccinic acid, in the rate law for the decomposition of the V(V)–2-mercaptosuccinate complex to form disulfides.

(10) L. G. Sillen and A. E. Martell, "Stability Constants," Special Publication No. 17, The Chemical Society, London, 1964.

(11) J. R. Jones and W. A. Waters, *J. Chem. Soc.*, 352 (1963).

(12) J. N. Kar, G. B. Behera, and M. K. Rout, *J. Indian Chem. Soc.*, **46**, 400 (1969).

(13) J. S. Littler and W. A. Waters, *J. Chem. Soc.*, 1299 (1959); 3014 (1959).

(14) W. F. Pickering and A. McAuley, *J. Chem. Soc. A*, 1173 (1968).

Table III: Influence of the Trace Species on the Rate. Initial V(V) = 6.09×10^{-3} *F*, $[H^+] = 0.626$ *M*, $[H_3PO_2] = 0.604$ *M*

Trace species	$k \times 10^4$, sec^{-1}	$R_0 \times 10^6$, $M\ sec^{-1}$
N_2 (1 atm)	3.93	2.39
O_2 (1 atm)	3.77	
C_2H_5OH (4% v/v)	4.35	
Cl^- (4.4×10^{-4} *F*)	3.72	
Ag^+ (4.0×10^{-5} *F*)		4.1

The V(V)–P(I) reaction is slightly retarded by 4.4×10^{-4} *F* HCl: $k(Cl^-)/k(N_2) = 0.95$. The negligible effect of trace $[Cl^-]$ is compared with the third-order dependence[15] of the rate of V(V) oxidation of alcohols on $[Br^-]$ in 0.1 *F* Br^-, which was interpreted in terms of the formation of V(V)–Br^- complexes. In our study, investigations at higher chloride concentrations were not undertaken.

The reaction is Ag^+-catalyzed: in 4.0×10^{-5} *F* $AgNO_3$, the initial rate is doubled and the rate law is nearly zero order in V(V). The Ag^+-catalyzed initial rate is about 10^{-3} that found[2a] for the tautomerization of free H_3PO_2 at this acidity. Mitchell[16] found that in silver ion concentrations greater than about 2×10^{-2} *F* the rate of H_3PO_2 oxidation by Ag^+ is independent of the silver ion concentration and is the same as the rate of tautomerization of H_3PO_2. This and the apparent zero-order dependence of the rate on V(V) in 4×10^{-5} *F* Ag^+ support the conjecture of Rao and Gowda[5] that Ag^+ catalysis proceeds by the reaction sequence given in eq III and IV.

$$Ag^+ + H_3PO_2 \longrightarrow Ag^0 + P(II) \qquad (III)$$

$$Ag^0 + V(V) \longrightarrow Ag^+ + V(IV) \qquad (IV)$$

The oxidation of H_3PO_2 by complex-forming cationic species differs from its oxidation by neutral or anionic species in the possibility of forming polyhypophosphito complexes with the oxidant. In the recent study[3a] of the oxidation of H_3PO_2 by Ce(IV), the rate data were interpreted in terms of an acid-catalyzed tautomerization of hypophosphite in Ce(IV)–P(I) complexes of the form $Ce(H_2PO_2)_n^{(4+)-n}$, $n = 1, 2, 3$. Although we have clear evidence only for the first $H_2PO_2^-$ complex with VO_2^+, formation of higher complexes with VO_2^+ seems plausible.

Formation of the $VO_2H_2PO_2$ complex is too fast to follow conventionally and rates of V(V) reduction are less than 10^{-3} those found[2a] for the tautomerization of free H_3PO_2, suggesting that oxidation of free, tautomerized $HP(OH)_2$ by VO_2^+, if it occurs, must be much slower than oxidation by, for example, the halogens. The form of the rate law suggests that the formation of the observed complex is followed by parallel, competing sequences of reactions. As usual, kinetics leave ambiguity in the order of multiple-step sequences. The k_0 term corresponds to the direct protonation of the complex by H^+ followed by a tautomerization step in which water abstracts a phosphinic proton. No evidence was found of a term corresponding to reaction of the neutral, unprotonated complex such as was found in the Cr(VI)–P(I) kinetics.[4] Similarly, the k_1 and k_2 terms correspond to protonation of the two neutral complexes, $VO_2(H_2PO_2)(H_3PO_2)$ and $VO_2(H_2PO_2)(H_3PO_2)_2$, followed by H^+ abstraction by water. An alternative possible mechanism involves hypophosphite anion abstraction of a phosphinic proton from doubly charged complexes such as $VO_2H(H_3PO_2)^{2+}$ and $VO_2H(H_3PO_2)_2^{2+}$. The high ionic charge and the absence of evidence for a kinetic term of the form $k_H[H^+]$ lead us to doubt the formation of doubly charged, protonated complexes such $VO_2H(H_3PO_2)^{2+}$ and $VO_2H(H_3PO_2)_2^{2+}$ considered above. In addition, the neutral $VO_2(H_2PO_2)(H_3PO_2)$ and $VO_2(H_2PO_2)(H_3PO_2)_2$ are more nearly analogous to the sulfato–V(V) complexes reported.[17] Our rate law is similar to that observed in the Ce(IV)–P(I) reaction[3a] except that the Ce(IV) complexes were of the unprotonated form, $Ce(H_2PO_2)_n^{4-n}$, due presumably to the high charge on these ions.

It is not possible to conclude that the tautomer, $HP(OH)_2$, does not react with V(V); however, the rates of oxidation of hypophosphorous acid by V(V) and by Cr(VI) are 10^{-2} and 10^{-3} the rate of tautomerization of free H_3PO_2, and the rate laws show no evidence of an oxidant-independent term. Thus the rate of oxidation of free tautomer, $HP(OH)_2$, by V(V) and by Cr(VI) must be, at most, 10^{-2} and 10^{-3} the rate of $HP(OH)_2$ oxidation by oxidants for which the rate law is zero order in the oxidant. We interpret this in terms of a rate-limiting formation of a complex between the tautomer and V(V) or Cr(VI) prior to the oxidation step. The equilibrium constant for formation of the tautomer has been estimated to be 10^{-9} to 10^{-11},[2b] leading to rate constants for oxidation of the free tautomer by halogens, for example, of the order of 10^8 to 10^{10} M^{-1} sec^{-1}. Rates of formation of V(V) and Cr(VI) complexes with an oxy-ligand such as H_2O_2[18] are much slower, with second-order rate constants 10^2 and 10^4, respectively. We attribute the reduced reactivity of H_3PO_2 to oxidation by V(V) and by Cr(VI), relative to the halogens, to the formation of a complex by either form of H_3PO_2 prior to the oxidation step.

Acknowledgments. We express our thanks to the Research Corporation and Bucknell University for grants in partial support of this work.

(15) K. Julian and W. A. Waters, *J. Chem. Soc.*, *A*, 818 (1962).

(16) A. D. Mitchell, *J. Chem. Soc.*, **123**, 629 (1923).

(17) J. S. Littler and W. A. Waters, *ibid.*, 4046 (1959); H. S. Mishra and M. C. R. Symons, *ibid.*, 4411 (1962).

(18) M. Orhanovic and R. G. Wilkins, *J. Amer. Chem. Soc.*, **89**, 279 (1967).

Electron Paramagnetic Resonance Studies of Carbon Monoxide Adsorbed on Thorium Oxide

by Wallace S. Brey, Jr.,* R. B. Gammage, and Y. P. Virmani

Department of Chemistry, University of Florida, Gainesville, Florida 32601 *(Received July 15, 1970)*

Publication costs borne completely by The Journal of Physical Chemistry

Adsorption of carbon monoxide on well-outgassed thorium dioxide at room temperature leads to the production of several radical species. Species A, formed first, may be related to the presence of impurities on the surface and has a lifetime of only a few minutes. In a rate process which continues over several days there are produced two interconvertible radicals, B, having an asymmetric g tensor, and C, having an axially symmetric tensor. At higher pressures, the equilibrium between the two radicals is temperature dependent, but pumping out excess CO causes conversion into radical C, as does the presence of water vapor. Following evacuation, the intensity of the signal of C grows slowly over a period of several hundred hours, and thus this species must arise from very tightly bound carbon monoxide. Increasing the temperature causes a sequence of reactions to occur on the surface, in contrast to the behavior of CO on MgO. Species D, stable around 100°, has some resemblance to species A and may represent nearly neutral or somewhat positive CO. It gives way, at about 200°, to species E, the spectrum of which indicates that it is CO_2^-. Following heat treatment of the sample at any temperature from 150 to 350°, a signal of low g value is observed, and its appearance seems to be at the expense of the adsorbed radicals. Finally, at about 500°, the adsorbate signal gives way to one which is characteristic of carbon.

Introduction

It is unexpected that the chemisorption of CO at room temperature on a stoichiometric, nonconducting and unirradiated oxide should produce a radical. Lunsford and Jayne[1] have reported that CO interacts with a well-outgassed MgO surface to produce a radical with uniaxial anisotropy of the g factor and with bonding of the type found in metal carbonyls, but this process was shown to be related to the presence of iron. Several nitro compounds adsorbed at the clean MgO surface also form radical ions, the suggestion being made by Tench and Nelson[2] that surface oxide lattice ions act as electron donors to adsorbed molecules with sufficiently high electron affinities (>0.5 eV).

Electron paramagnetic resonance evidence is here presented to show that CO can be adsorbed at the well-outgassed surface of ThO_2 to produce radicals. In relation to the conditions of adsorption leading to the paramagnetic state and the effects of pumping off the chemisorbed CO at elevated temperatures, it is relevant to mention previously reported studies of CO adsorbed on ThO_2 at elevated temperatures. Claudel, *et al.*,[3] have made a kinetic and conductivity study of CO oxidation by O_2 at the ThO_2 surface between 250 and 450°. They report that on the bare surface CO is adsorbed and O_2 is not. The CO is desorbed unchanged at 338° when O_2 is absent. The first reaction intermediate in the oxidation was believed to be adsorbed CO^+. In an infrared study of CO adsorbed at 240°, Pichat and Mathieu[4] found evidence for an OCO complex according to the spectrum of thorium formate. Disproportionation of CO at the ThO_2 surface becomes predominant at higher temperatures. Roberts, *et al.*,[5] claim, however, that at 850° the decomposition cannot be represented simply by the reaction $2CO \rightarrow CO_2 + C$ because CO_2 was produced in excess of the expected amount. The evidence pointed to the loss of surface oxygen; a rapid initial loss of 10–20% of the oxygen in the ThO_2 surface was followed by further loss of oxygen as carbon deposition proceeded. In view of this evidence it is, perhaps, not surprising that a variety of paramagnetic states should have been encountered in the present study of CO adsorbed on ThO_2.

Experimental Section

Materials. A high-purity sample of ThO_2 powder, supplied by A.E.R.E., Harwell, was used in this study. Spectroscopic analysis of the thoria, carried out at Oak Ridge National Laboratories, indicated the principal impurities to be 14 ppm Fe, 26 ppm Cu, and 19 ppm Cr. The specific surface area, measured by adsorption of nitrogen, was originally 7.8 m^2/g. After the sample was heated under vacuum at 1000°, as for the standard conditioning prior to CO adsorption, the BET area had fallen to 3.8 m^2/g.

(1) J. H. Lunsford and J. P. Jayne, *J. Chem. Phys.*, **44**, 1492 (1966).

(2) A. J. Tench and R. L. Nelson, *Trans. Faraday Soc.*, **63**, 2254 (1967).

(3) B. Claudel, F. Juillet, Y. Trambouze, and J. Veron, *Proc. Third Int. Congr. Catal., 1964*, **1**, 214 (1965).

(4) P. Pichat and M. V. Mathieu, *ibid.*, **1**, 224 (1965).

(5) L. E. J. Roberts, A. J. Walter, and V. J. Wheeler, *J. Chem. Soc.*, 2472 (1958).

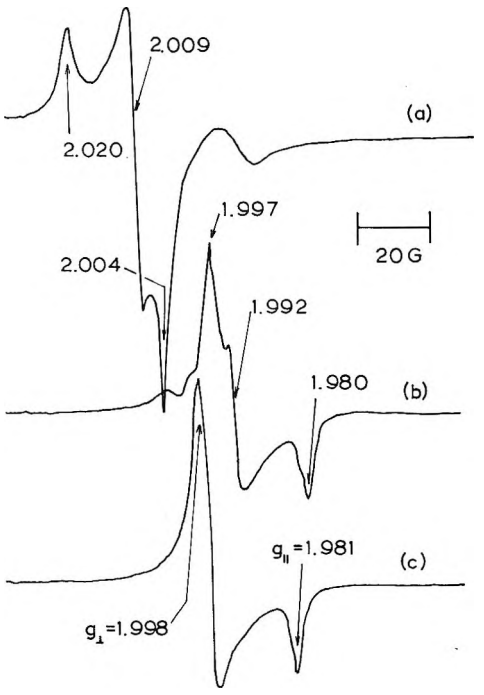

Figure 1. Epr derivative spectra: a, adsorbed CO on degassed ThO_2 at 100°K 5 min after admission of 100 Torr of gas at room temperature; b, same system at 100°K, after allowing the spectrum to develop for 240 hr at room temperature; c, same as for b, but with the spectrum obtained with the sample at 298°K.

The source of carbon monoxide was Matheson CP grade of stated minimum purity 99.5%. Infrared analysis revealed a trace of CO_2. On route to the CO reservoir attached to the vacuum system, the gas was passed in turn through soda lime and a cold trap at −196° to ensure the absence of CO_2 and H_2O.

Preparation. The powders were contained in the usual type of silica epr tube which could be evacuated through a stopcock which was lubricated with Apiezon T grease. The ThO_2 was outgassed overnight at 1000° to $<10^{-6}$ Torr. During the process of cooling the powder to room temperature and admitting the CO, a cold finger in the near vicinity of the powder was cooled with liquid nitrogen to minimize pickup of water vapor.

Electron Paramagnetic Resonance Spectroscopy. A conventional spectrometer (Varian 4502-14) was used to obtain the epr data. Operation was at 9.3 kMHz (X-band) with 100-kHz field modulation. A dual sample cavity was used, operating in the TE mode, with variable temperature assembly. A g value of 2.0036 was taken for the reference substance, DPPH, and g values are given relative to this standard. In some cases a sample of pitch with a g value of 2.0028 was used as the intermediate reference, to which samples were directly compared. The microwave power and field modulation were selected as optimum values for a particular signal or series of signals. The samples were in general cooled to 100°K before recording the spectra, but in several cases recordings were made with a sample at room temperature. For species with anisotropic g tensors, the principal g values were estimated according to the method of Kneubühl.[6] In view of the effects of adsorbed CO on γ-irradiated porous glass which have been reported,[7] checks were made to determine that epr signals were absent from sample tubes containing CO alone. In addition, blank determinations, with oxide but without CO, indicated that signals did not arise from the stopcock lubricant.

Results

Resonances in the Oxide. After outgassing the ThO_2 powder at 1000°, only an extremely weak absorption having a g value of about 2.005 was observed. At the spectrometer settings used to record the signals from the absorbed CO, this same signal was invisible. Treatment of the oxide with electromagnetic radiation (uv, X-, or γ rays) invariably produced a strong symmetrical line (signal G) with a g value of 1.969. The center was spin-lattice relaxed and its signal was absent from the spectrum at room temperature although easily seen at 100°K. It is likely that this is associated with an impurity cation which became paramagnetic during sample bombardment. The F center in single crystal ThO_2[8] possesses the same mean g value but is observable at room temperature and is readily bleached, unlike the center observed with the present sample of ThO_2.

CO Adsorbed at Room Temperature. When CO at 100 Torr pressure is allowed to adsorb on the clean ThO_2 at room temperature, two resonances are observed. We shall designate these signals A and B and apply the same letters to the species responsible for these signals. These are shown in Figures 1a and b. Signal A is characteristic of a center with an anisotropic g tensor, the principal components of which have values greater than the free electron value. The g values have been listed in Table I.

Species A has only a transient existence. Efforts to detect this signal immediately after admission of the CO, are usually, but not always, successful. Within 15 min of the entry of the CO, signal A decreases to a barely detectable level at the usual spectrometer settings. The variability in signal A is perhaps associated with the thoroughness with which the thoria surface has been cleaned and maintained clean to the instant of admitting the CO. Actually, it is impossible to maintain ThO_2 completely free of contamination on cooling from 1000°. The surface acts as an extremely effective desiccant, picking up water from other surfaces in the vacuum system.[9] One must accept the fact that a

(6) F. K. Kneubühl, *J. Chem. Phys.*, **33**, 1074 (1960).

(7) G. M. Muha and D. J. C. Yates, *J. Phys. Chem.*, **70**, 1399 (1966).

(8) V. I. Neeley, J. B. Gruber, and W. J. Gray, *Phys. Rev.*, **158**, 809 (1967).

(9) E. L. Fuller, Jr., H. F. Holmes, and C. H. Secoy, *J. Phys. Chem.*, **70**, 1633 (1966).

Table I: Values of g for CO on ThO_2 Following Various Treatments

Treatment	Spectrum at 100°K				Spectrum at 298°K		
	Signal	g_1	g_2	g_3	Signal	$g_{\|\|}$	$g_\perp$
Adsorption of 100 Torr CO at 298°K; spectrum recorded immediately	A	2.004	2.009	2.020			
Sample above after full growth of spectrum	B	1.980	1.992	1.997	C	1.982	1.999
Adsorption of 100 Torr CO at 298°K for 1.5 hr, followed by pumping of excess CO	C	1.981	1.998	1.998	C	1.982	1.998
Simultaneous adsorption of 100 Torr CO and 0.18 Torr H_2O at 298°K	B	1.980	1.991	1.996			
Above, followed by 24 Torr added H_2O after several hours	C	1.981	1.998	1.998	C	1.982	1.998
Simultaneous adsorption of 50 Torr CO and 0.08 Torr O_2 at 298°K	B	1.980	1.993	1.997			

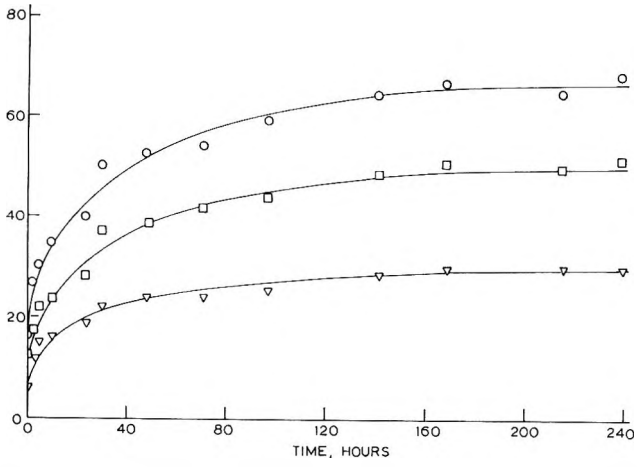

Figure 2. Growth of the three components of signal B for CO on thoria at room temperature and a pressure of 100 Torr CO. Ordinate is an arbitrary intensity.

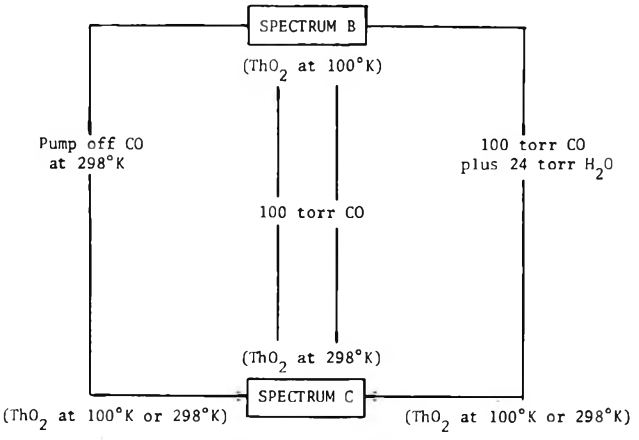

Figure 3. Scheme of interconversion of spectra B and C for adsorbed CO under various conditions.

small amount of water will have been picked up by the thoria surface before there is any possibility of adsorbing CO on the thoria at room temperature.

For signal B (Figure 1b), the g tensor is anisotropic with principal values below the free electron value. Signal B was never detected immediately following the admission of CO. However, it grows with time over a period of more than 100 hr. As signal B builds up to maximum intensity, there appear the first signs of signal G with $g = 1.969$. Also, in Figure 1b, a remnant of the decayed signal A can be seen to the low-field side of signal B. The rate of growth of signal B is shown in Figure 2. Each of the three components in the first derivative trace grows at the same rate, and this fact is strongly indicative of a single type of radical with an asymmetric g tensor. The process, not surprisingly, is temperature dependent. If the ThO_2–CO system is held at 100°K, no signal develops. Microwave saturation studies showed power effects at an attenuation of 20 db, the saturation effect on signal B becoming severe below 10-db attenuation.

Effects of Evacuation, Addition of Other Gases, and Variation in Temperature. Several variations of the original CO adsorption experiment were carried out. These included recording the spectra with the sample temperature at 298°K, pumping out the CO at room temperature, and the addition of water, oxygen, or carbon dioxide before or after adsorption of the CO. When mixtures of gases were employed for adsorption, the volume of vapor was always much larger than the amount adsorbed, so that no appreciable change in concentration of the mixture occurred.

On recording the spectrum with the sample at 298°K and under 100 Torr of CO, a new signal labeled C could be seen, as shown in Figure 1c. The g values, Table II, indicate axial symmetry. Recooling the sample to 100°K brings the return of signal B. This easy transi-

Table II: Value of g at 100°K for CO on ThO_2[a]

Outgassing temp, °C	Signal C		Signal D		Signal E		Signal F	Signal G
	$g_{\|\|}$	$g_\perp$	$g_{\|\|}$	$g_\perp$	$g_{\|\|}$	$g_\perp$	g	g
25	1.981	1.998	...	...	...	...	...	1.969
60	1.982	1.999	...	...	...	...	...	1.969
100	...	...	2.008	2.013	...	2.003	...	1.970
150	...	...	2.007	2.012	1.997	2.004	...	1.969
200	...	...	...	2.012	1.997	2.004	...	1.969
250	...	...	...	...	1.997	2.004	...	1.969
300	...	...	...	...	1.997	2.004	...	...
350	...	...	...	...	1.996	2.004	...	...
500	...	...	...	...	...	2.003	2.003	...

[a] The sample was pumped for 30 min while heating at each successively higher temperature.

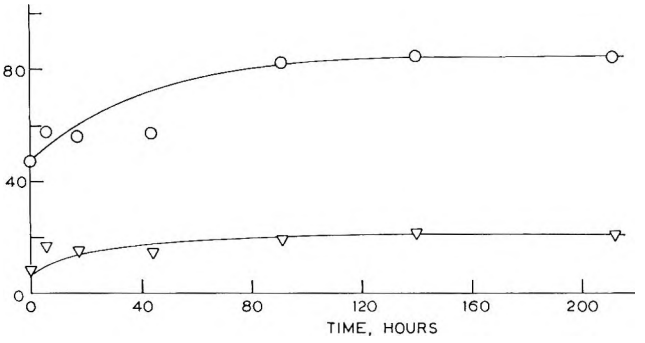

Figure 4. Growth of the two components of the signal C after adsorbing CO at 100 Torr for 1.5 hr and then pumping off the CO.

tion by temperature variation between the species responsible for B and C is stopped, in favor of the species C, upon pumping out the CO at room temperature. Signal C can now be recorded with the sample at either 100 or 298°K. These changes are shown in the schematic presentation of Figure 3.

The transition between species B and C can be affected by other factors, such as by the presence of H_2O. If a small amount of water vapor (0.18 Torr) is mixed with the CO prior to its adsorption on the ThO_2, spectrum B develops as before. However, if the sample is then exposed to additional water vapor at about 24 Torr, signal B is no longer obtained. Instead signal C is recorded with the sample at 100 and 298°K. The effect is sketched in Figure 3. It is clear that large amounts of water vapor have the capacity to stabilize structure C even in the presence of 100 Torr of CO. Under these circumstances it is visualized that water has somehow been adsorbed in the proximity of the radical species responsible for C to prevent the interconversion. If the water vapor at 25 Torr pressure is mixed with the CO before adsorption, then the radicals do not appear. A trace of oxygen (0.08 Torr) added to the CO does not prevent signal B from developing although the resolution is adversely affected. On the other hand, addition to the CO of 10% O_2 is sufficiently detrimental to prevent any observable paramagnetism. The remaining contaminant to be studied, CO_2, had no effect on the development of signal B. It was also determined that the adsorption of pure CO_2 produced no esr spectrum.

The radical responsible for signal C was examined in one more way. After allowing the signal B to grow in the usual way for 1.5 hr, the CO was pumped out to produce, as always, signal C. The intensity of signal C was then measured at intervals over 200 hr, the growth being shown in Figure 4. The increase in intensity is about twofold over this period of time. It would appear that the radical giving signal C is formed from strongly adsorbed CO molecules which are not removed in the evacuation procedure.

Effects of Evacuation at Elevated Temperature. Initially the spectrum (signal B) was allowed to build to full intensity, while the ThO_2 was exposed to CO at 100 Torr pressure. The system was then evacuated at room temperature to give the spectrum designated C. The temperature of evacuation was then raised to 60° and subsequently in steps to 500°. Pumping was always for 0.5 hr at each temperature. Signal C was destroyed to be replaced in turn by species D, E, and F. The spectra are shown in Figures 5, 6, and 7, and the g values are listed in Table II. Spectrometer settings were standardized at suitable levels to observe all the lines and at the same time gauge the overall relative changes in signal intensity.

After heating at 60° there was a slight increase in the intensity of signal C, which is seen in Figure 5. This same species was unstable at 100°; signal C had given way to a weaker broad band together with a new and much stronger signal D. The first signs of signal E were also evident. The species responsible for D and E appear to be radicals with g tensors that are axially symmetric. Signals for the temperature range 150–250° are shown in Figure 6. As the temperature is increased to 150° and then to 200°, the intensity of signal D is reduced drastically while signal E grows in intensity. In saturation studies both D and E signals show weakening and broadening effects for microwave

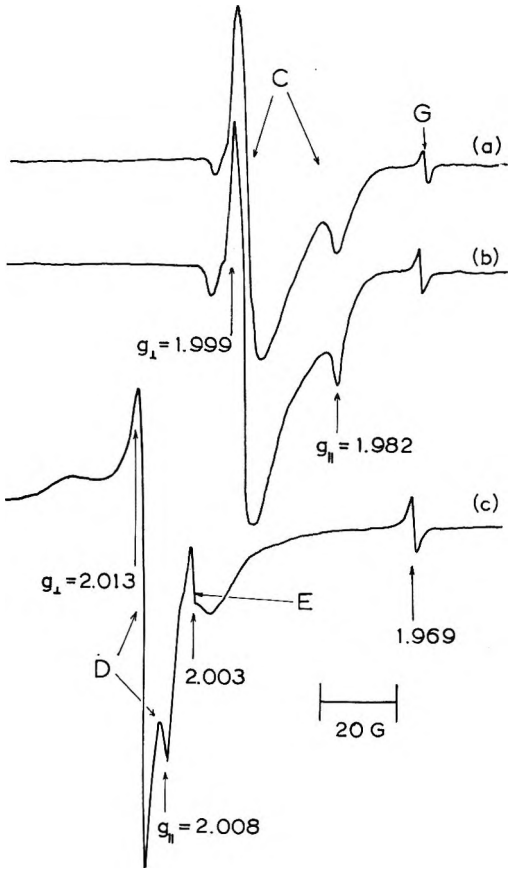

Figure 5. Epr derivative spectra (100°K) of adsorbed CO on degassed ThO_2 after pumping on the sample in sequence: (a) for 0.5 hr at room temperature, (b) then for 0.5 hr at 60°, (c) then for 0.5 hr at 100°.

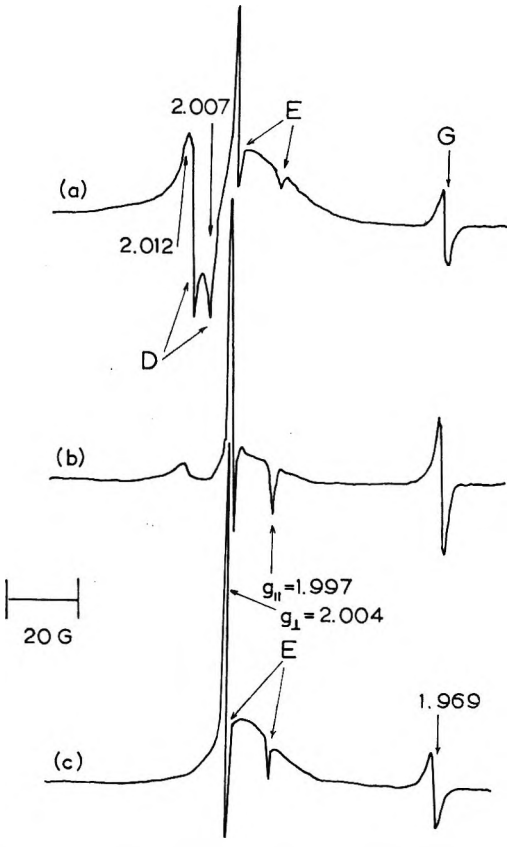

Figure 6. Epr derivative spectra (100°K) of adsorbed CO on degassed ThO_2 after pumping on the sample at up to 100° and: a, for 0.5 hr at 150°; b, then for 0.5 hr at 200°; c, then for 0.5 hr at 250°.

attenuations of 10 db or less. An interesting feature is that, concurrent with the loss in intensity of signal D to 200°, signal G at g = 1.969 increases about fivefold in intensity (Table II). On increasing the temperature from 200 to 350° in 50° steps, little further change occurs in the intensity of signal E. The paramagnetic cation or F center (signal G), however, no longer grows, but, as the temperature is extended beyond 200°, is returned to its diamagnetic state, the bleaching being completed at 350°.

The species with spectrum E has considerably more temperature stability than its predecessors. First appearing after heating at 100°, the center appears stable at temperatures up to 350°. The derivative signal from this center is very sharp (Figure 7) with $g_{||}$ and $g_\perp$ having values of 1.996 to 1.997 and 2.003 to 2.004, respectively. The narrowness of the line indicates that the center is sparsely distributed on the surface, so that there is very little dipole–dipole broadening.

After the sample is heated and pumped at 500°, there is evidence that reaction has taken place to yield carbon. The spectrum, shown in Figure 7, contains a symmetrical signal of peak to peak width 15 G, designated F. Superimposed on this is a remnant of

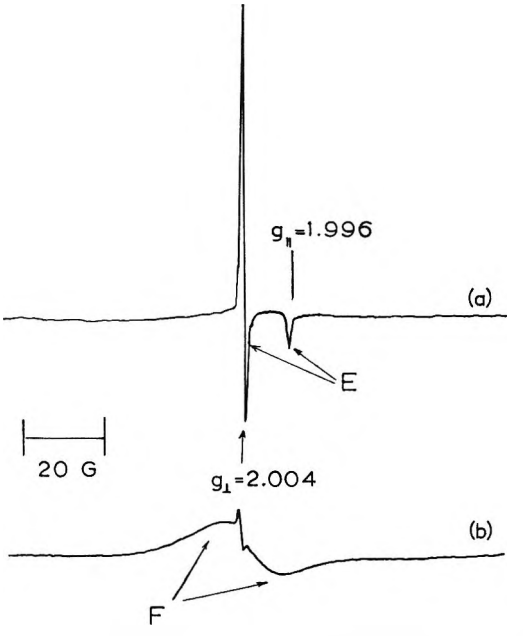

Figure 7. Epr derivative spectra (100°K) of adsorbed CO on degassed ThO_2 after pumping on the system at temperatures up to 300° and: a, for 0.5 hr at 350°; b, then for 0.5 hr at 500°.

signal E observed after the evacuation at 350°. Signal F is a single line with g = 2.003 and line shape

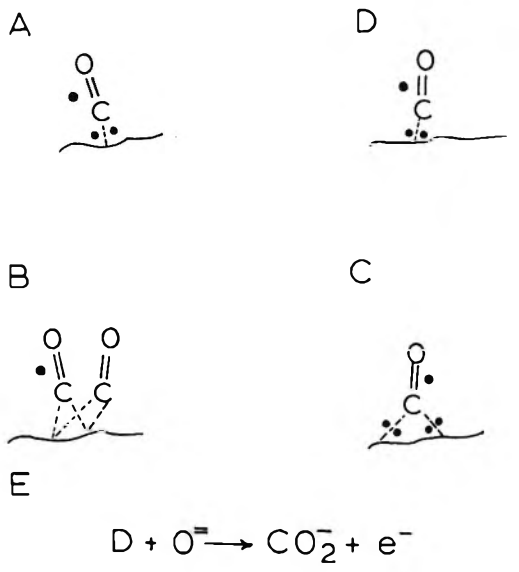

Figure 8. Assignment of carbon monoxide surface structures to observed epr signals. See text for description.

nearly Lorentzian. Raising the observation temperature from 100 to 298°K leaves the signal F unchanged in position and width.

Discussion

The initially formed and short-lived species A has a signal which resembles somewhat the resonance reported by Lunsford and Jayne[1] for carbon monoxide on magnesium oxide containing iron impurities. They observed values of 2.0021 for $g_{||}$ and 2.0055 for $g_{\perp}$ and proposed that the radical formed is neutral or slightly positive, with the adsorbate donating an electron pair to the oxide and receiving in return an electron in an antibonding π orbital, much as in the formation of a metal carbonyl. This structure is represented in "A" of Figure 8. A completely consistent picture of the nature of the defects on which the molecule is adsorbed could not be established, but it was proposed that the defect was either the ferric ion or a center for which the ferric ion acted as charge compensator. In the present material, there is not enough iron present to explain the number of adsorption sites, but formation of a similar complex is indicated. The rapid rate of formation of signal A compared to signals B and C indicates that A corresponds to molecules adsorbed on pre-existing surface defects which have immediately available an unpaired electron.

The slow growth of signals B and C and the fact that growth occurs in the absence of excess gaseous CO indicate that it is a diffusion process rather than the adsorption process which is the rate-determining step in the process of generating the species responsible for them. The most probable mechanism for this slow process is the diffusion of a bulk defect to the surface to combine with an adsorbed molecule. The initial adsorption of CO on the ThO_2 is so strong that pumping off the adsorbate at room temperature leaves bound molecules which can slowly convert into the radical species as shown by the curves in Figure 4.

A remarkable relationship exists between species B and C. While the pressure of CO is maintained at 100 Torr, transition between the two can be made at will simply by varying the temperature between 100 and 298°K. Furthermore, the structure C can be locked in by either of two procedures: simply by pumping out the CO or by adsorbing water along with species C in the presence of 100 Torr of CO. This behavior is consistent with a model in which the structure responsible for signal B consists of the species responsible for C plus an additional CO molecule adsorbed at the same site. The second molecule can only be added at low temperature and if water is absent, and when this second molecule is present, it slightly modifies the signal of the paramagnetic molecule.

A possible structure for the tightly held species C is shown in Figure 8, together with one schematic version of a structure of B which includes a second molecule of CO as has just been described.

One species which must be considered as a possible result of reaction of CO with the surface is CO^+. The epr spectrum of this cation has not been reported, although the isoelectronic CN radical has been observed.[10] An axially symmetric g tensor would be expected. Claudel, *et al.*,[3] in studying the catalytic oxidation of CO on thoria, concluded that the initial step involved the formation of adsorbed CO^+. Conductivity and thermoelectric power measurements in the temperature range 250–450° supported their contention. It is therefore possible to assign signal D to the carbon monoxide cation, although the temperature range in which it is observed is somewhat lower than that reported by Claudel. However, it seems more likely that D, resembling A in the magnitudes of the g values, is a nearly neutral species, differing from C in that one bond of the two to the surface has been broken, as shown in Figure 8.

Radicals derived from CO_2 are also expected to be formed, particularly in view of the previous reports of reaction at the thoria surface.[4,5] The CO_2^- radical has been well characterized, both within single crystals[11] and as an adsorbed surface species.[12,13] In the crystal, the g values were found to be 1.9975, 2.0014, and 2.0032. For the radical on irradiated MgO, the principal values of the g tensor were 1.9974, 2.0017, and 2.0029. A spectrum observed for the product of reaction of CO with the surface of irradiated silica–alumina was again

(10) E. L. Cochran and F. J. Adrian, Fifth International Symposium on Free Radicals, Uppsala, 1961.

(11) D. W. Ovenall and D. H. Whiffen, *Mol. Phys.*, **4**, 135 (1961).

(12) J. H. Lunsford and J. P. Jayne, *J. Phys. Chem. Solids*, **69**, 2182 (1965).

(13) R. R. Hentz and D. K. Wickenden, *J. Phys. Chem.*, **73**, 817 (1969).

anisotropic with values of 1.9974, 2.0013, and 2.0024, and was assigned to CO_2^-. Although signal E seems to have axial symmetry, the observed g values of 1.997 and 2.003–2.004 are very close to those for CO_2^-, and a slight degree of asymmetry might be concealed by line breadth. Accordingly, we assign signal E to this species. It is interesting that Muha and Yates observed a signal of axial symmetry for CO on silica, reporting g values of 1.995 and 2.002.[14] It is quite probable that this was produced by the same species as that responsible for signal E. In the present system, the narrowness of the lines for signal E indicates that the center is sparsely distributed on the surface, so that there is very little dipole–dipole broadening.

Signal F is similar to a narrow (10 ± 3 G) resonance which is exhibited by charcoals and other low-temperature carbons prepared by charring organic matter below 600°.[15,16] There are also the same insensitivity to temperature change, isotropy of the g value, and line shape which are observed for signal F. It is therefore evident that the last step in the progressive elimination of adsorbed CO complexes is the formation of carbon of which at least a portion represents paramagnetically active centers. The somewhat broader line seen for the ThO_2 system might reflect sparsely distributed carbon centers which cannot participate in an exchange narrowing process.

In progressing through the series of species C, D, E, and F, there is found a continuous reduction in signal intensity. It is tempting to think that there is a chain of events in which each paramagnetic species is the precursor of the species appearing at the immediately higher reaction temperature, leading to the final products, carbon on the surface and CO_2 in the gas phase. Very significantly, this behavior is in contrast to that of CO on MgO, where the CO radicals seem to be removed as CO molecules, without decaying through a series of intermediates.

If species D is identified with CO^+, then the sequence of events is the formation of D by loss of an electron from C, followed by the reaction of D with an oxide ion in the surface to form CO_2^-, species E. An alternative sequence, applicable if D is the neutral species shown in Figure 8, is the formation of D by breaking one of the bonds from C to the surface, and its disappearance by reaction with surface oxide to yield CO_2^- plus an electron. In the final stage, carbon may be formed by disproportionation reactions, such as

$$2CO \longrightarrow C + CO_2$$

$$2CO + e \longrightarrow CO_2^- + C$$

or

$$CO_2^- + CO + e \longrightarrow C + O^{2-} + CO_2$$

Signal G, which does not enter the main sequence of adsorbate changes, must now be considered. One explanation for this signal is the presence of an F center, for the g value agrees with that of about 1.97 found in single-crystal thoria for such a center.[8] However, signal G is not observable at room temperature, which is contrary to the usual behavior of an F center, as well as to that in the single-crystal thoria. It is conceivable, although unlikely, that the relaxation time of the F center might be modified by disorder or strain in the polycrystalline lattice.

The way in which the signal appears, being made visible by γ irradiation in thoria which has been previously evacuated at 1000°, and then appearing and growing in intensity from room temperature up to 250° in the CO–thoria system, only to disappear at higher temperatures, suggests that it is associated with an impurity of variable valence. The analysis of the oxide indicates that this impurity is chromium, and indeed the g value corresponds to that of a resonance found in chromia–alumina mixtures.[17] It is, of course, possible that one is seeing an electron lost from the impurity and trapped in an F center, since anion defects do occur rather readily in fluorite-type lattices.[18]

Since signal G grows as species B, C, and D are formed, it appears that electrons are being removed from the impurity, which we believe to be chromium, and transferred to the adsorbed CO. When the temperature is high enough so that D reacts, signal G falls in intensity, presumably then because electrons are supplied to it. If D is a neutral species, if affords a source of electrons. This scheme appears to be fairly strong evidence that the sequence shown in Figure 8 is correct, since D as a neutral species can reasonably react to supply electrons as well as to form CO_2^-.

Acknowledgment. The epr spectrometer used in this research was purchased with the assistance of a National Science Foundation equipment grant to the University of Florida Department of Chemistry.

(14) G. M. Muha and D. J. C. Yates, *J. Phys. Chem.*, **70**, 1399 (1966).

(15) D. J. E. Ingram and J. E. Bennett, *Phil. Mag.*, **45**, 545 (1954).

(16) D. J. E. Ingram, Third Carbon Conference, Buffalo, N. Y., June 1957.

(17) D. G. Howard and R. H. Lindquist, *J. Chem. Phys.*, **38**, 573 (1963).

(18) Y. Haven, Proceedings of the British Ceramics Society, No. 1, July 1964, p 93.

Electron Spin Resonance of the *p*-Quaterphenyl Cation Radical

by Melvin Keith Carter

Shell Development Company, Emeryville, California 94608 *(Received October 19, 1970)*

Publication costs assisted by Shell Development Company

The *p*-quaterphenyl cation radical has been produced in liquid solution by chemical oxidation of the parent hydrocarbon. Partially resolved esr spectra, centered at $g = 2.00246 \pm 0.00002$, have been analyzed and the proton hyperfine splitting constants determined: $|a_4^H| = 1.94$ G, $|a_{3'}^H| = 1.83$ G, $|a_2^H| = 1.27$ G, $|a_{2'}^H| = 0.56$ G, $|a_3^H| = 0.10$ G, and $\Delta H = 0.52$ G. Some of the proton hyperfine splitting constants for the cation are smaller in absolute value than those of the corresponding anion. This surprising result is in contradiction with results of other even–alternate cation, anion radical pairs and is explained by assuming that the para-bonded aromatic rings of the cation radical do not all lie in the same plane of symmetry.

The *p*-quaterphenyl cation radical (see Figure 1) exhibits properties similar to the well known even–alternate cation radicals;[1] however, it does not appear to be totally planar. Radical cations such as those generated from naphthalene, anthracene, naphthacene, pentacene, perylene, pyrene, and dibenzo(*a*,*c*)-triphenylene[2] are categorized by the following descriptive properties. (1) They are generated from even–alternate hydrocarbons. (2) They exhibit two or more proton hyperfine splitting constants. (3) The proton hyperfine splitting constants for the cations have been found, in general, to be larger than those at the same ring position for the anions,[2] with the possible exception of the anomalous 2 position.[1] (4) They belong to the D_{2h} symmetry point group. (5) They have electron spin resonance (esr) spectral line widths in the range of 0.1–0.5 G.[3] 6. The proton hyperfine splitting constants are accurately described by the McConnell relationship[4]

$$a_k^H = Q\rho_{kk} \quad (1)$$

for which Q is a proportionality factor determined from experiment. In addition, the unpaired electron spin densities calculated from the Hückel molecular orbital (MO) theory are in excellent agreement with the spin densities derived from experiment assuming an average value of Q. It is the purpose of this article to show the differences between the experimentally determined hyperfine splitting constants of the cation and anion may be explained by assuming that the *p*-quaterphenyl cation radical is not completely planar and hence does not exhibit properties 3 and 4.

The esr spectra of the polyphenyl anion radicals have been studied extensively[5] and the coupling constants of some of them are well known.[6] Resolved esr spectra of the polyphenyl cation radicals have not been reported previously, presumably because they are more difficult to prepare. Unresolved esr spectra have been reported for the biphenyl cation radical in solution at low temperatures.[2,7] Single line spectra have also been observed for photoionized biphenyl in rigid sulfuric and boric acid glasses.[8]

To the best of the author's knowledge this article, which describes the preparation of the *p*-quaterphenyl cation radical in solution, is the first report of a polyphenyl cation radical in which a resolved spectrum has been observed.

Experimental Section

The chemicals employed in this study for the preparation of the *p*-quaterphenyl cation radical were 20% fuming sulfuric acid (ACS, reagent grade obtained from Baker and Adamson) and *p*-quaterphenyl (obtained from K and K Laboratories). The impurity level of *p*-quaterphenyl, determined by mass spectroscopic analysis, was much less than 0.5% in aromatic impurities and less than 1% in total organic impurities (up to a mass number of 500).

p-Quaterphenyl was dissolved at −10° in 20% fuming sulfuric acid in quantities sufficient to form a dark green solution. A portion of the solution was rapidly transferred to a cold melting-point capillary tube. The tube was sealed under vacuum at the temperature of boiling liquid nitrogen and maintained in liquid nitrogen

(1) G. Vincow, "Radical Ions," E. T. Kaiser and L. Kevan, Ed., Interscience, New York, N. Y., 1968, Chapter 4. A good review of cation radicals is presented.

(2) I. C. Lewis and L. S. Singer, *J. Chem. Phys.*, **43**, 2712 (1965), and references cited therein.

(3) The lines are broader for the cations than for the corresponding anions. See ref 2 (and references therein) and ref 6.

(4) (a) H. M. McConnell, *J. Chem. Phys.*, **24**, 362 (1956); (b) E. deBoer, *ibid.*, **25**, 190 (1956); (c) T. R. Tuttle, R. L. Ward, and S. I. Weissman, *ibid.*, **25**, 189 (1956).

(5) (a) K. H. Hausser, L. Mongini, and R. van Steenwinkel, *Z. Naturforsch. A*, **19**, 777 (1964); (b) A. Carrington, F. Dravnieks, and M. C. R. Symons, *J. Chem. Soc.*, **1959**, 947; (c) E. deBoer and S. I. Weissman, *J. Amer. Chem. Soc.*, **80**, 4549 (1958).

(6) A. L. Allred and L. W. Bush, *J. Phys. Chem.*, **72**, 2238 (1968).

(7) M. K. Carter and G. Vincow, *J. Chem. Phys.*, **47**, 292 (1967).

(8) M. K. Carter, *Diss. Abstr. B*, **27** (1966).

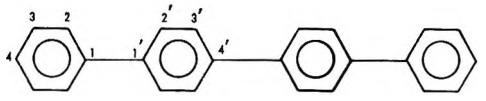

Figure 1. Molecular formula of *p*-quaterphenyl.

until ready for use. Samples which were warmed to room temperature turned blue in less than 2 min, possibly due to the formation of the dication. The blue solution was diamagnetic.

Electron spin resonance spectra were recorded using a Varian Associates Model V-4500 spectrometer with 100 kHz magnetic field modulation. Spectral spacings and g values were measured relative to a proton magnetic resonance signal using glycerin as a source of protons. The magnetic field strength was determined in the following manner. A reference signal from a Princeton Applied Research lock-in amplifier (Model JB-5) was amplified by a General Radio Company amplifier (Type 1206-B) which provided the modulation for an Alpha Scientific Laboratory nmr gaussmeter (Model AL-67).[9] The output was detected by the lock-in amplifier. The microwave frequency was determined by taking a portion of the microwave signal, through a Hewlett-Packard variable microwave attenuator (Model X-375A), producing a harmonic in a Hewlett-Packard transfer oscillator Model 540B and counting the frequency on a Hewlett-Packard electronic counter (Model 524D).[10,11]

Variable temperatures were generated using nitrogen gas cooled by liquid nitrogen in a heat exchanger. The cold gas was fed to the microwave cavity by a dewar sleeve. Temperatures were varied by changing the flow rate of the nitrogen gas and were measured at the cavity by means of a standardized copper–constantan thermocouple.[12]

Results

The esr spectrum of the green solution consists of 17 partially resolved components centered at $g = 2.00246 \pm 0.00002$. This spectrum, recorded at 6°, is ascribed to the *p*-quaterphenyl cation radical for which 5 proton hyperfine splitting constants are expected. The spectrum is strongly overlapped and the component widths change considerably with temperature and concentration of the radical in solution.[13] This situation is further complicated by the short lifetime of the radical ion in solution at room temperature (lifetime of the observed signal in the spectrometer is less than 2 min). At −5° the signal may be observed for 1 hr or more, although few hyperfine components are resolved at this temperature.

The best resolution is observed at +6° (see Figure 2a) where the intensity of the spectrum decays significantly during a 5-min scan (note the decrease in intensity on the high-field or right side of the spectrum). At this temperature the measured hyperfine splittings are $|a^H| = 1.86 \pm 0.01$, $|a^H| = 1.26 \pm 0.04$, and $|a^H| = 0.62 \pm 0.03$ G.[14,15] Component widths vary throughout the spectrum and are somewhat broader in the central portion of the spectrum. Measured components vary in width from 0.22 to 0.48 G. The spectrum displays a high degree of overlap of the individual components and thus can be analyzed quantitatively only in conjunction with an extensive overlap correction procedure.

A computer simulation overlap correction program[16] has been modified for use (in the Fortran V language) with a Univac 1108 computer. Input data consist of experimentally measured splittings, assumed line width, and number of spin 1/2 nuclei giving rise to each splitting. The program generates a first derivative esr spectrum using a Lorentzian line shape of constant width.[17] It measures the position, width, and relative height of each resolved component and tabulates the various splittings for each splitting constant. Averages of these splittings and line widths are compared with the experimental input data. If they do not agree new input parameters are systematically derived and the iterative procedure repeated until the measured splittings of a computed spectrum agree with the input data, or until a preselected number of cycles is reached. The complete spectrum and the overlap corrected values are tabulated and the final spectrum is plotted on a CalComp plotter.

A computer spectrum based on the hyperfine splitting constants $|a^H| = 1.88$, $|a^H| = 1.20$, $|a^H| = 0.56$, and $|a^H| = 0.10$ G (assumed) and line width $\Delta H = 0.56$ G[18] yields a plotted spectrum which is in fair agreement with the experimental spectrum. A spectrum is

(9) The accuracy of the field measurement is limited by the inhomogeneity of the magnetic field across the sample which is ≤ 50 mG.

(10) The stability of this unit is better than 1 count/10^7 during the time of measurement.

(11) Error limits cited throughout this report reflect only the precision of the measurements and are given as twice the standard deviation, $s = [\Sigma_i(X_i - \bar{X}_i)^2/(n-1)]^{1/2}$.

(12) Limits of error in the temperature reported are approximately ±1°.

(13) Concentrated solutions of *p*-quaterphenyl in fuming sulfuric acid exhibit a partially resolved esr spectrum in which a sharp, intense line is observed at the center of the spectrum. The sharp line is characteristic of exchange observed for small solid particles in suspension. Rapid preparation of more dilute solutions does not produce the intense single line.

(14) Line positions are determined as follows. Component heights are taken as the difference between the maximum and minimum vertical points of the component. Component positions are taken at the half-height of the component located on the horizontal axis, and component separations are the difference between components on that axis.

(15) The position assignment of the various splitting constants is based on results of π-MO calculations.

(16) M. K. Carter and G. Vincow, *J. Chem. Phys.*, **47**, 302 (1967).

(17) Program options are available for absorption components, Gaussian shapes and nuclear spin values of 1, 3/2, and 2.

(18) Line widths are measured at maximum slope of an absorption line (horizontal separation between the maxima and minima of the derivative line).

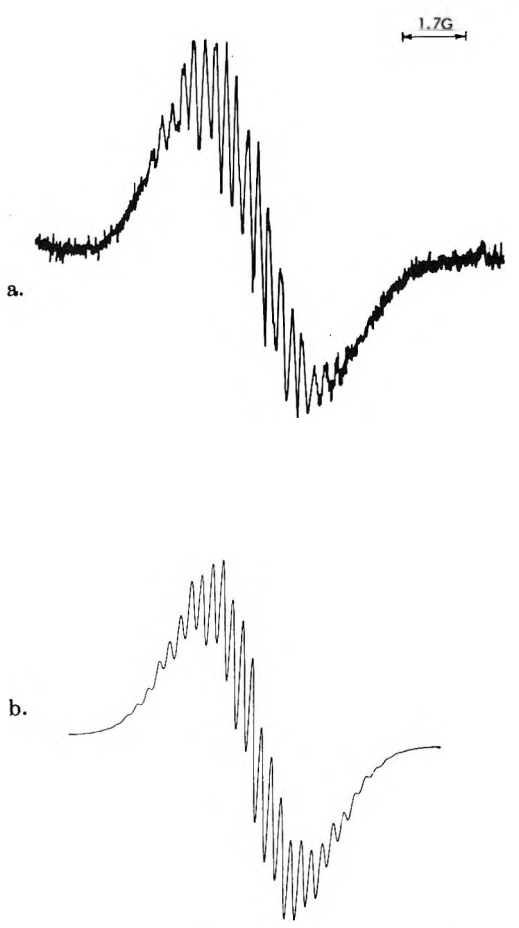

Figure 2. (a) Esr spectrum of the *p*-quaterphenyl cation radical at +6°. (b) Computer simulated spectrum generated for the values: $|a_4^H|$ = 1.94 G; $|a_{3'}^H|$ = 1.83 G; $|a_2^H|$ = 1.27 G; $|a_{2'}^H|$ = 0.56 G; $|a_3^H|$ = 0.10 G; and ΔH = 0.52 G.

generated in excellent agreement with the observed spectrum by assuming values of $|a_4^H|$ = 1.94, $|a_{3'}^H|$ = 1.83, $|a_2^H|$ = 1.27, $|a_{2'}^H|$ = 0.56, $|a_3^H|$ = 0.10, and ΔH = 0.52 G (see Figure 2b). These are the overlap corrected values which correctly describe the spectrum of Figure 2a.

Discussion

The effect of overlapped, broad lines on uncertainties in the assignment of the splitting constants has been investigated in detail. Computer-simulated overlap-corrected spectra have been generated for various splittings and line widths assuming Gaussian and Lorentzian line shapes. Individual component heights and widths as well as the overall pattern are compared with the experimentally observed spectrum. Agreement is poor for spectra generated assuming a Gaussian line shape; however, the spectra generated assuming a Lorentzian line shape are in good agreement with experiment (see Figure 2). Splitting constants have been varied by as much as half the line width from the assigned values. This causes the generated line heights and widths to deviate for small changes in the assumed splittings, and line separations to change for larger variations. For deviations of 0.02 G or less the spectrum shown in Figure 2b is generated.

Proton hyperfine splitting constants measured for cation radicals are, in general, larger than those for the corresponding anions (except for the anomolous 2 position). This is not the situation for the *p*-quaterphenyl ions, however. The proton hyperfine splittings are smaller for the cation in ring positions 2 and 4 (see Table I). This unexpected result is attributed to the nonplanarity of the cation and raises the question as to the cause of a nonplanar cation radical in light of a planar anion radical.[6]

Table I: Unpaired Electron Spin Density Distributions for Even-Alternate Cation Radicals

Compd	Position	ρ_{HMO}	$\lvert\rho_i\rvert_{exp}$	Q,[d] G	$\lvert a_i\rvert^+_{exp}$, G
Perylene	3	0.108[a]	0.109	37.0	4.04[a]
	1	0.083	0.082		3.04
	2	0.013	0.012		0.44
Anthracene	1	0.097[a]	0.095	32.5	3.08[a]
	2	0.048	0.042		1.38
	9	0.193	0.200		6.49
Naphthacene	1	0.056[a]	0.052	32.5	1.68[a]
	2	0.034	0.031		1.02
	5	0.147	0.154		5.01
Pyrene	1	0.136	0.143	37.5	5.38[a]
	2	0.000	0.031		1.18
	4	0.087	0.056		2.12
Naphthalene	1	0.181[a]	0.182	30.5	5.54[a]
	2	0.068	0.067		2.06
Pentacene	1	0.035[a]	0.029	33.9	0.98[a]
	2	0.025	0.022		0.76
	5	0.106	0.105		3.56
	6	0.141	0.150		5.08
Dibenzo(*a*,*c*)-triphenylene	1	0.027[a]	0.018	33.0	0.60[a]
	2	0.056	0.060		1.99
	3	0.002	<0.001		<0.03
	4	0.067	0.069		2.28
p-Quaterphenyl[c,e]	4	0.054	0.054	35.7	1.94
	3	0.004	(0.003)		(0.10)[b]
	2	0.040	0.036		1.27
	2′	0.028	0.016		0.56
	3′	0.048	0.051		1.83

[a] Reference 2. [b] Assumed. [c] This work. [d] Averaged over the various positions to give the lowest total deviation of $|\rho_i|_{exp}$ from ρ_{HMO}. [e] The splitting values for the *p*-quaterphenyl anion radical are $|a|_4$ = 2.10 G, $|a|_3$ = 0.42 G, $|a|_2$ = 1.47 G, $|a|_{2'}$ = 0.10 G, $|a|_{3'}$ = 1.47 G (ref 6).

Hyperfine splittings of the various protons measured from the esr spectrum are related to the unpaired electron spin densities of the adjacent carbon atoms by the McConnell relationship (eq 1). In order to compare experimentally derived spin densities for large molecules

such as the *p*-quaterphenyl cation radical with theoretically derived spin densities, simple π-electron MO treatments such as the Hückel method are useful. A simple MO treatment gives a highly successful account of the spectra of many alternate hydrocarbon radicals, and the agreement is excellent for the case of even–alternate radicals possessing the characteristics described in the introduction (Table I). In this regard it has been observed that the agreement of theoretically calculated spin densities with experimentally derived values is best for alternate hydrocarbon molecules, hydrocarbon molecules with a high degree of symmetry, and therefore totally planar molecules. Thus, it is assumed (for an even–alternate hydrocarbon) that disagreement between theoretically computed spin densities and spin densities derived from experimentally determined hyperfine splittings is an indication that the molecule has deviated significantly from the symmetry of a planar hydrocarbon.

X-Ray diffraction studies of crystalline biphenyl have been described by a number of authors.[19] In each case the molecule is found to be planar, probably as a result of intermolecular crystal forces. Crystal structures of *p*-terphenyl and *p*-quaterphenyl have also been investigated and these molecules have also been found to be totally planar.[20] However, the geometric configurations of *p*-polyphenyl molecules in the vapor phase are more characteristic of the molecules in dilute liquid solution since the intermolecular crystal forces are no longer present. Electron diffraction studies for biphenyl in the vapor phase have been reported. The interplanar angle has been determined as 41.6°.[21] Electron diffraction results are not available for *p*-quaterphenyl. Presumably it is also nonplanar in solution.

Unpaired electron spin densities have been calculated from the coefficients of the partially filled MO's as determined for a Hückel treatment by

$$\rho = \sum_k C_{0k}^2 \qquad (2)$$

for which C_{0k} is the kth coefficient of partially occupied orbital φ_0 in the single determinant wave function

$$\psi = \varphi_1^2, \varphi_2^2, \varphi_3^2, \ldots, \varphi_n^2, \varphi_0 \qquad (3)$$

Eigenvectors have been calculated for the *p*-quaterphenyl cation assuming all $\beta_{ij} = 1.0$ and all $\alpha_{ii} = 0$.[22] The π-electron spin densities derived from the Hückel MO calculation are listed in Table I according to the atomic assignment given in Figure 1.

Spin density distributions have also been calculated for the cation radicals derived from naphthalene, anthracene, naphthacene, pentacene, perylene, pyrene, and dibenzo(*a*,*c*)-triphenylene.[23]

Separate average Q values have been determined for each radical[24] so that the ρ_i calculated from the hyperfine splitting constants yield the best overall agreement with ρ_{HMO}. Agreement between ρ_{HMO} and ρ_i is excellent for all of the cations except for the pyrene and *p*-quaterphenyl cation radical (refer to Table I). The spin density distributions calculated by the McLachlan procedure for the *p*-polyphenyl anion radicals[6] are in better agreement with experiment than are the ρ_{HMO} values. This method leads to improved agreement for the cation radicals of pyrene[25,26] and *p*-quaterphenyl as well.

Simple π-MO theories cannot account for negative spin densities which are often found in alternating π-electron radicals. McLachlan[27] has shown that the use of an extended Hartree–Fock single determinant wave function with different orbitals for electrons with α and β spins can naturally predict both the sign and magnitude of unpaired electron spin densities. In a simple MO like φ_0 which describes the electron in a partially filled level, the spin density ρ is equal to the square of the function and is everywhere positive. McLachlan's approach is to use the wave function suggested by Pople and Nesbet[28] from which the spin density is derived. When the value of $|\psi'_i|^2$ [29] exceeds the values of $|\psi_i|^2$ at a node, the spin density is negative

$$\rho = |\psi_0|^2 + \sum_{i=1}^{n}[|\psi_i|^2 - |\psi_i'|^2] \qquad (4)$$

Unpaired electron spin densities have been calculated for the biphenyl anion radical in both the planar and twisted configuration.[27] The calculation for a planar molecule with all resonance integrals equal was in fair agreement with the experimental data,[30] while that which considered a possible twist in the molecule (by setting the inter-ring $\beta' = {}^1/_2\beta$) was not. It has been

(19) (a) G. B. Robertson, *Nature*, **191**, 593 (1961); (b) J. Trotter, *Acra Crystallogr.*, **14**, 1135 (1961); (c) A. Hargreaves and S. H. Rizvi, *ibid.*, **15**, 365 (1962); (d) references cited in (a), (b), and (c).

(20) G. W. Wheland, "Resonance in Organic Chemistry," Wiley, New York, N. Y., 1955, Appendix p 695; (b) *Acta Crystallogr.*, **3**, 46 (1950).

(21) A. Alminningen and O. Bastiansen, *Klg. Nor. Vidensk. Selsk. Skr.*, No. 4 (1958).

(22) The calculated energy level pattern shows the radical to be nondegenerate in agreement with conclusions based on the symmetry of the parent molecule.

(23) Refer to ref 2 for the atomic assignment of the molecules.

(24) These individual Q values compare favorably with the average value of 35.7 G (see ref 2).

(25) L. Salem, "The Molecular Orbital Theory of Conjugated Systems," W. A. Benjamin, New York, N. Y., 1966, p 273.

(26) It is interesting to note that pyrene is nonplanar in the crystalline state, A. Camerman and J. Trotter, *Acta Crystallogr.*, **18**, 636 (1965). It would be informative to determine whether or not pyrene is planar in the vapor state as determined by electron diffraction.

(27) A. D. McLachalan, *Mol. Phys.*, **3**, 233 (1960).

(28) J. A. Pople and R. K. Nesbet, *J. Chem. Phys.*, **22**, 571 (1954).

(29) The value of $|\psi_i|^2$ is the Hückel coefficient squared, C_{i0}^2, in the partially filled MO. The values of $|\psi_i'|$ are calculated by replacing the coulomb values by $\alpha_i = 2\lambda C_{0i}^2\beta$ and recomputing the wave function.

(30) See ref 6 for more quantitative agreement.

Table II: Unpaired Electron Spin Density Distributions Calculated for the *p*-Quaterphenyl Cation Radical. Distributions Have Been Calculated for Planar and Twisted Configurations

Position	ρ_{HMO}	ρ_{ML}[a]	ρ'_{ML}[b]	ρ^{θ}_{ML}[c]	$\lvert\rho_i\rvert^{+}_{exp}$[d]	$\lvert\rho_i\rvert^{-}_{exp}$[e]
4	0.054	0.063	0.057	0.055	0.054	0.075
3	0.028	0.018	0.019	0.019	0.016	0.015
2	0.040	0.047	0.038	0.036	0.036	0.052
2′	0.004	−0.010	−0.008	−0.007	(0.003)	0.004
3′	0.048	0.053	0.050	0.049	0.051	0.052

[a] The spin densities are from the McLachlan procedure for all $\beta = 1.0$ and $\lambda = 0.8$. [b] $\beta_0 = 1.019$ and $\beta_{IR} = 0.84$, ref 30. [c] $\beta_0 = 1.019$ and $\beta'_{IR} = \cos\theta\,\beta_{IR}$ for $\theta = 20°$, ref 24. [d] This work. [e] See ref 6.

concluded that the ion is planar.[31] Based on similar reasoning, it has also been concluded that the *p*-quaterphenyl anion radical is planar.[6]

Unpaired electron spin density distributions have been calculated for the *p*-quaterphenyl cation radical by the McLachlan method and are presented in Table II. Data of column ρ_{ML} are produced assuming that all $\beta_{ij} = 1.0$ for a value of $\lambda = 0.8$.[32] The spin density distribution calculated by assuming resonance integrals in the aromatic rings be given by $\beta_{ij} = 1.019$ (intra-ring distance = 1.388 Å) and the inter-ring values of $\beta_{IR} = 0.84$[33] (inter-ring distance 1.497 Å) is in fair agreement with the observed values. However, good agreement is obtained by assuming the aromatic rings to be disoriented from a common imaginary plane of symmetry. The interplanar angle is accounted for by assuming that the resonance integral of the inter-ring bond is proportional to overlap and is given by $\beta'_{IR} = (\cos\theta)\,\beta_{IR}$[34,35] for which $10° \leq \theta \leq 30°$. Based on this assumption and those stated previously, the spin density distribution of the *p*-quaterphenyl cation radical is best described for an interplanar angle of $\theta = 20°$.

The nonplanar configuration of the *p*-quaterphenyl cation radical may be considered in terms of two opposing effects. A deviation from planarity can be caused by interaction between opposing hydrogen atoms (atoms in the 2,2′ and 3′ positions of Figure 1), while the resonance effect tends to maintain planarity. Apparently the resonance effect is more important for the anion since it appears to be planar (see reference 36 for an alternate discussion). However, the cation has two less π electrons than the anion; the resonance effect is less important and hydrogen–hydrogen atom repulsion causes the resultant nonplanarity.

Some proton hyperfine splitting constants of the cation are smaller than the respective splittings for the anion. Since the spin density is decreased at positions 2 and 4 it must increase on the inter-ring carbon atoms. A local buildup of unpaired spin density is possible because the p orbitals on the inter-ring carbon atoms are in a less favorable bonding situation for a twisted configuration.

Acknowledgment. I wish to thank Dr. E. E. Genser for his helpful discussion and suggestions.

(31) It is interesting to note the cyclooctatetraene anion radical appears to be planar although the parent molecule is not; (a) T. J. Katz and H. L. Strauss, *J. Chem. Phys.*, **32**, 1873 (1960); (b) H. L. Strauss, T. J. Katz, and G. K. Fraenkel, *J. Amer. Chem. Soc.*, **85**, 2360 (1963).

(32) The value $\lambda = 0.8$ yields good results for all spin densities calculated in this work.

(33) A. Streitwieser, Jr., "Molecular Orbital Theory for Organic Chemists," Wiley, New York, N. Y., 1961, p 104 (bottom of page) and references cited therein.

(34) A. Golebiewski and A. Parczewski, *Theor. Chim. Acta*, **7**, 171 (1967).

(35) M. J. S. Dewar, *J. Amer. Chem. Soc.*, **74**, 3345 (1952).

(36) P. Carsky and R. Zahradnik, *Collect. Czech. Chem. Commun.*, **35**, 892 (1970).

A Spin-Label Investigation of Ion-Exchange Resins[1]

by D. B. Chesnut* and J. F. Hower

Paul M. Gross Chemical Laboratory, Duke University, Durham, North Carolina 27706 *(Received September 24, 1970)*

Publication costs assisted by the National Science Foundation

Rotational correlation times for a neutral spin label in the aqueous interior of a series of cation ion-exchange resins have been measured at room temperature from esr line width anisotropies. There is little indication of differences between the various ionic forms (Li^+, Na^+, K^+) of the resins studied but a significant dependence on cross linking. The correlation times increase with increasing cross linking up to 8 and 10% cross linking but then show a reduced value for the 12% resin. It is felt that the cause of this effect is probably due to the heterogeneous nature of the resin interior. Calibration of spectral parameters in solutions of known viscosity allows an approximate determination of the internal viscosity of the resins.

Introduction

Ion-exchange resins have been under investigation for two decades. For the most part reliance has been placed on the interpretation of thermodynamic data, diffusion studies, conductance, and equilibrium measurements to explain the chemical and physical properties of solvated resins. More recently, nuclear magnetic resonance (nmr) has been employed as an important and practical tool. For example, Gordon[2] used nmr to discuss exchange of proton-containing counterions, the change in counterion molality as a function of cross linking, loss of rotational freedom of the counterion as a function of swelling, and investigations of resin heterogeneity. Creekmore and Reiley[3a,b] employed nmr to estimate the hydration numbers of counterions in the resin phase and to measure the rate of exchange of protons between the interior and the exterior of the resin. Their results suggest that ion association occurs in the resin phase.

Spin labels[4] are stable organic free radicals which can be incorporated within a system to provide information concerning the system's internal structure; they provide a means of investigating systems whose chemical or physical complexity may resist attack by other techniques. The use of spin labeling has been confined mainly to systems of biological interest. For example, it has been employed successfully to observe structural changes associated with oxygen uptake in horse hemoglobin,[5,6] to study the motion of labeled steroids in synthetic membranes,[7] and to investigate micelles and the process of solubilization.[8]

The successful use of spin labels, particularly as applied to studies of membranes, prompted us to consider their use as probes in the interior of ion-exchange resins. Not only should the approach be particularly useful for this case of considerable interest in its own right, but there also exist certain parallels between resin interiors and biological systems of widespread interest today. In this paper we demonstrate the feasibility of applying the spin-labeling technique to the study of ion-exchange resins by using a spin label to investigate the interior of sulfonated polystyrene cation-exchange resins. The theory of magnetic resonance line widths allows one to calculate rotational correlation times (τ_c) of the spin probe from measurable spectral parameters of the label's electron spin resonance (esr) spectrum. Since the rotational correlation time is a direct measure of the motional freedom of the probe, we are able to discuss the environment inside the resin interior as seen by the label.

Theory

The system parameter from which our present information is derived is the anisotropy of the line widths in the esr spectrum. This effect is illustrated in Figure 1, which shows three spectra exhibiting three different degrees of anisotropy. The line width is described in terms of an inverse of a time, T_2^{-1}, the spin–spin or transverse relaxation time. For radicals in solution anisotropies in the g tensor and the hyperfine coupling with the nuclei both contribute to T_2. The physical situation corresponds to the electron spin experiencing randomly fluctuating magnetic fields whose frequency

(1) Supported in part by National Science Foundation Grant GP-8298 and the NIH Biomedical Sciences Support Grant (Duke University).

(2) J. E. Gordon, *J. Phys. Chem.*, **66**, 1150 (1962).

(3) (a) R. W. Creekmore and C. N. Reiley, *Anal. Chem.*, **42**, 570 (1970); (b) R. W. Creekmore and C. N. Reiley, *ibid.*, **42**, 725 (1970).

(4) Excellent reviews are to be found in: (a) C. L. Hamilton and H. M. McConnell in "Structural Chemistry and Molecular Biology," A. Rich and N. Davidson, Ed., W. H. Freeman, San Francisco, Calif., 1968; (b) O. H. Griffith and A. S. Waggoner, *Accounts Chem. Res.*, **2**, 17 (1969); (c) H. M. McConnell and B. G. McFarland, *Quart. Rev. Biophys.*, **3**, 91 (1970).

(5) J. C. A. Boeyens and H. M. McConnell, *Proc. Nat. Acad. Sci.*, **56**, 22 (1966).

(6) S. Ogawa, H. M. McConnell, and A. Horowitz, *ibid.*, **61**, 401 (1968).

(7) W. L. Hubbell and H. M. McConnell, *ibid.*, **63**, 16 (1969).

(8) A. S. Waggoner, O. H. Griffith, and C. R. Christensen, *ibid.*, **57**, 1198 (1967); A. S. Waggoner, A. D. Keith, and O. H. Griffith, *J. Phys. Chem.*, **72**, 4129 (1968).

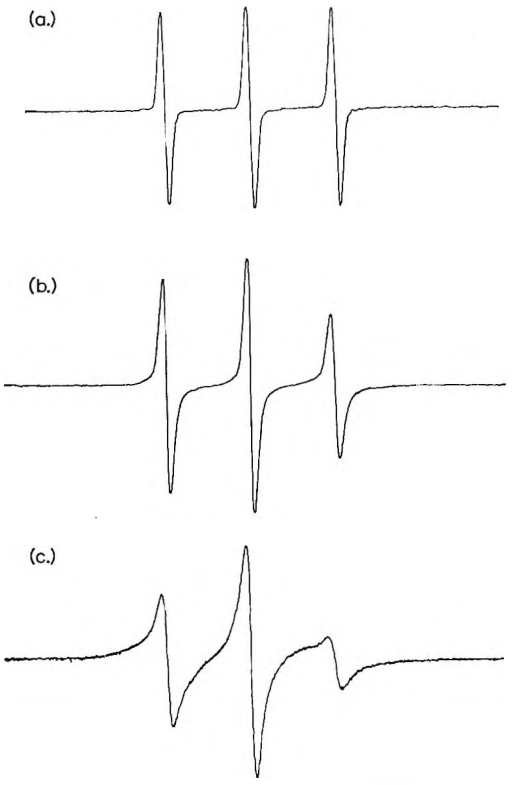

Figure 1. Sample spectra for solutions exhibiting three different correlation times: (a) 5 m LiCl, $\tau_c^{(m)} \approx 10^{-11}$ sec; (b) Li 2x resin, $\tau_c^{(m)} = 2.1 \times 10^{-10}$ sec; (c) Li 8x resin, $\tau_c^{(m)} = 8.4 \times 10^{-10}$ sec. The amplitude scale is arbitrary and not uniform while the magnetic field scale is the same in each spectrum and is defined by the splitting in spectrum (a) of 17.1 G.

distribution may be characterized by a correlation time, τ_c; the inverse of τ_c gives one a measure of the mean fluctuation frequency for the relaxation mechanism involved. Because both the g and hyperfine tensors are tied to the same molecular frame of reference, their effects are correlated, leading to a dependence of T_2^{-1} on the nuclear quantum number. Explicitly, the line width of the various lines in the hyperfine pattern may exhibit different widths, and by determining this line width anisotropy one can deduce the appropriate (in this case, rotational) correlation time. The usefulness of nitroxide radicals in deducing correlation times lies not only in their chemical stability and relative simplicity but also in the fact that, normally, a simple three-line esr spectrum is observed which is easily analyzed. The three lines of equal integrated intensity result from the coupling between the radical "odd" electron and the nitroxide nitrogen of nuclear spin one. With proper solvent degassing one can observe hyperfine coupling with the protons of such systems, but these couplings are small and are not observed in the usual spin-labeling studies.

For the system used here we consider only the nitrogen hyperfine coupling and use for $[T_2(m)]^{-1}$ the expression given by Kivelson.[9]

$$[T_2(m)]^{-1} = \tau_c\left\{\frac{1}{40}[3I(I+1) + 5m^2][b^2 + 3c^2] + \frac{4}{45}H_0^2[(\Delta\gamma)^2 + 3(\delta\gamma)^2] - \frac{4}{15}H_0 m[b(\Delta\gamma) + 3c(\delta\gamma)]\right\} + X \quad (1)$$

where

$$\Delta\gamma = \frac{-|\beta|}{\hbar}\left[g_{zz} - \frac{1}{2}(g_{xx} + g_{yy})\right]$$
$$\delta\gamma = \frac{-|\beta|}{\hbar}\frac{1}{2}(g_{xx} - g_{yy})$$
$$b = \frac{4\pi}{3}\left[\Gamma_{zz} - \frac{1}{2}(\Gamma_{xx} + \Gamma_{yy})\right] \quad (2)$$
$$c = \frac{4\pi}{2}\frac{1}{2}(\Gamma_{xx} - \Gamma_{yy})$$

are the anisotropies in the g tensor ($\Delta\gamma$ and $\delta\gamma$) and the hyperfine tensor (b and c). τ_c is the rotational correlation time, H_0 the applied field, $I = 1$ the nuclear spin for nitrogen, m the quantum number of spin projection ($\pm 1,0$) and the other symbols have their usual definitions. X represents all other contributions to the line width independent of m. Equation 1 takes on a simpler form when axial symmetry is present ($\delta\gamma = c = 0$) and we will assume this to be the case in the present study. Although the recent results of Libertini and Griffith[10] from single crystal work show axial symmetry to be lacking for the di-*tert*-butyl nitroxide in the solid state, the departure from axial symmetry is sufficiently small such that the error made in assuming axial symmetry is negligible.

The use of eq 1 assumes isotropic molecular tumbling, that the individual lines are not broadened beyond resolution, and correlation times such that $(\omega_0\tau_c)^2 \gg 1$ (ω_0 is the mean resonance frequency). Presuming axial symmetry eq 1 may be written in the convenient form

$$R(m) = \frac{T_2(0)}{T_2(m)} = 1 - \frac{4\tau_c}{15}b\Delta\gamma H_0 T_2(0)m + \frac{\tau_c}{8}b^2 T_2(0)m^2 \quad (3)$$

One can deduce τ_c by knowing b, $\Delta\gamma$, and H_0 and measuring relative widths of the various components.

There are several ways of approaching the calculation of τ_c. In the present case we choose to calculate it by two ways (eq 4a and 4b).

(9) D. Kivelson, *J. Chem. Phys.*, **33**, 1094 (1960).
(10) L. J. Libertini and O. H. Griffith, *ibid.*, **53**, 1359 (1970).

$$\tau_c^{(m)} = \frac{1}{2}\left\{\frac{R(-1) - R(+1)}{\frac{4}{15}b\Delta\gamma H_0 T_2(0)}\right\} \quad (4a)$$

$$\tau_c^{(m^2)} = \frac{1}{2}\left\{\frac{R(-1) + R(+1) - 2}{\frac{1}{8}b^2 T_2(0)}\right\} \quad (4b)$$

The superscripts m and m^2 indicate that in the two cases one relies upon knowledge of the linear (m) or quadratic (m^2) term in the expression of $R(m)$ as a function of m. Of course, the two correlation times are theoretically identical. As discussed later, if they differ it may indicate an error in the choice of input parameters or breakdown of one or more of the assumptions underlining the use of eq 1.

The initial parameters used for the hyperfine and g tensors were those of Stone, *et al.*,[11] which agree closely with Libertini and Griffith's values. Relative line widths were measured by taking the square root of the inverse amplitudes. This is a more sensitive way of determining the line width and is acceptable in the present case since the lines were shown to be Lorentzian.

Experimental Section

The spin label 2,2,6,6-tetramethylpiperidine-*N*-oxyl-4-ol (TMPOO) shown below was used in the present

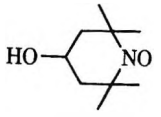

TMPOO

investigation and was prepared according to the procedure of Briere.[12] The cation-exchange resins were Dowex 50W obtained from the Bio-Rad Laboratories with nominal cross linking (x) of 2, 4, 8, 10, and 12% by weight of divinylbenzene copolymer. The resins were placed in columns and washed with methanol to remove organic impurities; when a colorless effluent was observed, the resins were washed with deionized H_2O, removed from the columns, and air dried. Each resin sample was then divided into three portions, placed in columns, and converted to the Li^+, Na^+, and K^+ forms by washing with copious amounts of alkali metal chloride solutions. When the effluent was negative to litmus the samples were washed with deionized water until a negative silver chloride test was achieved. The resins were then blotted dry and stored in amber bottles.

The damp resin (0.25 g) was allowed to equilibrate with 30 ml of a 10^{-3} M TMPOO aqueous solution. The equilibration period was varied from 1 day to 2 weeks although comparison of spectra as a function of time showed that equilibration occurred within 1 day. After the equilibration period, the resin was removed from the solution and carefully washed with deionized water to remove any excess spin label on the resin surface. The samples were then blotted dry and placed in preweighed melting point capillaries. By knowing the esr cavity dimensions and weight and height of the resin in the capillary it was possible to calculate the amount of resin in the cavity.

A standard glycerin solution 10^{-4} M in TMPOO was prepared by dissolving a preweighed amount of the probe in glycerin. Glycerin–water solutions containing 20, 40, 60, and 80% H_2O by volume and 10^{-4} M in TMPOO were prepared in a similar fashion.

The magnetic resonance work was carried out at room temperature (*ca.* 22°) on a standard Varian 12-in. system described previously.[13] Care was taken to avoid both saturation and exchange broadening of the spectral lines by working at low power and using dilute spin-label solutions.

Results and Discussion

In the present study ion-exchange resins with nominal cross linkings of 2, 4, 8, 10, and 12% were studied, each in the Li^+, Na^+, and K^+ forms. It was not possible to study the hydrogen form since the acidic medium destroyed the nitroxide radical.

The principal results of the present studies are shown in Table I and in Figure 2. In Figure 2 we have plotted the correlation time determined from the linear

Table I

		$\tau_c^{(m)} \times 10^{10}$, sec	$\tau_c^{(m)}/\tau_c^{(m^2)}$	K	I_{rel}, meq^{-1}	I_{rel}, mol H_2O^{-1}
$2x$	Li	2.1	0.73	0.19	1.00[a]	1.00
	Na	2.2	0.75	0.17	0.66	0.91
	K	2.5	0.80	0.16	0.45	0.83
$4x$	Li	3.4	0.66	0.14	0.44	0.72
	Na	3.6	0.71	0.14	0.35	0.74
	K	3.4	0.72	0.12	0.24	0.62
$8x$	Li	8.4	0.66	0.12	0.20	0.60
	Na	7.1	0.60	0.067	0.099	0.34
	K	9.8	0.67	0.087	0.11	0.45
$10x$	Li	8.7	0.67	0.085	0.15	0.44
	Na	8.3	0.59	0.067	0.10	0.34
	K	10.4	0.65	0.072	0.10	0.37
$12x$	Li	3.5	0.61	0.096	0.12	0.49
	Na	3.7	0.55	0.058	0.065	0.30
	K	3.3	0.59	0.073	0.071	0.38
Relative error, %		10–15	20–30	20–30	20–30	20–30

[a] Arbitrary reference.

(11) J. T. Stone, T. Buckman, P. L. Nordio, and H. M. McConnell, *Proc. Nat. Acad. Sci.*, **54**, 1010 (1964).

(12) R. Briere, H. Lemaire, and A. Rossat, *Bull. Soc. Chim. Fr.*, **32**, 3273 (1965).

(13) J. C. Bailey and D. B. Chesnut, *J. Chem. Phys.*, **51**, 5118 (1969).

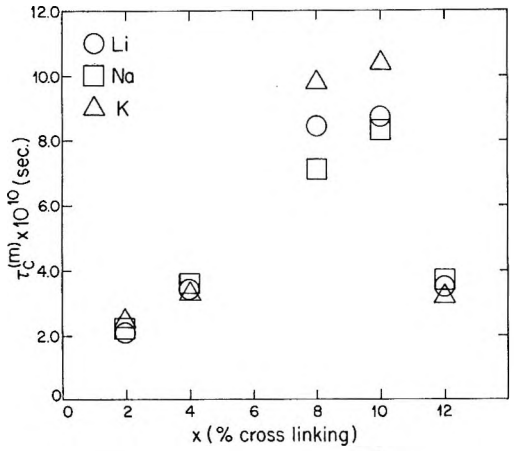

Figure 2. Rotational correlation times, $\tau_c^{(m)}$, for the Li, Na, and K resin forms as a function of cross linking (x).

terms (see eq 3 and 4a) as a function of cross linking. One observes the correlation times to increase with increasing cross linking up to and including the 8x and 10x resins. This is a result to be expected since with increasing cross linking one would expect the probe to experience less motional freedom. The unexpected result is the *drop* in the correlation times as one goes from the 10x to the 12x resin.

As one can see in Table I, the drop-off of the correlation time in the 12x case is the only property which does not show a smooth trend with cross linking. For example, relative intensities (I_{rel}) of the various cases were determined. The lithium form of the 2x resin was chosen as an arbitrary reference point. The data show that all intensities fall off smoothly with increasing cross linking. Using the resin data provided by the manufacturer the intensity per milliequivalent (meq) and the intensity per mole of water in the resin were determined. Again, one would expect fewer radicals to be able to enter the resin at higher cross linking and this is borne out by the figures in the table. The data on the relative intensities per mole of water show that the amount of spin label penetrating the resin falls off more rapidly than the amount of water entering the resin. It is well known that the hydration water falls off quite rapidly with increasing cross linking.

The resins were equilibrated with a 1.0×10^{-3} M solution of spin label. Rough estimates of the absolute number of spins in the resin were made which allowed an estimate of the equilibrium constant, K. As has been shown to be a good approximation,[14] it was assumed that the volume of water in the resin may be determined from the total weight of water and its normal density. K, which represents the ratio of concentration of spin label (moles per liter of water) inside the resin to concentration of spin label outside the resin (moles per liter of solution) falls from approximately 0.18 at 2% to approximately 0.07 at 12% cross linking.

The other column of data in the table is the ratio of $\tau_c^{(m)}$ to $\tau_c^{(m2)}$. It was indicated earlier that these two correlation times might differ for a variety of reasons and we shall discuss this point a bit later. The point we wish to establish right now is that, again, this ratio as a function of cross linking shows a smooth trend.

The indicated relative errors show that in most cases it is difficult to assess the significance of differences between the various ionic forms. The ordering of the ions for some of the intensity and equilibrium constant data seem to be real. Certainly, for the 8x resin the differences in the calculated correlation times are approaching significance.

The choice to list the correlation time, $\tau_c^{(m)}$, is an arbitrary one. The data in Table I allow one to calculate $\tau_c^{(m^2)}$. The fact that these two calculated times are not equal may be due to one or more of several causes. If one is looking at the superposition of spectra then the measured line widths will improperly reflect what one wishes to measure. As mentioned before, the line widths here are Lorentzian and we have no clear indications that a superposition of spectra is being observed. A more likely source of error lies in the input parameters b and $\Delta\gamma$ used in the calculation of the correlation times. These reflect the anisotropy of the hyperfine and g tensors and are known to vary from medium to medium.[15] Our initial calculations assumed a hyperfine anisotropy of 73 MHz based on the data of Stone, *et al.*[11] The observation of differing correlation times led us to a redetermination of these anisotropies in the following manner. The isotropic hyperfine coupling and g factors were determined for a 5 m aqueous LiCl solution of 10^{-4} M in the spin label. The lithium chloride solution was then frozen and the parallel components of the hyperfine and g tensors were determined at $-100°$ according to the method of Edelstein, Kwok, and Maki.[16] Knowledge of these components and of the average or isotropic values then allows the calculation of the desired anisotropies. The results obtained from this latter study indicated that the g factor anisotropy was approximately what had been employed initially while the hyperfine anisotropy instead of being 73 MHz was approximately 92 MHz. Use of the latter data does improve the agreement between the two correlation times but does not make them identical. We have decided to use the presently determined anisotropies since we believe that the measurements made in the highly ionic solutions more nearly approach the environment seen by the spin label inside an ion-exchange resin. It should also be mentioned that the initial set of input parameters did give identical correlations times for the glycerin and glycerin–water solutions. The choice of anisotropies leads to

(14) J. A. Kitchner in "Ion Exchangers in Organic and Biochemistry," C. Calmon and T. R. E. Kressman, Ed., Interscience, New York, N. Y., 1957.

(15) See ref 4a and 11.

(16) N. Edelstein, A. Kwok, and A. H. Maki, *J. Chem. Phys.*, **41**, 179 (1964).

at most a factor of 2 difference in the absolute values of the correlation times.

The magnitudes of the rotational correlation times found in the present study are approximately what one might expect. They range from approximately 10^{-10} to 10^{-9} sec, an intermediate range of rotational correlation times. The correlation time of 10^{-11} sec found for the spin label in the 5 *m* lithium chloride solution is considered fast. On the other hand, Hubbell and McConnell[7] estimate correlation times in the range of 10^{-7} to 10^{-8} sec for certain steroid spin labels in neuromembranes and sonicated phospholipid suspensions. The long correlation times are reflected in the loss of resolution in the esr spectrum, one which is approaching a solid like spectrum.

The unusual result in the present study is the drop-off of the correlation time in going from the 8*x* to the 12*x* resin. Although it was deemed unlikely, the possibility of surface effects was investigated by comparing spectra of 20–50, 50–100, 100–200, and 200–400 mesh resins for the 8*x* potassium form. No surface effects were observed over this range of resin size. As discussed previously, all other data indicate a smooth trend of properties with increasing cross linking. Two distinct sets of 12% cross-linked resin were investigated to rule out the possibility that the resin was improperly identified. We suspect that our result reflects a heterogeneity of the ion-exchange resins such that not all environments within a given resin are accessible to our spin label. A given cross linking will contain, of course, a statistical distribution of pore and cavity sizes. Furthermore, as the per cent cross linking increases the shape of the statistical distribution may well be expected to change. Schlögel and Schurig[17] have done some calculations which show that there are several preferred pore sizes in a resin as a function of its cross linking. We may only conclude that in the 12*x* resin those cavities available to our spin label are those much like the predominant ones found in the 4*x* resin, since the correlation times of these two resins are similar. Gordon's result in his nmr study[1] gave no hint of this effect; in fact, for the tetramethylammonium ion the line widths studied showed a smooth trend up to and including the 12*x* case. He did not, however, report any data beyond 8% for the *larger* cations involved. To investigate the present situation one might use spin labels of differing sizes. If an exclusion effect is operative, a larger spin label should exhibit the effect at lower cross linking while smaller spin labels should not show the effect at the higher cross linkings. Continued effort on this problem is underway in these laboratories. We may also point out that in the present study a neutral spin label was employed. Thus, in the resin interior one is probing the environment seen by a polar but neutral species. Experiments are also currently underway using charged spin labels which should reflect the environment near the charged resin sites. It is clear that the spin-labeling technique may offer considerable insight into the interior of ion-exchange resins.

During the course of our investigation the spin label in a series of glycerin and glycerin–water solutions was investigated. Knowledge of the viscosity of these solutions and the determined correlation times allows a determination of an effective molecular radius *via* Stokes' equation. For the radical under investigation we found a radius, *R*, of approximately 1.6 Å. This figure should be compared to a radius of approximately 3.6 Å obtained from estimates based on molecular models and from a value of 3.4 Å obtained from considerations involving atomic volume increments as given by Edward.[18] The small experimental value of *R* is not uncommon when one uses a bulk viscosity and a rotational correlation time. It reflects the fact that the rotational viscosity is less than the bulk viscosity of the solvent. One can use the solutions of known viscosity along with an appropriate spectral parameter to obtain a calibration curve. We found that plotting the ratio of the middle to the high field line first derivative amplitudes *vs.* bulk viscosity gave a smooth curve. Although it is a somewhat crude approximation, if we assume one can use such a calibration curve inside the ion-exchange resins one then has a rough experimental measure of the internal viscosity. Thus, for averages of the various ionic forms one obtains very rough estimates of 0.71, 2.3, 15, and 3.3 P for the 2, 4, 8, and 12% cross linked resins. The figures, while approximate, are, however, consistent with the measured internal correlation times. Thus, for the 5 *m* lithium chloride solution a rotational correlation time of approximately 1×10^{-11} is found. The viscosity of this solution is approximately 0.02 P.[19] One might also take the internal viscosity and use the empirically determined molecular radius to calculate a correlation time. If this is done one finds that the calculated correlation times compared to the experimentally determined correlation times match rather well for the 2*x* resin but become larger than the observed correlation times for the 4*x*, 8*x*, and the 12*x* resin. The ratios of the correlation times are approximately 1.3, 2.6, 7.5, and 3.8 for the 2, 4, 8, and 12*x* resin, respectively. The *change* in the agreement between the two values may well indicate a change in the effective molecular radius of the spin label inside the resin. Since the molecular species involved is undoubtedly hydrated and since the degree of hydration would be expected to change with cross linking, this explanation is exceedingly plausible. Creekmore and Reiley[3a] have shown that

(17) R. Schlögel and H. Schurig, *Z. Elektrochem.*, **65**, 863 (1961).

(18) J. J. Edward, *J. Chem. Educ.*, **47**, 261 (1970).

(19) "The International Encyclopedia of Physical Chemistry and Chemical Physics," E. A. Guggenheim, J. E. Mayer, and F. C. Tompkins, Ed., Pergamon Press, Oxford, Vol. 3, Appendix 2.1.

the hydration of the counterions in cation exchangers drops with increasing cross linking. This is just the trend needed in the present case to explain the discrepancy between the methods of determining the correlation times. Obviously, the direct determination of the rotational correlation times is the best one. We mentioned the viscosity experiments and the agreement between the two methods of calculation to illustrate some qualitative aspects of the resin interior provided by the present method of investigation.

Acknowledgment. We are indebted to Professor H. A. Strobel of this department for many informative discussions.

The Color of Liquid Sulfur

by B. Meyer,* T. V. Oommen, and D. Jensen

Chemistry Department, University of Washington, Seattle, Washington 98105 *(Received November 18, 1970)*

Publication costs assisted by the National Science Foundation

At the melting point, liquid sulfur is yellow; at the boiling point it is dark red. The color change is due to an apparently monotonous shift of the absorption edge toward the red, and to an increase of the visible absorption. At optical density 0.6 the average shift is 23.6 $cm^{-1}/°K$ between 114 and 700°C. In the temperature range between 114 and 250°, the rapid color change is primarily due to absorption by thermally populated excited vibrational levels of S_8 and to absorption by polymers. Above 250°, the color change is mainly due to the appearance of new absorption peaks at 4100 and 5300 Å. The intensity of these peaks increases with temperature and indicates that above 250° new species are formed. The absorption peaks at 4100 and 5300 Å are also observed in red sulfur quenched from 444°C to 77°K, in sulfur vapor, and in trapped molecular beams of vapor at 77°K. Photolysis products of S_3Cl_2 in an organic glass at 77°K and in a krypton matrix at 20°K absorb only at 4100 Å, while photolysis products of S_4Cl_2 absorb only at 5300 Å. This indicates that the 4100-Å band is due to S_3, while the 5300-Å band is due to S_4. Thus, liquid sulfur contains S_3 and S_4. Comparison of liquid and vapor indicates that the S_3 and S_4 concentrations increase with temperature and at the boiling point reach between 0.5 and 2 weight %. The discovery of S_3 and S_4 implies the presence of other small species.

Introduction

At the melting point, pure sulfur forms a clear, bright yellow liquid. Upon heating, the color monotonously changes to dark red. Above 350° a 1-cm path of the liquid is opaque. At high temperatures, the vapor above the liquid is also dark red. Upon slow cooling, the dark red color fades reversibly to yellow. Erdmann[1] suggested in 1908 that this color change was caused by the formation of S_3, and later, Kellas[2] thought that liquid sulfur contained S_{12} and S_{18}. It is now known that liquid sulfur is a complex system[3] and contains many allotropes. Only three spectral studies of the liquid have been reported. They all deal with the temperature dependence of the red absorption edge, rather than with the entire visible spectrum, because the absorptivity is so great that even in very thin films the entire absorption region, except the edge, appears opaque. Fukuda,[4] in 1921, observed that upon heating from 0° to 300° the absorption edge of plastic sulfur shifted by about 2 Å/°C to the red. Mondain-Monval,[5] in 1930, reported a shift of 2.94 Å/°C below 160°; above it was found to be 7.44 Å/°C. In 1953, Bass[6] reported shift rates for the temperature range between 112 and 400° and proposed that, as in the case of selenium,[7] thermal excitation of vibrational modes of S_8 causes the color change.

Our study had four goals. The first was to extend measurement of the absorption edge to higher temperatures, to record the visible absorption spectrum below the edge, and to compare the results with the present knowledge of the composition of the liquid in order to check whether the color change was due to thermal excitation or due to changing molecular composition.

At the melting point, the liquid is almost pure cyclo-

(1) H. Erdmann, *Justus Liebigs Ann. Chem.*, **362**, 133 (1908).
(2) A. M. Kellas, *J. Chem. Soc. London*, **113**, 903 (1918).
(3) R. E. Harris, *J. Phys. Chem.*, **74**, 3102 (1970).
(4) M. Fukuda, *Mem. Coll. Sci., Kyoto Imp. Univ.*, **4**, 351 (1921).
(5) P. Mondain-Monval, R. Job, and P. Gallet, *Bull. Soc. Chim.*, **4**, 47, 545 (1930).
(6) A. M. Bass, *J. Chem. Phys.*, **21**, 80 (1953).
(7) M. A. Gilleo, *ibid.*, **19**, 1291 (1951).

S_8 with about 5.5% S_π.[8] It has recently been concluded[3] that S_π, the fraction of sulfur which is insoluble in CS_2 at −78°, consists of a mixture of sulfur rings. At a temperature around 159°, liquid sulfur becomes highly viscous because polymers with up to 500,000 S_8 units are formed. The viscosity change can be quantitatively explained by a model which assumes chain scission and polymerization of catena-S_8 with cyclo-S_8.[9] When the temperature is increased beyond 250°, the average chain length decreases and with it the viscosity, until, at the normal boiling point, sulfur forms again a thin liquid. The molecular composition of hot liquid sulfur is not known.

The second goal of our study was to investigate the composition of hot liquid sulfur by recording the spectrum of quenched liquid sulfur. Many researchers have tried to analyze the composition of the liquid by quenching,[10,11] but this is difficult because sulfur is a very efficient insulator and cannot dissipate heat quickly. Thus, it changes its molecular composition during cooling. It was our aim to use improved quenching techniques and search for metastable allotropes. Such allotropes have been obtained from quenched vapor.[12−14]

Our third goal was to compare the spectrum of liquid sulfur with that of individual allotropes such as S_8, S_6, polymeric sulfur, and the spectrum of all those sulfur species which can be kept or prepared individually as solids, in solution, in organic glasses or in rare gas matrices. We also planned to study the photolysis of chlorosulfanes to see whether reactions analogous to that of S_2Cl_2[15] in inert matrices at 20°K

$$S_2Cl_2 \longrightarrow S_2 + 2Cl$$

could be used to prepare and isolate allotropes.

The fourth goal was to compare the color of liquid sulfur with that of sulfur vapor. Saturated sulfur vapor changes its color upon heating in a fashion similar to that of the liquid. It is originally yellow and upon heating becomes red and then turns brown and finally black. The spectrum and the molecular composition of sulfur vapor is fairly well known.[16−18] It was our aim to see whether the spectrum of the vapor and the liquid indicated the presence of the same species.

Experimental Section

High-purity sulfur samples of several manufacturers were compared. Traces of organic impurities can be visually recognized by heating because organic compounds react with the hot liquid and form brown products. Pure sulfur remains yellow. All the experiments described below were performed in sealed evacuated quartz cells containing 99.999% sulfur (Asarco, high purity) or filtered sulfur which was donated by the Freeport Sulphur Company.

Three types of optical cells were used. Solutions were studied in a Dewar cell with 1.5-cm diameter and 2.45-cm path length. Liquid samples were measured in specially built thin quartz cells of 2.5-cm diameter. The path length varied between 0.1 and 1.3 mm. Experiments on gas samples are described in a different publication.[16] Spectra were recorded on a Carry 14H photospectrometer with a high-temperature attachment; photographic work was done on a Jarrell-Ash f/6.3 Czerni-Turner spectrograph. More experimental details are given in ref 19.

For photolysis experiments, S_3Cl_2 was prepared from SCl_2 and liquid H_2S, and S_4Cl_2 was prepared by reaction of SCl_2 with H_2S_2 at −78° according to procedures described by Feher.[20] For studies at 77°K, a 10^{-3} M solution of the chlorosulfane in a 1:2 mixture of isopentane–methyl cyclohexane was photolyzed in the above described quartz cell by irradiation with the light from a General Electric AH6 high-pressure mercury lamp. Photolysis times were 1–60 min. Matrix experiments were performed at 20°K in equipment and according to techniques described before.[21]

Results

The results are presented in five parts. The first deals with the visible spectrum of liquid sulfur between the melting point and 700°, the boiling point of liquid sulfur, at 10 atm. This part also lists the absorption of S_8 crystals for comparison. The second part deals with spectra of solids which are obtained when liquid sulfur is quenched. In the third part, spectra of solutions of S_8 and S_6 are reported. In the fourth part, photolysis of chlorosulfane is discussed, and in the fifth part, gas phase spectra are compared.

1. Liquid Sulfur. The absorption of liquid sulfur is so strong that even thin films are opaque in the ultraviolet. Thus, the spectrum recorded by early researchers[4,5] consists only of a steep absorption edge. Figure 1 shows the absorption recorded with a Cary 14H spectrophotometer of the edge of a 100 μm thick

(8) B. Meyer, *Chem. Rev.*, **64**, 429 (1964).

(9) A. V. Tobolsky and A. Eisenberg, *J. Amer. Chem. Soc.*, **81**, 780 (1954).

(10) J. C. Kohn and W. Klement, Jr., *J. Phys. Chem.*, **74**, 4280 (1970).

(11) P. W. Schenk, *Angew. Chem.*, **65**, 325 (1953).

(12) H. Staudinger and W. Kreis, *Helv. Chim. Acta*, **8**, 71 (1924).

(13) F. O. Rice and C. Sparrow, *J. Amer. Chem. Soc.*, **75**, 848 (1953).

(14) B. Meyer and E. Schumacher, *Helv. Chem. Acta*, **43**, 1333 (1960).

(15) B. Meyer and J. J. Smith, U. S. Atomic Energy Comm. Report, UCRL 18060 (1968).

(16) B. Meyer, T. Stroyer-Hansen, D. Jensen, and T. Oommen, UCRL 19660, Nov 1970.

(17) D. Detry, J. Drowart, P. Goldfinger, H. Keller, and H. Rickert, *Z. Phys. Chem.*, **55**, 314 (1967).

(18) J. Berkowitz in "Elemental Sulfur," B. Meyer, Ed., Interscience, New York, N. Y., 1964, p 125.

(19) T. V. Oommen, Ph.D. Thesis, University of Washington, 1970.

(20) F. Feher and S. Ristic, *Z. Anorg. Allg. Chem.*, **293**, 307 (1958).

(21) B. Meyer, "Low Temperature Spectroscopy," Elsevier Publishers, New York, N. Y., 1970.

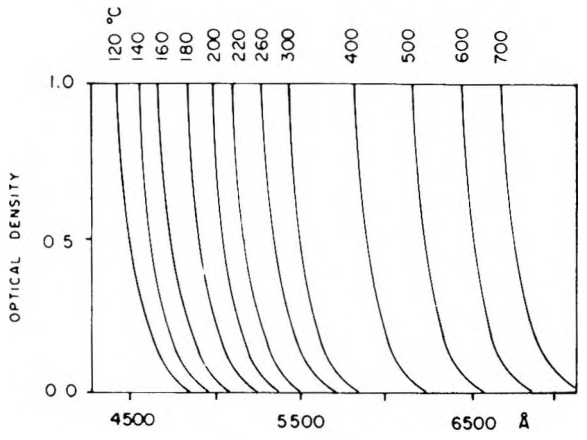

Figure 1. Absorption edge of 0.1-mm liquid sulfur film at various temperatures between 114 and 700°.

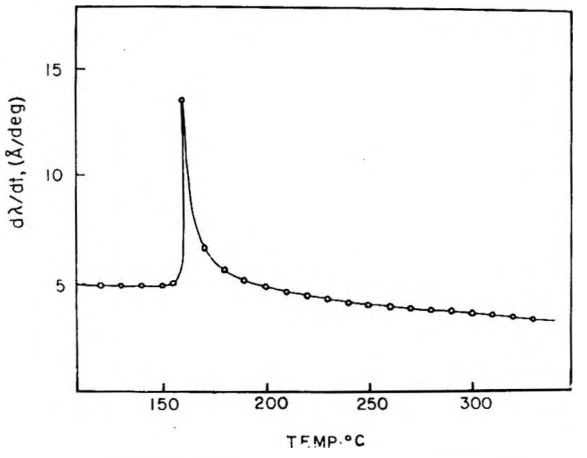

Figure 2. Temperature dependence of shift of absorption edge at optical density 0.6.

liquid sulfur film in an evacuated quartz cell at various temperatures between 114 and 700°. The absorption edge shifts to the red with increasing temperature but retains about the same slope. The temperature dependence of the shift is shown in Figure 2. The average shift rate at optical density 0.6 is about 23.6 $cm^{-1}/°K$. The shift decreases monotonously, except for a short but drastic increase with a maximum at 160°. Figure 3 is a tracing of a photograph of the absorption of the same sample as in Figure 1. Figure 3a and b shows that the absorption spectrum changes with temperature. At 500° shoulders are apparent at 4100 and 5300 Å which are not present below 250°.

Crystals. The spectrum of a 1.4 mm thick orthorhombic crystal of the S_8 molecule is similar to that of S_8 in solution. The average shift rate of the edge is 2.3 Å/°K between 77 and 300°K.[19]

2. Quenched Sulfur. Figure 3c shows the absorption of polymeric sulfur prepared by quenching liquid sulfur from 250 to 0°. The resulting film is yellow and has a characteristic absorption shoulder at 3600 Å.

The spectrum of red sulfur glass, prepared by quenching a thin film of boiling sulfur on a quartz plate in liquid nitrogen, is shown in Figure 3d. The spectrum shows uv absorption due to S_8 and S_μ and additional peaks at 4100 and 5300 Å. It is similar to that of hot liquid sulfur and that of purple sulfur prepared by quenching a molecular beam of hot sulfur vapor on a cold target.[14] The Franck–Condon curve and the location of the peaks at 4100 and 5300 Å is similar to that of sulfur vapor.

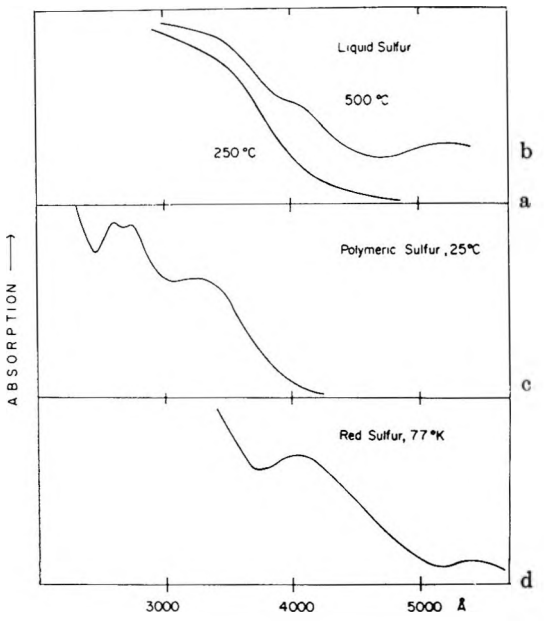

Figure 3. Absorption spectra of sulfur samples: (a) liquid sulfur film at 250°; (b) liquid sulfur film at 500°; (c) polymeric sulfur at 25°; and (d) red sulfur glass prepared by quenching boiling liquid to 77°K.

3. Allotropes in Solution. The spectra of S_8 solutions are shown in Figure 4. Figure 4a is a density tracing of the spectrum in isopentane–cyclohexane at 25°, and Figure 4b corresponds to a solution in 1:2 isopentane–cyclohexane (*i*PC) at 77°K. Both solutions show two peaks around 2700 Å which have been assigned to the transition $E_1 \leftarrow A_1$.[22] Except for small solvent shifts, and different bandwidths around the maxima, the difference between the spectra is due to temperature dependent broadening of the red absorption edge. The shift of the red edge at optical density 0.6 is about 2 $cm^{-1}/°K$.

The spectrum of S_6 is shown in Figure 4c. It has a shoulder at 2800 Å and a shallow tail which causes the golden tint of S_6 crystals.

4. Photolysis of Chlorosulfanes. Figure 5a shows the spectrum of a 10^{-3} *M* solution of S_3Cl_2 in a 1:2 isopentane–cyclohexane glass at 77°K. S_3Cl_2 has a continuous absorption with a peak at about 2700 Å. Upon 1 min of photolysis with a high-pressure mercury arc, the S_3Cl_2 absorption reduces and absorption bands

(22) L. B. Clark, Ph.D. Thesis, University of Washington, 1963.

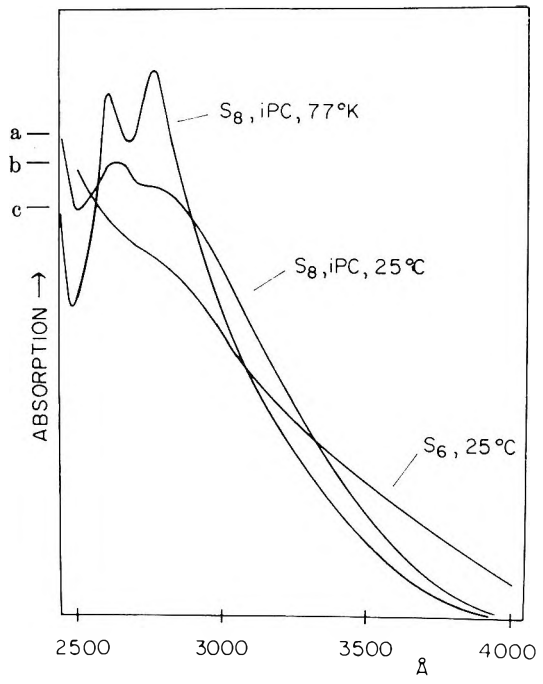

Figure 4. Absorption spectra of solutions: (a) 10^{-3} M solution of S_8 in isopentane–cyclohexane (iPC) glass at 25°; (b) S_8 in iPC at 77°K; (c) S_6 in ethyl ether at 25°.

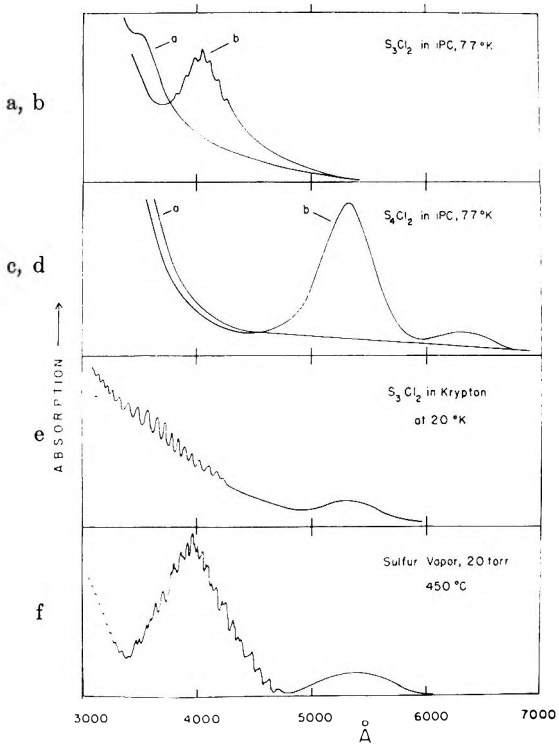

Figure 5. Absorption of low-temperature samples and vapor: (a) S_3Cl_2 in isopentane–cyclohexane (iPC) glass at 77°K; (b) same after photolysis; (c) S_4Cl_2 in iPC glass at 77°K; (d) same after photolysis; (e) S_3Cl_2 in krypton matrix at 20°K after photolysis, and (f) sulfur vapor at 20 Torr and 450°.

at 4100 and 5300 Å appear. The 4100 Å absorption is structured and overlaps the red end of the S_3Cl_2 con-

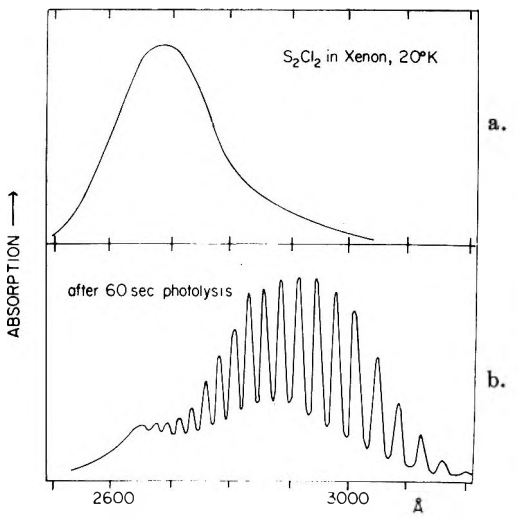

Figure 6. Absorption by S_2 species: (a) S_2Cl_2 in krypton matrix at 20°K; and (b) S_2, produced by photolysis of (a).

tinuum. Figure 5b shows the spectrum after 1 min of photolysis. If S_3Cl_2 is photolyzed in a krypton matrix at 20°K, the spectrum shown in Figure 5e obtains. This photolysis process is reminiscent of that of S_2Cl_2 in inert matrices at 20°K, Figure 6a, which yields S_2, as shown in Figure 6b.[15] The spectrum of S_4Cl_2 before and after photolysis is shown in Figure 5c and 5d. Photolysis yields a strong band at 5300 Å.

5. Sulfur Vapor. Below 300° the absorption of sulfur vapor is mainly due to S_8. At low pressure and high temperature, S_2 absorption, with an origin at 31690 cm^{-1}, predominates. Figure 5f shows the absorption spectrum of sulfur vapor at intermediate temperatures and pressures. A structured absorption around 4100 Å and a continuum at 5100 Å appears. At 20 Torr it is strongest at 450°. The composition of the vapor under these conditions is well known[17,18] and will be discussed below. A vibrational analysis of the 4100-Å bandwidth and isotope substitution indicates that the origin of the transition is at 23,671 cm^{-1} (4235 Å). Details of the analysis will be presented at some other location.[23]

Discussion

Our results indicate that the absorption edge of liquid sulfur at optical density 0.6 shifts by an average of 23.6 cm^{-1} (5.7 Å/°K). Bass[6] reported a value of 6.2 Å/°C between 110 and 444°, and Mondain-Monval[5] found 2.94 Å/°C below 160° and 7.44 Å/°C above 160°. Our value agrees very well with that of Bass, who explained the shift by thermal population of ground-state vibrational bands of S_8. This explanation is based on a model developed by Gilleo[7] for liquid Se. However, examination of the spectrum of liquid sulfur below the absorption edge and comparison with spectra of other

(23) B. Meyer, T. Stroyer-Hansen, and T. V. Oommen, unpublished work.

sulfur forms shows that this interpretation can only explain the color at low temperatures. Above 250°, this interpretation is insufficient because of at least four reasons. First, the shift rate is much larger in the liquid than in the solid or in solutions of S_8; second, although the absorption edge retains approximately the same slope (Figure 1), new absorption peaks appear at high temperature at 4100 Å and at 5300 Å (Figure 3b); third, it is known that molecules other than S_8 form when liquid sulfur is heated, and it can be expected that the absorption of other species contributes to the color;[3] and fourth, we have observed that boiling sulfur, when rapidly quenched, remains red (Figure 3d).

The shift rate in the liquid is more than twice larger than the value of 2.3 Å/°C measured on S_8 crystals between 77 and 300°K.[19] The spectrum of S_8 in various solvents between 77 and 300°K, Figure 4a–c, also indicates a smaller shift, of 1.3 cm^{-1}/°K. Thus, the question arises as to what causes such a large shift for the liquid phase. A marked discontinuity in the shift rate at 160° in Figure 2 coincides with polymerization. Thus, it is necessary to consider the spectrum of large sulfur chains. This spectrum is shown in Figure 3c. It shows a shoulder at 3600 Å which is not present in cyclo-S_8. This shoulder is 800 Å to the red of the absorption edge of S_8. Such a change in absorption is of the expected size for electronic transitions of a molecule whose chain length is increased from 8 to infinity. The observed shift from S_8 to S_∞ corresponds very closely to that observed for hydrocarbon chains.[24] Inspection of the polymer absorption and comparison with the spectrum of the liquid show that the concentration increase of polymer between 160 and 180° and simultaneous thermal broadening of the 3600 Å band can explain the large absorption shift rate in liquid sulfur up to 250° and the maximum of the shift rate at 160°.

The color above 250° cannot be explained by formation of polymeric sulfur, because of the absorption shoulders at 4100 and 5300 Å, Figure 3b, which are not present in polymeric sulfur or any other known allotrope, and because the increase in polymer concentration is insufficient to account for the continued large shift rate. Thus, at least one other species must be present between 250 and 700°.

Research on the composition of quenched sulfur samples is hampered because, as explained above, quenching leads to change in composition. In addition, the composition of quenched material depends on the initial and final temperature, the temperature gradient, and several other factors. Red quenched sulfur bleaches and converts to polymeric sulfur at −80°. Boiling sulfur quenched at −80° is yellow and yields an elastic, rubbery transparent film similar to that produced by polymeric sulfur quenched from 250 to 0° in ice water. The spectrum is the same as shown in Figure 3c. At room temperature, all quenched films crumble, turn opaque and dull, and eventually convert to orthorhombic sulfur. If organic impurities are present, quenched sulfur is brown because organic polysulfides are formed in the hot liquid. Their color is similar to that of the hot pure liquid, and thus has been the cause of much confusion because some early researchers thought that the brown color was due to unstable species. However, impure quenched sulfur remains brown at room temperature, while our quenched red sulfur is metastable at 77°K and converts to yellow sulfur at −80°.

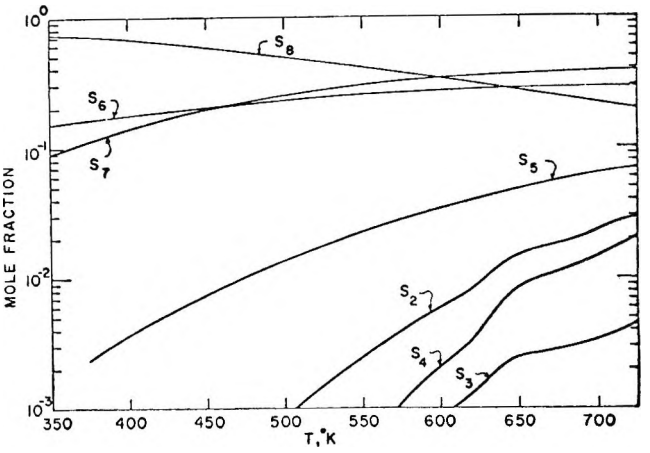

Figure 7. Saturated vapor composition, after ref 18.

The red metastable solid is similar to a solid which can be obtained by trapping vapor.[14] The composition of the trapped vapor is complex, but fortunately, the composition of equilibrium vapor is now known,[17,18] as shown in Figure 7.[21] At an intermediate temperature, the concentrations of S_3, S_4, and S_5 increase at a rate which is comparable to the red shift of the absorption of the liquid. The color of vapor is similar to that of the liquid. Thus, it is reasonable to consider these small species in the liquid, as Erdmann, without the benefit of modern knowledge, had already done in 1908.[1]

A continuous gas phase absorption with a peak at 5100 Å has been assigned to S_3 or S_4,[25] and a band system with vibrational structure at 4100 Å has also been tentatively assigned to S_3 or S_4.[26] The vapor spectrum shown in Figure 5e fits the color of the liquid well. Since it is difficult to identify or analyze the red component of sulfur vapor, hot liquid sulfur, or quenched sulfur, we aimed at finding other systems containing elemental sulfur species and at isolating or synthesizing pure sulfur allotropes in matrices and glasses. After exploring various methods and procedures, we discovered that the best preparation method for small sulfur allotropes is the photolysis of the corresponding chloro- or bromosulfane in an organic glass or a rare gas matrix at 20°K.[15,27]

(24) J. W. Raymonda and W. Simpson, *J. Chem. Phys.*, **47**, 430 (1967).

(25) H. Braune and E. Steinbacher, *Z. Naturforsch.*, **7a**, 486 (1952).

(26) L. d'Or, *Compt. Rend. Acad. Sci. Fr.*, **201**, 1026 (1935).

In a detailed study on S_2Cl_2 and S_2Br_2 in rare gas matrices,[15,27] we found that photolysis at 255.5 nm produces over 90% yield of S_2 (Figure 6b). The S_2 synthesized in this manner has the same absorption and emission spectrum as that produced by trapping S_2 vapor from a Knudsen cell. Figures 5a and b show the visible absorption of S_3Cl_2 before and after photolysis in a 1:2 isopentane–cyclohexane glass. The spectrum of photolyzed S_3Cl_2 shows a very strong absorption band at 4100 Å and a very weak band at 5200 Å. Both systems also absorb below 3500 Å due to undecomposed materials. No uv evidence for Cl–S_3 was found, although such species surely must be present. Figure 5e shows the spectrum of S_3Cl_2 photolyzed in a krypton matrix at 20°K. The spectrum consists of one single progression with $v'_1 = 400$ cm^{-1} with an origin $T_{00} = 23600 \pm 100$ cm^{-1}. This corresponds to a gas phase value of $v'_1 = 405$ cm^{-1} and $T_{00} = 23671$ cm^{-1}. The similarity between gas phase and matrix data suggests that these systems are due to absorption by the same molecule. In the iPC glass the shift of the transition origin is about 700 cm^{-1}. This red shift is of the order expected for such a system.[21] The vapor contains only elemental sulfur, the matrix only S_3Cl_2, S_3Cl, S_3, or smaller species. Since the absorption of S_2 and S_2Cl_2 photolysis products is further to the blue, Figure 6a and 6b, the 4100-Å band can only belong to S_3. A similar argument for the photolysis band of S_4Cl_2 at 5300 Å, Figure 5d, leads to the conclusion that it belongs to S_4. Neither in the vapor nor in the glass does this band show vibrational structure. The weak band at 5300 Å in photolyzed S_3Cl_2 (not shown in Figure 5b) is obviously due to S_4Cl_2 impurities in the sample, and the weak band at 6200 Å in photolyzed S_4Cl_2 might likewise belong to impurities, perhaps S_5 or even higher sulfane derivatives.

The combined evidence from photolyzed chlorosulfanes, sulfur vapor, trapped vapor, liquid and quenched liquid sulfur indicates that the color of hot liquid sulfur is due to absorption of S_3 and S_4. However, neither S_3 nor S_4 is the major constituents of liquid sulfur. If one compares the integrated absorption of a 10-cm path of vapor at 450° and equilibrium pressure with the absorption of the liquid, one computes a concentration of red colored species of 1 to 2 weight % ± 200% at 400° and 0.01% ± 200% at 250°. Thus, the colored species are comparatively minor constituents of the liquid, with the bulk being an as yet unanalyzed mixture of S_8, S_n, etc. Much more work will be necessary to elucidate the properties of S_3 and S_4 and to identify and characterize the other species. However, some predictions are possible. As Figure 7 shows, the presence of S_3 and S_4 implies the presence of S_5, S_6, and S_7. They all have similar thermal properties.[17,18] From Figure 7 one would also expect some S_6 and probably all of the molecules with S_n, $3 < n < 12$, to be present. However, the exact composition of the liquid cannot simply be deduced from the composition of the vapor because each species has a somewhat different heat of vaporization and heat of solution and because the equilibrium between the species in the liquid is affected by the presence of polymers and S_8, which, even at high temperature, are probably prevailing species. A further[28] difference between vapor and liquid is that the relative stability of rings and chains might change. In the vapor S_n rings with $n \geq 4$ might be more stable than the corresponding chains, while in solution the reverse might be true. Unfortunately, we do not yet know much about the shape of these molecules[18,28] and cannot make predictions about their properties.

Conclusion

Our study shows that the temperature dependence of the color of liquid sulfur is not due to thermal broadening of the S_8 spectrum alone, but is also determined by the overlap of absorption of S_8, polymeric sulfur, S_3 and S_4, which are in thermal equilibrium with many other allotropes. The unraveling of the exact composition of the liquid is difficult and far from complete.

However, it seems that the color of liquid sulfur can now be explained. In the low range between the melting point and 250°, the spectrum of the liquid is mainly due to broadened S_8, but with increasing temperature the contribution of polymeric sulfur increases. In the upper temperature range, between 250 and 700°, the color and the absorption edge are essentially determined by the concentration of S_3 and S_4. The combination of contributors explains the complicated shift rate of the absorption edge which puzzled earlier workers who had erroneously concluded from the approximately constant slope of the tail of the red absorption edge that the opaque part of the spectrum was always due to S_8.

The presence of S_3 and S_4 and other species in liquid sulfur necessitates rethinking of our views on elemental sulfur. The small molecules seem to be thermally more stable than anticipated; their presence and their reactivity, rather than the presence of polymers, explain why hot sulfur reacts with all solvents at or above 250° and why even traces of organic impurities lead to discoloring of elemental sulfur. It will be challenging to learn more about the small sulfur allotropes and to prove their presence through direct reaction.

Acknowledgment. This work was supported by the National Science Foundation (GP-9234) and by the National Air Pollution Control Administration (AP-639). The Cary spectrophotometer was purchased for the Chemistry Department with a National Science Foundation grant (GP-10506). We wish to thank Miss B. Gotthard for help with experimental work.

(27) A. Morelle, Ph.D. Thesis, University of Washington, 1970.
(28) N. W. Luft, *Monatsh. Chem.*, 86, 474 (1955).

The Crystal and Molecular Structure of L-Alanyl-L-alanine

by R. J. Fletterick, Chun-che Tsai, and R. E. Hughes*

Department of Chemistry, Cornell University, Ithaca, New York 14850 *(Received June 18, 1970)*

Publication costs assisted by the National Institutes of Health and the Materials Science Center, Cornell University

L-Alanyl-L-alanine crystallizes in the tetragonal space group, $I4$, with $a = 17.985 \pm 0.005$ Å and $c = 5.154 \pm 0.003$ Å. The crystal structure of this dipeptide was solved using noncentrosymmetric direct methods on 1396 reflections measured with Mo Kα radiation on an automatic four-circle diffractometer; details of the phasing procedure are briefly discussed. Full-matrix least-squares refinement of the structure yielded a conventional $R = 0.066$, with standard deviations of 0.005 Å and 0.3° in the bond lengths and bond angles. Comparison of the peptide bonding parameters with a weighted average set of available data presented by Marsh and Donohue reveals small but statistically significant differences. The conformation of the molecule in this zwitterion structure differs markedly from the more nearly planar form found in the hydrochloride derivative. The intricate hydrogen bond network, atypical of other known peptide crystal structures, interlocks tetragonally-packed columnar arrays of four-membered rings of molecules.

Introduction

The application of direct statistical methods to noncentrosymmetric structures typically involves space groups of orthorhombic or lower symmetry and the structures usually include a moderately heavy atom or a substantial planar group. This report on L-alanyl-L-alanine describes a unique and curious equal-atom dipeptide structure in a remarkably rare tetragonal space group, $I4$. In addition to its intrinsic interest as an unusual example of a zwitterion dipeptide structure unperturbed by heavy atom or salt interactions, it provides an interesting comparison with the recently reported[1,2] structure of L-alanyl-L-alanine hydrochloride; significant differences are revealed in the conformation of the molecule in the two states. Such comparisons are of fundamental importance to any analysis of the effects of hydrogen bonding and ionic interactions on the conformation of peptide linkages. The ultimate success of *a priori* calculations of peptide and protein conformations must surely depend upon the successful analysis of such perturbations in suitable model systems.

Experimental Section

Colorless, lath-like single crystals of L-alanyl-L-alanine (Mann Research Laboratories) were slowly grown at room temperature from aqueous solution. Preliminary Weissenberg and precession photographs revealed a centered tetragonal cell with no additional extinctions; the space group, $I4(C_4^5)$, uniquely indicated for an acentric structure displaying this diffraction symmetry, was further confirmed in the subsequent structural analysis.

The lattice constants, $a = 17.985 \pm 0.005$ Å and $c = 5.154 \pm 0.003$ Å, were determined in a least-squares analysis of the angular settings of 26 automatically centered reflections (at $\pm 2\theta$) within the angular range $20° < |2\theta| < 35°$ using Zr filtered Mo Kα radiation on a Picker FACS-1 four-circle diffractometer. The experimental density of 1.28 g/cc agrees with the value 1.28 g/cc calculated for $Z = 8$.

The diffraction intensities were measured on a crystal having dimensions 0.70 mm × 0.25 mm × 0.10 mm using Zr-filtered Mo Kα radiation with the diffractometer operating in the θ–2θ scan mode. Of the 1485 independent data investigated within the angular range $2\theta < 62°$, 1396 were retained as objectively observed with $|F_o| > 0.675\sigma_F$, where σ_F is defined by $\sigma_F = 0.02|F_o| + \sqrt{C + k^2B}/(2|F_o|L_p)$; C is the total count from the scan, and k is the ratio of scanning time to the total background counting time for the background count B. Approximately $1/2$ of those reflections which were rejected had negative net counts. Monitoring of three reflections throughout the course of the data collection showed no evidence of crystal degradation. Standard L_p corrections were applied, but neither absorption nor extinction corrections were required.

Structure Determination

The structure was solved using noncentrosymmetric direct methods[3] starting with 119 three-dimensional data with $|E| > 1.6$. The starting set of known phases included three $hk0$ reflections; the (3,11,0) was assigned a phase angle of π, and the (15, 1, 0) was signed using the Σ_2 relation. The phase of the (12, 8, 0) reflection was computed to be zero from the approximate Σ_1 relationship, $sE_{2h2k0} \sim s[\Sigma_l(|E_{hkl}|^2 - 1) + \Sigma_l(|E_{h+k,k-h,l}|^2 - 1)]$. The starting sets, shown in

(1) Y. Tokuma, T. Ashida, and M. Kakudo, *Acta Crystallogr. Sect. B*, 25, 1367 (1969).

(2) See also R. A. Pasternak and J. E. Leonard, *ibid.*, 5, 152 (1952).

(3) J. Karle and I. L. Karle, *ibid.*, 21, 849 (1966).

Table I: Starting Phase Assignments

h	k	l	$\|E\|$	Phase
15	1	0	2.53	0
3	11	0	2.14	π
12	8	0	1.72	0
4	4	2	1.87	$-\pi/5$
2	8	4	1.70	$\pm\pi/2$
11	4	1	1.82	$\pm\pi/2$

Table I, were completed by an arbitrary assignment of $-(\pi/5)$ to the phase of (4, 4, 2), and of $\pm\pi/2$ to both the (2, 8, 4) and the (11, 4, 1) reflections.

These four starting sets were each expanded in a computer formalism[4] using the expression $\varphi_{\vec{h}} = \langle\varphi_{\vec{k}} + \varphi_{\vec{h}-\vec{k}}\rangle$. From these four sets, the one with the largest consistency index, $\bar{C} = 0.48$, and the largest $\bar{\alpha}$ index, $\bar{\alpha} = 15.6$, was chosen for tangent refinement with the inclusion of 25 additional data. The $\bar{\alpha}$ index[3] is given by $\bar{\alpha} = \langle 2\sigma_3\sigma_2^{-3/2}|E_{\vec{h}}|(A^2 + B^2)^{1/2}\rangle$ and the consistency index[5] is defined by $\bar{C} = \langle(A^2 + B^2)^{1/2}/\Sigma|E_{\vec{k}}E_{\vec{h}-\vec{k}}|\rangle$, where $A = \Sigma|E_{\vec{k}}E_{\vec{h}-\vec{k}}|\cos(\varphi_{\vec{k}} + \varphi_{\vec{h}-\vec{k}})$ and $B = \Sigma|E_{\vec{k}}E_{\vec{h}-\vec{k}}|\sin(\varphi_{\vec{k}} + \varphi_{\vec{h}-\vec{k}})$. After three iterations, the quantities $\bar{C}$ and $\bar{\alpha}$ increased to 0.62 and 22.0, respectively, and all 144 phases were statistically acceptable. A Fourier synthesis based upon these results was structurally interpretable; eight atomic positions were assigned among the 11 strongest peaks in the E map. When six of these atom positions were used to phase a standard Fourier synthesis utilizing all the observed data ($R = 0.45$), peaks corresponding to the remaining five atoms of the molecule appeared. The initial positional parameters for least-squares refinement were deduced from the E map and the Fourier synthesis. A subsequent comparison with the final refined model revealed an average error of 26° for the 144 tangent refined phases.

A single cycle of full-matrix least-squares[6,7] weighted with $w_1 = 1/\sigma_F^2$ yielded a residual, $R = (\Sigma||F_o| - |F_c||)/(\Sigma|F_o|) = 0.15$. The positions of all 12 hydrogen atoms were located in a difference Fourier and included in a single cycle of refinement of all nonhydrogen atom parameters with anisotropic thermal factors which reduced R to 0.091. An alternate weighting scheme was introduced with $w_2 = 1/\sigma^2$, and $\sigma = \sum_0^3 a_n|F_o|^n$; the expansion coefficients, a_n, were derived from a least-squares fitting of the curve $||F_o| - |F_c|| = \sum_0^3 a_n|F_o|^n$. One cycle of refinement of the hydrogen atom positions with isotropic thermal parameters further reduced R to 0.071. Two final refinement cycles were run; in the first, all parameters were allowed to vary, while in the second, only the nonhydrogen atom parameters were refined. The final weighted residual, $R_{w_2} = [\Sigma w_2(|F_o| - |F_c|)^2]^{1/2}/(\Sigma w_2|F_o|^2)^{1/2}$ was 0.094 and the final unweighted $R = 0.066$. It is interesting to note that the final structure parameters derived from the refinement based upon weighting with w_2 yielded a final value of $R_{w_1} = 0.067$.

Results and Discussion

The final atomic coordinates and the anisotropic thermal parameters for all nonhydrogen atoms are given in Tables II and III; the corresponding data for the hydrogen atoms are listed in Table IV. The appropriate atom labels can be identified in the perspective view of the molecule in Figure 1.

Table II: Fractional Coordinates with Estimated Standard Deviations

Atom	10^4x	10^4y	10^4z
O(1)	−1259 (1)	2719 (2)	292 (9)
O(2)	711 (2)	2396 (2)	−3284 (10)
O(3)	1452 (1)	2580 (2)	0
N(1)	−1900 (1)	2070 (1)	4397 (9)
N(2)	−104 (1)	2770 (1)	2159 (9)
C(1)	−794 (2)	1296 (3)	4076 (19)
C(2)	−1069 (2)	2093 (2)	4355 (11)
C(3)	−824 (1)	2568 (2)	2044 (10)
C(4)	265 (1)	3180 (2)	91 (10)
C(5)	618 (3)	3882 (2)	1167 (15)
C(6)	857 (2)	2678 (2)	−1175 (10)

Relatively few precise structures have been reported for peptides, especially in the nonhydrohalide form, but in a recent review,[8] a set of bond lengths and bond angles has been developed from a weighted average of the available data. The bonding parameters for L-al-

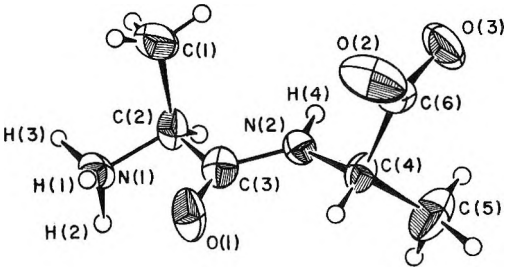

Figure 1. An ORTEP drawing of the L-alanyl-L-alanine molecule.

(4) Chun-che Tsai, Ph.D. Thesis, Indiana University, 1968.

(5) M. G. B. Drew, D. H. Templeton, and A. Zalkin, *Acta Crystallogr.*, **B25**, 261 (1969).

(6) W. R. Busing and H. A. Levy, "A Fortran Crystallographic Least-Squares Program," ORNL-TM-305, Oak Ridge National Laboratory, Oak Ridge, Tenn., 1962.

(7) Detailed information concerning $|F_o|$,$|F_c|$ will appear following these pages in the microfilm edition of this volume of the journal. Single copies may be obtained from the Reprint Department, ACS Publications, 1155 Sixteenth St., N. W., Washington, D. C. 20036, by referring to author, title of article, volume, and page number. Remit $3.00 for photocopy of $2.00 for microfiche.

(8) R. E. Marsh and J. Donohue in *Advan. Protein Chem.*, **22**, 235 (1967).

Table III: Thermal Parameters,[a] Å²

Atom	B_{11}	B_{22}	B_{33}	B_{12}	B_{13}	B_{23}	B^b
O(1)	2.9 (1)	5.3 (1)	3.0 (1)	−0.9 (1)	−0.4 (1)	1.5 (1)	3.39
O(2)	6.0 (2)	6.4 (2)	3.2 (1)	2.7 (1)	−0.3 (1)	−1.3 (1)	4.49
O(3)	2.4 (1)	5.0 (1)	5.1 (1)	0.5 (1)	−0.3 (1)	−1.6 (1)	3.73
N(1)	2.6 (1)	2.6 (1)	3.0 (1)	−0.1 (1)	0.6 (1)	0.4 (1)	2.69
N(2)	2.4 (1)	3.2 (1)	2.3 (1)	−0.3 (1)	0.5 (1)	0.1 (1)	2.53
C(1)	3.2 (1)	4.3 (2)	11.2 (5)	1.0 (1)	1.9 (2)	3.4 (3)	4.71
C(2)	2.8 (1)	3.0 (1)	2.7 (1)	−0.7 (1)	−0.2 (1)	0.7 (1)	2.70
C(3)	2.3 (1)	2.4 (1)	2.2 (1)	−0.2 (1)	0.4 (1)	−0.1 (1)	2.28
C(4)	2.2 (1)	2.4 (1)	2.8 (1)	0.0 (1)	0.6 (1)	0.3 (1)	2.40
C(5)	6.0 (2)	3.0 (1)	6.6 (3)	−1.4 (1)	2.5 (2)	−1.5 (2)	4.42
C(6)	2.2 (1)	2.7 (1)	2.4 (1)	0.3 (1)	0.6 (1)	0.5 (1)	2.34

[a] The B_{ij} in Å² are related to the dimensionless β_{ij} employed during refinement by $B_{ij} = 4\beta_{ij}/a_i^* a_j^*$. [b] The isotropic thermal parameter is calculated from $B = 4[V^2 \det(\beta_{ij})]^{1/2}$.

Table IV: Fractional Coordinates and Thermal Parameters for the Hydrogen Atoms

Atom	10^3x	10^3y	10^3z	B_A[a]	B, Å²
H(1)	−205 (5)	192 (5)	311 (24)	3	1 (2)
H(2)	−208 (3)	252 (4)	445 (19)	3	3 (1)
H(3)	−207 (3)	178 (3)	560 (14)	3	3 (1)
H(4)	17 (2)	267 (2)	368 (10)	3	1 (1)
H(5)	−90 (2)	232 (2)	593 (9)	3	1 (1)
H(6)	−5 (3)	328 (3)	−121 (12)	2	3 (1)
H(7)	−35 (6)	129 (5)	395 (26)	5	8 (2)
H(8)	−94 (3)	101 (3)	571 (12)	5	3 (1)
H(9)	−102 (5)	107 (5)	206 (24)	5	6 (3)
H(10)	86 (4)	413 (4)	18 (18)	4	6 (2)
H(11)	31 (5)	425 (5)	165 (22)	4	5 (2)
H(12)	107 (5)	368 (5)	252 (21)	4	5 (2)

[a] This quantity is the thermal parameter for the atom to which the hydrogen is bonded.

Table V: Interatomic Distances and Bond Angles for Nonhydrogen Atoms

	Angle, deg		Length, Å
C(3)–N(2)–C(4)	122.9 (3)	O(1)–C(3)	1.226 (4)
C(1)–C(2)–N(1)	107.4 (3)	O(2)–C(6)	1.228 (5)
C(1)–C(2)–C(3)	110.9 (4)	O(3)–C(6)	1.241 (4)
C(3)–C(2)–N(1)	108.4 (3)	N(1)–C(2)	1.494 (4)
N(2)–C(3)–O(1)	125.9 (3)	N(2)–C(3)	1.344 (4)
N(2)–C(3)–C(2)	113.2 (3)	N(2)–C(4)	1.457 (4)
C(2)–C(3)–O(1)	120.9 (3)	C(1)–C(2)	1.523 (5)
N(2)–C(4)–C(5)	110.1 (3)	C(2)–C(3)	1.530 (4)
N(2)–C(4)–C(6)	109.2 (2)	C(4)–C(5)	1.518 (5)
C(5)–C(4)–C(6)	110.7 (3)	C(4)–C(6)	1.539 (4)
O(2)–C(6)–O(3)	123.9 (3)		
O(2)–C(6)–C(4)	118.0 (3)		
O(3)–C(6)–C(4)	118.1 (3)		

Table VI: Bond Lengths and Bond Angles for the Hydrogen Atoms

	Angle, deg		Length, Å
H(1)–N(1)–H(2)	103.0	N(1)–H(1)	0.77
H(1)–N(1)–H(3)	106.1	N(1)–H(2)	0.88
H(2)–N(1)–H(3)	113.8	N(1)–H(3)	0.87
H(4)–N(2)–C(4)	119.4	N(2)–H(4)	0.95
H(4)–N(2)–C(3)	117.6	C(1)–H(7)	0.79
H(7)–C(1)–H(8)	108.4	C(1)–H(8)	1.02
H(7)–C(1)–H(9)	105.1	C(1)–H(9)	1.19
H(8)–C(1)–H(9)	117.5	C(2)–H(5)	0.96
H(5)–C(2)–N(1)	108.5	C(4)–H(6)	0.90
H(5)–C(2)–C(1)	112.2	C(5)–H(10)	0.94
H(5)–C(2)–C(3)	109.4	C(5)–H(11)	0.89
H(6)–C(4)–N(2)	111.0	C(5)–H(12)	1.14
H(6)–C(4)–C(5)	111.5		
H(6)–C(4)–C(6)	104.1		
H(10)–C(5)–H(11)	98.6		
H(10)–C(5)–H(12)	105.6		
H(11)–C(5)–H(12)	120.9		

anyl-L-alanine are listed in Tables V and VI; in general, the agreement with the averaged values is excellent although a number of statistically significant differences do appear. In the peptide group, the bond C(2)–C(3) = 1.53 Å corresponds to the value proposed by Pauling and Corey[9] rather than the 1.51 Å given by Marsh and Donohue.[8] The angle C(2)–C(3)–N(2) = 113.2° is substantially smaller than the 116° weighted average; this contraction appears to arise from the general constraints on the molecule rather than from a specific interaction.

All of the bond lengths and angles at the N-terminal end of the molecule are equal within experimental error to those derived[8] from a weighted average of amino acid structures. The two C–O distances in the carboxylate group are somewhat smaller than the value of 1.25 Å found in the amino acids. This is only partly compensated for by the fact that the oxygen atoms have two of the highest thermal parameters in the struc-

(9) L. Pauling and R. B. Corey, *Proc. Nat. Acad. Sci. U. S.*, **39**, 253 (1953).

ture; corrections of 0.010–0.015 Å might be required to offset librational foreshortening of these bonds. Similar corrections are probably appropriate for the two bonds to the methyl carbons which also have high temperature factors.

Despite the fact that it forms four strong intermolecular hydrogen bonds, the carboxylate group maintains its planarity within one estimated standard deviation; the parameters of the least-squares plane are given in Table VII. The group also displays nearly perfect twofold symmetry with only modest deviations from 120° angles.

Table VII: Mean Planes and Atomic Displacements Therefrom

Peptide group[a]		Carboxyl group[b]	
Atom	Dev, Å	Atom	Dev, Å
C(2)	−0.002	O(2)	0.0005
C(3)	0.007	O(3)	0.0005
O(1)	−0.003	C(6)	−0.0015
N(2)	−0.002	C(4)	0.0004
C(4)[c]	−0.09		

[a] Equation of plane: $-0.26317x + 0.83117y + 0.48979z = 4.73551$. [b] Equation of plane: $0.39149x + 0.79475y - 0.46379z = 4.70950$. [c] This atom was not included in the calculation of the mean plane.

The peptide group, C(2), C(3), O(1), N(2), is planar within experimental error (see Table VII). The atom C(4), not included in the calculation of the mean plane, lies 0.09 Å out of the plane; this corresponds to a dihedral angle, $\omega = 355.8 \pm 0.5°$. The angle between the carboxylate plane and the peptide plane is 110.0 ± 0.5°, nearly 90° from the value found in the hydrochloride structure.[1] The values of the dihedral angles associated with the peptide group are listed in conventional form[10] in Table VIII; the corresponding values for the hydrochloride structure[1] are also presented for comparison. The major differences in the conformation of the molecule, revealed in the values of ψ_1, ψ_2, and φ, clearly arise from the strikingly different hydrogen bonding and ionic interactions in the two crystal environments. The potential energy functions representing rotational states of these dihedral angles are of considerable importance in the analysis of equilibrium conformations of peptide sequences. The derivation of information from a comparison of peptide crystal structures is a formidable task, complicated by intricate hydrogen bonding networks. Nevertheless, such comparisons may provide useful tests for model energy functions and parameters.

Table VIII: A Comparison of the Dihedral Angles of L-Alanyl-L-alanine with Those of L-Alanyl-L-alanine Hydrochloride

Angle, deg	Bond	L-Alanyl-L-alanine hydrochloride	L-Alanyl-L-alanine
ψ_1	C(2)–C(3)	334.2	345.4 (4)
ψ_2	C(4)–C(6)	341.3	282.9 (3)
φ	N(2)–C(4)	26.5	67.1 (4)
ω	N(2)–C(3)	0.8	355.8 (5)

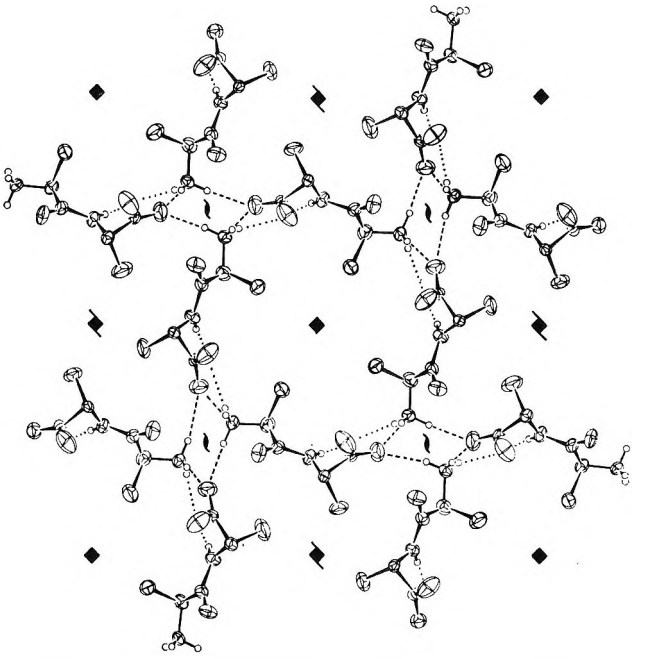

Figure 2. A view along the tetragonal axis of the packing of L-alanyl-L-alanine. Hydrogen bonds between molecules related by a cell translation along the z axis are represented by dotted lines; the other hydrogen bonds are shown as dashed lines.

The molecular packing of L-alanyl-L-alanine is dominated by a curious fourfold symmetry (Figure 2). Each molecule is bonded to its neighbors through a total of eight hydrogen bonds. The protonated nitrogen atom, N(1), forms three links to carboxylate oxygens in three different molecules. The first of these bonds is involved in a four-membered head-to-tail ring around the fourfold axis; the second one joins this ring to the equivalent group at the center of the cell; the third bond interlocks the ring with the one directly below it along the z axis. This columnar array is further stabilized by another hydrogen bond between the peptide nitrogen and a carboxylate oxygen in the adjacent molecule along the z axis. The remaining four intermolecular links are, of course, the complementary ones formed by the two carboxylate oxygen atoms. All of these hydrogen bond lengths lie in the range 2.80–2.86 Å, indicating that the interactions are moderately strong, but within the normal range (Table IX).

(10) J. T. Edsall, P. J. Flory, J. C. Kendrew, A. M. Liquori, G. Nemethy, G. N. Ramachandran, and H. A. Scheraga, *J. Mol. Biol.*, **15**, 399 (1966).

Table IX: Lengths and Angles for the Hydrogen Bonds

	H–O, Å	N–O, Å	Angles, deg (O–H–N)	Angles, deg (O–N–H)	Angles, deg (N–O–C)
N(1)–H(1)–O(3)	2.05	2.805 (4)	171.8	6.0	142.9 (3)
N(1)–H(2)–O(3)	1.96	2.834 (4)	172.5	5.2	135.0 (3)
N(1)–H(3)–O(2)	2.09	2.863 (4)	148.2	22.6	108.4 (3)
N(2)–H(4)–O(2)	1.90	2.849 (5)	176.5	2.3	137.9 (3)

An alternative description of these columnar arrays along the tetragonal axis invokes a somewhat artificial multiple helical model. Each column can be regarded as an interstranded set of four, 4_1 helices of molecules joined along the helix by head-to-tail hydrogen bonding. Each helix, of pitch 20.6 Å, is bonded to two other helices within the column and each column is bonded to four other columns.

The carbonyl oxygen, O(1), is not involved in any intermolecular hydrogen bond. However, the dihedral angle about C(2)–C(3) is only −14.6°; the sequence N(1)–C(2)–C(3)–O(1) is much more nearly planar than it is in the hydrochloride or in many related structures. Moreover, the O(1)–N(1) distance is only 2.68 Å. Since the atom H(1) is about 2.4 Å from O(1), the possibility of an intramolecular interaction between O(1) and N(1) cannot be excluded. The analysis of such a nonlinear system is clearly difficult, although a recent study[11] of similar five- and seven-membered ring systems in nonpolar solvents suggests that the interactions are significant.

A few secondary features of the structure are worthy of note. The refined hydrogen positions on the methyl carbon atoms precisely correspond, in each case, to a staggered conformation about the respective C–C bonds. Similarly, within experimental error, the three hydrogen atoms on N(1) are also staggered with respect to the substituents on atom C(1). The significance of this fact is obscured by the intricate hydrogen bonding geometry around N(1). Finally, there are no unusually short nonbonded contact distances in the structure. Methyl–methyl separations of 3.86 Å occur around the fourfold axis; intercolumnar methyl–methyl interactions of 4.15 and 4.59 Å around the 4_2 axis reflect the fact that only two of the eight hydrogen bonds are directed between the columns.

Acknowledgment. Financial support by the National Institutes of Health (GM-14832-03) is gratefully acknowledged. Additional support was received through the Materials Science Center, Cornell University. The authors also acknowledge the contributions of P. T. Ward during the early stages of this work.

(11) N. Avignon, P. U. Huong, and J. Lascombe, *Biopolymers*, **8**, 69 (1969).

Dependence of Vibrational Transition Probabilities on the Rotation Angles and Impact Parameter in BC + A Collisions[1a]

by Hyung Kyu Shin

Department of Chemistry, University of Nevada,[1b] Reno, Nevada 89507 *(Received October 5, 1970)*

Publication costs assisted by the U. S. Air Force Office of Scientific Research

Vibrational transitions in BC + A collisions are investigated by use of the sudden approximation. The transition probability P_{mn} is formulated for an arbitrary system of BC + A collisions, but the O_2 + Ar system is chosen for specific consideration. P_{01} is calculated as a function of the collision velocity v, impact parameter b, and molecular rotation angles θ, ϕ. Dependence of P_{01} on these collision parameters at different values of b is discussed. For $b < \sigma$, the angle-averaged transition probability increases with increasing v, while for $b > \sigma$ it decreases as v increases, where σ is the Lennard-Jones potential parameter.

Introduction

The problem of vibrational energy transfer at high collision energies (in the electron-volt region) is a subject of great interest from both experimental and theoretical standpoints. The recent progress in high-energy beam experiments is beginning to provide important information on absolute magnitudes of vibrational transition probabilities and related quantities.[2,3] With the advent of large memory high-speed computers, theoretical calculations of vibrational transition probabilites at high collision energies are becoming available[4-7] and are contributing to our understanding of vibrationally inelastic scattering. However, almost all of such calculations are based on the model of collinear collisions, which does not adequately represent the physics of molecular collisions, and a realistic model should explicitly consider collisions taking place at nonzero impact parameters and at different molecular orientations.

In a recent paper,[8] we considered low-energy collisions by use of the method of distorted waves and investigated collisions at different molecular orientations without specific reference to the role of impact parameters. In a subsequent paper,[9] we treated collisions at nonzero impact parameters and at different molecular orientations. The transition probability was formulated such that it can be used to investigate the problem of vibrational energy transfer at various impact parameters and orientation angles in high-energy collisions. Cosby and Moran[3] showed that the model and formulation reported in the latter paper gave vibrational transition probabilities of O_2 in $O_2 + O^+$ collisions which are in good agreement with their measured data in the collision energy range of 10–20 eV.

In studying vibrational energy transfer in the three-dimensional collision, we must recognize that the orientation angle changes during the course of energy transfer. Although this situation is intuitively clear, there has been no rigorous consideration of it in the calculation of vibrational transition probabilities. In the present paper we consider this problem in diatomic molecule–atom (BC + A) collisions by extending the collision model given in ref 9. The collision system is simple enough to allow an explicit consideration of this problem in calculating transition probabilities. After attempting several different methods for the derivation of vibrational transition probabilities in high-energy collisions, we found that the "sudden" approximation[10,11] is most suitable and simple to apply here; we use it in this paper. For BC + A collisions at energies in the electron-volt region, the use of this method should be appropriate. The orientation dependent interaction potential will be assumed to be of the Lennard-Jones form. In numerical illustrations we consider the $0 \rightarrow 1$ transition in O_2 + Ar collisions.

Formulation of Vibrational Transition Probability

In Figure 1 we show the three-dimensional collision

(1) (a) This work was carried out under Grant AFOSR-68-1354 from the Air Force Office of Scientific Research. (b) Theoretical Chemistry Group Contribution No. S-1029.

(2) (a) P. F. Dittner and S. Datz, *J. Chem. Phys.*, **49**, 1969 (1968). (b) J. Schottler and J. P. Toennies, *Z. Phys.*, **214**, 472 (1968).

(3) P. C. Cosby and T. F. Moran, *J. Chem. Phys.*, **52**, 6157 (1970).

(4) D. Secrest and B. R. Johnson, *ibid.*, **45**, 4556 (1966).

(5) J. D. Kelley and M. Wolfsberg, *ibid.*, **44**, 324 (1966).

(6) D. J. Wilson, *ibid.*, **53**, 2075 (1970); also see earlier papers by Wilson and his associates.

(7) Also, see D. Rapp and T. Kassal, *Chem. Rev.*, **69**, 61 (1969); they present an excellent review of recent work.

(8) H. Shin, *J. Chem. Phys.*, **49**, 3964 (1968).

(9) H. Shin, *J. Phys. Chem.*, **73**, 4321 (1969).

(10) K. Alder and A. Winther, "Coulomb Excitation," Academic Press, New York, N. Y., 1966, pp 209–280; the original article was published in *Kgl. Dan. Vidensk. Selsk., Mat.-Fys. Medd.*, **32**, No. 8 (1960).

(11) K. H. Kramer and R. B. Bernstein, *J. Chem. Phys.*, **40**, 200 (1964), presents the application of the sudden approximation to rotational transitions. Recently, M. A. Wartell and R. J. Cross, Jr., applied this approximation to vibrational inelastic scattering, *Chem. Phys. Lett.*, in press.

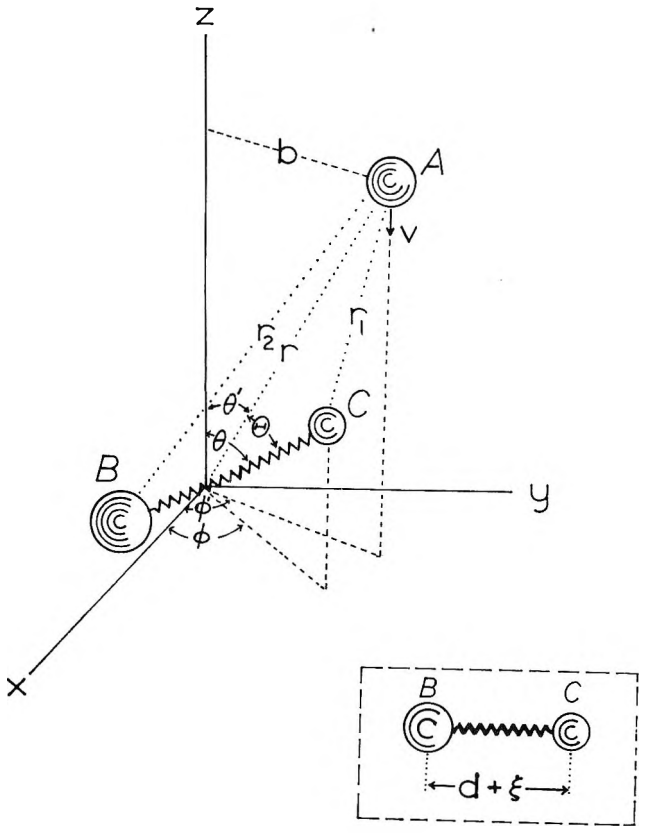

Figure 1. Collision model. Insertion shows the vibrational coordinate.

model for a general case of the BC + A interaction defining the collision coordinates needed to describe the encounter. According to the sudden approximation, the probability of the vibrational transition m to n is[10,11]

$$P_{mn}(v,b,\Theta) = \langle n|\exp[2i\eta(v,b,\Theta,\xi)]|m\rangle^2 \quad (1)$$

where the phase shift is

$$\eta(v,b,\Theta,\xi) = -\frac{1}{2\hbar}\int_{-\infty}^{\infty} V[v,b,\Theta,\xi,r(t)]\,dt \quad (2)$$

Here ξ is the vibrational coordinate, b the impact parameter, v the relative collision velocity [$E = (1/2)\mu v^2$], μ the reduced mass of the collision system, Θ the orientation angle, and V the potential energy which causes the transition. We use the linear trajectory approximation for the present high-energy collision system; then from Figure 1, we get the relations $r^2 = b^2 + z^2$ and $z = vt$. To see the effect of varying collision velocity, orientation angle, and impact parameter on transition probabilities it is then necessary to find an interaction potential function which is simple enough to allow the integration of eq 2 and yet complicated enough to be realistic in describing the dependence of transition probabilities on relevant collision variables. The assumed form of the interaction potential is[9]

$$U(r_1,r_2) = 2D\sum_{i=1}^{2}[(\sigma/r_i)^{12} - (\sigma/r_i)^6] \quad (3)$$

where $r_{1,2}^2 = r^2 \mp 2(d + \xi)S_{2,1}r\cos\Theta + (d + \xi)^2S_{2,1}^2$, $S_{1,2} = m_{B,C}/(m_B + m_C)$, d is the equilibrium distance of the B–C bond, and D, σ are the Lennard-Jones potential parameters for BC + A. The summation affects only two terms, since there are two interactions, *i.e.*, B–A and C–A. By use of the relations $r^2 = b^2 + z^2$ and $z = vt$, we can parameterize the interaction potential in the time variable. By introducing $r_{1,2}$ into eq 3 and by expanding each term in a power series, we extract out the ξ-dependent energy terms from eq 3. The result is expressed by

$$V[v,b,\xi,\Theta,r(t)] = 24(D/\sigma)[(\sigma/r)^{13} - {}^1/_2(\sigma/r)^7](S_2 - S_1)\xi \times \cos\Theta + 8D(d/\sigma^2)[(42\cos^2\Theta - 3)(\sigma/r)^{14} - (12\cos^2\Theta - {}^3/_2)(\sigma/r)^8](S_1^2 + S_2^2)\xi \quad (4)$$

where the third- and higher-order terms in $(d + \xi)/r$ are neglected. For homonuclear diatomic molecules, the first part disappears since $S_1 = S_2$. For heteronuclear diatomic molecules such as hydrogen halides $S_1 \ll S_2 \simeq 1$ so that we can approximate $(S_2 - S_1) \simeq S_1^2 + S_2^2 \simeq 1$. In the following the formulation of the vibrational transition probability will be made including all these terms of the interaction potential so that the result can be directly applied to both heteronuclear and homonuclear diatomic molecules.

From the collision geometry shown in Figure 1, the relative orientation angle can be obtained by

$$\cos\Theta = \frac{z\cos\theta + b\sin\theta\cos\phi}{(b^2 + z^2)^{1/2}} \quad (5)$$

where by rotating the coordinate system about the z axis the azimuthal angle ϕ' has been eliminated. This equation describes the variation of the molecular orientation angle Θ with the impact parameter, the collision velocity (as well as the time since $z = vt$), and the molecular rotation angles θ, ϕ during the collision process. The introduction of this relation into eq 5 leads to a complicated dependence of V on θ, ϕ, and b, and because of this relation the oriented collision is much more difficult to treat than the conventional collinear or three-dimensional case in which the orientation angle Θ is assumed to be independent of other coordinates. Equation 4 with the above relation for Θ can now be substituted into the phase shift given by eq 2.

The phase shift can be determined through trivial integrations. From eq 4, we have

$$\int_{-\infty}^{\infty} V[v,b,\xi,\Theta,r(t)]dt = 24D\sigma^{12}(S_2 - S_1) \times \left[\int_{-\infty}^{\infty} r^{-13}\cos\Theta\,dt - (2\sigma^6)^{-1}\int_{-\infty}^{\infty} r^{-7}\cos\Theta\,dt\right]\xi + 336Dd\sigma^{12}(S_1^2 + S_2^2)\left[\int_{-\infty}^{\infty} r^{-14}\cos^2\Theta\,dt -$$

$$(14)^{-1}\int_{-\infty}^{\infty} r^{-14}\mathrm{d}t - (^2/_7\sigma^6)\int_{-\infty}^{\infty} r^{-8}\cos^2\Theta\mathrm{d}t + (28\sigma^6)^{-1}\int_{-\infty}^{\infty} r^{-8}\mathrm{d}t\Big]\xi \quad (6)$$

With eq 5 for cos Θ and with the relations $r^2 = b^2 + z^2$ and $z = vt$, each integral in eq 6 can be reduced to the form of the β function. A straightforward simplification of the function leads to the result

$$\int_{-\infty}^{\infty} V[v,b,\xi,\Theta,r(t)]\mathrm{d}t =$$
$$(693/256)(D\pi/v)(S_2 - S_1)\xi[(\sigma/b)^{12} -$$
$$(160/231)(\sigma/b)^6]\sin\theta\cos\phi +$$
$$(9009/512)(D\pi/v)(d/\sigma)(S_1^2 + S_2^2)\xi \times$$
$$(\sigma/b)^{13}(\cos^2\theta + 2\sin^2\theta\cos^2\phi - {}^2/_{13}) -$$
$$(15/8)(D\pi/v)(d/\sigma)(S_1^2 + S_2^2)\xi(\sigma/b)^7 \times$$
$$(\cos^2\theta + 7\sin^2\theta\cos^2\phi - 1) \equiv G(v,b,\theta,\phi)\xi \quad (7)$$

Equation 7 is formulated such that it can also be applied to the collisions involving heteronuclear diatomic molecules. For O_2 + Ar collisions, the first term containing $(S_2 - S_1)$ of course vanishes. By multiplying eq 7 by $-(2\hbar)^{-1}$, we obtain the phase shift needed for the calculation of vibrational transition probabilities as a function of the impact parameter, the molecular rotation angles, and the collision velocity. It may be noted that the result for the collinear collision case cannot be obtained from eq 7. Rather, we need to set cos Θ = 1 in eq 4 and obtain the phase shift; the derivation is simpler than the present nonlinear oriented case. However, it is important to recognize that for nonzero impact parameter collisions the collinear arrangement of the oscillator with the incident atom would mean that the rotational angles continually vary so as to maintain Θ = 0. Of course, for $b = 0$, the collinear collision is a head-on encounter along the z axis and the problem of continual change in the angles does not arise. It is also important to point out that the orientation $\theta = \phi = 0$ represents the configuration in which the molecule is lying on the z axis; it does not imply the collinear configuration. From eq 5, for $\theta = \phi = 0$ we have Θ = $\cos^{-1}[z/(b^2 + z^2)^{1/2}]$, which approaches 0 and $\pi/2$, respectively, as $b \to 0$ and $\to \infty$. The latter two situations correspond to the collinear and perpendicular orientations, respectively.

In eq 4 we have only terms linear in the vibrational coordinate. The second part resulted from the terms containing $(d + \xi)^2$ of which the linear term is $2d\xi$. The vibrational transition probability now appears in the form

$$P_{mn} = \left\langle n\left|\exp\left[-\frac{i}{\hbar}G(b,v,\theta,\phi)\xi\right]\right|m\right\rangle^2 \quad (8)$$

We approximate the BC molecule by a harmonic oscillator; since we are interested only in the $0 \to 1$ transition particularly for the homonuclear diatomic molecule, the harmonic oscillator model should be satisfactory. With the harmonic oscillator wave functions for m and n states, we find[12]

$$P_{mn} = \frac{m!}{n!}K^{2(n-m)}\exp(-K^2)[L_m^{n-m}(K^2)]^2 \quad (9)$$

where $K = G(v,b,\theta,\phi)/(2M\hbar\omega)^{1/2}$, L_m^{n-m} is the Laguerre polynomial with $n \geq m$, and M, ω are the reduced mass and vibrational frequency of the oscillator, respectively. For $0 \to 1$, we then have the simple result

$$P_{01} = K^2\exp(-K^2) \quad (9a)$$

Since K is a function of v, b, θ, and ϕ, the functional dependence of eq 9 is $P_{mn}(v,b|\theta,\phi)$. The form of eq 9a is identical with the one derived from the solution of the time-dependent Schrödinger equation[13,14] or with the solution of the time-independent Schrödinger equation by use of the Green function method.[15] In the latter approaches, K^2 is replaced by $\Delta E_v/\hbar\omega$, where ΔE_v is the amount of the vibrational energy transferred to the oscillator. However, as can be easily seen from eq 9 that for transitions other than $0 \to 1$, the present formulation differs from those derived from the solutions of the Schrödinger equation.

If we consider the orientation angle as a parameter and ignore its θ- and ϕ dependence, the resulting expression for the transition probability is different from the above result and should be denoted by $P_{mn}(v,b|\Theta)$. As shown by eq 7 and 9, the θ- and ϕ dependence of P_{mn} appear in both the exponential and preexponential parts, thus leading to a complicated dependence of the efficiency of vibrational transitions on molecular orientations.

Numerical Results and Discussions

A. Validity of the Sudden Approximation. The sudden approximation can be used when the collision time t_c is small compared to the vibrational period t_v, which may be defined by $2\pi/\omega$. Therefore, before making use of the above formulation to calculate vibrational transition probabilities, we must show the range in which the approximation is valid and restrict the calculation to this range. In ref 9, the collision time for the interaction energy given by eq 3 is shown to be

$$t_c = \frac{\Gamma(^7/_{12})}{\Gamma(^1/_{12})}\left(\frac{\pi\mu}{2}\right)^{1/2}\frac{(4D\rho_1)^{1/12}\sigma}{E^{7/12}} \times \left[1 - \frac{1}{72}\left(\frac{\Gamma(^1/_{12})}{\Gamma(^7/_{12})}\right)^2\left(\frac{D}{E}\right)^{1/2}\frac{\rho_2}{\rho_1^{1/2}}\right] + \frac{5}{144}\frac{\Gamma(^5/_{12})}{\Gamma(^{11}/_{12})}\left(\frac{\pi\mu}{2}\right)^{1/2}\frac{b^2}{\sigma(4D)^{1/12}\rho_1^{1/6}E^{5/12}} \quad (10)$$

(12) D. Rapp and T. E. Sharp, *J. Chem. Phys.*, **38**, 2641 (1963).
(13) E. H. Kerner, *Can. J. Phys.*, **36**, 371 (1958).

where

$$\rho_1 = 1 + 6.321(\cos^2\Theta - {}^1/_{14})$$

$$\rho_2 = 1 + 1.806(\cos^2\Theta - {}^1/_8)$$

For O_2 + Ar collisions we take the following parameters:[16,17] $D = 1.63 \times 10^{-13}$ erg, $\sigma = 3.42$ Å, $d = 1.207$ Å, $\omega = 3.535 \times 10^{14}$ sec^{-1}. Then, by calculating the coefficients of $E^{7/12}$, $E^{1/2}$, and $E^{5/12}$ in eq 10 with these parameters, we obtain

$$t_c = \frac{2.46 \times 10^{-21}\rho_1^{1/12}}{E^{7/12}}\left[1 - \frac{1.01 \times 10^{-7}\rho_2}{(\rho_1 E)^{1/2}}\right] + \frac{2.05 \times 10^{-19}}{\rho_1^{1/6}E^{5/12}}\left(\frac{b}{\sigma}\right)^2 \text{ sec} \quad (10a)$$

where E is in erg units. For example, when $b/\sigma = 1.3$ the condition $t_c < t_v$ is satisfied for velocities above 8×10^5 cm/sec, while for $b/\sigma = 0.8$ it is satisfied above 4×10^5 cm/sec. For given velocities, the approximation therefore works better in small-b collisions than in large-b collisions. At collision velocities above these values, the oscillator executes only a very small fraction of its one complete vibrational motion during the approach and recession of the incident atom. Therefore, the phase and direction of the oscillator should be given careful consideration in making use of the above formulation. We note that eq 10 explicitly shows that the collision time becomes shorter as b decreases; it also becomes shorter as the molecular attraction becomes stronger.

In the following calculation, we take two values of the impact parameter, $b/\sigma = 0.8$ and 1.3. For these two values of the impact parameter, we calculate the following expressions for K, respectively

$$K = (9.73\cos^2\theta + 18.1\sin^2\theta\cos^2\phi - 1.26)10^5/v$$

and

$$K = (8.80\cos^2\theta + 29.1\sin^2\theta\cos^2\phi + 6.50)10^2/v$$

Equation 9 shows that $t_c \to 0$ as E (or v) $\to \infty$, which may be called "the sudden limit." In this limit $K \propto 1/v \to 0$, so that at sufficiently high collision velocities $P_{01} = c/v^2$, the proportionality coefficient c being dependent on the rotation angles. In addition, the variation of P_{01} would be seriously affected by the magnitude of the impact parameter. This situation can best be considered by taking the values of b greater than and smaller than the characteristic potential parameter σ and by calculating the corresponding transition probabilities.

B. Velocity Dependence of P_{01}. In Figure 2 we plot the transition probability as a function of the collision velocity at $\theta = 0$, 50, and 90° for $b/\sigma = 0.8$. A similar plot for $b/\sigma = 1.3$ is made in Figure 3. For $v > 4 \times 10^5$ cm/sec, we find $t_c < t_v$. To show the velocity dependence of P_{01} at different rotation angles, we choose the motion to be in the xz plane, parallel to the z axis ($\phi = 0$). Although other values of ϕ would give significantly different curves, the calculation for $\phi = 0$ would furnish sufficient information about the velocity variation of P_{01} at different molecular orientations. As v increases, P_{01} sharply rises to the maximum value $1/e$, and then slowly decreases as v continues to increase; it should be noted that P_{01} is a decreasing function of v in high-velocity collisions. The maximum value shifts toward higher velocities as the angle increases from 0 to $\pi/2$. The calculated transition probabilities do not exceed unity, in contrast to the result of the usual perturbation approximation.[7] The curves shown in Figure 2 (also Figure 3) are symmetrical about

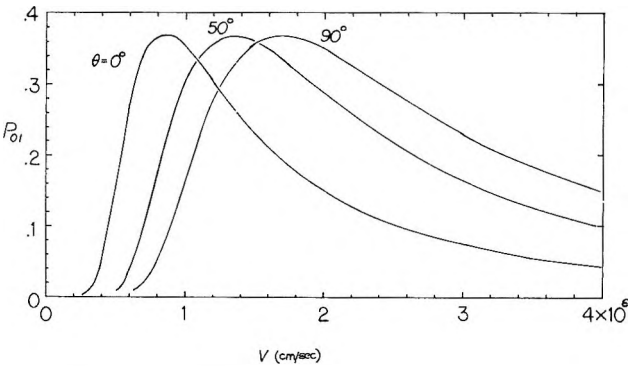

Figure 2. Dependence of the transition probability P_{01} on the collision velocity v for $b/\sigma = 0.8$. The chosen values of the rotation angle θ are 0, 50, and 90°. For this calculation, as well as those shown in Figures 3–5, the angle ϕ is set at zero. The range of validity of the sudden approximation slightly changes as θ varies; however, above $v = 4 \times 10^5$ cm/sec, the approximation is satisfactory.

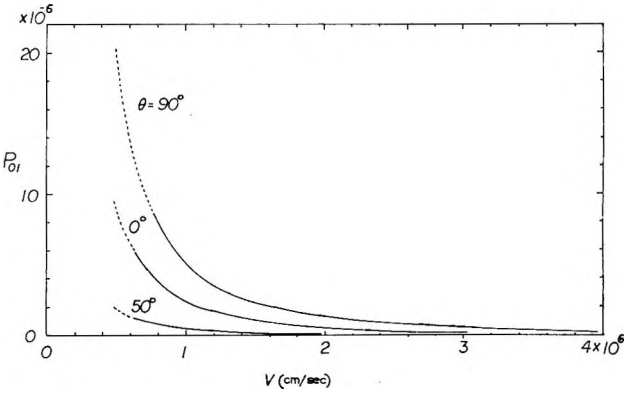

Figure 3. Dependence of P_{01} on v for $b/\sigma = 1.3$ at different values of θ. The dashed portion of the curve represents the range where the sudden approximation becomes invalid.

(14) C. E. Treanor, *J. Chem. Phys.*, **43**, 532 (1965); **44**, 2220 (1966).

(15) H. Shin, *Chem. Phys. Lett.*, **3**, 125 (1969).

(16) J. O. Hirschfelder, C. F. Curtiss, and R. B. Bird "Molecular Theory of Gases and Liquids," Wiley, New York, N. Y., 1964, pp 1110–1111.

(17) G. Herzberg, "Spectra of Diatomic Molecules," Van Nostrand, Princeton, N. J., 1950, Table 39.

the polar coordinates of 0–π and $\pi/2$–$3\pi/2$; we therefore only consider the variations in the first quadrant, but the discussion can be readily generalized to effect the variations in other quadrants. The transition probability is large for smaller θ at lower velocities, while it becomes small at higher velocities. Over the velocity range considered, the figure shows that the transition is very efficient.

For $b > \sigma$, the situation is very different from the above case. As seen in Figure 3, the probability always decreases as v increases. Furthermore, P_{01} is very small, of the order of 10^{-6}. Still another important result is that P_{01} for $\theta = 90°$ is always the largest, followed by the cases with $\theta = 0°$ and $50°$. This variation clearly shows that for large-b collisions the molecular orientation affects the collision process much more strongly than do small-b collisions. The orientation dependence is shown in the following section.

C. Orientation Dependence of P_{01}. To show the orientation dependence of P_{01}, it is useful to make polar plots of P_{01} as a function of θ and ϕ. In Figure 4 we show such plots for $b/\sigma = 0.8$ at $v = 8 \times 10^5$, 1.2×10^6, 2×10^6, and 4×10^6 cm/sec. We again choose the rotation angle $\phi = 0$. At the lowest velocity considered, the probability is largest at $\theta = 0°$, and decreases as the angle increases toward 90° at which P_{01} attains a minimum value. As v increases, P_{01} is largest at $\theta = 90°$ and smallest at 0°; *e.g.*, see the curve for $v = 2 \times 10^6$ cm/sec. At intermediate velocities, P_{01} is largest between these two angles. The symmetrical variation of P_{01} from one quadrant to another is due to the property that the molecule is homonuclear. We notice that a gradual change in the effectiveness of energy transfer occurs from $\theta = 0$ to 90° as v increases.

In Figure 5 a similar plot for $b/\sigma = 1.3$ is shown for $v = 8 \times 10^5$ and 1.2×10^6 cm/sec; the probability varies very rapidly as v changes. At higher velocities, P_{01} is very small and such cases are not plotted here. Unlike the case with $b/\sigma = 0.8$, we find that $P_{01} = 0$ at $\theta = 39.5°$ regardless of the collision velocity; at this angle $K = 0$. A word should be said about this situation. In general, the interaction potential between BC and A will require more than one term for a reasonable description of the collision system; in fact here we used several terms up to the second order of the power series in $(d + \xi)/r$. With these terms we find that $K = 0$ at 39.5°. However, if we included the third- and higher-order contributions in eq 4, there would be additional terms in K which are nonzero but small. In connection with the appearance of K zero here, we note that K for $b/\sigma = 0.8$, shown above, does not vanish at any angle.

D. Angle-Averaged Transition Probability. All the above results show a complicated angle dependence of P_{01}. If we also considered the ϕ dependence, the calculation would be much more complicated, and the result would be different from those shown above. The

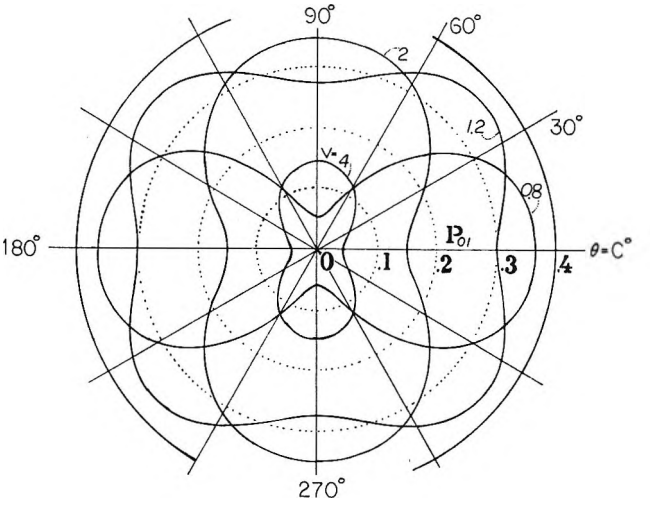

Figure 4. Polar plots of P_{01} for $b/\sigma = 0.8$ at different collision velocities. The chosen values of v are 0.8×10^6, 1.2×10^6, 2.0×10^6, and 4.0×10^6 cm/sec.

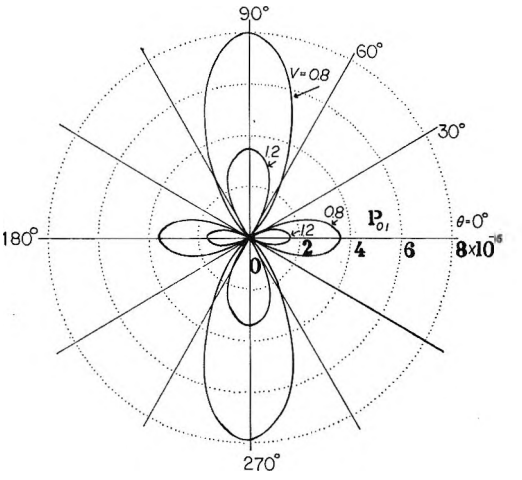

Figure 5. Polar plots of P_{01} for $b/\sigma = 1.3$ at different velocities (0.8×10^6 and 1.2×10^6 cm/sec). Note that $P_{01} = 0$ at $\theta = 39.5°$.

potential used here is also suited for calculating rotational transition probabilities[11] although actual procedures may involve difficult mathematical and numerical steps, but in the present paper we are not interested in such an aspect. Therefore, it should be appropriate to make some type of angle average of P_{01}. In the problems such as the present one it has been customary to obtain P_{01} as a function of Θ and finally average it over all possible values of the angle. However, we have witnessed above that Θ can also change during the collision, and as a result we have derived P_{01} as a complicated function of θ, ϕ, and other relevant collision parameters. Hence, an average of P_{01} over these two rotation angles should be physically more reasonable than the former averaging. Such an average will now give the transition probability as a function only of v and b, and the importance of a particular impact parameter can be deduced from such an expression.

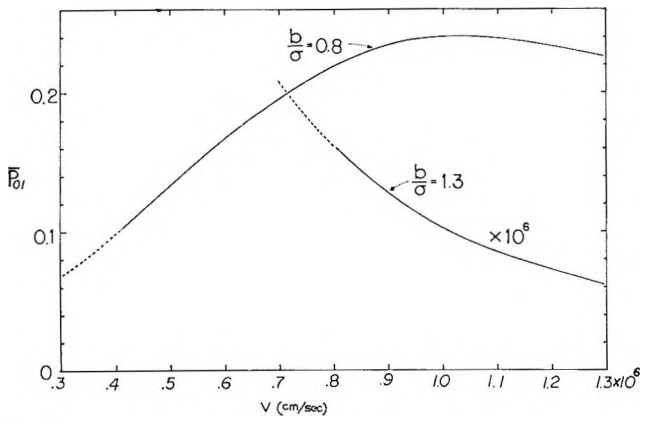

Figure 6. Dependence of the average transition probability $\bar{P}_{01}$ on v for $b/\sigma = 0.8$ and 1.3. A Sigma 7 computer was used to carry out numerical integration.

During the approach and the recession of the incident atom the oscillator is rotating, and at the moment of the collision, it can take any values of the angle θ between 0 and $\pi/2$ and ϕ between 0 and 2π; the former angle region should be extended to $0 - \pi$, if the molecule is heteronuclear. Therefore, we can define the average transition probability by

$$\bar{P}_{01} = \frac{1}{2\pi} \int_0^{2\pi} \int_0^{\pi/2} P_{01}(v,b|\theta,\phi) \sin\theta \, d\theta \, d\phi \quad (11)$$

Because the nonlinear θ- and ϕ dependence of P_{01}, explicit integrations of eq 11 were not possible. Thus we carried out numerical integrations on a Sigma 7 computer by use of the Simpson method. The results up to $v = 1.3 \times 10^6$ cm/sec are shown in Figure 6.

As shown by eq 10, the b-dependent term affects the collision time significantly. For example, when $b/\sigma = 1.3$ and $\theta = 90°$, this term is 1.24×10^{-14} sec at $v = 10^6$ cm/sec, while the first part of eq 10 is only 4.61×10^{-15} sec, which is comparable to the b-independent part. Since the collision time sensitively depends on the magnitude of b, the change in b would also mean a change in the range of validity of the sudden approximation. For $b/\sigma = 1.3$ the approximation is satisfactory above $v = 8 \times 10^5$ cm/sec; for $b/\sigma = 0.8$ the corresponding velocity is as low as 4×10^5 cm/sec. In Figure 6, we show the numerical result of $\bar{P}_{01}$ for the two b values. Note that for both curves, the dashed portion represents the region where the sudden approximation becomes invalid; we show these portions only for comparison.

The curve for $b/\sigma = 0.8$ raises to a maximum value at about 10^6 cm/sec, then *very* slowly declines as the velocity increases. For velocities up to 10^6 cm/sec, the probability continues to rise as v increases. The opposite variation is seen for $b/\sigma = 1.3$. For such large-b collisions, $\bar{P}_{01}$ always decreases as v increases and its magnitude is very small. This is a noteworthy feature of the collision process and will be discussed below.

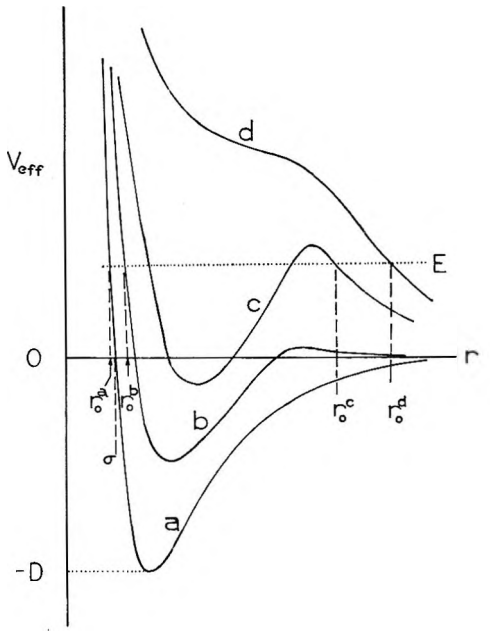

Figure 7. Schematic presentation of $V_{eff}(r)$. The distance of closest approach is denoted by r_0^i for the ith curve.

For the present model the effective interaction potential is $V_{eff} = V + {}^1/_2\mu v^2(b/r)^2 = V + E(b/r)^2$. For $b = 0$, the potential curve can be represented by a typical curve, curve a, in Figure 7. For nonzero impact parameter collisions, a maximum value of the effective potential, V_{eff}^{max}, may show up at the outside of the potential minimum (curves b and c). If b is sufficiently large, then the curve is obliterated and it might even become a decreasing function of r (curve d). It is obvious that this situation would also occur when both b and E are large.

If $E < V_{eff}^{max}$, the distance of closest approach (r_0) is r_0^c indicated in Figure 7; see curve c. Therefore, with the collision partners approaching at large r with $E < V_{eff}^{max}$, they will repel each other at r_0^c regardless of the nature of the potential at smaller values of r. When $b > \sigma$, an increase in E counteracts the magnitude of the potential minimum and straightens out the trajectory, thus leading to an increase in r_0. The transition probability for $b > \sigma$ decreases with increasing E (or velocity) as seen in Figure 6. Furthermore, since the collision occurs near "the outer closest distance" r_0^c for $b > \sigma$, the energy transfer can be very inefficient (the probability being order of 10^{-6} in the O_2 + Ar collision). On the other hand, when $b < \sigma$, the potential energy will be mainly repulsive (nearly direct collisions). In this case an increase in the collision energy decreases r_0 and straightens out the trajectory. Therefore, with $b < \sigma$, the probability increases for increasing v and values of the transition probability are very large. Figure 6 shows such variations up to an intermediate velocity where $\bar{P}_{01}$ takes a maximum value of about 0.24. At higher velocities

where $\bar{P}_{01}$ very slowly decreases, multilevel transitions ($0 \rightarrow 2$, $0 \rightarrow 3$, etc.) would compete with the $0 \rightarrow 1$ transition, thus leading to smaller values of $\bar{P}_{01}$. The result also shows that for a given v the probability normally decreases with increasing b. In general the present calculation of the average transition probability correctly reflects the physics of molecular collisions at different values of b.[18]

Acknowledgment. I wish to thank Dr. Young O. Koh of the Computer Center, University of Nevada, for assisting with the programming.

(18) B. Widom and S. H. Bauer, *J. Chem. Phys.*, **21**, 1670 (1953).

Kinetics of Hydrolysis of Ferric Ion in Dilute Aqueous Solution

by Paul Hemmes, Larry D. Rich, David L. Cole, and Edward M. Eyring*

Department of Chemistry, University of Utah, Salt Lake City, Utah 84112 *(Received August 21, 1970)*

Publication costs assisted by the Air Force Office of Scientific Research

Dilute aqueous solutions of ferric perchlorate have been studied by the electric field jump relaxation kinetic technique. At 25° and ionic strengths less than $3 \times 10^{-4} M$ the specific rates of the reactions $FeOH^{2+}(aq) \underset{}{\overset{k_2}{\rightleftharpoons}} Fe(OH)_2^+(aq) + H^+(aq)$ were found to be $k_2 = 6.1 \times 10^4\ sec^{-1}$ and $k_{-2} = 8.0 \times 10^9\ M^{-1}\ sec^{-1}$. A preceding hydrolysis step $Fe^{3+}(aq) \rightleftharpoons FeOH^{2+}(aq) + H^+(aq)$ was found to reach equilibrium too rapidly for rate measurements by this method.

Introduction

The hydrolysis of metal ions in aqueous solution is an important process in many areas of pure and applied chemistry. In some cases, the normal solution chemistry of an element in a given oxidation state is not the chemistry of the aquo ion at all but rather that of a hydrolyzed form of the ion. A classic example of such behavior is the case of aqueous ferric ion.[1]

While for many years thermodynamic studies of aqueous metal ion hydrolysis have been made,[2] especially in Scandinavia, the kinetics of hydrolysis have been susceptible to study only since the advent of relaxation techniques.[3] Kinetic investigations of the hydrolysis of aqueous metal ions

$$M^{3+} + H_2O \underset{}{\overset{k_1}{\rightleftharpoons}} MOH^{2+} + H^+ \qquad {}^*K_1 = k_1/k_{-1} \quad (1)$$

$$MOH^{2+} + H_2O \underset{}{\overset{k_2}{\rightleftharpoons}} M(OH)_2^+ + H^+ \qquad {}^*K_2 = k_2/k_{-2} \quad (2)$$

have revealed a surprising sameness of the hydrolysis rate constant $k_1 \cong 10^5\ sec^{-1}$ at 25° and nearly zero ionic strength for aqueous trivalent aluminum,[4] chromium,[5] scandium,[6] and indium ions.[7] As would be expected from Debye's equation[8] for the specific rate of diffusion-controlled ion recombination reactions, the values of k_{-1} also do not differ markedly for these metals lying as they do between $\sim 4 \times 10^9$ and $\sim 10^{10}\ M^{-1}\ sec^{-1}$. A possible case in which k_1 could differ significantly from $\sim 10^5\ sec^{-1}$ would be aqueous iron(III) since for this ion p^*K_1 is variously reported[9,10] as 2.2 to 2.5 (at zero ionic strength) in contrast to 5.02 for aluminum(III)[4] and 3.98 for chromium(III),[5] for example. The electric field jump relaxation method[3] kinetic study of dilute aqueous ferric perchlorate reported below confirms this expectation.

Experimental Section

The ferric perchlorate was reagent grade (G. F. Smith Co.). Stock solutions were analyzed volumetrically

(1) F. A. Cotton and G. Wilkinson, "Advanced Inorganic Chemistry," 2nd ed, Interscience, New York, N. Y., 1966, p 859.

(2) L. G. Sillen and A. E. Martell, "Stability Constants," The Chemical Society, London, 1964, p 39 ff.

(3) M. Eigen and L. DeMaeyer, "Technique of Organic Chemistry," Vol. VIII, Part II, S. L. Friess, E. S. Lewis, and A. Weissberger, Ed., Interscience, New York, N. Y., 1963, Chapter 18.

(4) L. P. Holmes, D. L. Cole, and E. M. Eyring, *J. Phys. Chem.*, **72**, 301 (1968).

(5) L. D. Rich, D. L. Cole, and E. M. Eyring, *ibid.*, **73**, 713 (1969).

(6) D. L. Cole, L. D. Rich, J. D. Owen, and E. M. Eyring, *Inorg. Chem.*, **8**, 682 (1969).

(7) P. Hemmes, L. D. Rich, D. L. Cole, and E. M. Eyring, *J. Phys. Chem.*, **74**, 2859 (1970).

(8) P. Debye, *Trans. Electrochem. Soc.*, **82**, 265 (1942).

(9) A. B. Lamb and A. G. Jacques, *J. Amer. Chem. Soc.*, **60**, 1215 (1938).

(10) R. M. Milburn and W. C. Vosburgh, *ibid.*, **77**, 1352 (1955).

Table I: Calculated Molar Concentrations and Experimental Electric Field Jump Relaxation Times in Dilute Aqueous Ferric Perchlorate at 25°

C_0,[a] 10^{-6} M	pH[b]	μ,[c] 10^{-4} M	$[H^+]$,[d] 10^{-4} M	$[Fe^{3+}]$,[e] 10^{-7} M	$[FeOH^{2+}]$,[e] 10^{-5} M	$[Fe(OH)_2^+]$,[e] 10^{-6} M	$[Fe_2(OH)_2^{4+}]$,[e] 10^{-9} M	$\bar{\tau}$,[f] μsec	n[g]
6.83	3.788	3.19	1.663	28.0	5.83	6.99	101.9	0.68 ± 0.16	6
4.88	3.972	2.17	1.082	12.5	4.01	7.39	48.2	1.02 ± 0.10	6
2.91	4.196	1.10	0.644	4.06	2.19	6.80	14.4	1.72 ± 0.10	6
0.977	4.633	0.393	0.234	0.354	0.525	4.48	0.827	3.53 ± 0.14	3
0.781	4.466	0.404	0.344	0.487	0.491	2.85	0.724	2.47 ± 0.12	6

[a] Total molar concentration of ferric perchlorate. [b] Glass electrode pH of the sample solution. [c] Ionic strength calculated from eq 7 of the text. [d] Concentration of hydrogen ion calculated from eq 9 of the text. [e] Molar concentrations calculated from eq 3–6 of the text. [f] Average experimental electric field jump relaxation time with standard deviation calculated from the range. [g] Number of independent determinations of the relaxation time.

using stannous chloride and potassium dichromate.[11] Other experimental procedures and the conductometric electric field jump apparatus have been described before in considerable detail.[4-7] Solutions were all freshly prepared, dilute, low in pH, and never heated above room temperature, and thus were out of equilibrium insofar as the eventual formation of polymeric precipitates is concerned.

Results

Table I contains the values of total iron(III) perchlorate concentration, C_0, measured pH, and experimental relaxation times. Also shown are calculated concentrations of the several types of ions present. On the basis of results of several equilibrium studies[2] we have assumed the existence of dimer but no higher polymeric species in our dilute, freshly prepared sample solutions. Concentrations were calculated from the following set of equations

$$*K_1 = \frac{[H^+][MOH^{2+}]}{[M^{3+}]} \quad (3)$$

$$*K_2 = \frac{[H^+][M(OH)_2^+]}{[MOH^{2+}]} \quad (4)$$

$$^\dagger K_{22} = \frac{[M_2(OH)_2^{4+}]}{[MOH^{2+}]^2} \quad (5)$$

$$C_0 = [M^{3+}] + [MOH^{2+}] + [M(OH)_2^+] + 2[M_2(OH)_2^{4+}] \quad (6)$$

$$\mu = {}^1/_2(9[M^{3+}] + 4[MOH^{2+}] + [M(OH)_2^+] + 16[M_2(OH)_2^{4+}] + [H^+] + 3C_0) \quad (7)$$

$$-\log \gamma_\pm = 0.509\sqrt{\mu} \quad (8)$$

$$[H^+] = \frac{10^{-pH}}{\gamma_\pm} \quad (9)$$

where brackets denote molar concentration, μ denotes the ionic strength, and $\gamma_\pm$ is the mean ionic activity coefficient for monovalent ions. Lamb and Jacques,[9] in a glass electrode potentiometric study of aqueous iron(III), determined that $p*K_1 = 2.46$ and $p*K_2 = 4.7$ at high dilutions, 25°, and corrected to zero ionic strength. Hedstrom's[12] $p*K_1 = 3.05$, $p*K_2 = 3.26$, and $p^\dagger K_{22} = -3.19$ for iron(III) at 25° and $\mu = 3.0$ M are unsuited for use with electric field jump kinetic data that are obtainable only in solutions approaching zero ionic strength. The fairly pronounced ionic strength dependence of $*K_1$ and $^\dagger K_{22}$ for aqueous iron(III) found by Milburn and Vosburgh[10] is ample warning against an extrapolation of $*K_1$, $*K_2$, and $^\dagger K_{22}$ from Hedstrom's 3.0 M ionic strength constants.[12] Milburn and Vosburgh[10] reported $p*K_1 = 2.17$ and $p^\dagger K_{22} = -1.48$ at 25° and extrapolated to zero ionic strength. However, the neglect of equilibrium 2 (and the omission of $*K_2$) by these authors explicitly contradicts the kinetic results described below. Thus we are obliged to use a composite set of equilibrium constants in our calculations of the concentrations given in Table I: $*K_1 = 10^{-2.46}$, $*K_2 = 10^{-4.7}$, and $^\dagger K_{22} = 30$. As we will see later, the dominance of $[H^+]$ over $[FeOH^{2+}]$, $[Fe(OH)_2^+]$, and $[Fe_2(OH)_2^{4+}]$ under our experimental conditions makes a fairly reliable determination of rate constants possible in spite of the uncertainties just noted in these equilibrium constants.

Discussion

Relaxation method rate studies of the dimerization of aqueous ferric ion (in more concentrated solutions than we have considered here) have invariably been conducted on a much longer time scale (~1 sec) than the microsecond relaxation time scale of the present work.[13,14] It is therefore reasonable to seek an explanation of our electric field jump relaxations in terms of hydrolysis rather than dimerization kinetics. Since ferric ion reportedly undergoes two hydrolysis steps

(11) D. A. Skoog and D. M. West, "Fundamentals of Analytical Chemistry," Holt, Rinehart and Winston, New York, N. Y., 1963, p 457.

(12) B. O. A. Hedstrom, *Ark. Kemi*, **6**, 1 (1953).

(13) H. Wendt, *Z. Elektrochem.*, **66**, 235 (1962); *Inorg. Chem.*, **8**, 1527 (1969).

(14) B. A. Sommer and D. W. Margerum, *ibid.*, **9**, 2517 (1970).

(eq 1 and 2), we conceivably could by judicious choices of concentration observe two relaxations within the 0.3–10 μsec time range accessible to our electric field jump relaxation method apparatus. Experimentally, however, we have observed only one relaxation. The anticipated two relaxations associated with the equilibria 1 and 2 are given by

$$\tau_{1,2}^{-1} = \frac{a_{11} + a_{22}}{2} \pm {}^1/_2\sqrt{(a_{11} + a_{22})^2 - 4(a_{11}a_{22} - a_{12}a_{21})} \quad (10)$$

where, omitting the charges of the ionic species for brevity

$$a_{11} = k_{-1}(*K_1 + [H] + [MOH]) \equiv k_{-1}\theta \quad (11)$$

$$a_{22} = k_{-2}(*K_2 + [H] + [M(OH)_2]) \equiv k_{-2}\varphi \quad (12)$$

$$a_{12} = k_{-1}([H] - [MOH]) \quad (13)$$

$$a_{21} = k_{-2}(*K_2 - M(OH)_2) \quad (14)$$

In cases where either a_{11} or a_{22} is very much larger than the other, eq 10 reduces to

$$\tau_{fast}^{-1} \cong a_{ii} \quad (15)$$

$$\tau_{slow}^{-1} \cong a_{jj} \quad (16)$$

where a_{ii} is the larger of the two terms a_{11} or a_{22} and a_{jj} is the smaller. This reduced form (eq 15 and 16) is not generally true. The reduced form for an ionic association process, for example, is quite different.[15]

The problem is to determine whether a reduced form of eq 10 can be used to describe the data and if so, whether we are observing the fast or the slow process.

In order to decide whether a reduced form can be used, we first consider the ratio $a_{11}/a_{22} = k_{-1}\theta/k_{-2}\varphi$. In all solutions studied the ratio $\theta/\varphi \geq 19$. Since on the basis of the Debye equation for diffusion-controlled rates,[8] the ratio k_{-1}/k_{-2} is expected to be about 0.3–0.5, it follows that $a_{11}/a_{22} \geq 6$. A ratio of this magnitude indicates that eq 15 and 16 will represent reasonable approximations at the very least. It further indicates that for ferric ion the relaxation time associated with the first hydrolysis step, eq 1, is substantially shorter than the τ associated with eq 2.

A decision must now be made as to whether the experimental value of τ is given by eq 15 or 16, that is, if we are observing the slow or the fast process. Let us, as a zeroth approximation, neglect the radical in eq 10. Then

$$\tau^{-1} = \frac{k_{-1}}{2}\theta + \frac{k_{-2}}{2}\varphi \quad (17)$$

or

$$\frac{\tau^{-1}}{\varphi} = \frac{k_{-1}}{2}\frac{\theta}{\varphi} + \frac{k_{-2}}{2} \quad (18)$$

A plot of τ^{-1}/φ *vs.* θ/φ gives a line with negative slope. This indicates that the left-hand side of eq 18 is too small and that it requires the addition of the radical. This is the same as taking the negative root in eq 10. Hence we conclude that the slow process is being observed.

We can now make the assignment $\tau_{exp}^{-1} = a_{22} = k_{-2}([H] + [M(OH)_2]) + k_2$ and plot τ^{-1} *vs.* $([H] + [M(OH)_2])$. The least-squares slope of this line is $8.0 \pm 1.0 \times 10^9\ M^{-1}\ sec^{-1} = k_{-2}$ and the intercept is $6.1 \pm 0.4 \times 10^4\ sec^{-1} = k_2$. The ratio k_2/k_{-2} is $10^{-5.1}$ which is in reasonable agreement with the value of $*K_2 = 10^{-4.7}$ reported in the literature[9] and used initially to calculate concentrations. The agreement of this quotient of specific rates with the equilibrium, $*K_2$ is especially gratifying since the dominant term in the sum $([H] + [M(OH)_2])$ is the measured [H] concentration. In no case is $[M(OH)_2]$ more than 19% of [H]; hence the kinetic value of $*K_2$ is nearly independent of errors in the literature value of this constant.

As in previous kinetic studies of aqueous trivalent metal ion hydrolyses, we have observed a nearly diffusion-controlled rate of recombination of a hydrolyzed metal ion, in this case $Fe(OH)_2^+$(aqueous), with a proton. We have also observed a deprotonation step, in this case of $FeOH^{2+}$(aqueous), having a specific rate $k_2 \sim 10^5\ sec^{-1}$. The unusual feature of the ferric ion system is, however, the great rapidity of the first hydrolysis reaction, k_1 probably equal to $\sim 3 \times 10^7\ sec^{-1}$.

The reason that $a_{11} \gg a_{22}$ is that the term $*K_1$ which appears in θ is so large that it dominates all other terms. This is equivalent to saying that the value of k_1 is so large that the minimum value of τ^{-1}, which can be obtained as $([H] + [MOH])$ becomes very small, is $10^7\ sec^{-1}$ or larger. If we assume that k_{-1} is diffusion controlled, it is very likely that a relaxation due to the first step in the hydrolysis of ferric ion could be observed using ultrasonics or perhaps Brillouin scattering of an argon ion laser beam.

A more important consequence of the present work is the recognition of a systematic method of determining the equilibrium responsible for an observed relaxation in one of these hydrolyzing metal ion systems. From τ^{-1}/φ *vs.* θ/φ plots of our kinetic data we can say for the two-step hydrolysis systems we have previously studied [thorium(IV),[16] chromium(III),[5] scandium(III),[6] indium(III),[7] and gallium(III)[7]] that it is always the slower of two anticipated hydrolysis relaxations that we actually observed. Then since $a_{11}/a_{22} = k_{-1}\theta/k_{-2}\varphi$, in order for the slow process to correspond to a_{11} it is necessary that $a_{11}/a_{22} < 1$. This follows from the fact that $a_{11}/a_{22} \cong \tau_1^{-1}/\tau_2^{-1}$. To discover whether $a_{11}/a_{22} < 1$, we examine the ratio θ/φ. Since the Debye

(15) Reference 3, p 910.

(16) E. M. Eyring and D. L. Cole in "Fast Reactions and Primary Processes in Chemical Kinetics," S. Claesson, Ed., Interscience, New York, N. Y., 1967, p 255.

equation leads to a predicted ratio $k_{-1}/k_{-2} \cong 0.3$ to 0.5 for these hydrolyzing metals, $a_{11}/a_{22} < 1$ if θ/φ is less than approximately 2–3.3. If θ/φ exceeds this range and we are still observing the slower of two relaxation processes, then this slow process must correspond to a_{22} (since $a_{11}/a_{21} > 1$ implies $\tau_1^{-1} > \tau_2^{-1}$).

The results of this sort of analysis can then be summarized as

	ϕ/φ	Slow process
Iron(III)	19–61	a_{22}
Gallium(III)	5.2–6.7	a_{22}
Chromium(III)	1.8–3.4	?
Thorium(IV)	1.3–1.5	a_{11}
Scandium(III)	1.0–1.7	a_{11}
Indium(III)	0.38–0.60	a_{11}

The chromium(III) case cannot be resolved by this argument although we see no reason to doubt our earlier assignment of specific rates based on a concordance of kinetic and thermodynamic equilibrium constants.[5] On the other hand, our previous assignment of specific rates k_1 and k_{-1} in the case of aqueous gallium(III) hydrolysis was in error. We correctly determined that the slower of the two anticipated gallium(III) hydrolysis reactions was the one we could observe. However we mistakenly assumed a_{11} to be the slow process.[7] In the gallium(III) case as with iron(III) it is actually the second hydrolysis step (eq 2) that is slower. Thus the corrected specific rates for gallium(III) are $k_{-2} = 4.5 \times 10^9\ M^{-1}\ \text{sec}^{-1}$ and $k_2 = 1.7 \times 10^5\ \text{sec}^{-1}$ with $k_2/k_{-2} = 10^{-4.4}$, in rough agreement with the potentiometric[17] $^*K_2 = 10^{-3.5}$.

Acknowledgment. This research was supported by the Directorate of Chemical Sciences, Air Force Office of Scientific Research, Grant AF-AFOSR-69-1717-D.

(17) R. Fricke and K. Meyring, *Z. Anorg. Allg. Chem.*, 176, 325 (1928).

A Study of Nitrogen-15 Nuclear Magnetic Resonance Shifts in Pure Methylamines and Pure $CH_3C^{15}N$[1a]

by Mohammed Alei, Jr.,* Alan E. Florin, William M. Litchman,[1b] and James F. O'Brien

University of California, Los Alamos Scientific Laboratory, Los Alamos, New Mexico 87544 *(Received September 29, 1970)*

Publication costs assisted by the Los Alamos Scientific Laboratory

The ^{15}N liquid association shifts and temperature dependences of the ^{15}N chemical shifts of $^{15}NH_3$, $CH_3{}^{15}NH_2$, $(CH_3)_2{}^{15}NH$, $(CH_3)_3{}^{15}N$, and $CH_3C^{15}N$ are presented and discussed. In the order given above, the vapor chemical shifts are 0, −14.5, −26.1, −28.7, and −273.4 ppm, respectively. The liquid association shifts at the melting point are −22.6, −9.4, −3.2, −6.9, and +11.3 ppm, respectively, and the temperature coefficients are +4.3, +1.6, +0.5, +2.0, and −2.1 (all $\times 10^{-2}$ ppm/°C), respectively. The difference in the shift data between the amines and acetonitrile is attributed to the dominance of the diamagnetic term in the case of the amines compared to the dominance of the paramagnetic term in acetonitrile.

Introduction

In recent publications[2a,b] we have demonstrated that the ^{17}O resonance in pure liquid water and the ^{15}N resonance in pure liquid ammonia are both considerably downfield of the resonances in their respective vapor-phase molecules. The liquid-phase resonance also shifts, in each case, to lower field with decreasing temperature in linear fashion. Moreover, taking pure $^{15}NH_3$ as an example, the ^{15}N shift between vapor and liquid and the temperature coefficient of the ^{15}N shift in the liquid are both more than ten times as large as the corresponding parameters for the NH_3 proton resonance. It is thus possible for the ^{15}N resonance to be a sensitive probe for study of liquid-phase intermolecular interactions traditionally studied by proton resonance measurements. We have, in fact, more recently shown[3,4]

(1) (a) Work supported by the U. S. Atomic Energy Commission; (b) AWU Faculty Research Participant at Los Alamos Scientific Laboratory.

(2) (a) A. E. Florin and M. Alei, Jr., *J. Chem. Phys.*, **47**, 4268 (1967); (b) W. M. Litchman, M. Alei, Jr., and A. E. Florin, *ibid.*, **50**, 1031 (1969).

that when $^{15}NH_3$ or $Me_3{}^{15}N$ is dissolved in a solvent the ^{15}N resonance undergoes a shift which may be correlated with the types of interactions which can occur between the amine and the given solvent.

In the present work, we report results of a study of the ^{15}N resonance in the pure compounds $^{15}NH_3$, $CH_3{}^{15}NH_2$, $(CH_3)_2{}^{15}NH$, and $(CH_3)_3{}^{15}N$. We were primarily interested in measuring the shift of the ^{15}N resonance in the pure liquid relative to the pure vapor and comparing this "liquid-association shift" with the temperature dependence of the ^{15}N shift in the pure liquid for a series of structurally related compounds. For compounds which are monomolecular in the gas phase, the liquid-association shift is presumably produced by intermolecular interactions in the liquid and since the variation with temperature of the ^{15}N shift in the liquid is almost surely due to some sort of thermal perturbation of these interactions, we felt there might be some correlation between these two nmr parameters.

In previous work,[3] we observed that protonation or dilution with H_2O produces strong *downfield* shifts of the ^{15}N resonance in the $^{15}NH_3$ molecule. For the CH_3CN molecule, on the other hand, Lowenstein and Margalit[5] have reported that the ^{14}N resonance shifts *upfield* on dilution with H_2O or methanol and Olah and Kiovsky[6] have reported a strong *upfield* shift of the ^{15}N resonance on protonation. We have therefore also measured the ^{15}N liquid-association shift and the temperature dependence of the ^{15}N shift in the liquid for pure $CH_3C^{15}N$ to determine whether or not these shifts also differ in direction from those for the amines.

Experimental Section

1. Synthesis of ^{15}N-Labeled Compounds. The original source of ^{15}N for this work was nitric oxide gas, isotopically enriched by low-temperature distillation.[7] The following sequence of reactions was used to convert this material to isotopically enriched $^{15}NH_3$ or $^{15}NH_4Cl$.

$$^{15}NO + H_2 \xrightarrow[800^\circ]{\text{Ni catalyst}} \tfrac{1}{2}\,{}^{15}N_2 + H_2O$$

$$\tfrac{1}{2}\,{}^{15}N_2 \xrightarrow[700^\circ]{\text{Ca metal}} Ca_3{}^{15}N_2 \xrightarrow{H_2O} {}^{15}NH_3 \xrightarrow{\text{aqueous HCl}} {}^{15}NH_4Cl$$

Starting material containing essentially 100% ^{15}N was available to us and was occasionally used for preparing vapor samples where the low density of nuclei makes signal detection more difficult. For liquid samples, material containing ~50% ^{15}N generally gave adequate nmr signals.

a. $^{15}NH_3$. This material was prepared as indicated above. $^{15}NH_3$ stored in a stainless steel cylinder attached to a Pyrex vacuum system through a stainless steel valve could be measured out and transferred by standard techniques either for nmr sample preparation or for use in other syntheses.

b. $CH_3{}^{15}NH_2$. This material was prepared by the sequence of steps listed below.

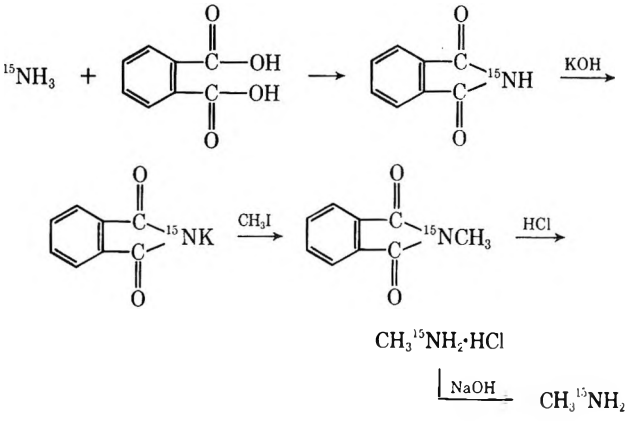

The above steps are a combination of two published syntheses with obvious minor modifications.[8]

c. $(CH_3)_2{}^{15}NH$. This compound was prepared by the following sequence of reactions.

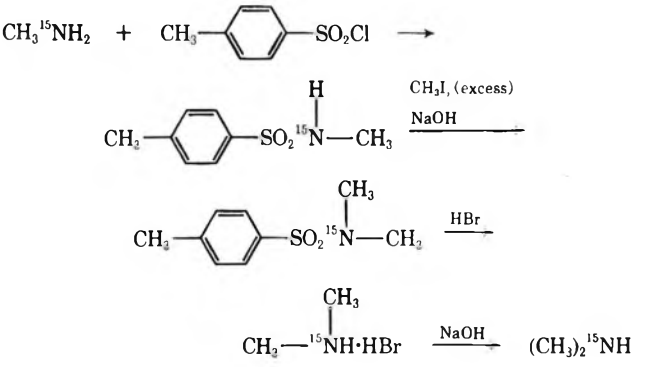

The above synthesis is a slight modification of a published procedure.[9]

d. $(CH_3)_3{}^{15}N$. $(CH_3)_3{}^{15}N \cdot HCl$ was prepared by refluxing $^{15}NH_4Cl$ in an aqueous solution of formic acid and formaldehyde according to a published procedure.[10] The procedure reports a yield of 75.4% of $Me_3{}^{15}N \cdot HCl$, but we found that carrying out the reaction exactly as directed resulted in a product containing significant quantities of $Me^{15}NH_2 \cdot HCl$ and $Me_2{}^{15}NH \cdot HCl$. By doubling the ratio of formaldehyde to $^{15}NH_4Cl$ and refluxing for 16–24 hr instead of the indicated 10 hr, we were able to obtain pure $Me_3{}^{15}N \cdot HCl$ in over 90%

(3) W. M. Litchman, M. Alei, Jr., and A. E. Florin, *J. Amer. Chem. Soc.*, **91**, 6574 (1969).

(4) M. Alei, Jr., A. E. Florin, and W. M. Litchman, *ibid.*, **92**, 4828 (1970).

(5) A. Lowenstein and Y. Margalit, *J. Phys. Chem.*, **69**, 4152 (1965).

(6) G. A. Olah and T. E. Kiovsky, *J. Amer. Chem. Soc.*, **90**, 4666 (1968).

(7) We are indebted to Dr. B. B. McInteer and Mr. R. M. Potter of this laboratory for supplying us with this material.

(8) "Organic Syntheses with Isotopes," A. Murray III and D. L. Williams, Ed., Interscience, 1958, Part II, p 1731, and Part I, p 491.

(9) See ref 8, Part I, p 598.

(10) See ref 8, Part II, p 1837.

yield.[11] The free amine was liberated from this salt by adding concentrated aqueous NaOH.

e. $CH_3C^{15}N$. This material was prepared by initially reacting $^{15}NH_3$ with excess CH_3COCl at Dry Ice temperature to form a mixture of $CH_3CO^{15}NH_2$ and $^{15}NH_4Cl$. After pumping off the excess CH_3COCl, the $CH_3CO^{15}NH_2$ was separated from the $^{15}NH_4Cl$ by a low-temperature (50–75°) sublimation in a stream of Ar. The $CH_3(O=)C^{15}NH_2$ was mixed with an excess of P_2O_5 and the mixture heated to ~100° in a distillation apparatus which was continually flushed with dry Ar. The overall yield of $CH_3C^{15}N$ was 40–50%.

2. Nmr Measurements. The nmr measurements were made on a Varian DP-60A instrument in which the external lock-on mechanism was utilized to fix the magnetic field so that H_2O protons resonated at exactly 60 MHz. The ^{15}N resonances were then observed by using a General Radio Co. digital frequency synthesizer and the ramp voltage of a Varian C-1024-time-averaging computer to sweep the working frequency in the region of 6.08 MHz.

The liquid amine samples were sealed in Pyrex tubes of ~8 mm o.d. diameter. A thin-walled glass thermocouple well was sealed into the tube so that the tip of the well was immersed several millimeters at the top of the liquid sample. Sample volumes were ~1 cc. The temperature of the sample, was varied by flowing hot or cold N_2 around the sample tube. The temperature was read on a thermocouple inserted in the thermocouple well.

Gas samples were generally prepared by sealing ~1 mmol of liquid in an ampoule ~35 mm long prepared from 15-mm o.d. standard-wall Pyrex tubing. Vaporization of the entire liquid sample would thus produce vapor pressures of the order of 5 atm. The vapor resonance was easily observed under these conditions by using the Varian C-1024 time-averaging computer.

Results and Discussion

The principal experimental results are listed in Table I. The temperature coefficient of ^{15}N shift in each pure liquid is derived from the plot of ^{15}N shift *vs.* temperature for that liquid (*cf.* Figures 1 and 2). In every case, the dependence of shift on temperature showed no significant departure from linearity over the temperature range studied (in the case of $CH_3C^{15}N$, nearly the entire liquid range). The vapor resonances, on the other hand, were not measurably shifted by temperature changes of 40 to 50°, indicating no significant degree of vapor-phase association for any of the compounds studied.

The first two rows of Table I list parameters derived from the vapor resonances. They display some interesting features which we think are noteworthy. Confining our attention to the amine data, the $J_{^{15}N-H}$ values demonstrate that the coupling between ^{15}N and directly

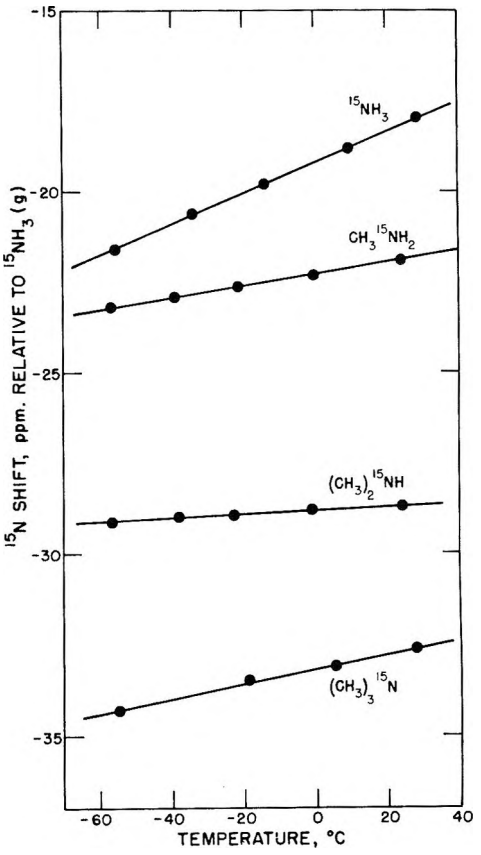

Figure 1. Temperature coefficient for ^{15}N shift in pure liquid amines.

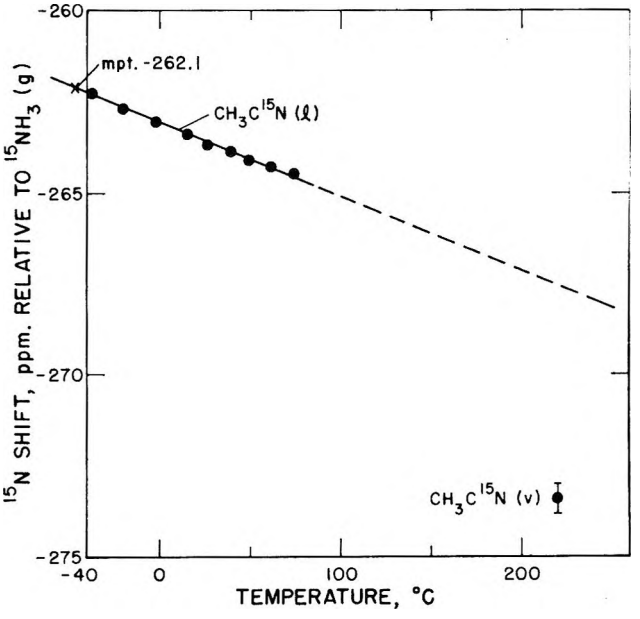

Figure 2. ^{15}N shifts for $CH_3C^{15}N$ liquid and vapor.

(11) It was convenient to follow the reaction by periodically taking a few drops of the reaction mixture and examining its pmr spectrum. The methyl proton resonances for the species $(CH_3)_3NH^+$ (doublet), $(CH_3)_2NH_2^+$ (1:2:1 triplet), and $CH_3NH_3^+$ (1:3:3:1 quartet) are easily differentiated.

Table I: ^{15}N Nmr Parameters for Simple Amines and $CH_3C^{15}N$

	$^{15}NH_3$	$CH_3{}^{15}NH_2$	$(CH_3)_2{}^{15}NH$	$(CH_3)_3{}^{15}N$	$CH_3C^{15}N$
$J_{^{15}N-H}$, vapor[a]	61.2	64.5	67.0		
^{15}N shift, vapor[b]	(0)	−14.5	−26.1	−28.7	−273.4
^{15}N shift, liquid[c,d]	−22.6 (−77.7)	−23.9 (−93.5)	−29.3 (−96)	−35.6 (−117)	−262.1 (−45.7)
Liquid-assoc shift	−22.6	−9.4	−3.2	−6.9	+11.3
Temp coeff of ^{15}N shift, liquid[e]	4.3×10^{-2}	1.6×10^{-2}	0.5×10^{-2}	2.0×10^{-2}	-2.1×10^{-2}

[a] Units are Hz. Uncertainty = ±0.3 Hz. [b] Units are ppm relative to $^{15}NH_3$(v). Uncertainty = ±0.2 ppm. Negative sign indicates shift is downfield. [c] Shifts, in ppm relative to $^{15}NH_3$(v), are for the ^{15}N resonance at the melting point (listed in °C in parentheses). These are obtained by extrapolating data in Figures 1 and 2. Volume susceptibility corrections between vapor and liquid at ~30° have been made but changes in susceptibility due to changes in liquid density with temperature have been ignored. The trend in these data between $CH_3{}^{15}NH_2$ and $(CH_3)_3{}^{15}N$ follows very closely that reported by Witanowski and Januszewski[d] for the ^{14}N shifts in these same compounds but their shifts are all 1–2 ppm farther downfield than ours when both sets of data are referred to the same reference. [d] M. Witanowski and H. Januszewski, *Can. J. Chem.*, 47, 1321 (1969). [e] Units are ppm/°C. Uncertainty = $\pm 0.2 \times 10^{-2}$ ppm/°C.

bonded hydrogen increases with increasing methyl substitution. Roberts, *et al.*,[12] have suggested a linear relationship between s character of the ^{15}NH bond and the ^{15}NH coupling constant provided, among other things, that the mean electronic excitation energy remains constant throughout a given series. Using the equation proposed by these authors, an increase in s character from 20.3% to 22.8% would account for the increase in $J_{^{15}N-H}$ in going from $^{15}NH_3$ to $(CH_3)_2{}^{15}NH$. The bond angle data[13] for the series NH_3, CH_3NH_2, and $(CH_3)_2NH$ are not sufficiently precise to provide any independent evidence with regard to such small changes in hybridization. Thus, a small increase in s character of the ^{15}NH bond might reasonably explain the observed increase in $J_{^{15}N-H}$. However, Tannenbaum, Coffin, and Harrison[14] have shown that the absorption bands in the region of 50,000 cm^{-1} undergo appreciable shifts to lower frequency with methyl substitution in the series NH_3, CH_3NH_2, $(CH_3)_2NH$, and $(CH_3)_3N$. This result is consistent with a decrease in electronic excitation energy but it is not completely clear which electronic excitation is involved. If the uv absorption is due to excitation of an electron in the lone-pair orbital, there may be no necessary correlation between the uv and $J_{^{15}N-H}$ data. However, if the excitation energy for an electron in the $^{15}N-H$ bond were being lowered, then the $1/\Delta E$ dependence of the coupling constant might lead to the observed increase in $J_{^{15}N-H}$. In addition, calculations utilizing the principle of "bond-effective nuclear charge"[15] can account for the observed trend in $J_{^{15}N-H}$. Following the same procedure for $^{15}NH_3$ as for $^{13}CH_4$, the value of 0.29 for the charge transfer, Q_{NH}, in the NH bond satisfactorily determines the couplings. The lone-pair charge transfer, while taken to be zero, is not greatly significant in this calculation. The value of 0.29 for Q_{NH} is slightly larger than the Q_{CH} found in the methane case but is reasonable considering the electronegativities of the two atoms. As a result, since most of the parts of the contact term of the directly bonded coupling constant expression can individually account for the observed changes in coupling, relying on any one of them in a specific case is highly suspect.

The shift of the ^{15}N resonance in the amine vapor to progressively lower field with increasing methyl substitution (*cf.* second row of Table I) is roughly in accord with the uv absorption data cited above. A decrease in mean excitation energy should lead to an increase in the paramagnetic contribution to the shift. However, the results of Tannenbaum, *et al.*,[14] indicate that if Δ is the total decrease in excitation energy between NH_3 and $(CH_3)_3N$, the decrease between NH_3 and CH_3NH_2 is $\sim 2/3\Delta$ and between NH_3 and $(CH_3)_2NH$, $\sim 7/8\Delta$. If the change in ΔE were the only factor influencing the ^{15}N shifts, one would expect the shifts to follow the same pattern. Since the shifts depart significantly from this pattern it is likely that other factors are also involved.

The ^{15}N liquid-association shifts listed in the fourth row of Table I represent the downfield shift of the ^{15}N resonance in the liquid at its melting point relative to the gas-phase resonance whose position, within the experimental uncertainty, is independent of temperature. Thus, for each compound, this shift is assumed to be the result of changing the ^{15}N environment from that in the free molecule to that in the most highly structured liquid. We note that the ^{15}N liquid-association shifts for all the amines are downfield (liquid resonance downfield of vapor resonance) but of varying magnitude. Since we had concluded from our previous

(12) G. Binsch, J. B. Lambert, B. W. Roberts, and J. D. Roberts, *J. Amer. Chem. Soc.*, 86, 5564 (1964).

(13) "Tables of Interatomic Distances and Configuration in Molecules and Ions," The Chemical Society, London, 1958.

(14) E. Tannenbaum, E. M. Coffin, and A. J. Harrison, *J. Chem. Phys.*, 21, 311 (1953).

(15) D. M. Grant and W. M. Litchman, *J. Amer. Chem. Soc.*, 87, 3994 (1965).

studies[3,4] that the interaction of the amine nitrogen lone-pair electrons with an N–H proton (hydrogen-bond formation) makes a larger contribution to the ^{15}N shift than does interaction of the nitrogen lone-pair electrons with solvent methyl groups, we anticipated that the liquid-association shifts for the amines in Table I would *decrease* in magnitude on replacement of protons by methyl groups. This does indeed occur as we go from $^{15}NH_3$ to $(CH_3)_2{}^{15}NH$. The *increase* in magnitude of the liquid-association shift on replacing the proton of $(CH_3)_2{}^{15}NH$ with another methyl group to form $(CH_3)_3{}^{15}N$ was unexpected.

The temperature coefficient of nmr shift for the proton resonance in hydrogen-bonded liquids is generally believed to arise from thermal perturbation of the hydrogen-bonded structure either by altering the ratio of hydrogen-bonded to nonhydrogen-bonded species[16] or by changing the degree of excitation of the hydrogen-bond-stretching vibrational mode.[17] In liquid primary and secondary amines, one would expect these types of thermal perturbations to also influence the shift of the ^{15}N nucleus since the nitrogen lone-pair electrons are involved in any hydrogen-bonds which are present. In addition, our previous studies[3,4] of the ^{15}N shifts for $^{15}NH_3$ or $(CH_3)_3{}^{15}N$ in a number of solvents indicate that interaction of the nitrogen lone-pair electrons with solvent molecule methyl or ethyl groups contributes significantly to the ^{15}N shift. Thermal perturbation of this type of interaction might also cause the ^{15}N resonance to shift with temperature. The plots in Figure 1 demonstrate that in the liquid amines the ^{15}N shift has a significant temperature dependence not only in the hydrogen-bonding liquids $^{15}NH_3$, HC_3NH_2, and $(CH_3)_2NH$, but also for $(CH_3)_3{}^{15}N$. Thus, as Hindman, *et al.*,[18] have previously shown for proton NMR shifts, the ^{15}N resonance can shift appreciably with temperature in systems which would not generally be considered as "hydrogen-bonded." It is also interesting to note that for all the liquid amines in Figure 1, (1) the ^{15}N resonance shifts to lower field with decreasing temperature and (2) the shift, within experimental uncertainty, is a linear function of the temperature. The first observation is consistent with the expectation that lowering the temperature strengthens the intermolecular interactions in the liquid and therefore causes the liquid-association shift to increase in magnitude. The linearity of the temperature dependence of the ^{15}N shift seems, at first glance, to be inconsistent with the models proposed for explaining temperature dependences of nmr shifts in liquids. Thus, for example, if we assume that lowering the temperature increases the fraction of ^{15}N atoms in hydrogen bonds, the simplest shift expression is

$$\delta = \frac{\delta_2 K_0 e^{-\Delta H/RT}}{1 + K_0 e^{-\Delta H/RT}} \qquad (1)$$

where δ_2 is the shift of the ^{15}N resonance in the hydrogen-bonded environment relative to its position in a liquid-phase "monomeric" or nonhydrogen-bonded species, K_0 is a constant of integration, and ΔH is the enthalpy difference between the hydrogen-bonded and monomeric species.

Equation 1 clearly will not generally yield a linear variation of shift with temperature. Thus, if the proposed model is to be consistent with the experimentally observed linearity, it must be demonstrated that for a reasonable set of values for the parameters δ_2, K_0, and ΔH, eq 1 will fit the experimental observations within experimental uncertainty. We therefore attempted to fit eq 1 to the ^{15}N shift *vs.* temperature data for liquid $^{15}NH_3$ (*cf.* Figure 1) using a nonlinear least-squares computer program to find best values for the parameters δ_2, K_0, and ΔH. The results are $\delta_2 = -24.5 \pm 0.7$ ppm, $K_0 = 0.22 \pm 0.05$, and $\Delta H = -1.5 \pm 0.2$ kcal/mol. With these best parameter values, eq 1 duplicates the experimental data to well within the experimental uncertainty. Moreover, the best parameter values seem reasonable. Thus, accepting the model on which the parameters are based, we consider the ^{15}N in liquid $^{15}NH_3$ as rapidly exchanging between two environments in equilibrium with each other. In the hydrogen-bonded environment, the ^{15}N resonance is shifted 24.5 ppm downfield of its position in the monomeric environment, and the enthalpy of stabilization of the hydrogen-bonded with respect to the monomeric species is -1.5 kcal. Taking all three parameter values together we calculate that liquid ammonia is 91% hydrogen bonded (*i.e.*, 91% of the N atoms are involved in hydrogen bonding) at its melting point and 83% hydrogen bonded at its boiling point. None of these conclusions seems untenable except perhaps the value of -1.5 kcal/mol for the enthalpy of hydrogen-bond formation in liquid NH_3. This value seems rather low compared with the heat of vaporization of ~5.5 kcal/mol for liquid NH_3[19] or the enthalpy of formation of -4.4 kcal/mol reported[20] for a hydrogen-bonded gas-phase ammonia dimer. However, we know of no directly measured values of the hydrogen bond strength in liquid NH_3 and therefore cannot rule out the value of -1.5 kcal/mol. It thus appears that the model is reasonably consistent with the experimental observations although we do not wish to imply that it is the only model which adequately interprets the data.

Whatever the exact source of the variation of ^{15}N shift with temperature in the liquid amines, the linear dependence yields a temperature coefficient which is

(16) U. Liddel and N. F. Ramsey, *J. Chem. Phys.*, 19, 1608 (1951).

(17) N. Muller and R. C. Reiter, *ibid.*, 42, 3265 (1965).

(18) J. C. Hindman, A. Svirmickas, and W. B. Dixon, *J. Chem. Phys.*, 47, 4658 (1967).

(19) "C. R. C. Handbook of Chemistry and Physics," 48th ed, 1968, p E-20.

(20) G. C. Pimentel and A. L. McClellan, "The Hydrogen Bond," New York, N. Y., Reinhold, 1960, p 224.

constant over a rather wide temperature range. A comparison of these temperature coefficients (5th row of Table I) with the liquid association shifts (fourth row of Table I) for the amines shows a striking similarity in behavior of these two parameters. Thus, for the series $^{15}NH_3$, $CH_3{}^{15}NH_2$, and $(CH_3)_2{}^{15}NH$, both parameters progressively decrease in magnitude with the ratio between them remaining approximately constant. Both parameters increase in magnitude in going from $(CH_3)_2{}^{15}NH$ to $(CH_3)_3{}^{15}N$. These results are clearly consistent with the view that the variation of shift in the liquid is due to thermal perturbation of the intermolecular interactions responsible for the liquid-association shift. However, the minimum in both parameters at $(CH_3)_2{}^{15}NH$ suggests that even for a series of structurally related compounds in which the electronic environment is not grossly altered from one molecule to the next, relatively subtle changes in bond hybridization or in the anisotropy of the electronic distribution about the nitrogen may obscure any correlation between the magnitudes of the ^{15}N shift parameters and the types and/or strengths of the liquid-phase interactions involving the nitrogen.

The data for $CH_3C^{15}N$ (*cf.* Figure 2 and column 5 of Table I), when compared with corresponding data for the amines, clearly demonstrates the difference in behavior which may be brought about by gross alteration of the electronic structure around the nitrogen. For $CH_3C^{15}N$ condensation from vapor to liquid leads to an *upfield* shift of the ^{15}N resonance. Moreover the ^{15}N shift in the liquid continues to move to *higher* field with *decreasing* temperature. Thus the data for $CH_3C^{15}N$ remain consistent with the premise that the temperature variation of shift in the liquid is due to thermal perturbation of the interactions responsible for the liquid-association shift. However, $CH_3C^{15}N$ appears to differ consistently from the simple aliphatic amines in the direction of ^{15}N shift produced by similar types of changes in the nitrogen environment. We suggest that this is due to dominance of the paramagnetic term in the ^{15}N chemical shift for $CH_3C^{15}N$ while the ^{15}N shifts in the amines are dominated by the diamagnetic term. Thus, in the gaseous molecules, the ^{15}N resonance in $CH_3C^{15}N$ is strongly shifted paramagnetically (273.4 ppm downfield) relative to $^{15}NH_3$. This is consistent with the large increase in anisotropy of the electron distribution about the nitrogen in $CH_3C^{15}N$ relative to $^{15}NH_3$. If the paramagnetic term dominates, any intermolecular interactions which tend to displace electrons away from the ^{15}N nucleus would, through the $(1/r^3)$ dependence of the paramagnetic term, lead to a decrease in the paramagnetic term or an upfield shift of the ^{15}N resonance. For ammonia or the methylamines on the other hand, dominance of the diamagnetic term would, through its $(1/r)$ dependence, lead to a downfield shift of the ^{15}N resonance for an increase in the average value of r.

The rather good constancy of the ratio of ^{15}N liquid-association shift to temperature coefficient of ^{15}N shift in all the liquids studied here (ratio $\cong -500 \pm 100$) prompted us to compile a larger list of liquids and nuclei for which these parameters had been measured. Table II is a compilation of such data that we were able to find readily in the literature. As anticipated, the ratio of liquid association shift at the melting point to the temperature coefficient of shift in the liquid does not vary greatly over the entire table. Thus, from a purely empirical point of view, one could get a quite good approximation to the temperature coefficient of shift for a particular nucleus in any of these liquids by taking $-1/500$ of the liquid-association shift for that nucleus. It is interesting that the ratio of the enthalpy change on

Table II: Correlation of Liquid-Association Shifts with Other Data

Compd	Nucleus	Liquid-assoc shift, S, ppm	Temp coeff of shift in liquid, $\partial S/\partial T$, ppm/°C	$\frac{S}{\partial S/\partial T}$	$\left(\frac{\Delta H}{\Delta C_p}\right)_{evap}$
$^{15}NH_3$	^{15}N	−22.6	4.3×10^{-2}	−525	−587[f]
NH_3	^{1}H	−1.05[a]	2.7×10^{-3}[e]	−389	−587[f]
$CH_3{}^{15}NH_2$	^{15}N	−9.4	1.6×10^{-2}	−587	
$(CH_3)_2{}^{15}NH$	^{15}N	−3.2	0.5×10^{-2}	−640	−370[g]
$(CH_3)_3{}^{15}N$	^{15}N	−6.9	2.0×10^{-2}	−345	
$CH_3C^{15}N$	^{15}N	+11.3	-2.1×10^{-2}	−538	−810[h]
$H_2{}^{17}O$	^{17}O	−36[b]	4.8×10^{-2}[b]	−743	−1000[f,i]
H_2O	^{1}H	−4.66[c]	9.9×10^{-3}[c]	−471	−1000[f,i]
H_2S	^{1}H	−1.46[d]	4.2×10^{-3}[d]	−349	
H_2Se	^{1}H	−1.85[d]	4.6×10^{-3}[d]	−402	
H_2Te	^{1}H	−3.29[d]	6.6×10^{-3}[d]	−500	

[a] J. A. Pople, W. G. Schneider, and H. J. Bernstein, "High Resolution NMR," McGraw-Hill, 1959, p 403. [b] A. E. Florin and M. Alei, Jr., *J. Chem. Phys.*, **47**, 4268 (1967). [c] J. C. Hindman, *ibid.*, **44**, 4582 (1966). [d] J. C. Hindman, A. Svirmickas, and W. B. Dixon, *ibid.*, **47**, 4658 (1967). [e] M. Alei, Jr., and A. E. Florin, *J. Phys. Chem.*, **73**, 863 (1969). [f] *U. S. Bur. Mines Bull. No. 592*, 111, 119 (1961). [g] *Nat. Bur. Stand. (U. S.) Circ.* **500**, 623 (1952). [h] "Techniques of Organic Chemistry," Vol. VII, 2nd ed, Interscience, 1955 p 224. [i] *U. S. Bur. Mines Bull. No. 584*, 80 (1960).

evaporation to the difference in specific heat between liquid and vapor, $(\Delta H/\Delta C_p)_{evap}$, is also of this order of magnitude for a number of liquids. There is a crude rationale for this similarity if one assumes that the liquid association shift, S, is proportional to the heat of evaporation. Thus, if $S \propto \Delta H_{evap}$, then $(\partial S/\partial T) \propto (\partial \Delta H_{evap}/\partial T) \propto (\Delta C_p)_{evap}$ or $[S/(\partial S/\partial T)] \cong (\Delta H/\Delta C_p)_{evap}$. This is obviously an oversimplification since the thermodynamic properties are influenced by energy changes in all the degrees of freedom of the systems involved while the shifts may be primarily determined by the energies of interactions along certain bonds or directions. However, if this type of model, applied to those interactions which influence the shift, is valid, the temperature dependence of shift in the liquid would be considered as simply due to increasing strength of interaction with decreasing temperature and the linearity of the temperature dependence of shift in the liquid would be attributed to the near constancy of the rate of change of this interaction energy with temperature. Thus, since this "continuum" model could probably fit the nmr observations as well as the "two-state-model" represented by eq 1, the nmr evidence alone cannot rule out either possibility.

Self-Association of Butylamines[1]

by John C. Schug* and Wen M. Chang

Department of Chemistry, Virginia Polytechnic Institute and State University, Blacksburg, Virginia 24061
(Received November 23, 1970)

Publication costs assisted by the National Science Foundation

An iterative matrix technique is described for solving the quasichemical equations. The method is then applied to interpret the amino proton dilution chemical shift of four butylamines in cyclohexane. Comparison of the results with equilibrium calculations indicates that the best stoichiometry for butylamine self-association is the formation of noncyclic trimers.

In the course of other work,[2] it became desirable for us to learn something about the strength and extent of hydrogen bonding in the four isomeric primary butylamines. We therefore studied their proton magnetic resonance spectra upon dilution with the inert solvent, cyclohexane, and sought a model to describe the data over the entire concentration range. The data were successfully interpreted both by a simple monomer–n-mer equilibrium model and in terms of the quasichemical approximation.[3-5] Comparison of the two sets of results leads to the conclusion that the best self-association model is the formation of noncyclic trimers.

The amines were the best grades available from Fisher and Eastman Kodak. They were further purified by distilling twice or more over potassium hydroxide pellets using a Vigreux reflux column; the last distillation of each amine was carried out immediately before its use. Experiments were done using both Fisher Certified cyclohexane which was refluxed overnight over calcium hydride and then fractionated[6] and Fisher spectrograde cyclohexane without further purification. No differences were observed between these two solvents. Tetramethylsilane (TMS) from NMR Specialties was used as an internal standard.

All glassware was thoroughly dried and was flushed with dry nitrogen gas just before use. Samples were prepared by pipetting and the nmr sample tubes were degassed and sealed under vacuum. The chemical shift measurements were obtained with a Jeolco Model C-60H (60 MHz) spectrometer employing external locking and running in the frequency-sweep mode. The frequency of the sweep oscillator was measured with a Hewlett-Packard Model SRC counter. Chemical shifts were determined by the difference between the frequency at the proton of interest and that at the TMS

(1) Supported by a grant from the National Science Foundation.

(2) J. C. Schug, W. M. Chang, and M. J. Kogan, *J. Magn. Res.*, in press.

(3) E. A. Guggenheim, "Mixtures," Oxford University Press, Oxford, 1952.

(4) J. A. Barker, *J. Chem. Phys.*, **19**, 1430 (1951); **20**, 1526 (1952).

(5) I. Satake, M. Arita, H. Kimizuka, and R. Matuura, *Bull. Chem. Soc. Jap.*, **39**, 597 (1966).

(6) C. S. Springer and D. W. Meek, *J. Phys. Chem.*, **70**, 481 (1966).

reference signal. The probable uncertainty in these measurements is about ±0.6 Hz. This is a pessimistic estimate resulting from various instrumental factors that arise in the frequency-sweep experiments. The probe temperature was 24.5 ± 1°, the normal operating temperature.

The remainder of this note deals only with the amino protons, and their chemical shifts are referred to the resonance positions of these protons in the pure amines. For completeness, the $-NH_2$ proton chemical shifts for the pure amines are located with respect to TMS in Table I. The points indicated in Figure 1 are the experimental data showing the upfield shifts observed upon dilution of the amines with cyclohexane.

Table I: Chemical Shift of Amino Hydrogens in the Pure Amines Relative to Internal Tetramethylsilane

Amine	δ_{NH_2}, ppm
n-Butyl	−1.091
Isobutyl	−1.142
sec-Butyl	−1.131
tert-Butyl	−1.118

For an equilibrium description of the data, it was assumed that only a single process was important, namely

$$n(RNH_2) = (RNH_2)_n \quad (1)$$

and that the observed chemical shift is determined by the weighted average

$$\delta = (x_1\delta_1 + nx_n\delta_n)/(x_1 + nx_n) \quad (2)$$

In this equation, x_1 and x_n are equilibrium mole fractions of monomer and *n*-mer, and δ_1 and δ_n are the chemical shifts typical of monomer and *n*-mer, respectively. For each amine, various values of n and the equilibrium constant, K, for reaction 1, were examined in a trial and error search. For each set of these, δ_1 and δ_n were determined by minimizing the root mean square deviation between observed and calculated chemical shifts. When the appropriateness of the model is judged solely by the root mean square deviation between calculated and observed shifts, it is concluded that essentially any value of n is satisfactory. (The values of K, δ_1, and δ_n of course vary with n for each amine.) However, at infinite amine dilution the intercept of the curve is equal to δ_1, the monomer shift. It was found that for each amine the empirical δ_1 continuously decreases as n increases. This can be seen by reference to Figure 1, on which the curves are the chemical shifts calculated for $n = 3$. For the typical case of *n*-butyl amine, the optimum δ_1 determined for $n = 2$, 3, 4, and 5 were 0.458, 0.423, 0.411, and 0.406 ppm, respectively. The last two of these values are too small to be compatible

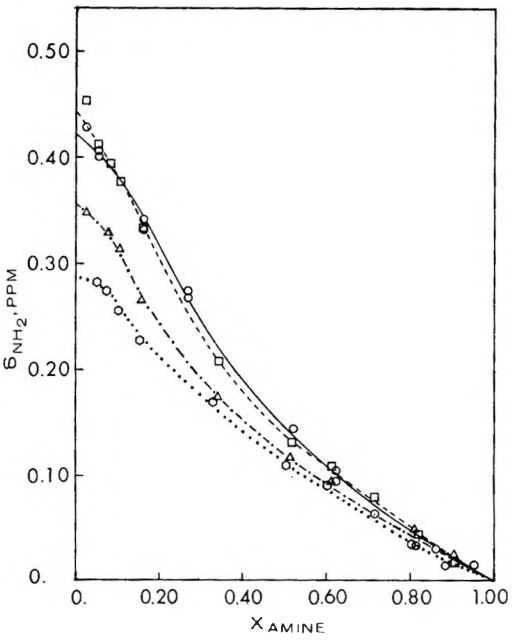

Figure 1. Amino hydrogen chemical shifts relative to pure amines in cyclohexane solution. In order of decreasing intercept at zero mole fraction amine, the curves refer to isobutyl-, *n*-butyl-, *sec*-butyl-, and *tert*-butylamines.

with reasonable extrapolations of the experimental data. Since the same type of results was obtained for all four amines, it was concluded that the most suitable value of n is 2 or 3 in all cases. The optimum parameters found for the case of trimerization are listed in Table II.

Table II: Optimum Parameters for Equilibrium Description ($n = 3$) of Self-Association

Amine	K[a]	δ_1, ppm[b]	δ_3, ppm[b]	$\delta_3 - \delta_1$, ppm
n-Butyl	2.75	0.423	−0.180	−0.603
Isobutyl	4.25	0.441	−0.139	−0.580
sec-Butyl	3.95	0.354	−0.108	−0.462
tert-Butyl	2.30	0.285	−0.124	−0.408

[a] Equilibrium constant for reaction 1 in mole fraction units. [b] Relative to NH_2 resonance in pure amines.

Sometimes the value of n can be better determined by making measurements at lower amine concentrations. This method could not be used here because the NH_2 resonance peak broadens considerably at lower concentrations than those employed. On the other hand, we have investigated the utility of the quasichemical approximation in interpreting these data, and a comparison of the findings with the preceding equilibrium results does seem to fix $n = 3$ in all four amines.

In the quasichemical treatment,[3-5] one considers a lattice model for the liquid solution and focuses attention on the interactions that occur as the molecules contact one another in the various ways possible. All

lattice sites are assumed to be occupied, so that every contact point of each molecule is always in contact with some point on another molecule. This leads to a conservation equation for each site type of every molecular species. For the ith site type of molecular species B, this is

$$2N_{ii} + \sum_{j \neq i} N_{ij} = Q_{i\mathrm{B}} N_{\mathrm{B}} \tag{3}$$

where N_{B} is the number of B molecules in solution, $Q_{i\mathrm{B}}$ is the number of ith type sites on each B molecule, and N_{ij} is the equilibrium number of i–j pairs in contact. The N_{ij} satisfy the quasichemical equation

$$(N_{ij})^2 = 4N_{ii}N_{jj} \exp(-2U_{ij}/kT) \qquad (i \neq j) \tag{4}$$

where $(2U_{ij})$ is the energy required to break one i–i and one j–j constant and form two i–j contacts. For each particular solution, defined by specifying all the N_{B}, and for a set of assumed energies, U_{ij}, it is necessary to solve the set of nonlinear equations of the form (3) in order to determine the equilibrium values of N_{ij}. Rather than following the algebraic method developed by Barker[4] and used by Satake, *et al.*,[5] we have utilized an iterative matrix method.

To do this, let N be the total number of molecules in solution and define the quantities

$$\begin{gathered} Y_i = (N_{ii}/N)^{1/2}; \quad X_{\mathrm{B}} = N_{\mathrm{B}}/N \\ \eta_{ij} = \exp(-U_{ij}/kT); \quad Z_i = Q_{i\mathrm{B}} X_{\mathrm{B}}/2Yi \\ D_{ii} = Z_i/Y_i; \quad D_{ij} = 0 \ (i \neq j) \end{gathered} \tag{5}$$

The entire set of equations of the form (3) can then be written in matrix form as

$$\mathbf{V} = \mathbf{n}\mathbf{Y} - \mathbf{Z} = \mathbf{0} \tag{6}$$

where $\mathbf{0}$ is a null column vector, $\mathbf{Y}$ and $\mathbf{Z}$ are column vectors whose components are the Y_i and Z_i, and $\mathbf{n}$ is the matrix of η_{ij}.

Now suppose we have for eq 6 a trial solution vector, $\mathbf{Y}^{(t)}$, and use it to calculate

$$\mathbf{V}^{(t)} = \mathbf{n}\mathbf{Y}^{(t)} - \mathbf{Z}^{(t)} \tag{7}$$

If $\mathbf{V}^{(t)} \neq \mathbf{0}$, then $\mathbf{Y}^{(t)}$ is not the correct solution. It is necessary to add to $\mathbf{Y}^{(t)}$ a correction vector, $\mathbf{\Delta Y}^{(t)}$. The logical way to choose $\mathbf{\Delta Y}^{(t)}$ is by requiring that the corresponding $\mathbf{\Delta V}^{(t)}$ exactly cancel $\mathbf{V}^{(t)}$. Differentiation of eq 6 with respect to the Y_i shows that, to first order

$$\mathbf{\Delta V} = (\mathbf{n} + \mathbf{D})\mathbf{\Delta Y} \tag{8}$$

where $\mathbf{D}$ is specified in eq 5. Thus, setting $\mathbf{\Delta V}^{(t)} = -\mathbf{V}^{(t)}$, we obtain the required correction vector, to first order

$$\mathbf{\Delta Y}^{(t)} = -(\mathbf{n} + \mathbf{D}^{(t)})^{-1}\mathbf{V}^{(t)} \tag{9}$$

This yields a new trial solution vector

$$\mathbf{Y}^{(t+1)} = \mathbf{Y}^{(t)} + \mathbf{\Delta Y}^{(t)} \tag{10}$$

and the whole process can be repeated until either $\mathbf{V} = \mathbf{0}$ or $\mathbf{\Delta Y} = \mathbf{0}$ to sufficient accuracy. It was sometimes necessary to check each iteration to ensure that every Y_i was positive and remained below its physically acceptable upper limit. It was furthermore helpful to avoid overshoot problems by multiplying $\mathbf{\Delta Y}^{(t)}$ in eq 10 by a damping factor which is less than unity. Convergence was always obtained in fewer than ten iterations.

When the equilibrium numbers of each type of contact are known in a solution, they can be used to calculate observed chemical shifts for the protons of interest. The protons are assumed to be at contact points, and for protons of the αth type, the observed chemical shift is equal to the weighted average

$$\delta(\alpha) = \left(\sum_k N_{\alpha k}\delta_{\alpha k}\right) \Big/ \sum_k N_{\alpha k} \tag{11}$$

The sums are extended over all possible kinds of contact in which the αth proton can engage, and $\delta_{\alpha k}$ is the chemical shift that would be observed for an isolated α–k pair in contact.

The only difference between this approach and the equilibrium model is that the equilibrium constants are replaced by the interaction energies, U_{ij}, or the parameters η_{ij}. Parameter evaluation was therefore approached in the same way, and the same number of parameters were used. Nonzero interaction energies were assigned only to the hydrogen-bond contacts, *i.e.*, –NH–N–. The interaction energy for this is denoted U_{HN}, with the corresponding parameter η_{HN}. The amino proton chemical shift in these contacts is called δ_{N}; for all other types of contacts, the amino proton chemical shift is assumed to have the common value of δ_{F}. For each amine, various η_{HN} were examined by trial and error, and the chemical shift parameters were determined by least-squares calculation based upon eq 11.

A tetrahedral lattice was used, so each lattice site has four nearest neighbors, one or more of which is occupied by bonded portions of the same molecule. For the amines, it was assumed that each carbon or nitrogen atom occupies one lattice site. Each butylamine molecule thus experiences twelve contacts with neighboring molecules. Of these, two correspond to interactions with the amino hydrogens, one with the nitrogen lone-pair electrons, and the remaining nine correspond to noninteresting hydrocarbon interactions. Using the notation described above, we have

$$Q_{\mathrm{HA}} = 2, \ Q_{\mathrm{NA}} = 1, \ Q_{\mathrm{CA}} = 9$$

where A refers to the amine molecule and H, N, and C indicate hydrogen-bonding hydrogen, nitrogen lone pair, and hydrocarbon portion, respectively. The cyclohexane molecule is denoted by the subscript B, and it was assumed that there are twelve (hydrocarbon-type) contact points on it

$$Q_{CB} = 12$$

With the assumptions described earlier, the set of four nonlinear equations of the form (3) or (6) are

$$\begin{aligned} Y_H + \eta_{HN}Y_N + Y_{CA} + Y_{CB} &= X_A/Y_H \\ \eta_{HN}Y_H + Y_N + Y_{CA} + Y_{CB} &= X_A/2Y_H \\ Y_H + Y_N + Y_{CA} + Y_{CB} &= 9X_A/2Y_{CA} \\ Y_H + Y_N + Y_{CA} + Y_{CB} &= 6X_B/Y_{CB} \end{aligned} \tag{12}$$

The interaction parameters η_{HN} and corresponding energies, U_{HN}, along with the chemical shift parameters δ_F and δ_N that gave the best agreement with experiment are shown for the four amines in Table III. In all cases, the root mean square deviation from experimental shifts was less than the estimated uncertainty in the data, so it is concluded that this model also gives an adequate description of the data.

Table III: Parameters for Quasichemical Description of Self-Association Data

Amine	η_{HN}	U_{HN}, kcal/mol	δ_F,[a] ppm	δ_N,[a] ppm	$(\delta_N - \delta_F)/2$, ppm	$2(\delta_N - \delta_F)/6$, ppm
n-Butyl	5.5	−1.01	0.453	−1.491	−0.972	−0.645
Isobutyl	8.9	−1.30	0.482	−1.182	−0.832	−0.555
sec-Butyl	8.5	−1.27	0.384	−0.432	−0.658	−0.439
teri-Butyl	5.4	−1.00	0.311	−1.011	−0.661	−0.441

[a] Relative to NH_2 resonance in pure amines.

The interaction energies, U_{HN}, were found to be in the range -1.2 ± 0.2 kcal/mol. These are small in magnitude compared with values of $\Delta H^\circ = -4 \pm 1$ kcal/mol[7] which are generally expected for the formation of NH–N hydrogen bonds. However, $\Delta H^\circ = -1.5 \pm 0.5$ kcal/mol has been reported once before[8] from an nmr study of dimer amines. For $U_{HN} = -3$ to -5 kcal/mol, η_{HN} is 158–4620. Calculations using interaction parameters in this range were carried out, and the agreement with experiment was exceedingly poor.

It is possible to make comparisons between the chemical shift parameters from the quasichemical and the equilibrium calculations. In the first place, it is clear that the values of δ_F from the quasichemical approach are comparable to the corresponding δ_1 from the equilibrium calculations. The other quasichemical parameter, δ_N, refers to a single amino proton in a hydrogen bond, while δ_n of the equilibrium approach is the average amino proton chemical shift in an n-mer. If the association complex is noncyclic, the n-mer contains $(n - 1)$ hydrogen-bonded and $(n + 1)$ nonbonded amino protons, and it is expected that

$$\delta_n = [(n - 1)\delta_N + (n + 1)\delta_F]/(2n) \tag{13}$$

Further, since $\delta_1 = \delta_F$, the hydrogen-bond shift should be

$$\begin{aligned} \delta_n - \delta_1 &= \delta_n - \delta_F \\ &= (n - 1)(\delta_N - \delta_F)/2n \end{aligned} \tag{14}$$

If the complex were cyclic, half of the amino hydrogens would be hydrogen bonded, and we would expect

$$\delta_n - \delta_1 = (\delta_N - \delta_F)/2 \tag{15}$$

The last column of Table II contains $(\delta_n - \delta_1)$ for $n = 3$, and the right-hand-sides of eq 14 and 15 are listed in the last two columns of Table III. It is seen that the equality of eq 14 is nearly borne out, but that eq 15 is far from being satisfied. Similar comparisons were made for the optimum parameters determined from the $n = 2$, 4, and 5 models, also. In no other case did eq 14 or 15 come close to being satisfied. The discrepancies were always in excess of 50% and rose in some cases to close to 300%. We must therefore conclude that open trimers are the best self-association models for all four amines.

This finding is in disagreement with a paper of Feeney and Sutcliffe,[9] who stated that isobutylamine forms tetramers. It is further interesting that they quoted a hydrogen-bond shift of −0.875 ppm, while ours was only −0.480 for the tetramer model and −0.580 ppm for the preferred trimer model.

In conclusion, we have found that the quasichemical approximation is easy to use, that it provides comparable results with the equilibrium calculations, and that it can be very helpful in choosing the most appropriate equilibrium stoichiometry.

(7) G. C. Pimental and A. L. McLellan, "The Hydrogen Bond," W. H. Freeman, San Francisco, Calif., 1960.

(8) R. A. Murphy and J. C. Davis, Jr., *J. Phys. Chem.*, 72, 3111 (1968).

(9) J. Feeney and L. H. Sutcliffe, *Proc. Chem. Soc. London*, 118 (1961); *J. Chem. Soc. London*, 1123 (1962).

Investigation of Micelle Structure by Fluorine Magnetic Resonance. V. Sodium Perfluorooctanoate[1]

by Norbert Muller* and Harvey Simsohn

Department of Chemistry, Purdue University, Lafayette, Indiana 47907 *(Received October 29, 1970)*

Publication costs assisted by the National Science Foundation

Chemical shifts of five structurally nonequivalent types of fluorine atom have been determined for aqueous solutions of sodium perfluorooctanoate by nuclear magnetic resonance and double irradiation techniques. The concentration dependence of the shifts yielded three values for the critical micelle concentration (cmc) in good agreement with each other and with results from nonspectroscopic observations. The cmc is 0.030 *M* at 35° and when studied as a function of temperature exhibits a minimum between 30 and 40°. The shifts support the conclusion that in the micelles all fluorine atoms are exposed to water to some extent, with the average environment becoming progressively more aqueous as one moves along the chain toward the ionic end. Potassium perfluorooctanoate (cmc = 0.027 *M* at 35°) acts very much like the sodium salt, but the tetramethylammonium salt forms smaller micelles and has a cmc near 0.015 *M*. In 2.0 *M* tetrahydrofuran the aggregation numbers for all three salts are reduced to about 3 or 4; 1,4-dioxane at the same concentration has a much less drastic effect.

Introduction

The great solvent sensitivity of fluorine chemical shifts allows micelle formation in solutions of fluorine-labeled surfactants to be studied conveniently by nuclear magnetic resonance (nmr) spectroscopy.[2-5] When the intent is to elucidate hydrophobic interactions between hydrocarbon chains, the number of fluorine atoms introduced into the chains should be kept small; because of their spectroscopic properties and relative ease of preparation, terminal trifluoromethyl derivatives have been found useful. The physical properties of these compounds are not very different from those of their unfluorinated analogs, even though the CF_3CH_2R structure should have an electric dipole moment of about 2.3 D, the value reported[6] for CF_3CH_3. Interactions between this dipole and those of adjacent water molecules probably account for the finding[2-5] that for a variety of detergents replacing the terminal methyl group of the alkyl chain by a trifluoromethyl group reduces the favorable free energy of micellization by 0.4 kcal/mol.

Perfluoroalkyl detergents obviously are also amenable to study by this technique. It has been known for some time that these materials, unlike the trifluoro compounds, form micelles at much lower concentrations than hydrocarbon detergents with the same number of carbon atoms.[7-9] An especially interesting feature of these compounds is that nmr signals originate from nuclei at several sites on the alkyl chain,[10,11] so that the spectra can be expected to reveal how the effect of micellization on the local environment varies with the distance between the probe nucleus and the hydrophilic group.

We present here the results of such a study for sodium perfluorooctanoate, chosen because it is easy to obtain, its cmc falls in a convenient range, and it produces an nmr spectrum in which signals belonging to several sets of structurally distinct fluorine nuclei can be identified. With the usual convention that the carbon atom of the carboxyl group is designated as number 1, shifts can be found directly for fluorines attached to carbons 2, 7, and 8. For sufficiently concentrated solutions, shifts of fluorines bound to carbons 4 and 6 can be determined indirectly using a double resonance technique. Some observations of the effects of temperature changes, introduction of organic additives, and replacement of the counterions by potassium or tetramethylammonium ions are also reported.

Experimental Section

Perfluorooctanoic acid (Pierce Chemical Co.) was recrystallized twice from carbon tetrachloride. The melting point of the product (55.5 ± 1°, literature value[12] 54.9–55.6°) was somewhat higher than that of the

(1) Financial support from the National Science Foundation under Grant G.P. 8370 is gratefully acknowledged.

(2) N. Muller and R. H. Birkhahn, *J. Phys. Chem.*, **71**, 957 (1967).

(3) N. Muller and R. H. Birkhahn, *ibid.*, **72**, 583 (1968).

(4) N. Muller and T. W. Johnson, *ibid.*, **73**, 2042 (1969).

(5) N. Muller and F. E. Platko, *ibid.*, in press.

(6) R. G. Shulman, C. H. Townes, and B. P. Dailey, *Phys. Rev.*, **78**, 145 (1950).

(7) H. B. Klevens and M. Raison, *J. Chim. Phys.*, **51**, 1 (1954).

(8) H. B. Klevens and M. Raison, *1er Congr. mondial détergence et prods. tensio-actifs, Paris*, **1**, 66 (1954).

(9) K. Shinoda and K. Katsura, *J. Phys. Chem.*, **68**, 1568 (1964).

(10) R. E. Bailey and G. H. Cady, *ibid.*, **73**, 1612 (1969).

(11) R. E. Haque, *ibid.*, **72**, 3056 (1968).

(12) M. K. Bernett and W. A. Zisman, *ibid.*, **63**, 1911 (1959).

unpurified acid, but samples made with either material yielded identical nmr spectra under similar conditions. Stock solutions of the several salts were made by neutralizing weighed amounts of the acid with the required amount of a standard solution of the appropriate base in a volumetric flask and adding distilled, deionized water as required. More dilute solutions were made volumetrically using aliquots of the stock solutions. When appropriate, tetrahydrofuran or 1,4-dioxane, freshly distilled, was added as required to make the concentration of the additive in the stock solution 2.0 M, and dilutions were made using 2.0 M solutions of the additive in water.

Nmr determinations were made with a Varian HA60-IL spectrometer operated at 56.445 MHz, using a Hewlett-Packard 200CD wide range oscillator in place of the internal "manual oscillator" to increase the upfield range of the instrument. 1,3-Dichlorotetrafluoroacetone (Peninsular Chemresearch, Inc.) was used as an external reference, neglecting bulk susceptibility corrections because they are small and nearly constant. At 35° the shifts are related to shifts measured from the more common (but less convenient) reference, trifluoroacetic acid, by the equation

$$\delta(CF_2ClCOCF_2Cl) = \delta(CF_3COOH) + 12.85 \text{ ppm} \quad (1)$$

The temperature was controlled with a Varian V-4341/V-6057 variable temperature accessory, allowing 15 min for each sample to reach a steady temperature before making nmr measurements. Temperatures were determined and periodically checked by replacing the working sample with a tube containing 2% 1,2-difluorotetrachloroethane in 1,1,2-trichlorotrifluoropropene.[13]

Results and Discussion

Determination of Chemical Shifts. The gross features of the nmr spectrum of aqueous sodium perfluorooctanoate are essentially independent of concentration. There is a well-defined triplet at about 17 ppm (all shifts are to higher fields from the reference), a poorly resolved triplet near 52 ppm, a large peak obviously formed by several overlapping signals but with no resolvable fine structure near 58 ppm, and a broad, symmetrical peak near 62 ppm. The relative areas of these four resonances are 3:2:8:2, suggesting at once that the peak near 17 ppm belongs to the CF_3 group.[14] This assignment is consistent with shifts reported[15] for terminal CF_3 groups in other perfluoroalkyl compounds.

The intensity, position, and fine structure of the peak near 52 ppm suggest that it belongs to C2. Supporting evidence is provided by the spectra of perfluorooctanoic acid and its sodium salt in absolute ethanol. These are quite similar to that of the salt in aqueous solution, and the 52-ppm peak is the only one which moves appreciably when the acid is replaced by the salt. The difference is 2.15 ppm, the shift for the acid being to higher field.

Comparison of the spectrum with those of normal fluoroalkanes[15] further suggests that the complex peak near 58 ppm arises from C3, C4, C5, and C6, while the peak at 62 ppm belongs to C7.

The procedure for obtaining the shifts of C4 and C6 is based on the observation[15] that in perfluoroalkyl derivatives the spin–spin coupling constants for fluorine atoms separated by four bonds, $J_{F-C-C-C-F}$, are substantially larger than those for atoms separated by only three bonds, $J_{F-C-C-F}$, the latter being often less than 1 Hz. Thus the triplet structure of the C8 signal reflects coupling of the nuclei in C8 with those in C6, and the resonance of C2 is split primarily because of the interaction between nuclei in C2 and C4. Consequently, if the C8 signal is observed while exposing the sample to radiation at a frequency equal to the resonant frequency of C6, the nuclei of C8 and C6 are decoupled,[16] and the C8 resonance appears as a singlet.

In practice, the "second" radiofrequency may be generated by modulating the first upper side band of the lock signal with the output, ν_2, of a tuneable audio oscillator. One scans repeatedly over the C8 peak while varying the value of ν_2 in small steps, *e.g.*, 5 Hz. The peak amplitude is plotted as a function of ν_2, yielding a symmetrical curve with a maximum, corresponding to optimal decoupling, that can be located with a precision of about ±2 Hz (0.04 ppm). The C6 shift, in hertz, is then given by the difference between the manual oscillator frequency and the value of ν_2 at the maximum. The C4 shift is similarly determined by finding the value of ν_2 which produces complete decoupling of C2 and C4. This procedure worked well when the surfactant concentration was at least 0.1 M but failed for more dilute samples because of low-signal-to-noise ratios.

Chemical shifts for aqueous sodium perfluorooctanoate at 35° at a number of concentrations are presented in Table I.

Critical Micelle Concentration. When the shifts for C2, C7, or C8 are plotted as a function of the reciprocal of the total detergent concentration, the results[17] closely resemble analogous plots[2-4] for other surfactants, and the monomer shifts, the micelle shifts, and the cmc's can be found as described earlier.[2-4] At 35° the cmc's determined using the data for C2, C7, and C8 are 0.031, 0.032, and 0.030 M, respectively. The accuracy is greatest when the difference between the

(13) N. Muller and T. W. Johnson, *J. Phys. Chem.*, 73, 2460 (1969).

(14) Hereafter the abbreviation C8 will be used for the fluorines of the CF_3 group, and C2, C3, ..., C7 will be used for the fluorines attached to carbons 2 through 7.

(15) J. W. Emsley, J. Feeney, and L. H. Sutcliffe, "High Resolution Nuclear Magnetic Resonance Spectroscopy," Vol. 2, Pergamon Press, Elmsford, N. Y., and Oxford, 1966, Chapter 11.

(16) Reference 15, Vol. 1, Section 6.8.

(17) H. Simsohn, Ph.D. Thesis, Purdue University, 1970.

Table I: Chemical Shifts (ppm from External 1,3-Dichlorotetrafluoroacetone) of Various Groups of Fluorine Atoms for Aqueous Sodium Perfluorooctanoate at 35°

Molarity	δ(C2)	δ(C4)	δ(C6)	δ(C7)	δ(C8)
0.500	52.04	56.77	57.32	61.90	17.25
0.300	51.99	56.76	57.29	61.86	17.15
0.200	51.97	56.65	57.23	61.79	17.04
0.125	...	56.58	57.16	61.61	16.79
0.100	51.88	56.49	57.11	61.45	16.65
0.080	51.83	...	...	61.33	16.47
0.060	51.76	...	...	61.08	16.10
0.050	51.68	...	...	60.82	15.85
0.040	51.60	...	...	60.53	15.48
0.030	51.45	...	...	60.23	15.04
0.025	51.45	...	...	60.23	14.91
0.020	51.45	...	...	60.21	14.89
0.017	...	...	...	...	14.89

monomer shift and the micelle shift is maximal, and hence the C8 data should yield the best value. Accordingly, to evaluate the cmc with other counterions or at other temperatures only data for C8 were taken, with results summarized in Table II. The precision of each such cmc determination is about ± 0.001 M.

Table II: Critical Micelle Concentrations Derived from Chemical Shift Data for the CF_3 Group of Perfluorooctanoate Salts

Cation	Temp, °C	Cmc, M
Sodium	18	0.033
Sodium	25	0.031
Sodium	30	0.031
Sodium	35	0.030
Sodium	44	0.031
Sodium	60	0.033
Potassium	35	0.027
Tetramethyl-ammonium	35	0.015

The C8 dilution shift curve for potassium perfluorooctanoate is nearly identical with that for the sodium salt, but the cmc is a little lower, 0.027 M. In contrast with earlier results,[11] this agrees exactly with values based on colligative property measurements.[7-9] The data points for the tetramethylammonium salt define a slightly sigmoidal curve[17] with a cmc of 0.015 M. The form of the curve implies that the micelles are much smaller than those formed by the two alkali metal salts and that the concentration of monomeric perfluorooctanoate ions passes through a maximum as the total detergent concentration increases. Such a maximum is consistent with calculations based on a simple mass-action model allowing for counterion binding.[3,18]

Sodium perfluorooctanoate resembles other anionic detergents in that the cmc varies only slowly with temperature between 20 and 60° and passes through a minimum between 30 and 40°. The equation[19]

$$\Delta H_m^\circ = -RT^2 \frac{d \ln \text{cmc}}{dT} \qquad (2)$$

then requires that the enthalpy of micellization, ΔH_m°, be small and positive at the lower temperature and become negative as the temperature is raised. The validity of this equation has been challenged[20] on the grounds that, for potassium octanoate, heat of dilution measurements appeared to show that ΔH_m° remained positive over the whole interval from 15 to 60° even though cmc data indicated the usual change in sign near 40°. Both approaches require assumptions which are not readily verified experimentally, and the conflict cannot be resolved on the basis of this work, but it seems appropriate to stress here that is is not at all intrinsically implausible to suppose that ΔH_m° changes sign near 40°. Measured heat capacity changes accompanying micellization of nonionic detergents[5] and denaturation of proteins[21] together with the rationale presented for these observations[21] strongly suggest that micellization of anionic detergents should likewise involve a sizeable negative heat capacity change. Since all workers are agreed that ΔH_m° for the anionics is small and positive at 25°, such a heat capacity change would then require the change of sign at somewhat elevated temperatures.

Micelle Chemical Shifts. Since the immediate environment of a fluorine atom in a perfluorooctanoate micelle should contain primarily fluorocarbon chains and, perhaps, water molecules, one is led to attempt to characterize this environment by a quantity Z, derived from the micelle shift[2] and defined as

$$Z = (\delta_{\text{micelle}} - \delta_{\text{aq}})/(\delta_{\text{fc}} - \delta_{\text{aq}}) \qquad (3)$$

where δ_{aq} is the shift for the fluorine atom in an aqueous medium (*i.e.*, the monomer shift) and δ_{fc} is the shift in a fluorocarbon solvent. As stated above, the required values of δ_{micelle} and δ_{aq} for C2, C7, and C8 are readily determined. For C4 and C6 the shifts are available only for fairly concentrated solutions, but since the cmc is fixed by the C8 data, δ_{micelle} and δ_{aq} for these groups can be found graphically by extrapolating the linear plot of chemical shift *vs.* reciprocal concentration to the intercept and to the cmc. Values of δ_{fc} are less easily come by, since sodium perfluorooctanoate does not dissolve in fluorocarbons. Approximate values were found indirectly using a sample consisting of 1 g of perfluorooctanoic acid and 0.35 g of perfluorocyclohexane (Pierce Chemical Co.). Guided by the results (above) for the acid and the sodium salt in ethanol,

(18) E. W. Anacker in "Cationic Surfactants," E. Jungerman, Ed., Marcel Dekker, New York, N. Y., 1970, p 212.

(19) G. Stainsby and A. E. Alexander, *Trans. Faraday Soc.*, **46**, 587 (1950).

(20) P. White and G. C. Benson, *ibid.*, **55**, 1052 (1959).

(21) C. Tanford, *Advan. Protein Chem.*, **23**, 121 (1968); **24**, 1 (1970).

it was assumed that the shifts for all groups except C2 would be the same in this mixture as in a hypothetical solution of the salt in fluorocarbon, and that for C2 the required value would be given by

$$\delta(C2)_{fc}^{salt} = \delta(C2)_{fc}^{acid} - 2.15 \text{ ppm} \quad (4)$$

The results appear in Table III. It is surprising that the Z values are so large; leaving out C2, the average is 0.74, larger by 0.2 than the corresponding quantity for the terminal CF_3 groups of trifluoroalkyl carboxylates.[2] Published shifts[2,22] for the other organofluorine compounds in various solvents raise the possibility that our δ_{fc} values may be systematically low, and therefore it would be dangerous to conclude that there is a significant difference between the degrees of hydration of the two kinds of micelles. Nevertheless, the more or less steady increase in Z from C2 to C8 is certainly significant, and it mirrors the anticipated decrease in the amount of water "seen" by the probe nucleus as it is moved farther from the micelle surface.

Table III: Chemical Shifts (ppm from External 1,3-Dichlorotetrafluoroacetone) for Sodium Perfluorooctanoate in Various Environments, and Values of $Z = (\delta_{micelle} - \delta_{aq})/(\delta_{fc} - \delta_{aq})$

Group	δ_{aq}	$\delta_{micelle}$	δ_{fc}	Z
C2	51.45	52.08	53.16	0.37
C4	55.60	56.87	57.52	0.66
C6	56.50	57.38	57.89	0.63
C7	60.22	62.07	62.45	0.83
C8	14.89	17.37	17.85	0.84

Effect of Organic Cosolvents. Measurements in the mixed solvents, 2.0 M aqueous 1,4-dioxane and 2.0 M tetrahydrofuran, were undertaken because of the unexpected behavior of other detergents in these solvents. Addition of dioxane to solutions of trifluorododecyl sulfate slightly raises the cmc and reduces the micelle size, and the detergent is unassociated when the concentration is 0.01 M or less.[4] The same amount of tetrahydrofuran reduces the micelle size much more drastically, the principal species being apparently a tetramer, and appreciable association persists in the concentration range 0.0025 to 0.01 M. In contrast with these findings, the two additives have very similar effects on micelles of the nonionic surfactant $CF_3(CH_2)_7S(O)CH_3$; in neither case is the aggregation number so very small, nor is there residual association in very dilute solutions.[5] These differences seem to rule out the possibility that the additives act simply by changing the effectiveness of hydrophobic interactions between alkyl chains. The possibility that specific interactions between the organic species and the counterions are involved is not very appealing, but we thought it best not to discard it without attempting to test it experimentally and therefore determined dilution curves for sodium, potassium, and tetramethylammonium perfluorooctanoate in both mixed solvents.

The three salts gave very similar results in 2.0 M tetrahydrofuran;[17] again the aggregation number was very low, perhaps 3 or 4. Since these three cations must be solvated rather differently, it seems unlikely that specific ether–counterion interactions are responsible for the change in micelle size. The conclusion is consistent also with a small number of observations[17] of the ^{23}Na resonances from sodium dodecyl sulfate in water and mixed solvents. In 2.0 M dioxane, the sodium and potassium salts form smaller micelles than in water, but with aggregation numbers perhaps in the range 10–20. For the tetramethylammonium salt, which forms rather small micelles in water, addition of dioxane appears actually to *increase* the micelle size somewhat. We remain unable to explain why the two cyclic ethers affect association of anionic (but not nonionic) surfactants so differently.

(22) D. F. Evans, *J. Chem. Soc.*, 877 (1960).

Thermodynamics of Mixed Electrolyte Solutions. Ionic Entropy Correlations and Volume Fraction Statistics

by J. V. Leyendekkers

Division of Fisheries and Oceanography, CSIRO, Cronulla, N.S.W. 2230, Australia *(Received March 25, 1970)*

Publication costs borne completely by The Journal of Physical Chemistry

Linear correlations are illustrated between the ionic entropy and various thermodynamic properties of mixing of two electrolytes with a common ion, *viz.* Harned coefficients, excess free energy, and enthalpy of mixing. The Harned coefficients are resolved into pairwise-interaction components and correlations between the ionic and structural entropy shown. Volume fraction statistics are used to predict the activity coefficients of electrolytes in 1:1/1:1 mixtures. A comparison between the experimental and predicted results indicates that the theory needs modification to account for changes in the hydration parameters and long-range interactions. If such changes are negligible the agreement is good.

Introduction

A survey of the theory of multicomponent electrolyte solutions was published in 1968.[1] Recently,[2] equations were given which enable the free energy and related properties of a mixed electrolyte solution to be calculated from data on single electrolyte solutions and common-ion mixtures. Equations based on the ion–component treatment of Scatchard enable the mean activity coefficient of any electrolyte in any mixture of ions to be calculated in a related way.[3] A recent report[4] gives the parameters of these equations for 22 aqueous mixtures of two electrolytes. The effect of temperature on some of these parameters has also been studied.[5] These references constitute much practically useful information on the theory of mixed electrolyte solutions. In the present paper an attempt is made to extend this information in a somewhat different direction, more emphasis being given to ion–solvent interactions and solution structure. A number of developments[6] take account of effects of ion–solvent interactions, or hydration, on the activity coefficients in single electrolyte solutions but these theories have been somewhat neglected in dealing with mixed electrolyte solutions. The only application seems to have been to the calcium–strontium chloride system[7] where volume fraction and mole fraction statistics were used. In this paper, volume fraction statistics (VFS) are investigated for univalent electrolyte mixtures. In addition, the correlation between Harned coefficients and ionic entropy[8] is examined in more detail.

Entropy Correlations

H Lines. For an aqueous mixture of two electrolytes (say A and B) at constant ionic strength, I (equal to $I_A + I_B$), the simple relationship

$$\log \gamma_A/\gamma_A^0 = -\alpha_{AB} I_B \qquad (1)$$

often applies, where γ represents the activity coefficient and α the Harned coefficient. Generally, the data have been correlated in terms of the system A–B with I as the variable. However, by keeping A and I fixed and varying B it has been shown that the corresponding Harned coefficients can be simply related to a thermodynamic property of the ions, *viz.*, the ionic entropy. For a large number of chloride systems α_{AB} is a linear function of the standard entropies of the ions, suitably weighted to normalize charge asymmetric systems.[8] For example, for a 2:1/1:1 chloride system such as $CaCl_2$–NaCl the entropy function is

$$\bar{S}^0_{CaCl_2(NaCl)} = \frac{7}{12}\bar{S}^0_{Ca^{2+}} + \bar{S}^0_{Na^+} - \frac{9}{8}\bar{S}^0_{Cl^-}$$

and for 2:1 mixtures, such as $CaCl_2$–$MgCl_2$

$$\bar{S}^0_{CaCl_2(MgCl_2)} = \frac{1}{4}\bar{S}^0_{Mg^{2+}}$$

(1) H. S. Harned and R. A. Robinson, "Multicomponent Electrolyte Solutions," Topic 15, Vol. 2, The International Encyclopedia of Physical Chemistry and Chemical Physics, Pergamon Press, Edinburgh, 1968.

(2) (a) P. J. Reilly and R. H. Wood, *J. Phys. Chem.*, **73**, 4292 (1969); (b) R. H. Wood, M. Ghamkhar, and J. D. Patton, *ibid.*, **73**, 4298 (1969).

(3) Y. C. Wu, R. M. Rush, and G. Scatchard, *ibid.*, **73**, 2047 (1969).

(4) R. M. Rush, Oak Ridge National Laboratory Report, ORNL-4402, UC-4-Chemistry (1969).

(5) M. H. Lietzke, H. B. Hupf, and R. W. Stoughton, *J. Phys. Chem.*, **69**, 2395 (1965).

(6) (a) R. H. Stokes and R. A. Robinson, *Trans. Faraday Soc.*, **53**, 301 (1957); (b) R. A. Robinson and R. H. Stokes, "Electrolyte Solutions," 2nd ed, Butterworths, London, 1959; (c) E. Glueckauf, *Trans. Faraday Soc.*, **51**, 1235 (1955); (d) E. Glueckauf, "Structure of Electrolyte Solutions," W. J. Hamer, Ed., Wiley, New York, N. Y., 1959, p 106; (e) R. H. Stokes and R. A. Robinson, *J. Amer. Chem. Soc.*, **70**, 1870 (1948); (f) D. G. Miller, *J. Phys. Chem.*, **60**, 1296 (1956); (g) T. Ikeda, *Rep. Liberal Arts Fac., Shizuoka Univ. Japan, Natur. Sci.*, **1**, 25 (1960).

(7) S. Wu, Ph.D. Thesis, University of Kansas, University Microfilms, Inc., Ann Arbor, Mich., 1965.

(8) J. Leyendekkers, *J. Phys. Chem.*, **74**, 2225 (1970).

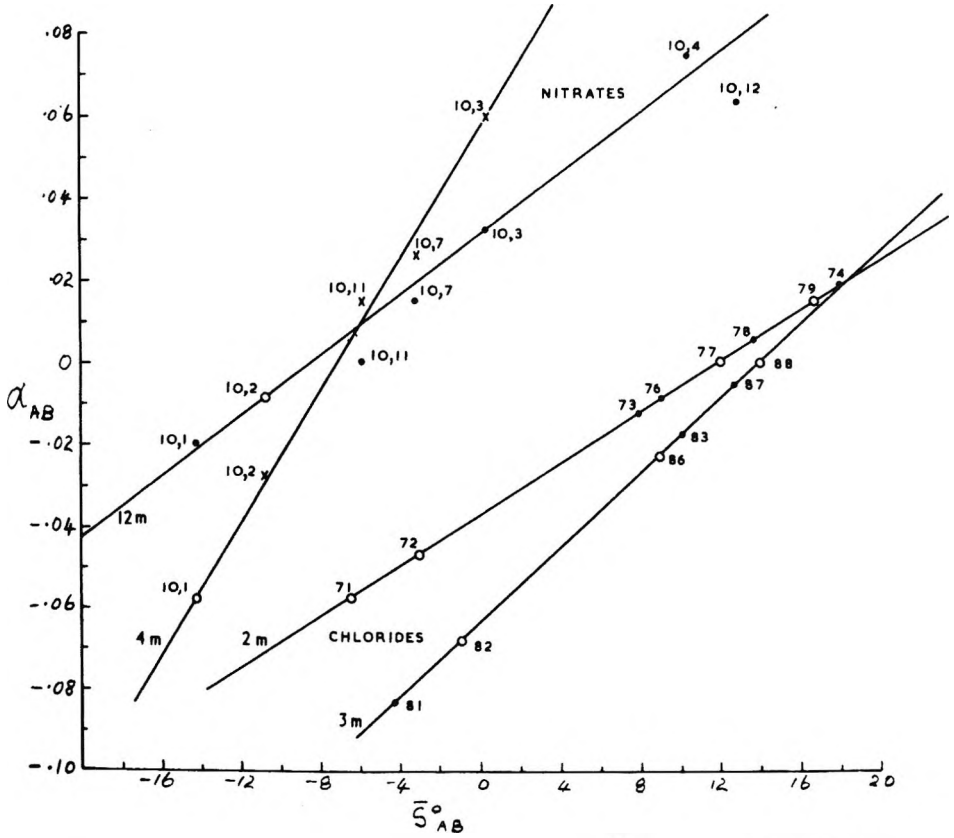

Figure 1. H lines[8] of $CaCl_2$, $SrCl_2$, and $UO_2(NO_3)_2$ at various ionic strengths. $\bar{S}_{AB}^{\circ}$ in cal deg^{-1} mol^{-1} (at 25° and computed relative to $\bar{S}_{H^+}^{\circ} = 0$),[16] α_{AB} in reciprocal ionic strength: ●, × experimental; ○, predicted. Code: 1, H^+; 2 Li^+; 3, Na^+; 4, K^+; 5, Cs^+; 6, Mg^{2+}; 7, Ca^{2+}; 8, Sr^{2+}; 9, Ba^{2+}; 10, UO_2^{2+}; 11, Cu^{2+}; 12, NH_4^+.

The characteristic line for a given electrolyte at a given ionic strength has been called an H line. Figure 1 shows some of these lines for the chlorides of calcium and strontium and for uranyl nitrate. The data used are given in ref 7 and 9. For convenience the weights for chloride systems were represented as functions of the ionic charges;[8] however, the anion weighting function was not suitable for the nitrate ion, the entropy function for asymmetric uranyl nitrate systems being

$$\bar{S}^0_{UO_2(NO_3)_2(MNO_3)} = \frac{7}{12}\bar{S}^0_{UO_2^{2+}} + \bar{S}^0_{M^+} - \frac{1}{8}\bar{S}^0_{NO_3^-}$$

The entropy of an oxyanion is correlated with the charge in a different way from that for a monatomic ion[10] and complexing is more marked in nitrate systems; however, no satisfactory theoretical basis for the weighting values is available yet.

Thermodynamic quantities such as the ionic entropies and the structural entropy ΔS^{st} [11] represent potentially very useful reference quantities so that experimental data can be used to characterize structural effects in a quantitative way. A number of other linear correlations have been noted between ionic entropies and parameters related to ion–solvent and ion–ion interactions such as the viscosity coefficient B of the Jones–Dole equation[12] and, for dilute solutions of alkali halides, the b coefficient in the well known equation[13]

$$\log \gamma^0_A = \frac{-D|z_+z_-|I^{1/2}}{1 + \rho I^{1/2}} + (2\nu_+\nu_-/\nu)bm \qquad (2)$$

where[1] $D = 0.5107$ $mol^{-1/2}kg^{1/2}$ for water at 25°, ρ is a parameter characteristic of the electrolyte, ν represents the number of moles of ions formed from one mole of electrolyte, and z is the charge number of an ion.

The structural entropy ΔS^{st} or a quantity proportional to it has been correlated successfully with D_2O/H_2O transfer enthalpies and entropies, and has been shown to be useful in interpreting trends in the data.[14] The transfer entropies are believed to result primarily from long-range ion–solvent interactions while solution

(9) (a) H. S. Harned and B. B. Owen, "The Physical Chemistry of Electrolytic Solutions," 3rd ed, ACS Monograph 137, Reinhold, New York, N. Y., 1958, Chapter 14; (b) R. A. Robinson and V. E. Bower, *J. Res. Nat. Bur. Stand.*, **70A**, 305 (1966); (c) R. A. Robinson and A. K. Covington, *ibid.*, **72A**, 239 (1968); (d) R. D. Lanier, *J. Phys. Chem.*, **69**, 3992 (1965); (e) L. Jenkins and H. A. C. McKay, *Trans. Faraday Soc.*, **50**, 107 (1954); (f) E. Glueckauf, H. A. C. McKay, and A. R. Mathieson, *J. Chem. Soc., Suppl.*, **2**, S299 (1949).

(10) J. W. Cobble, *J. Chem. Phys.*, **21**, 1443 (1953).

(11) H. S. Frank and M. W. Evans, *ibid.*, **13**, 507 (1945).

(12) R. W. Gurney, "Ionic Processes in Solutions," McGraw-Hill, New York, N. Y., 1953.

(13) D. T. Burns, *Electrochim. Acta*, **11**, 1545 (1964).

(14) (a) E. M. Arnett and D. R. McKelvey in "Solute-Solvent Interactions," J. F. Coetzee and C. D. Ritchie, Ed., Interscience, New York, N. Y., 1969; (b) C. V. Krishnan and H. L. Friedman, *J. Phys. Chem.*, **74**, 2356 (1970).

viscosity variations result from a balance of both short- and long-range interactions.[15] Consequently it is assumed that the ionic entropy is an indicator of both types of interactions while ΔS^{st} distinguishes the long-range type. A breakdown of the Harned coefficients into components on the basis of simple ion–ion interaction theory and a comparison with these entropy terms should therefore be interesting. Such an analysis might also give information on the general applicability of the H lines.

Ion Interaction Equations. Following the treatment given in ref 1 (p 11) and taking account of interactions between cations it can be shown that for the electrolyte system A (cation 1 and anion 2) and B (cation 3, and anion 4 identical with 2), and assuming eq 1 holds

$$-(2.303/2)\alpha_{AB} = w_c B_{12} + w_d B_{23} + w_e \delta_{13} - w_f \delta_{11} \quad (3)$$

$$-(2.303/2)\alpha_{BA} = u_c B_{12} + u_d B_{23} + u_e \delta_{13} - u_f \delta_{33} \quad (4)$$

where

$$w_c = (\nu_1\nu_4/\nu_A\nu_B z_3 z_4 - 2\nu_1\nu_2/\nu_A^2 z_1 z_2)$$

$$w_d = (\nu_2\nu_3/\nu_A\nu_B z_3 z_4)$$

$$w_e = (\nu_1\nu_3/\nu_A\nu_B z_3 z_4)$$

$$w_f = (2\nu_1^2/\nu_A^2 z_1 z_2)$$

$$u_c = \nu_1\nu_4/\nu_A\nu_B z_1 z_2$$

$$u_d = (\nu_3\nu_2/\nu_A\nu_B z_1 z_2 - 2\nu_3\nu_4/\nu_B^2 z_3 z_4)$$

$$u_e = \nu_1\nu_3/\nu_A\nu_B z_1 z_2$$

$$u_f = 2\nu_3^2/\nu_B^2 z_3 z_4$$

Here, z represents the absolute charge value of the ion; note that $z_2 = z_4$, while $\nu_2 \neq \nu_4$ may apply. The B terms represent interactions between ions of opposite charge and δ terms represent the interaction between ions of like charge.

For charge symmetric systems when $\delta_{13} = (\delta_{33} + \delta_{11})$ or the δ terms are negligible, then $\alpha_{AB} = -\alpha_{BA}$, obviously a special case.

The excess free energy of mixing when Harned's rule applies, and $I_A = I_B = {}^1/_2 I$, is given by

$$G^E/RTI^2 = -(2.303/4)(\alpha_{AB}/z_1 z_2 + \alpha_{BA}/z_3 z_4)$$

$$= y_c B_{12} + y_d B_{23} + y_e \delta_{13} + y_f \delta_{11} + y_g \delta_{33} \quad (5)$$

where

$$y_c = {}^1/_2(w_c/z_1 z_2 + u_c/z_3 z_4)$$

$$y_d = {}^1/_2(w_d/z_1 z_2 + u_d/z_3 z_4)$$

and so on, from eq 3 and 4, or, in terms of the charge values

$$y_c = (z_1 - z_3)/z_1 z_2 (z_1 + z_2)^2 (z_3 + z_2)$$

$$y_d = -(z_1 - z_3)/z_3 z_2 (z_1 + z_2)(z_3 + z_2)^2$$

$$y_e = 1/(z_1 + z_2)(z_3 + z_2) z_1 z_3$$

$$y_f = -1/z_1^2 (z_1 + z_2)^2$$

$$y_g = -1/z_3^2 (z_3 + z_2)^2$$

These weights are equivalent to those given by Reilly and Wood[2] for the pairwise interaction terms (the numbering here is different and all z values are positive).

Cation–Anion Interactions. The B_{12} and B_{23} terms in eq 3 and 4 are characteristic of solutions A and B, respectively. It is assumed that these terms may be represented by the B' values listed by Pitzer and Brewer[16] (*i.e.*, equivalent to b in eq 2 when $\rho = 1$). These values have been weighted on the basis of ionic strength and plotted against the entropy of the corresponding cation (Figure 2). For electrolytes with negligible complexing, B' fits the line

$$(2\nu_1\nu_2/\nu_A z_1 z_2) B_{12} = a - (b'/z_1 z_2)\bar{S}^0_1 \quad (6)$$

to within ±0.01. The coefficients a and b' are functions of the ionic strength but at higher concentrations, following the trend of B', become effectively constant. At 1 m and above b' has a value around −0.004. Similar correlations are found for other electrolytes such as the nitrates and chlorates of uni- and divalent cations.

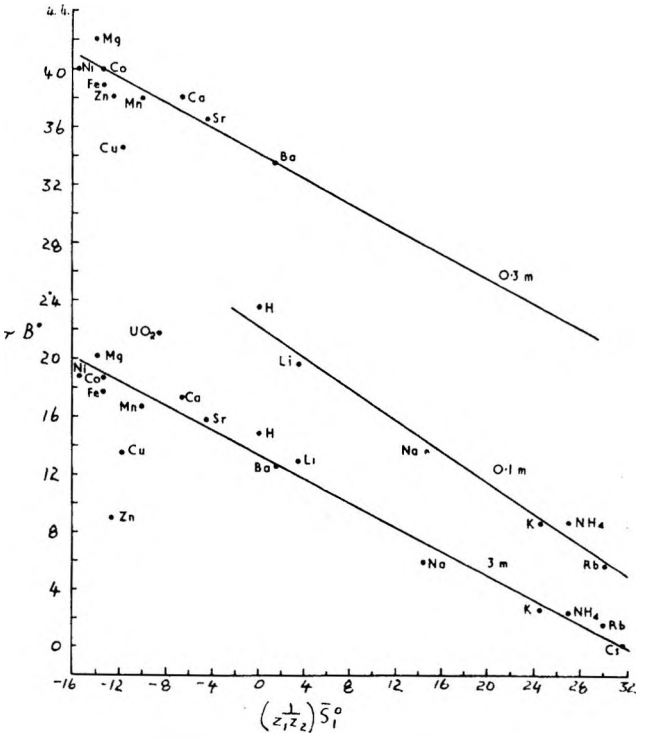

Figure 2. Chloride interaction parameters for the single electrolyte solutions *vs.* the conventional entropy of the cation, at various ionic strengths. Units as in Figure 1. $rB' = {}^1/_2\nu$ (log $\gamma_\pm + z^+z^-$D.H.)/I (where $r = 2\nu^+\nu^-/\nu z^+z^-$).

(15) J. Greyson and H. Snell, *J. Phys. Chem.*, **73**, 3208 (1969).

(16) G. N. Lewis and M. Randall, "Thermodynamics," revised by K. S. Pitzer and L. Brewer, 2nd ed, McGraw-Hill, New York, N. Y., 1961.

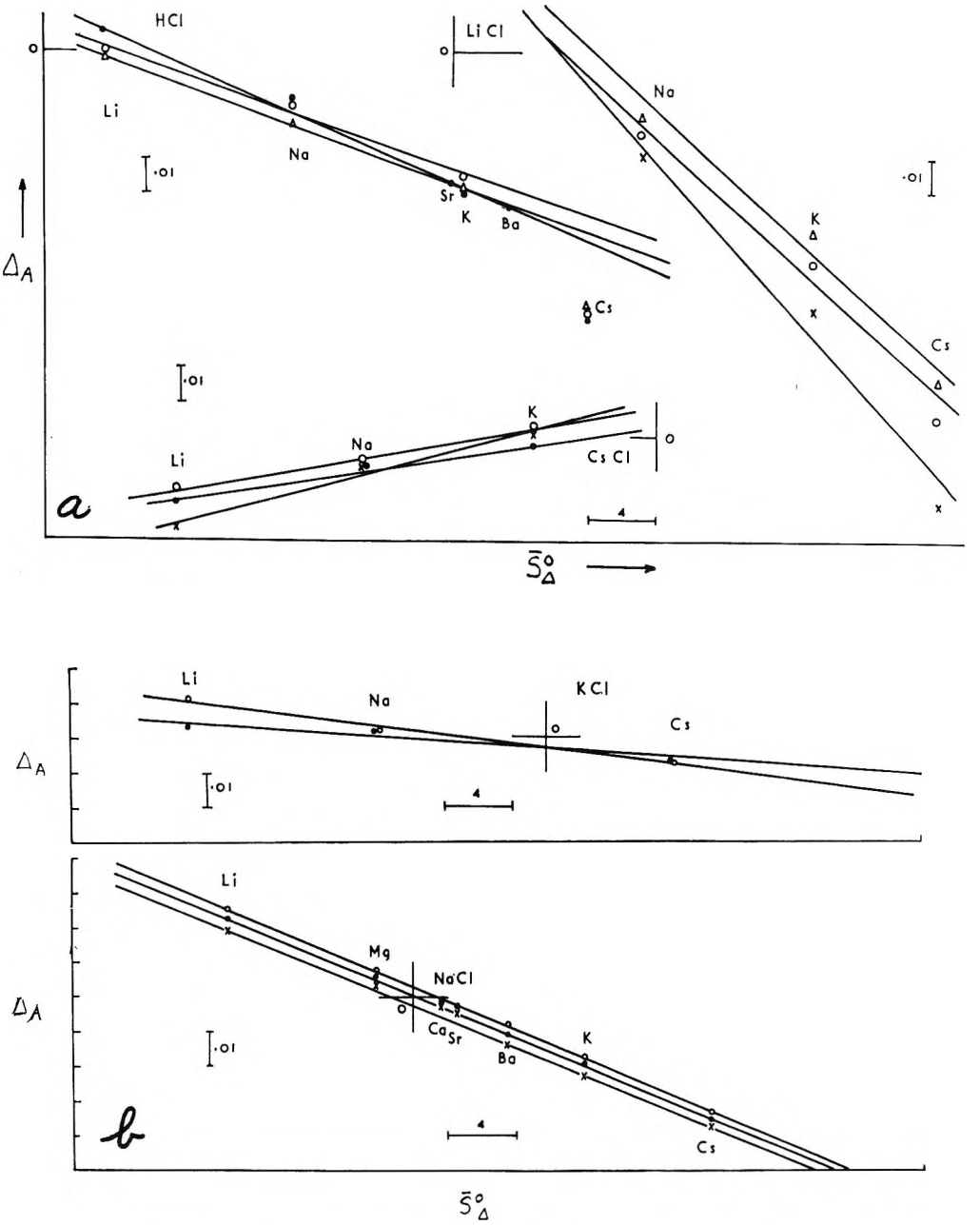

Figure 3. The cation–cation interaction terms of chloride systems *vs.* the conventional ionic entropy function: charge symmetrical systems, $\bar{S}_\Delta^\circ = \bar{S}_3^\circ - \bar{S}_1^\circ$; asymmetric, $\bar{S}_\Delta^\circ = (1/4\bar{S}_3^\circ - 1/2\bar{S}_1^\circ + 2\bar{S}_2^\circ) - \bar{S}_1^\circ$. Units as in Figure 1: Δ, 0.5 *M*; ○, 2 *M*; ●, 3 *M*; ×, 6 *M*.

Single electrolyte solutions that exhibit complexing are in reality multicomponent systems. The B' value therefore does not represent B_{12} but the resultant of a number of interaction terms. In addition, associated changes in the ionic strength and charge symmetry introduce further complications. However, for some of these systems it might be useful to correlate B' with weighted sums of the entropies of the constituent ions, or alternatively, simply correct for the entropy change due to complex formation. A reasonable amount of data are available on entropies of formation of complexes[17] and an equation for predicting the entropies of complex ions has been derived.[18] For example, the deviations from eq 6 for the copper and zinc chloride systems are of the order of the expected ΔS, the entropy change due to complex formation.[17] For the more complicated system of cadmium chloride the deviation is quite spectacular (the experimental rB' is −0.28) but is consistent with the ΔS associated with the release of five or more water molecules. Extension to mixed solutions will introduce further complications since different complex species might dominate; *e.g.*, in mix-

(17) (a) G. M. Nancollas, "Interactions in Electrolyte Solutions," Elsevier Publishing Co., Amsterdam, 1966; (b) C. W. Davies, "Ion Association," Butterworths, London, 1962.

(18) J. W. Cobble, *J. Chem. Phys.*, 21, 1446 (1953).

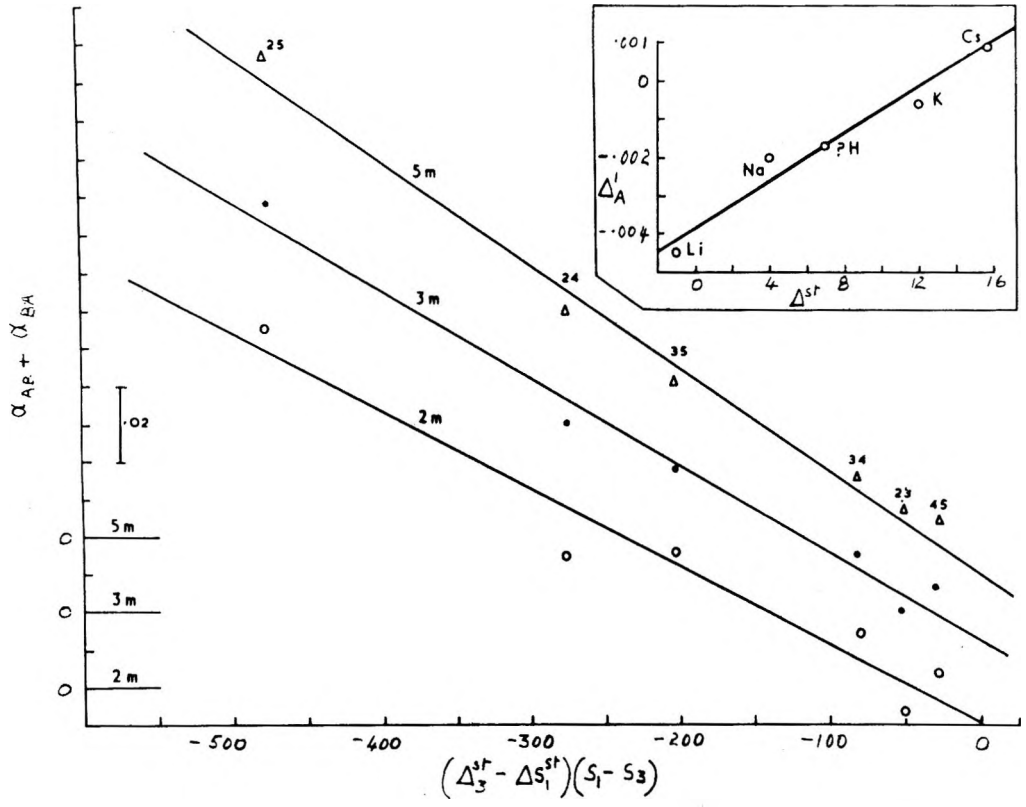

Figure 4. Excess free energy of alkali halide systems ($-(\alpha_{AB} + \alpha_{BA}) = 4G^E/2.303RTI^2$ for equimolal mixtures) as a function of the ionic entropy and structural entropy ΔS^{st}. Coding and units as in Figure 1. Inset: slopes of lines in Figure 3 *vs.* the structural entropy (2 *m*).

tures of cadmium chloride and sodium chloride the species $CdCl_2$ becomes much more important.[19]

Cation–Cation Interactions. An estimate of the cation interaction terms can be obtained from eq 3 using the experimental Harned coefficients and B values, *viz.*

$$\Delta_{AB} = w_e\delta_{13} - w_f\delta_{11} = -(1.15\alpha_{AB}\,\alpha_{AB} + w_cB_{12} + w_dB_{23}) \quad (7)$$

Values of Δ_{AB} have been calculated for the alkali halide systems and plotted against a simple function of the ionic entropies (Figure 3). This was taken as $\bar{S}_3^0 - \bar{S}_1^0$ for symmetric systems and $(^1/_4\bar{S}_3^0 - {}^1/_2\bar{S}_1^0 + 2\bar{S}_2^0) - \bar{S}_1^0$ for asymmetric systems to conform to the H line weights which were derived empirically. The results may be summarized by the equation

$$\Delta_{AB} = d + b''\bar{S}_\Delta^0 \quad (8)$$

where $\bar{S}_\Delta^0$ is the appropriate entropy function and $d = (w_e - w_f)\delta_{11}$ for the case where cation 3 is equivalent to cation 1, *i.e.*, a mixture of the single electrolyte with itself. The quantity d is also equal to $b''S_1 + \Delta_{A(HCl)}$ for the symmetric systems with the acid as a component.

The H line can therefore be interpreted in terms of eq 3, 6, and 8. For a simple 1:1/1:1 system the line is given by

$$\alpha_{AB} = -d/1.15 + B\bar{S}_1^0 - B\bar{S}_3^0 = a_A + b_A\bar{S}_3^0 \quad (9)$$

where $b_A = -B = -(^1/_4b' + b'')/1.15$ and $a_A = -d/1.15 + B\bar{S}_1^0$.

In summary, the H lines should apply generally to strong-electrolyte mixtures with a common ion but for charge asymmetric systems the weights will depend on the common ion.

Free Energy and Enthalpy Correlations. The above analysis indicates that the slopes of the H lines are related to the cation interactions. In addition, b'' was found to be linearly related to the structure entropy ΔS^{st} (inset, Figure 4). This suggests that a combined entropy function of the type

$$(\Delta S_3^{st} - \Delta S_1^{st})(S_1 - S_3)$$

would be proportional to the free energy for symmetric systems where only cation interaction terms apply (eq 5). The difference in the δ_{11} terms will cause some scatter but the correlation is quite good (Figure 4).

These free energy estimates cannot be expected to be very accurate and the data are limited. Accurate enthalpy data are readily available, however, and these have been used to extend the analysis.[20] The experi-

(19) P. J. Reilly and R. H. Stokes, *Aust. J. Chem.*, **23**, 1397 (1970).

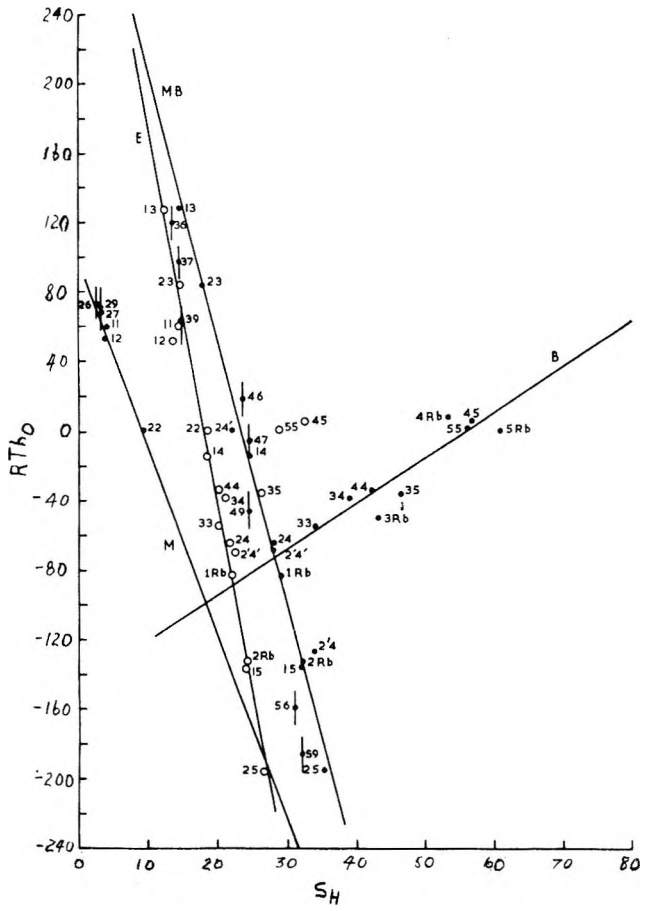

Figure 5. The parameter h_0 for cation–cation interactions at an ionic strength of 1 m, at 25° (derived from enthalpy data[20]), as a function of the ionic and structural entropies: O, S_H values corrected for ΔS^{st}. Coding (and units of $\bar{S}°$) as in Figure 1. A dashed number indicates bromide salt. Units of h_0: cal/kg of solvent/ional².

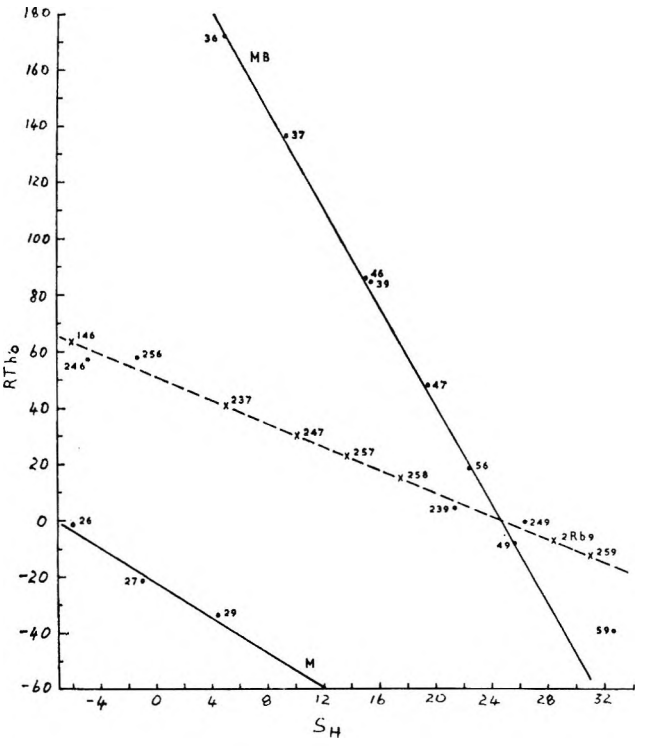

Figure 6. The parameter h_0 (asymetric charge systems) as a function of the ionic entropy. Coding as in Figure 1, *e.g.*, 237 represents a LiCl–NaCl–$CaCl_2$ mixture. Units as in Figure 5.

mental data for excess enthalpy of mixing, H^E are usually expressed in the form[20]

$$H^E = y_A y_B I^2 RT(h_0 + h_1(y_A - y_B)) \qquad (10)$$

where y is the ionic strength fraction of the electrolyte, h_0 is a measure of the ion interactions, and h_1 a measure of skew. The correlation indicated in Figure 4 did not apply for enthalpy data. However, when h_0 (for $y_A = y_B = 0.5$) values are plotted against the sum of the cation entropies (Figure 5), the points fall into three groups which can be correlated with the water structure concepts; *viz.* electrolytes are classified, according to their effect on the water structure, as makers (M) or breakers (B). Mixtures of structure promoting electrolytes (M + M) fall on line M, (M + B) mixtures fall on line MB, and (B + B) on line B. On this basis sodium chloride is a B, contrary to its usual classification. However, the sodium ion seems to have only a small net effect on solvent structure.[15,21]

These classifications are based on a combination of short- and long-range structure effects, whereas classifications for dilute solutions are based on long-range effects,[15] *e.g.*, all the alkaline earths are considered M types here but in dilute solutions this only applies to the magnesium ion. For charge asymmetric systems (alkali chloride/alkaline earth) the contribution of the cation interactions to h_0 has been estimated,[20c] although the accuracy is uncertain.[20d] The values fall close to the MB line when plotted as a function of the entropy of the monovalent cation; apparently the contributions of the alkaline earth cations are all small or approximately the same value. This result is consistent with the very low RTh_0 values for alkaline earth mixtures.[20e]

The lines M, MB, and B can be made to closely coincide (line E) if the entropy function is corrected for the long range structural entropy.[11] This correction is given by a weighted sum of the ΔS^{st} values of the component ions for the B and M points and the weighted difference for the MB points. The sum is

$$\epsilon_+ = (z_1z_3 + z_2z_3)(f_1\Delta S_1{}^{st} + f_2\Delta S_2{}^{st} + f_3\Delta S_3{}^{st}) \qquad (11a)$$

where f represents the ionic strength fraction of the ion, *e.g.*, for the point 34 (NaCl–KCl)

$$\epsilon_+ = {}^1/_2(\Delta S_{Na^+}{}^{st} + \Delta S_{K^+}{}^{st} + 2\Delta S_{Cl^-}{}^{st})$$

(20) (a) T. F. Young, Y. C. Wu, and A. A. Krawetz, *Discuss. Faraday Soc.*, 24, 37, 77, 80 (1957); (b) Y. C. Wu, M. B. Smith, and T. F. Young, *J. Phys. Chem.*, **69**, 1868 (1965); (c) R. H. Wood, J. D. Patton, and M. Ghamkhar, *ibid.*, **73**, 346 (1969); (d) R. H. Wood and M. Ghamkhar, *ibid.*, **73**, 3959 (1969); (e) R. H. Wood and H. L. Anderson, *ibid.*, **70**, 992 (1966).

(21) M. Kaminsky, *Discuss. Faraday Soc.*, **24**, 171 (1957).

and the difference is

$$\epsilon_- = (z_1z_3 + z_2z_3)(f_1\Delta S_1^{st} - f_2\Delta S_2^{st}) \quad (11b)$$

as the anion contributions cancel out.

The open circles in Figure 5 indicate the corrected entropies.

A mixture of the single electrolyte solution with itself represents either an (M + M) or a (B + B) mixture and therefore should fall on line M or line B. The entropy should correspond to $2\bar{S}_{AA}{}^0$, where $\bar{S}_{AA}{}^0$ is the value of the entropy function of the H line equation when the Harned coefficient is zero. This is not equivalent to $\bar{S}_1{}^0$ as can be seen from eq 9. The points for these single electrolyte "mixtures" were therefore estimated by using $\bar{S}_{AA}{}^0$ values from the H lines and eq 11 for the structure correction. The resultant h_0 values correspond to the δ_{11} interaction term.

These enthalpy correlations should prove useful for filling in gaps in the data (the structural corrections, which are only approximate, are not necessary for this). Similar plots are obtained for asymmetric systems[20c] when all the interaction terms are included (Figure 6). For the system NCl–MCl_2 the entropy function is $(\bar{S}_{N^+}{}^0 + {}^1/_3\bar{S}_{M^{2+}}{}^0)$. For more complicated mixtures the lines can be combined, *e.g.*, for the chloride system of structure breaking (B) and structure making (M) cations $M^{2+}/B^+/M^+$ the heat of mixing 50–50 mol% of B^+/M^+ chloride mixtures with the divalent chloride is given by[2b]

$$\Delta H_m = ({}^1/_8I^2)(RTh_{M^{2+}B^+Cl} + RTh_{M^{2+}M^+Cl} - {}^1/_2RTh_{M^+B^+Cl}) \quad (12)$$
$$= 2I^2(\text{constant} + \bar{S}_{B^+}{}^0 + {}^5/_8\bar{S}_{M^+}{}^0 + 2\bar{S}_{M^{2+}}{}^0)$$

the entropy coefficients have been derived from the lines MB (Figure 5) and MB and M (Figure 6). Experimental values of ΔH_m for alkali chloride mixtures with magnesium and barium chlorides have been plotted against this entropy function (dashed line, Figure 6); predictions for other systems of this type are indicated for interest.

Volume Fraction Statistics (VSF) Method of Predicting Activity Coefficients in Mixed Electrolyte Solutions

This method, despite its present shortcomings, is not bounded by linearity restrictions, and Wu[7] has shown that it can be usefully applied to ternary systems and has certain advantages over the mole-fraction-statistics approach; *e.g.*, the hydration parameters are additive.

The activity of a strong electrolyte may be represented by

$$\log \gamma_\pm = \log \gamma^{el} + \log \gamma^s \quad (13)$$

where, on the basis of Glueckauf's treatment of 1:1 electrolytes,[6d] the electrostatic term is given by

$$\log \gamma^{el} = |z^-z^+|(\text{D.H.} + X(m)) \quad (14)$$

where, at 25°

$$\text{D.H.} = -0.509I^{1/2}/(1 + \rho I^{1/2}) \quad (14a)$$

The symbol ρ represents an empirical parameter estimated by an iterative method, $X(m)$ is an empirically derived deviation function which for a 1:1 electrolyte (at molality m) has the form[6d]

$$X(m) = -0.06m^2/(1 + {}^1/_2m)^2 \quad (14b)$$

A similar function has not yet been derived for 2:1 electrolytes but the following equation fitted both calcium and strontium chloride down to $I = 0.3m$[7]

$$2X(m) = 0.0079 - 0.0195m + 0.0073m^2 \quad (14c)$$

This is a less satisfactory form than (14b) since at $I = 0.1$ m the value is still relatively large.

The following equations, based on those statistically derived by Kirkwood, have recently been given by Glueckauf[22] and apply up to values of $\rho I^{1/2} = 20$ for all types of aqueous electrolyte solutions. At 25° and $\rho I^{1/2} < 2$

$$\log \gamma^{el} = -0.511|z^+z^-|I^{1/2}\left[\frac{1 + {}^1/_2\rho I^{1/2}}{1 + \rho I^{1/2}}\right]^2 p \quad (14d)$$

and when $\rho I^{1/2} > 2$

$$\log \gamma^{el} = -0.511|z^+z^-|\frac{4}{9}\left(\frac{2I}{\rho}\right)^{1/3} p \quad (14e)$$

where $p = ({}^3/_4 + {}^1/_4(c/d_0m))$ and c = molarity of electrolyte.

Equation 14 may be written

$$\log \gamma^{el} = |z^+z^-|\left[\text{D.H.} - \frac{0.511\rho^2I^{3/2}}{4(1 + \rho I^{1/2})^2}\right]p$$

so that $X(m) = -0.511\rho^2I^{3/2}/4(1 + \rho I^{1/2})^2$ up to about $I = 2$.

While it would be preferable to work with the general eq 14d and 14e, values of the parameters ρ and h (see eq 15) have been derived on the basis of eq 14b and 14c so that it is convenient to use these equations here.

The entropy term is given by

$$\log \gamma^s = fmr(r + h - \nu)/2.303(1 + fmr) + ((h - \nu)/\nu)\log(1 + fmr) - (h/\nu)\log(1 - fmh) \quad (15)$$

where $f = 0.018$, r = apparent molar volume of electrolyte (at $m = 1$ for 1:1 electrolytes, $m = 0.7$ for 1:2 electrolytes) divided by the molar volume of water, m = molality of electrolyte, ν = number of moles of ions produced by the dissociation of 1 mol of electrolyte, and h = hydration parameter, derived in conjunction with ρ.

(22) E. Glueckauf, *Proc. Roy. Soc., Ser. A*, **310**, 449 (1969).

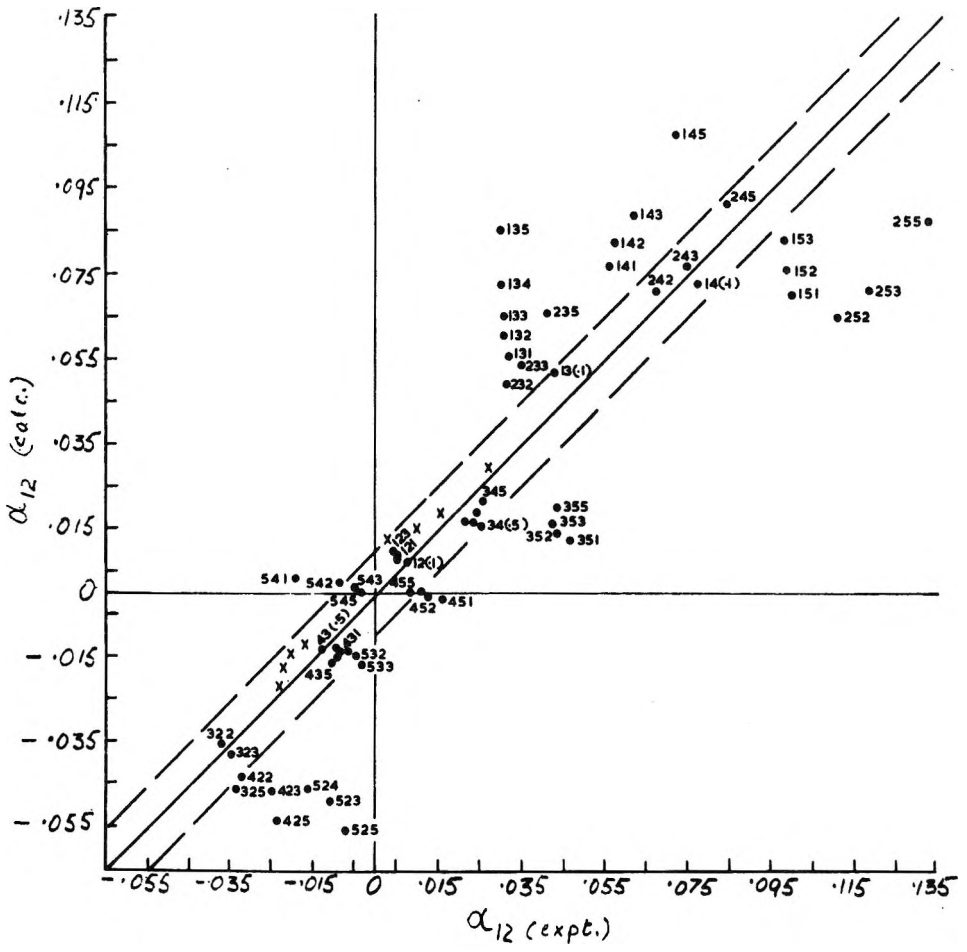

Figure 7. A survey of the comparison of VFS theory with experiment over the range of I = 0.1 to 5 m (Table II, linear fit). The first two numbers represent the electrolyte system (Figure 1) and the last number (or number in brackets) represents I; *e.g.*, 352 represents NaCl–CsCl at 2 m; × represents $LiNO_3$–LiCl system. When the points for a given system are too crowded only key identification numbers are shown.

For solutions containing two electrolytes A and B the activity coefficients may be expressed in the form of an activity coefficient ratio, *viz.*

$$\log (\gamma_A/\gamma_A^0) = \log \gamma_{AB}^{el} - \log \gamma_{A(0)}^{el} + \log \gamma_{AB}^{s} - \log \gamma_{A(0)}^{s}$$

$$\log (\gamma_B/\gamma_B^0) = \log \gamma_{BA}^{el} - \log \gamma_{B(0)}^{el} + \log \gamma_{BA}^{s} - \log \gamma_{B(0)}^{s} \quad (13a)$$

where

$$\log \gamma_{AB}^{s} - \log \gamma_{A(0)}^{s} = \Delta \log \gamma_{AB}^{s} = ((h_A - \nu_A)/\nu_A) \log (1 + fm_A r_A + fm_B r_B)/(1 + fm_A^0 r_A) + (h_A/\nu_A) \log (1 - fm_A^0 h_A)/(1 - fm_A h_A - fm_B h_B) + (fr_A/2.303\nu_A) \times [(m_A(r_A + h_A - \nu_A) + m_B(r_B + h_B - \nu_B))/(1 + fm_A r_A + fm_B r_B) - m_A^0(r_A + h_A - \nu_A)/(1 + fm_A^0 r_A)] \quad (15a)$$

and $\Delta \log \gamma_{BA}^{s}$ is obtained by symmetry. m^0 represents the molality of the single electrolyte solution.

When the electrolytes are of the same charge type and the ionic strength is constant the electrostatic terms should not change appreciably. This was found to hold for the system $CaCl_2$–$SrCl_2$.[7] For such systems the activity coefficient ratio reduces to $\Delta \log \gamma^s$.

In systems where the electrolytes are of different charge type, variation in the electrostatic term might be appreciable. An approximate estimate of this variation could be made on the following basis.

In the derivation of the deviation functions, which characterize the charge type, the distance of closest approach has a fixed value for a particular electrolyte. In the mixed electrolyte the D.H. term for either electrolyte may be considered constant and the deviation functions will be some combination of the individual deviation functions suitably weighted according to the charge type; *e.g.*, for a system such as NaCl–$CaCl_2$ it could be assumed that as $m_A \to 0$

$$\log \gamma_{AB}^{el} = (\nu_A/\nu)x(m)_B^0 - x(m)_A^0 = 0.4x(m)_B^0 - x(m)_A^0, \text{ since } \nu = \nu_A + \nu_B \quad (14f)$$

and as $m_B \to 0$

$$\log \gamma_{BA}^{el} = 1.2x(m)_A^0 - 2x(m)_B^0 \quad (14g)$$

Table I: Harned Coefficients Calculated on the Basis of VFS and Compared with Experimental Values

1:1 Electrolytes

I	a	α_{AB}[b]	Exp	α_{AB}[c] / β_{AB}	a	α_{BA}[b]	Exp	α_{BA}[c] / β_{BA}
				LiCl–HCl[d,e]				
0.025	−0.0068	−0.0101		−0.0068	0.0071	0.0106		0.0071
				−0.0000				−0.0000
0.05	−0.0068	−0.0102		−0.0068	0.0071	0.0106		0.0711
				−0.0000				−0.0000
0.075	−0.0068	−0.0102		−0.0068	0.0071	0.0106		0.0713
				−0.0000				−0.0000
0.1	−0.0068	−0.0102		−0.0068	0.0071	0.0106	0.007	0.0071
				−0.0000			0.0013	0.0000
0.5	−0.0071	−0.0104		−0.0071	0.0074	0.0108	0.006	0.0074
				−0.0000				−0.0000
1	−0.0074	−0.0107		−0.0074	0.0077	0.0111	0.005	0.0076
				−0.0000				−0.0000
2	−0.0081	−0.0113		−0.0081	0.0085	0.0118	0.005	0.0085
				−0.0000				−0.0000
3	−0.0090	−0.0122		−0.0089	0.0094	0.0127	0.004	0.0095
				−0.0000				−0.0000
4	−0.0103	−0.0133		−0.0101	0.0107	0.0139	−0.0025	0.0109
				−0.0000				−0.0000
5	−0.0120	−0.0150		−0.0118	0.0125	0.0156		0.0128
				−0.0001				−0.0001
6	−0.0145	−0.0176		−0.0141	0.0152	0.0183	−0.0086	0.0158
				−0.0001				−0.0001
				NaCl–HCl[d]				
0.025	−0.0359	−0.0599		−0.0359	0.0514	0.0759		0.0514
				−0.0005				−0.0008
0.05	−0.0360	−0.0600		−0.0359	0.0515	0.0760		0.0515
				−0.0005				−0.0008
0.1	−0.0361	−0.0600		−0.0360	0.0517	0.0761	0.043	0.0518
				−0.0005				−0.0008
0.5	−0.0372	−0.0609		−0.0369	0.0534	0.0777	0.037	0.0540
				−0.0005				−0.0008
1	−0.0384	−0.0620		−0.0378	0.0553	0.0794	0.032	0.0564
				−0.0006				−0.0009
2	−0.0411[f]	−0.0640		−0.0399	0.0597[f]	0.0836	0.031	0.0623
				−0.0007				−0.0011
3	−0.0446[f]	−0.0677		−0.0423	0.0651[f]	0.0888	0.031	0.0698
				−0.0009				−0.0014
4	−0.0489[f]	−0.0719		−0.0450	0.0718[f]	0.0956	0.030	0.0798
				−0.0011				−0.0017
5	−0.0544[f]	−0.0775		−0.0482	0.0805[f]	0.1046	0.030	0.0933
				−0.0014				−0.0022
6	−0.0619[f]	−0.0855		−0.0518[f]	0.0921[f]	0.1172	0.029	0.1129
				−0.0019				−0.0030
				KCl–HCl[d]				
0.025	−0.0438	−0.0872		−0.0438	0.0712	0.1036		0.0712
				−0.0009				−0.0018
0.05	−0.0439	−0.0872		−0.0439	0.0713	0.1038		0.0714
				−0.0009				−0.0018
0.1	−0.0400	−0.0873		−0.0439	0.0715	0.1040	0.077	0.0717
				−0.0009				−0.0018
0.5	−0.0450	−0.0880		−0.0445	0.0738	0.106	0.062	0.0752
				−0.0010				−0.0020
1	−0.0461[f]	−0.0889		−0.0451	0.0764	0.109	0.056	0.0790
				−0.0010				−0.0021
2	−0.0486[f]	−0.0910		−0.0464	0.0821[f]	0.114	0.057	0.0880
				−0.0012				−0.0025
3	−0.0516[f]	−0.0937		−0.0478	0.0889[f]	0.121	0.062	0.0993
				−0.0014				−0.0029

Table I (*Continued*)

I	a	α_{AB}[b]	Exp	α_{AB}[c] / β_{AB}	a	α_{BA}[b]	Exp	α_{BA} / β_{BA}
4	−0.0552[f]	−0.0973		−0.0493	0.0972[f]	0.130	0.066	0.1138
				−0.0017				−0.0035
5	−0.0598[f]	−0.1021		−0.0507	0.1074[f]	0.1417	0.072	0.1330
				−0.0021				−0.0044
6	−0.0657[f]	−0.1087		−0.0520[f]	0.1206[f]	0.1570		0.1596
				−0.0026				−0.0056
				CsCl–HCl[d]				
0.025	−0.0464	−0.1017		−0.0464	0.0629	0.0882		0.0630
				−0.0013				−0.0021
0.05	−0.0465	−0.1018		−0.0464	0.0631	0.0884		0.0632
				−0.0013				−0.0021
0.1	−0.0466	−0.1019		−0.0460	0.0634	0.0886	0.140	0.0636
				−0.0013				−0.0022
0.5	−0.0477	−0.1034		−0.0470	0.0662	0.0917	0.105	0.0677
				−0.0013				−0.0023
1	−0.0488[f]	−0.1048		−0.0475	0.0691	0.0950	0.100	0.0722
				−0.0014				−0.0025
2	−0.0514[f]	−0.1079		−0.0486	0.0757[f]	0.1022	0.099	0.0826
				−0.0016				−0.0029
3	−0.0543[f]	−0.1115		−0.0496	0.0833[f]	0.1107	0.098	0.0954
				−0.0018				−0.0034
4	−0.0578[f]	−0.1156		−0.0507	0.0923[f]	0.1209		0.1116
				−0.0020				−0.0041
5	−0.0621[f]	−0.1207		−0.0516	0.1032[f]	0.1336		0.1327
				−0.0024				−0.0051
6	−0.0675[f]	−0.1273		−0.0522	0.1168[f]	0.1502		0.1614
				−0.0029[f]				−0.0064

[a] Least-squares linear fit. [b] Value of α_{ij} when component i at trace concentration. [c] Least-squares quadratic fit. [d] Reference 9a. [e] Source of experimental values. [f] Poor fit.

Table II: Constants for Statistical Term of Equation 13

Electrolyte	h	r	Ref
HCl	5.57	1.05	6d
LiCl	5.31	1.03	
NaCl	3.60	1.03	
KCl	2.58	1.40	
CsCl	2.27	2.30	
$LiNO_3$	4.54	1.68	
KOH	5.23	0.40	
HBr	5.80	1.42	
LiBr	5.29	1.40	
NaBr	3.94	1.40	
KBr	2.66	1.98	

The variations of the ratios of (13a) with solution composition were computed for a number of mixed electrolyte solutions. As an example Table I gives the results for alkali halide–hydrochloric acid systems (the rest of the tables are available on request). The values of h and r used in the calculations are listed (Table II).

Results

Figure 7 gives a survey for 1:1 electrolytes over the range 0.1 to 5 m ionic strength. The most notable feature is the large deviations for systems of cations with opposing structural influences on water (*e.g.*, H–Cs, Li–Cs, H–Na, H–K). Quite accurate predictions are possible if the cations are similar, *e.g.*, Ca–Sr[7] and Li–H. A detailed analysis of the error pattern is not attempted in view of the difficulty in sorting out the contributions from the various types of interactions. Instead, a few general points are noted.

The main errors in prediction arise from errors in the two parameters ρ and h. The problem is that these quantities do not represent physical realities. If this were ignored then h values for charge symmetrical mixtures could be derived empirically. These parameters would then be forced to absorb all the ion–ion and ion–solvent interaction effects; *e.g.*, for the $CaCl_2$–$SrCl_2$ system,[7] for which interactions between the cations are small, the h parameters in the mixture showed little variation above 2 m, the values being approximately those of the single electrolytes. At 0.5 m the values were about two-thirds lower and increased to a maximum around 1.5 m. For the 1:1 systems the values in the mixtures were generally lower than those in the single electrolyte with the exception of sodium chloride at molalities below 5, and the chlorides of lithium and hydrogen, in mixtures with cesium chloride, above 3 m.

A better approach would be to look for an unequiv-

ocal way to define the hydration number of an electrolyte (*e.g.*, on the basis of entropy[6c,23]) and treat it as a function of the concentration (*e.g.*, by reassessing the single electrolyte data on the basis of eq 14d and 14e). This would provide a firmer theoretical framework and simplify the treatment of mixed solutions. Recently, some very interesting near-infrared studies of the hydration of alkali halides were reported.[24] The hydration number of sodium chloride was calculated to vary from 4.8 at a concentration of 0.5 M to 3.5 at 5.0 M, while the values for cesium and potassium chlorides (at 3 M) were about 1.0 higher than those in Table II.

The excess thermodynamic functions of symmetrical systems give a complete description of the formation of a solution from its components since they include effects of solvation and solute–solute interaction. A check on the accuracy of VFS in predicting these effects can be made by comparing the experimental H coefficient sums (eq 5) with the corresponding sums of the calculated values. The results are poor for many systems, notably 25 (Li–Cs) and to a lesser extent 15 (H–Cs), and 35 (Na–Cs), the magnitude of the predicted excess free energy being much too low. It seems likely that changes in the log γ^{el} term are superimposed on changes in h for these systems.

The quantity $(\alpha_{AB} - \alpha_{BA})$ approximately characterizes the end solutions but contains contributions from the mixture in the form of the terms[16]

$$m(d\alpha_{BA}/dm) + 2m\beta_{BA}$$

where β is the coefficient of the I_{BA}^2 term in the extended form of eq 1.

For one of the electrolytes in the pair the error in prediction of this quantity partly cancels the error in the prediction of the excess free energy. This usually favors the more structure breaking cation of the pair. For systems containing cesium, the errors decrease with increasing ionic strength, whereas they increase for the other systems. This merely summarizes the trends to be observed from Figure 7, notably the lack of symmetry in the prediction errors for the components of the system.

The VFS method of prediction is, in general, limited now by failure to treat the h values as variables and to account for variations in the electrostatic term. However, generally the correct sign and order of magnitude is predicted and the accuracy is good for systems containing cations with similar properties. The form of the VFS equations indicate that Harned's rule cannot be exact but the expansion converges quite rapidly. The linear fit is poor for many systems, yet the β coefficients are small and would be difficult to measure. The VFS method is therefore also useful for predicting the relative complexity of various systems and provides a reasonable estimate of the β coefficient.

Acknowledgments. I thank Dr. M. Whitfield and Dr. R. Hunter for helpful discussions.

(23) S. L. Bertha and G. R. Choppin, *Inorg. Chem.*, **8**, 613 (1969).

(24) W. C. McCabe and Harvey F. Fisher, *J. Phys. Chem.*, **74**, 2990 (1970).

Measurement of Activity Coefficients with Liquid Ion-Exchange Electrodes for the System Calcium(II)-Sodium(I)-Chloride(I)-Water

by J. V. Leyendekkers* and Michael Whitfield

Division of Fisheries and Oceanography, CSIRO, Cronulla, N.S.W. 2230, Australia *(Received October 20, 1970)*

Publication costs borne completely by The Journal of Physical Chemistry

The Harned coefficients of calcium chloride in the above system over the ionic strength range 0.03–0.70, at 25°, were estimated from activity measurements. These measurements were made with two liquid ion-exchange electrodes, Orion 92-20 for calcium(II) and Orion 92-17 for chloride ion. The Brønsted theory is shown to be unreliable as a basis for extrapolating the Harned coefficient *vs.* ionic strength curves to very low concentrations. Volume fraction statistics gives a better prediction.

Introduction

There are only limited data available on the properties of mixed electrolyte solutions in the intermediate concentration range (0.01–1 *m*) characteristic of natural aqueous systems. In such systems calcium ions, which are of considerable biological and geochemical importance, are usually associated with an excess of sodium ions. The Ca^{2+}–Na^{+}–Cl^{-}, H_2O system is therefore of particular interest in the study of natural waters. This ternary system has been studied over the range 0.7–7 *m* using isopiestic techniques[1] and the sodium activity has been measured over the ranges 1–6 *m*[2] and 0.05–0.5 *m*[3] using potentiometric methods. We have measured the calcium activity over the range 0.03–0.7 *m* and thus made the study more complete. The measurements were made with liquid ion-exchange electrodes which have not yet been tested in enough detail thermodynamically to be accepted unreservedly as reliable and accurate sensors. It seems clear, however, from a recently published critical review,[4] that ion-selective electrodes are reliable and accurate within the "accessibility window" that characterizes them,[5] *i.e.*, within certain limits of pH, temperature, and concentrations of interfering ions. The system studied here lies partly beyond the specifity "window" of the Orion calcium activity electrode and it is necessary to consider how this will affect the interpretation of the results.

Liquid Ion-Exchange Electrodes in Mixed Electrolyte Solutions

When an electrode of the above type, such as the Orion calcium activity electrode, is immersed in a mixed solution of, say, sodium and calcium chlorides, the potential relative to some fixed potential may be simply given by[6]

$$E_{Ca} = \text{constant} + S \log (a_{Ca^{2+}} + K a_{Na^{+}}^{2}) \quad (1)$$

or, as is sometimes more convenient

$$E_{Ca} = \text{constant} + S \log a_{Ca^{2+}} - S \log N_{CaX_2} \quad (1a)$$

where a represents the activity and N_{CaX_2} represents the mole fraction of sites occupied by calcium(II) in the exchanger. K represents the selectivity ratio which has been found to be a function of solution composition and ionic strength and which reaches values greater than 1 for certain solution compositions at high ionic strengths.[7] The last term on the right-hand side of (1a) becomes more significant as this ratio increases. S is generally assumed to be 29.58 mV at 25° in solutions of calcium chloride alone. It is difficult to verify this exactly since certain assumptions have to be made regarding the single ion activity coefficients and the liquid junction potential.[8] In a mixed solution it is even more difficult to determine the value of S, but the assumption that it has the Nernst value seems a reasonable one on the basis of the work done by Eisenman.[9]

If, in practice, the slope has a value of $S(1 - n)$, say, where n may be a variable, then eq 1a becomes

$$E_{Ca} = \text{constant} + S \log a_{Ca^{2+}} - S \log (a_{Ca^{2+}}{}^{n})(y)^{1-n} \quad (1b)$$

where N_{CaX_2} is now represented by y for simplicity.

(1) R. A. Robinson and V. E. Bower, *J. Res. Nat. Bur. Stand.*, **70A**, 313 (1966).

(2) (a) R. D. Lanier, *J. Phys. Chem.*, **69**, 3992 (1965); (b) J. N. Butler and R. Huston, *ibid.*, **71**, 4479 (1967).

(3) E. W. Moore and J. W. Ross, *J. Appl. Physiol.*, **20**, 1332 (1965).

(4) R. A. Durst, Ed., "Ion-Selective Electrodes," National Bureau of Standards Special Publication 314, U. S. Government Printing Office, Washington, D. C., 1969.

(5) Reference 4, Chapter 9.

(6) (a) M. Whitfield and J. V. Leyendekkers, *Anal. Chim. Acta*, **46**, 63 (1969); (b) M. Whitfield and J. V. Leyendekkers, *ibid.*, **45**, 383 (1969); (c) M. Whitfield, J. V. Leyendekkers, and J. D. Kerr, *ibid.*, **45**, 399 (1969).

(7) (a) R. Huston and J. N. Butler, *Anal. Chem.*, **41**, 200 (1969); (b) M. Whitfield and J. V. Leyendekkers, *ibid.*, **42**, 444 (1970).

(8) (a) Reference 4, Chapter 6; (b) R. G. Bates, B. R. Staples, and R. A. Robinson, *Anal. Chem.*, **42**, 867 (1970).

(9) (a) G. Eisenman, *ibid.*, **40**, 310 (1968); (b) ref 4, Chapter 1.

Naturally, this would complicate the analysis of the experimental results and, in general, the effect would be to increase the experimental errors.

The equation corresponding to (1a) for a liquid anion exchange electrode (*e.g.*, the Orion chloride electrode used here) is

$$E_{Cl} = \text{constant} - S \log a_{Cl^-}{}^2 + S \log z^2 \quad (1c)$$

where z represents the mole fraction of sites occupied by the chloride ion. In the system studied here z will be equal to unity, but its value can vary widely in other systems.[10]

When the two electrodes are incorporated in a cell such as (I)

$$\begin{array}{l|l|l} \text{reversible} \\ \text{Ca electrode} \end{array} \mathrm{NaCl}(m_1),\ \mathrm{CaCl_2}(m_2) \begin{array}{l|l} \text{reversible} \\ \text{Cl electrode} \end{array}$$

the resultant potential is given by

$$E_{Ca} - E_{Cl} = \Delta E = C + S \log a_{Ca^{2+}}\, a_{Cl^-}{}^2 - S \log y \quad (2)$$

with $z = 1$.

The constant C no longer contains the contribution from the liquid junction potential and is therefore more likely to be a true constant. In practice, variations can occur in C, especially in mixed solutions, and care must be taken to either minimize this as described by Huston and Butler[7a] or adjust for it as we have done here.

Provided the last term of eq 2 is negligible, or constant, the effect of solution composition on the mean activity coefficient ($\gamma_\pm$) can be determined relatively simply, since in this case the quantity $\Delta E/S - \log [\mathrm{Ca}][\mathrm{Cl}]^2$ will be proportional to $\log \gamma_{\pm \mathrm{CaCl_2}}$, where the bracketed terms represent concentrations. This should apply to the system studied here, at least up to a sodium/calcium ratio around 0.4 since, over the concentration range 0.03–0.7 m the average value of K is about 0.001.[6,7b] A further problem in mixed solutions is the change in electrode response rates that commonly occurs; *e.g.*, with the Orion calcium electrode there is a lag in the response to calcium changes when magnesium ions are present.[5] This should only be of critical concern in rate studies.

Experimental Section

Apparatus. Measurements were made with cell I. Orion liquid ion-exchange calcium (Cat. 92-20) and chloride (92-17) electrodes were used together with a Jenaer thalamid reference electrode (B183). The potential of each working electrode in turn was measured relative to the reference electrode using a pH switch (Cary 4010750) in conjunction with a Dynamco Digital Voltmeter (Dm2022); 700 mV was backed off *via* a Biddle-Gray potentiometer (605002-1) in order to increase the sensitivity.

Materials. Calcium chloride solutions were prepared from primary standard calcium carbonate[11] (Mallinckrodt, assay 99.95–100.05%, dried at 130° for 2 hr) and hydrochloric acid (constant bp). A small quantity of Et_4NOH (*ca.* 10^{-5} M) was added to bring the pH to 8–8.5. Sodium chloride solutions were prepared from AR grade crystals (dried at 130° overnight).

Method. Transfer of the electrodes from one solution to another sometimes resulted in shifts of the potential (up to 0.2 mV) which were unrelated to the solution composition or controllable environmental factors such as depth of immersion, rate of stirring, and temperature. This was particularly noticeable in solutions with high sodium to calcium ratios and is possibly due to changes in the electrostatic charge distribution of the interface between the liquid ion exchanger and the aqueous solution. The effect was minimized by using a titration procedure to alter the solution composition, so that the cell was undisturbed during a series of readings. There were two titration sets for each ionic strength, one commencing with pure calcium chloride solution using sodium chloride as titrant, and the other commencing with sodium chloride and using calcium chloride as the titrant. Each set was done in sections with overlapping portions, the sections usually covering 15–20% change in the ionic strength fraction of either component. The overlaps provided reference points to check on changes of interface potentials. Readings were taken when the potential remained steady for 5 min. The average time between the addition of each aliquot was 10 min. The overall accuracy is estimated at ± 50 μV. The solutions were stirred magnetically at a constant rate and temperature was maintained at 25 $\pm$ 0.1°. A check on the cell response in pure calcium chloride was made before each titration set. This was considered more unambiguous in view of the problems associated with single ion activity coefficients and the liquid junction effects.[8] When the response was not satisfactory the electrode(s) was cleaned and made up again according to the manufacturer's instructions. For a number of runs the chloride activity was measured simultaneously with the Orion electrode and the Beckman chloride ion electrode. The two electrodes recorded activity changes to within 50 μV of each other.

Results

The data were analyzed on the basis of eq 2 with the value of S taken as 29.58 mV. The term $\Delta E/S - \log [\mathrm{Ca}][\mathrm{Cl}]^2$ was computed for each titration section and fitted by least squares to the corresponding set of sodium chloride concentrations. For all ionic strengths linearity held at least up to 0.4 ionic strength fraction of sodium chloride. The value of the slope was obtained from the average of the slope sections in this linear region. The deviations from linearity occurred

(10) K. Srinvasan and G. A. Rechnitz, *Anal. Chem.*, **41**, 1203 (1969).

(11) W. J. Blaedel and H. T. Knight, *ibid.*, **26**, 743 (1954).

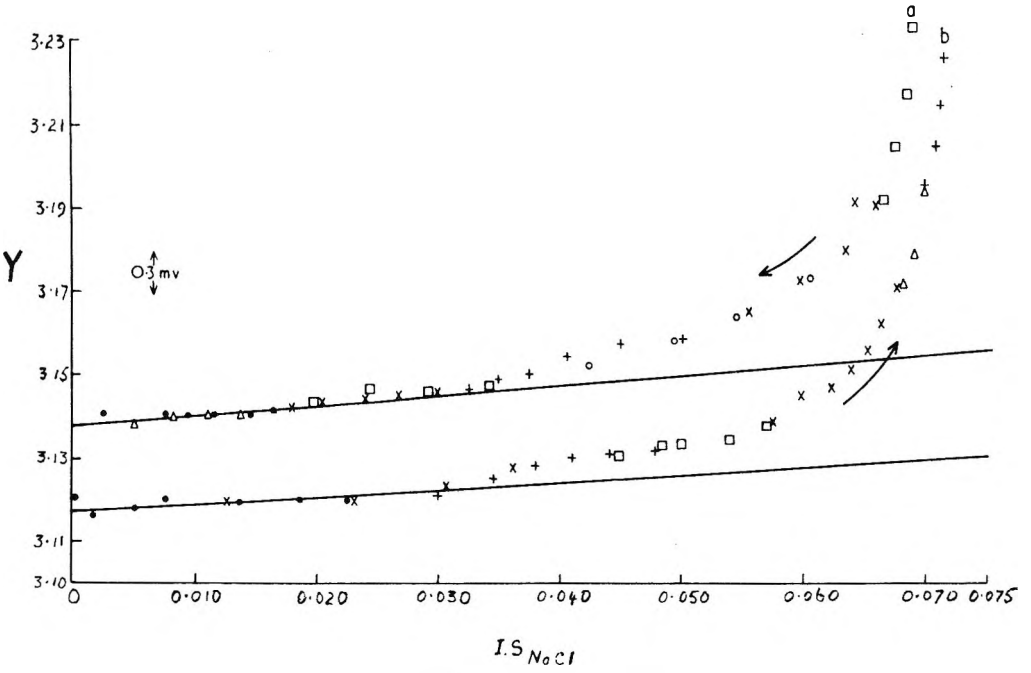

Figure 1. Titration curves for IS 0.075. Overlapping parts of sections are matched to correct for emf shifts; individual sections are shown with contrasting symbols. Arrows indicate direction of titration, *viz.*: a, calcium as titrant; b, sodium as titrant; $Y = 3 \log \gamma_{\pm CaCl_2} +$ constant $- \log N_{CaX_2}$, calculated from eq 2 (*i.e.*, $Y = \Delta E/S - \log [Ca][Cl]^2$). The curves are separated out for clarity.

Table I: Harned Coefficients

Ionic strength	α_{BA}[a]	Mean	α_{Ca}[b]	α_{Cl}[b]	α_{AB}[c]
0.03	−0.118[d]				
	−0.098[e]	−0.108	−1.05 ± 0.05	0.37 ± 0.1	0.044
0.05	−0.085[d]				
	−0.075[e]	−0.080	−0.72 ± 0.04	0.24 ± 0.04	0.030
0.075	−0.078[d]				
	−0.065[e]	−0.072	−0.48 ± 0.08	0.14 ± 0.05	0.026
0.10	−0.052[d]				
	−0.041[e]	−0.047	−0.34 ± 0.04	0.10 ± 0.03	0.013
0.70	−0.012[d]				
	−0.010[e]	−0.011	−0.05 ± 0.01	0.01 ± 0.003	−0.005

[a] A and B represent NaCl and $CaCl_2$, respectively. [b] Based on $\log \gamma_{Ca^{2+}}/\gamma_{Ca^{2+0}} = -\alpha_{Ca}[Na^+]$; $\log \gamma_{Cl^-}/\gamma_{Cl^{-0}} = -\alpha_{Cl}[Na^+]$. [c] Calculated from eq 3 and values in column 3. [d] Decreasing Na. [e] Increasing Na.

only at one end of the curve (the region of high ionic fraction of sodium chloride) and thus may be attributed to variations in y. A representative plot, corrected for emf shifts (by superimposing the overlaps) is given in Figure 1. The values of log y could be obtained also and have been used to investigate the selectivity characteristics of the calcium electrode in NaCl–$CaCl_2$ mixtures.[7b]

The same technique was used to compute the change in the single ion activity coefficients with solution composition from eq 1a and 1c.

The values obtained for the Harned coefficients using calcium chloride (B) and sodium chloride (A) as titrants agree reasonably closely (Table I); *i.e.*, they show the same (or smaller) range as that obtained for measurements of the changes in the activity coefficient of sodium chloride using a glass electrode.[3] The slopes obtained with calcium chloride as the titrant are consistently higher than the corresponding slopes with sodium chloride as titrant. This bias might be due to a lag in the response to calcium arising from slow replacement of the sodium in the exchanger. In this case the Harned coefficients will be too large.

The magnitude of the Harned-type coefficients obtained for the single ion activity coefficients (Table I) are much larger than the corresponding α_{BA} values, so that the problems associated with the use of single ion activities in single electrolyte solutions[8] might be am-

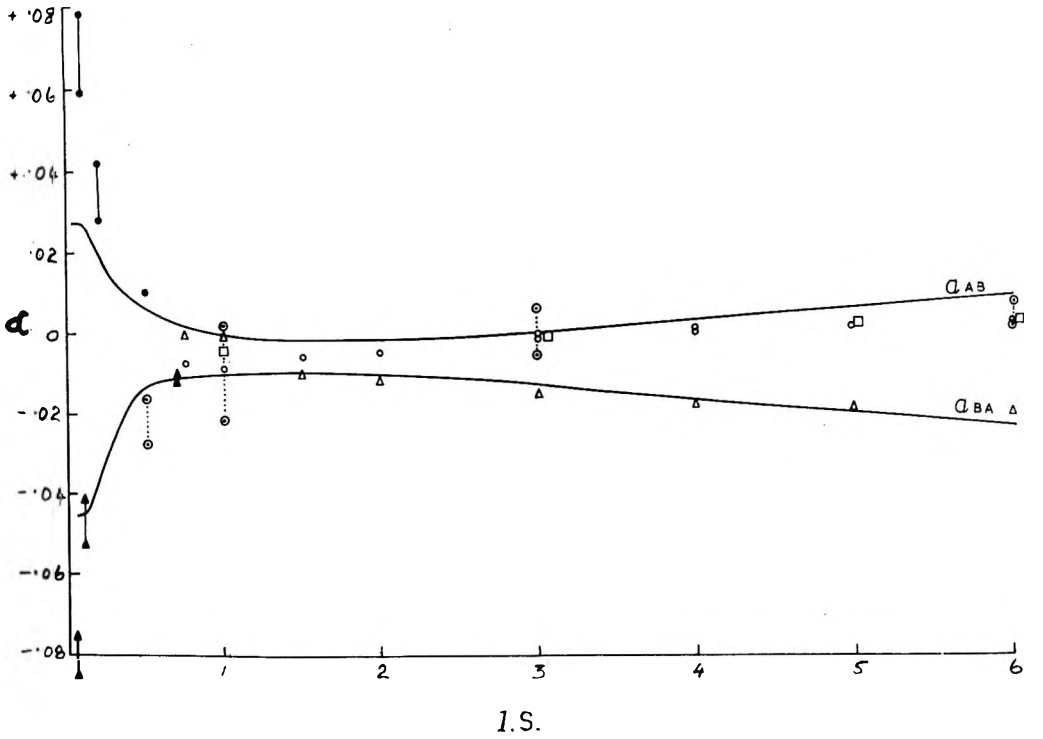

Figure 2. Harned coefficients (reciprocal ionic strength units) as functions of ionic strength: theoretical curves, ——; experimental points for α_{AB}: ●, Moore and Ross; □, Lanier; ○, Robinson and Bower; ⊙, Butler and Huston; for α_{BA}: △, Robinson and Bower; ▲, this work.

plified in mixed solutions. More work is needed to determine the general applicability of results such as these, especially since the single ion activity coefficient lacks a rigorous thermodynamic definition and problems relating to the liquid junction potential still remain to be solved.

Discussion

Our experimental values of α_{BA} disagree in both sign and magnitude with those calculated by Moore and Ross from their experimental values of α_{AB}, but the calculations do not seem to be thermodynamically consistent. The values obtained by the McKay method agree with those obtained *via* the Harned–Gary relationship, which implies that Harned's rule applies for both electrolytes; however, the calculated values of α_{BA}, combined with the experimental values of α_{AB}, do not conform with the requirements defined by the relationship[12]

$$\nu_A k_A \alpha_{AB} + \nu_B j_B \alpha_{BA} = C' \qquad (3)$$

where ν, k and j are the valence parameters for the electrolytes and C' is a constant (for the system studied here $\nu_A k_A = 6$ and $\nu_B j_B = 3$). The isopiestic results suggest that Harned's rule applies below an ionic strength of 4 m with a value of -0.063 for C'. The values of α_{BA} calculated from eq 3 with this value of C', and the experimental results of Moore and Ross for α_{AB}, are much larger (numerically) than our experimental values. This is contrary to the trend expected from the hysteresis effect mentioned above. However, the predicted sign of the values (negative) agrees with that obtained experimentally.

Another discrepancy observed is that both sets of experimental results (those of Moore and Ross, and ours) do not fit the curve extrapolated from the values at higher concentrations on the basis of the Brønsted theory.[1,2b] The assumption that specific interactions between ions of like charge can be neglected does not seem to be generally valid. This was illustrated by accurate calorimetric measurements of the heat of mixing of dilute electrolyte solutions[13] and by the theoretical model developed by Friedman.[14] Extrapolations based on this assumption cannot be expected to be very reliable except perhaps for a restricted number of systems. Recently,[15] it has been shown that the Brønsted theory is inadequate for HCl–alkaline earth chloride systems at an ionic strength of 0.1 m.

In view of these somewhat conflicting theoretical and experimental results we used the volume fraction statistics method discussed previously[16] to predict the Harned coefficients independently. The activity coefficients are given by

(12) E. Glueckauf, H. A. C. McKay, and A. R. Mathieson, *J. Chem. Soc.*, 5, 299 (1949).

(13) R. H. Wood and R. W. Smith, *J. Phys. Chem.*, 69, 2974 (1965)

(14) H. L. Friedman, "Ionic Solution Theory." Interscience, New York, N. Y., 1962.

(15) C. J. Downes, *J. Phys. Chem.*, 74, 2153 (1971).

(16) J. V. Leyendekkers, *ibid.*, 74, 946 (1971).

Table II: Harned Coefficients Calculated on the Basis of VFS and Compared with Experimental Values ($h_A = 3.60$, $h_B = 7.85$; $r_A = 1.03$, $r_B = 1.293$)

Ionic strength, m	a	α_{AB}[b]	Exp	α_{AB}[c] / β_{AB}	a	α_{BA}[b]	Exp	α_{BA}[c] / β_{BA}
0.025	0.0197[e]	0.0270		0.0747	−0.0297	−0.0453	−0.108[d]	−0.0297
				−2.409				−0.0001
0.05	0.0197[e]	0.0270	0.118[3]	0.0747	−0.0297	−0.0453	−0.080	−0.0297
			0.128	−1.206				−0.0001
0.1	0.0198[e]	0.0270	0.060	0.0748	−0.0294	−0.0453	−0.047	−0.0297
			0.079	−0.6037				−0.0001
0.2		0.0200	0.028					
			0.042					
0.5	0.0201[e]	0.0044	0.011	0.0761	−0.0302	−0.0127		−0.0302
				−0.1023				−0.0001
0.7						−0.012	−0.011	
0.75		0.002	−0.0106[1]			−0.012	0.0005[1]	
1	0.0204[e]	−0.0005	−0.0092	0.0774	−0.0308	−0.0110	−0.002	−0.0306
			−0.0040[2]	−0.0568				−0.0001
2	0.0212[e]	−0.0021	−0.0047[1]	0.0804	−0.0320[e]	−0.0109	−0.0126	−0.0316
				−0.0309				−0.0002
3	0.0221[e]	−0.0001	−0.0018	0.0840[e]	−0.0334[e]	−0.0135	−0.0165	−0.0326
			−0.0020[2]	−0.0219				−0.0002
4	0.0231[e]	0.0027	0.0000[1]	0.0882[e]	−0.0350[e]	−0.0168	−0.0186	−0.0338
				−0.0174				−0.0003
5	0.0244[e]	0.0058	0.0007	0.0933[e]	−0.0370[e]	−0.0201	−0.0192	−0.0352
				−0.0148				−0.0003
6	0.0259[e]	0.0088	0.0016	0.0995[e]	−0.0393	−0.0235	−0.0198	−0.0367
			0.0013[2]	−0.0132				−0.0004

[a,c] Least-squares linear and quadratic fits, respectively, with $\Delta \log \gamma^{el}$ equal to zero. [b] Value of α_{ij} with component i at trace concentration. $\Delta \log \gamma^{el}$ given by eq 4a or 5a when $I > 0.1$. [d] Table I values. [e] Poor fit.

$$\log \gamma_A/\gamma_A^0 = \Delta \log \gamma_{AB}^{el} + \Delta \log \gamma_{AB}^{s} \quad (4)$$

with the same notation as before,[16] and

$$\Delta \log \gamma_{AB}^{el} = 0.4X(m)_B^0 - X(m)_A^0 \quad (4a)$$

where $X(m)_A^0$ and $X(m)_B^0$ are the deviation functions of NaCl and $CaCl_2$, respectively, and are given by

$$X(m)_A^0 = -0.06m^2/(1 + {}^1/_2m)^2$$

$$X(m)_B^0 = {}^1/_2(0.0079 - 0.0195m + 0.0073m^2)$$

and

$$\Delta \log \gamma_{AB}^{s} = \frac{(h_A - \nu_A)}{\nu_A} \log \frac{(1 + fm_Ar_A + fm_Br_B)}{(1 + fm_A^0r_A)} + \frac{h_A}{\nu_A} \log \frac{(1 - fm_A^0h_A)}{(1 - fm_Ah_A - fm_Bh_B)} + \frac{fr_A}{2.303\nu_A} \times \left[\frac{(m_A(r_A + h_A - \nu_A) + m_B(r_B + h_B - \nu_B)}{(1 + fm_Ar_A + fm_Br_B)} - \frac{m_A^0(r_A + h_A - \nu_A)}{(1 + fm_A^0r_A)} \right] \quad (4b)$$

where $f = 0.018$ and the values of h and r are given in Table II.

Similarly, we find that

$$\log \gamma_B/\gamma_B^0 = \Delta \log \gamma_{BA}^{el} + \Delta \log \gamma_{BA}^{s} \quad (5)$$

where

$$\Delta \log \gamma_{BA}^{el} = 1.2X(m)_A^0 - 2X(m)_B^0$$

and $\Delta \log \gamma_{BA}^{s}$ is obtained from (4b) by symmetry.

The values of $\log \gamma_A/\gamma_A^0$ and $\log \gamma_B/\gamma_B^0$ obtained from eq 4 and 5 were fitted by least squares to the solution composition to find the Harned coefficients (Table II). The limiting calculated values (with trace concentration of one component) and the experimental values are compared in Figure 2. The agreement is more consistent with the overall experimental results than that obtained with the Brønsted theory, even though our correction for changes in $\log \gamma^{el}$ is only a rough approximation. The experimental values for α_{AB} at 0.5 m and below seem comparatively too large. Our experimental results, combined with the isopiestic data and used in eq 3, predict α_{AB} values lower than the experimental ones (Table I). The prediction for 0.7 m is good on the basis of the H line fit[17] and comparison with the isopiestic data at 0.75 m. As a further check we have plotted some H lines for ionic strengths of 0.5, 0.3, and 0.1 m (Figure 3). The most extensive set of data was for hydrochloric acid[15,18] and, with the

(17) J. V. Leyendekkers, *ibid.*, **74**, 2225 (1970).

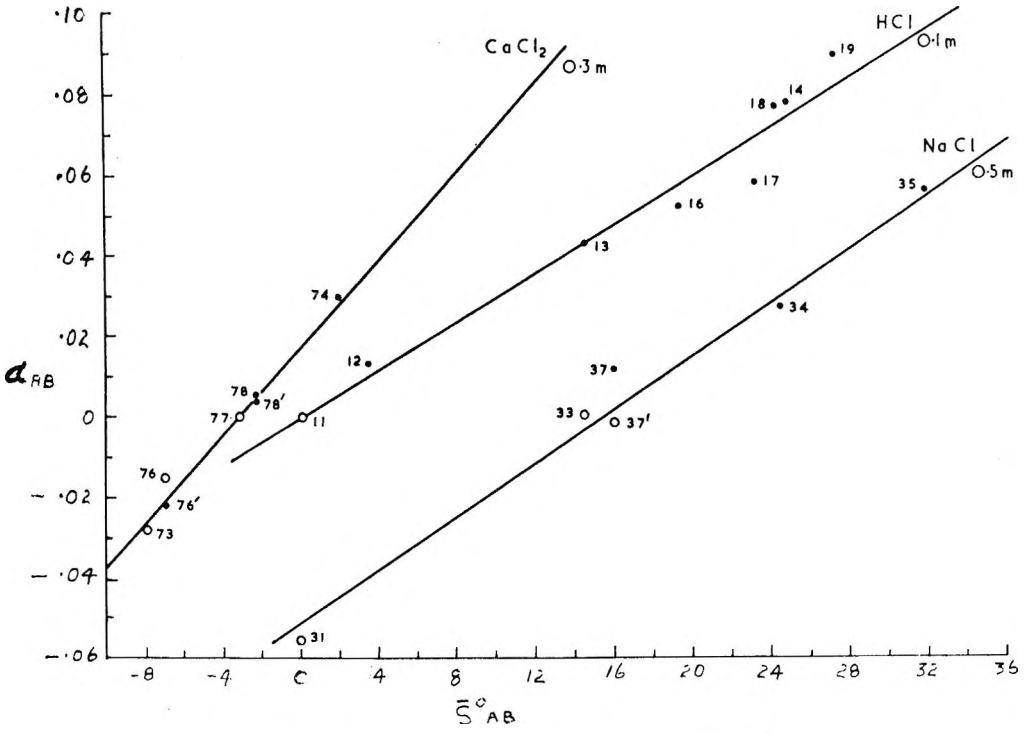

Figure 3. H lines at intermediate ionic strengths: α_{AB} in reciprocal ionic strength units. $\bar{S}_{AB}°$ values (cal deg^{-1} mol^{-1}) calculated as in ref 17. Code: H, 1; Li, 2; Na, 3; K, 4; Cs, 5; Mg, 6; Ca, 7; Sr, 8; Ba, 9; *e.g.*, 37 represents NaCl–$CaCl_2$. O, estimated values (see text).

exception of calcium chloride, the linear fit is good (generally better than ±0.005). This suggests that the H lines for chloride systems are valid for the intermediate ionic strength range, at least down to 0.1 *m*. The limited data for the other lines[19] have been supplemented with estimates. These are based on extrapolation from the experimental values at an ionic strength of 1 *m*[20] (or estimates from Figure 2) for the $CaCl_2$ line. The NaCl–HCl point (31) on the NaCl H line corresponds to the calculated value given by Harned and Owen[21] while the point 37′ has been estimated from interpolation of our results and eq 3. The value of the Harned coefficient for the single electrolyte mixture with itself[16,17] has been taken as zero and this seems justified on the basis of the results for the HCl line. Finally, we have made some preliminary measurements of α_{AB}, at an ionic strength of 0.1 *m*, using the Orion sodium electrode (94-11) coupled with the Orion chloride electrode. Our results gave a value of 0.032 ± 0.007 for α_{AB} compared with the value 0.069 of Moore and Ross. This represents a difference of about 1% in γ_{NaCl}. Altogether, this further evidence supports the conclusion that the results of Moore and Ross are somewhat high.

On the other hand, the values of α_{AB} predicted from our results at lower ionic strengths (less than 0.1 *m*) seem much too low. The response of the calcium electrode might not have been Nernstian (*i.e.*, S < 29.58 mV) in this region, which would result in low values for α_{BA} and consequently underestimates of α_{AB}. The only way of checking this is to measure the activity coefficients by an independent and thoroughly reliable and accurate method. Isopiestic data (above an ionic strength of 1 *m*) were used to check the response of the cell used here in the charge symmetric systems $CaCl_2$–$MgCl_2$ and $CaCl_2$–$SrCl_2$ and it was found that Nernstian behavior was closely followed.[19b] This does not necessarily mean that such behavior applies in the more complex system studied here at the lower ionic strengths, even though the selectivity is very much more favorable.

Another consideration is the selectivity results for the NaCl–$CaCl_2$ system which were obtained on the assumption of Nernstian behavior and are consistent with the data obtained at higher concentrations by

(18) (a) E. Güntleberg, *Z. Phys. Chem.*, **123**, 199 (1926); (b) E Güntleberg, "Studier over Elektrolyter Activiteter," G. E. C. Gads Forlag, Copenhagen, 1939; (c) A. K. Covington, *J. Chem. Soc.*, 4906 (1965). The linear fit of the experimental points was taken, no weight being given to γHCl(0).

(19) (a) S. Wu, Ph.D. Thesis, University of Kansas, University Microfilms Inc., Ann Arbor, Michigan, 1965; (b) J. V. Leyendekkers and M. Whitfield, *Anal. Chem.*, in press. (c) These two references give data for the $CaCl_2$ H line, and the dashed code numbers (Figure 3) represent data from (b); the following two references give data for the NaCl H line; (d) R. A. Robinson, *J. Phys. Chem.*, **65**, 662 (1961); (e) R. A. Robinson, *J. Amer. Chem. Soc.*, **74**, 6035 (1952).

(20) (a) R. A. Robinson and A. K. Covington, *J. Res. Nat. Bur. Stand.*, **72A**, 239 (1068); (b) R, A. Robinson and V. E. Bower, *ibid.*, **70A**, 305 (1966).

(21) H. S. Harned and B. B. Owen, "The Physical Chemistry of Electrolytic Solutions," 3rd ed, Reinhold, New York, N. Y., 1963.

Huston and Butler.[7] While small increases in the slope values (*i.e.*, α_{BA} values) would not produce any inconsistency, a change in the sign of the slope would. Our final conclusion is that the α_{BA} values have the right sign but might be somewhat low in value, especially at ionic strengths below 0.1 *m*.

For the two-electrolyte systems studied so far, the intermediate concentration region appears to be characterized by interesting features. Further studies in this region, by a variety of methods, would certainly be useful from both a practical and theoretical point of view.

Diffusion in Mixed Solvents. II. Iodine in Binary Solutions of Ethanol with Hydrocarbons and Carbon Tetrachloride

by Koichiro Nakanishi,* Teruko Ozasa, and Kazuyoshi Ashitani

Department of Industrial Chemistry, Kyoto University, Kyoto, Japan *(Received July 9, 1970)*

Publication costs assisted by the Asahi Glass Foundation

The diffusion coefficients of iodine dilute in binary solutions of ethanol with benzene, toluene, *n*-hexane, cyclohexane, and carbon tetrachloride at 25.00° have been measured by the capillary cell method. Both the diffusion coefficient D_{11}° and the product $D_{11}^{\circ}\eta_{23}/T$, where η_{23} is the viscosity of solvents and T is the temperature, do not vary linearly with the molar composition x of mixed solvents. For all cases studied, the $D_{11}^{\circ}\eta_{23}/T$ *vs.* x relation shows negative deviations from additivity, which increase in the order of toluene, benzene, CCl_4, cyclohexane, and *n*-hexane. Existing semiempirical equations based on Eyring theory cannot be successful in interpreting the present results. The discrepancies are discussed in terms of the ability of complex formation and preferential solvation of iodine with solvents.

Introduction

In a previous paper[1] (cited hereafter as P-I), we have reported the molecular diffusion coefficients of iodine in aqueous alcohol solutions. We have called special attention to an anomalous $D_{11}^{\circ}\eta_{23}/T$ *vs.* x_2 relation in the low mole fraction portion of alcohols.[2] Another kind of associated solutions, which might be of interest from the standpoint of the effect of specific interactions on diffusivity, must be the binary solutions of the lower aliphatic alcohol with nonpolar liquids. Considerable amounts of both theoretical and experimental work have been done on the thermodynamic and spectroscopic properties of these solutions and semiquantitative descriptions on molecular basis are now possible.[3] On the other hand, the charge-transfer type interactions of iodine with various organic molecules have been studied extensively.[4] In this paper, we present data for the diffusion coefficients of iodine dilute in binary solutions of ethanol with five nonpolar liquids, *i.e.*, benzene, toluene, CCl_4, *n*-hexane, and cyclohexane.

Experimental Section

Solvents. All the liquids except *n*-hexane used in this study were of E.P. grade [JIS (Japan Industrial Standards) extra pure reagent] commercially available. They were used without further purification. It was proved that the liquids were free from any impurities which interact chemically with dissolved iodine. The density of these liquids agreed with the accepted literature value.[5,6] As for *n*-hexane, we have used G.R. (JIS guaranteed reagent) grade samples. Although this liquid gave a single peak on gas chromatograms, its density was somewhat lower than that in the literature.[6] Therefore, we have checked the diffusion data by using Merck spectrograde *n*-hexane. Two results coincided with each other within the limit of experimental error.

(1) K. Nakanishi and T. Ozasa, *J. Phys. Chem.*, **74**, 2956 (1970).

(2) Subscripts 1, 2, and 3 refer to iodine, ethanol, and the second solvent, respectively. Therefore, D_{11}° is the main diffusion coefficient of iodine at an infinite dilution, η_{23} is the viscosity of mixed solvents, and x_2 is the mole fraction of ethanol in mixed solvents.

(3) See for review, *e.g.*, J. S. Rowlinson, "Liquids and Liquid Mixtures," 2nd ed, Butterworths, London, 1969.

(4) See, *e.g.*, E. M. Voigt, *J. Phys. Chem.*, **72**, 3300 (1968).

(5) J. Timmermans, "Physico-Chemical Constants of Pure Organic Compounds," Vol 1 and 2, Elsevier, Amsterdam, 1950 and 1965.

(6) R. R. Dreisbach, *Advan. Chem. Ser.*, **No. 15** (1955), **No. 22** (1959), **No. 29** (1961).

Diffusion and Viscosity Measurements. The diffusion coefficients D_{11}° of iodine diluted in pure and mixed solvents were measured by the capillary cell method. The apparatus and procedures (including viscosity measurement) were the same as given in P-I. The time required for one diffusion run depended upon the viscosity of the solvent; it was between 1 and 3 days. The initial concentration of iodine was always less than 0.04 *M*. This condition can be regarded safely as an infinite dilution of iodine in the solvents.

Results and Discussion

Viscosity of Solvents. Of five binary solutions of ethanol studied, the viscosity coefficient data at 25° are available only for EtOH + CCl_4 solutions.[7] Therefore, we have measured η_{23} at 25.00° for the rest of the four solvent systems. (The measurements were made with the Ostwald-type viscosimeter used in P-I.) To convert flow time data to η_{23}, density values available in the literature[8-10] were used. The results are shown in Table I.

Table I: Viscosity Coefficients of Binary Solutions of Ethanol with Benzene, Toluene, *n*-Hexane, and Cyclohexane at 25.0°

Mole fraction of ethanol, x_{EtOH}	Viscosity coefficient, η, cP	Mole fraction of ethanol, x_{EtOH}	Viscosity coefficient, η, cP
Ethanol + Benzene		Ethanol + *n*-Hexane	
0.000	0.610	0.000	0.318
0.104	0.598	0.100	0.325
0.198	0.592	0.250	0.363
0.301	0.618	0.500	0.464
0.404	0.642	0.750	0.674
0.498	0.677		
0.699	0.794	Ethanol + Cyclohexane	
0.799	0.865	0.000	0.894
1.000	1.085	0.099	0.845
Ethanol + Toluene		0.256	0.832
0.000	0.560	0.500	0.872
0.249	0.578	0.752	0.941
0.499	0.664		
0.751	0.826		

Diffusion Coefficients. The data for the diffusion coefficients of iodine D_{11}° in binary solutions of ethanol with benzene, toluene, CCl_4, *n*-hexane, and cyclohexane at 25.00° are given in Table II. Literature values of D_{11}° for ethanol,[11] benzene,[12] *n*-hexane[11,12] and cyclohexane[11] are 1.32, 2.14, 4.24 or 4.05, and 1.79 (interpolated), respectively. Except for *n*-hexane, the agreement is satisfactory.

Figures 1 and 2 show the variation of D_{11}° and the product $D_{11}^{\circ}\eta_{23}/T$ with the mole fraction of ethanol x_2 in mixed solvents. The D_{11}° *vs.* x_2 plots indicate

Table II: Diffusion Coefficients of Iodine Dilute in Several Mixed Solvent Systems Containing Ethanol at 25.00°

Mole fraction of ethanol, x_{EtOH}	Diffusion coefficient, $D_{11}^{\circ} \times 10^5$, cm²/sec	$D_{11}^{\circ}\eta/T$[a] $\times 10^{10}$
Ethanol + Benzene		
0.000	2.18 ± 0.02	4.44
0.100	2.09 ± 0.01	4.15
0.250	1.95 ± 0.02	3.94
0.500	1.77 ± 0.03	4.02
0.750	1.61 ± 0.01	4.48
1.000	1.35 ± 0.03[b]	4.96
	1.38 ± 0.01	5.04
Ethanol + Toluene		
0.000	2.13[c]	4.01
0.250	2.02 ± 0.01	3.92
0.500	1.87 ± 0.04	4.16
0.750	1.64 ± 0.02	4.54
Ethanol + Carbon Tetrachloride		
0.000	1.47 ± 0.03[b]	4.45
0.250	1.32 ± 0.01	3.93
0.500	1.14 ± 0.05	3.65
0.750	1.25 ± 0.02	4.43
Ethanol + *n*-Hexane		
0.000	4.65 ± 0.08	4.95
0.100	3.12 ± 0.01	3.41
0.250	2.48 ± 0.03	3.02
0.500	2.05 ± 0.01	3.19
0.750	1.81 ± 0.02	4.08
Ethanol + Cyclohexane		
0.000	1.82 ± 0.01	5.47
0.100	1.56 ± 0.01	4.43
0.250	1.35 ± 0.01	3.77
0.500	1.30 ± 0.02	3.80
0.750	1.41 ± 0.02	4.47

[a] The values of viscosity coefficient used to calculate this quantity are obtained from Table I and literature values in ref 7. [b] Our previous data given in P-I.[1] [c] Stokes, *et al.*[12]

that D_{11}° does not vary linearly with x_2 and that the curve depends remarkably on the second solvent used. A positive deviation from additivity is seen in EtOH + toluene solutions, while negative deviation is observed with CCl_4, *n*-hexane, and cyclohexane solutions. For EtOH + benzene solutions, the curve is of an extended S shape. On the other hand, the $D_{11}^{\circ}\eta_{23}/T$ *vs.* x_2 plot

(7) W. J. Jones, S. T. Bowden, W. W. Yarnold, and W. H. Jones, *J. Phys. Chem.*, **52**, 753 (1948).

(8) I. Brown and F. Smith, *Aust. J. Chem.*, **15**, 1 (1962).

(9) F. Pardo and H. C. van Ness, *J. Chem. Eng. Data*, **10**, 163 (1965).

(10) I. Brown, W. Fock, and F. Smith, *J. Chem. Thermodyn.*, **1**, 273 (1969).

(11) P. Chang and C. R. Wilke, *J. Phys. Chem.*, **59**, 592 (1955).

(12) R. H. Stokes, P. J. Dunlop, and J. R. Hall, *Trans. Faraday Soc.*, **49**, 886 (1953).

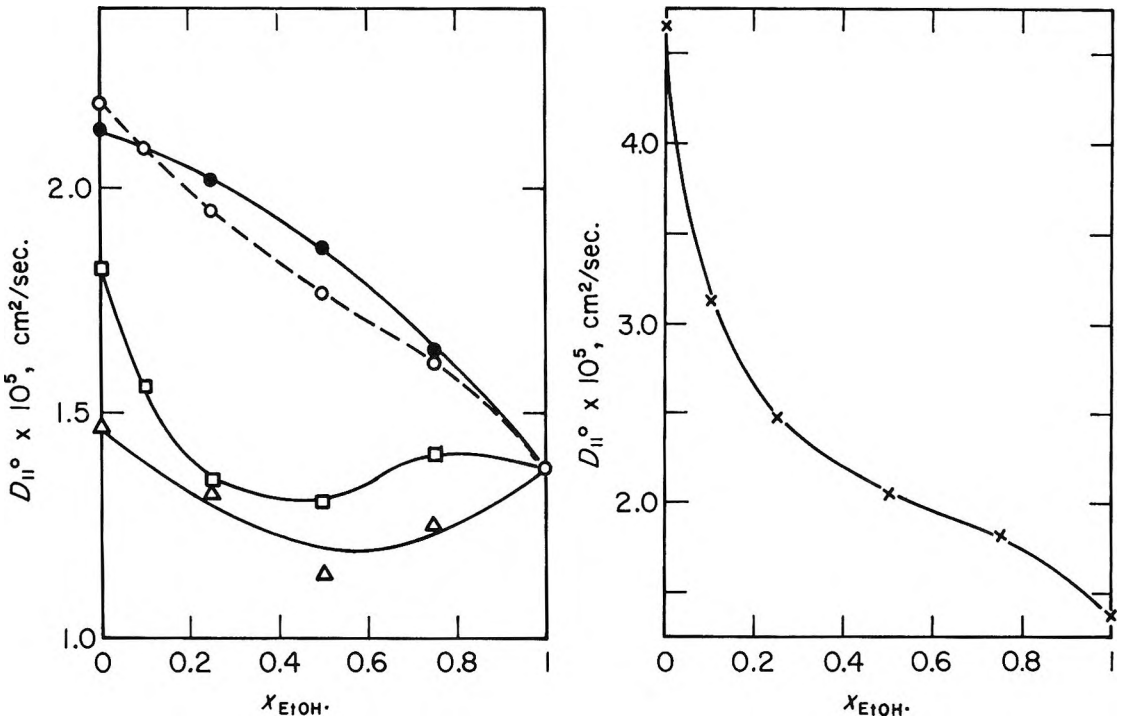

Figure 1. Diffusion coefficients D_{11}° of iodine in several mixed solvents containing ethanol at 25.00°: ○, benzene; ●, toluene; △, CCl_4, ×, *n*-hexane; □, cyclohexane.

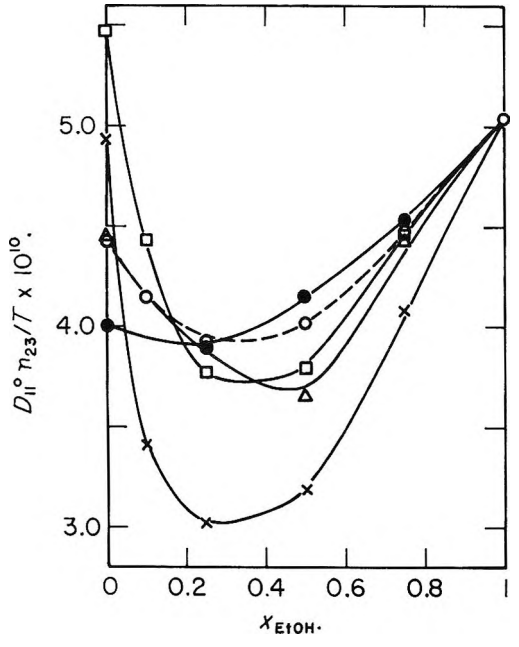

Figure 2. The product $D_{11}^{\circ}\ \eta_{23}/T$ for several mixed solvent systems containing ethanol. Marks are the same as in Figure 1.

shows large negative deviations from the additivity relation. Moreover, it is asymmetrical with respect to x_2. The magnitude (absolute value) of the deviation decreases in the order, *n*-hexane > cyclohexane > CCl_4 > benzene > toluene.

Semiempirical Correlations. Wilke, *et al.*,[13] have proposed the linear correlation between $D_{11}^{\circ}\eta_{23}/T$ and x_2.

$$D_{11}^{\circ}\eta_{23}/T = D_{12}^{\circ}\eta_2 x_2/T + D_{13}^{\circ}\eta_3(1 - x_2)/T \quad (1)$$

where D_{1i}° is the limiting value of the binary diffusion coefficient of I_2 in solvent i. As is evident from Figure 2, the present data do not obey such a simple additivity rule. Other semiempirical correlations have been given by Tang and Himmelblau,[14] and by Leffler and Cullinan.[15] Based essentially on the idea developed by Eyring,[16] they have derived the equations

$$\log [D_{11}^{\circ}(\eta_{23})^n] = x_2 \log [D_{12}^{\circ}(\eta_2)^n] + (1 - x_2) \log [D_{13}^{\circ}(\eta_3)^n] \quad (2)$$

where $n = 1/2$ in ref 14 and $n = 1$ in ref 15. Tang and Himmelblau have also derived an equation which assumes the additivity of $D_{1i}^{\circ}(\eta_i)^{1/2}$ with respect to x_2.[14] Except for EtOH + toluene system, these equations could not also reproduce the present diffusion data.

In the semiempirical equations cited above, the effect of viscosity of solvent is directly taken into account. Alternatively, the frictional properties may be correlated with thermodynamic properties.[16] If the inter-

(13) J. T. Holmes, C. R. Wilke, and D. R. Olander, *A.I.Ch.E. J.*, **8**, 646 (1962).

(14) T. P. Tang and D. M. Himmelblau, *ibid.*, **11**, 54 (1965).

(15) J. Leffler and H. T. Cullinan, Jr., *Ind. Eng. Chem. Fundam.*, **9**, 8 (1970).

(16) S. K. Glasstone, K. J. Laidler, and H. Eyring, "Theory of Rate Processes," McGraw-Hill, New York, N. Y., 1941.

Table III: Thermodynamic and Spectroscopic Properties of Solvent Systems Used[a,b]

Solvents	G^E, J/mol	TS^E, J/mol	H^M, J/mol	V^E, ml/mol	λ_{max}, mμ
EtOH + $C_6H_5CH_3$	1170 (35)[c]	−290 (35)	880 (35)	−0.06	496
EtOH + C_6H_6	1110	−360	750	+0.03	502
EtOH + CCl_4	1190 (45)	−340	850	−0.05	517
EtOH + c-C_6H_{12}	1320	−670	650	+0.58 (27)	523
EtOH + n-C_6H_{14}	1405	−850	555	+0.41	522[d]

[a] The values of thermodynamic excess functions for equimolar mixture given in this table are taken from ref 8–10, 17–24. [b] Spectroscopic data are taken from ref 4. [c] Numbers in parentheses indicate the temperature. Unless otherwise specified, the values are those at 25°. [d] Data for n-C_7H_{16}.

actions of the solute to both solvents are not too strong, the D_{11}° *vs.* x_2 relation must be primarily dependent on the nature of solvent. Table III[8−10,17−24] summarizes the literature values of four principal thermodynamic excess functions for five solvent systems used. If V^E is fairly large, it would be possible that the number and total volume of holes available for diffusional processes change appreciably. As is evident from Table III, however, the absolute values of V^E for the present solvent systems are generally small and, contrary to our expectation, positive volume of mixing is associated with large negative deviations of $D_{11}^\circ\eta_{23}/T$ or D_{11}° itself from the additivity with respect to x_2 (*e.g.*, EtOH + n-hexane). No significant correlations could be found with other excess functions either.

Solute–Solvent Interactions. From the above considerations, we can expect that solute–solvent interactions play an important role in determining the diffusivity of dilute I_2 in such associated solutions. In order to elucidate these interactions, we may utilize the activity data. The activity coefficients of iodine can best be evaluated from the solubility data. Although Hildebrand and his collaborators[25] have made extensive studies on pure solvents, no data for toluene and n-hexane and for mixed solvents (except for CCl_4 + C_7F_{16} system) have been reported.

Alternatively, we may use the shift in the absorption peak of visible light due to the formation of charge-transfer complex of I_2 with organic solvents.[4] In the last column of Table III are given the absorption maxima for each solvent. These values are to be compared with 443 mμ for ethanol.[4] We may conclude that the largest interaction occurs between EtOH and I_2 and that the difference between the interaction of the second solvent with I_2 and that of ethanol with I_2 parallels with the negative deviation of D_{11}° or $D_{11}^\circ\eta_{23}/T$ from the additivity with respect to x_2.

In certain cases shown in Figure 1, the diffusion coefficients in mixed solvents are appreciably smaller than those in pure solvents. A tentative explanation for this phenomenon may be given as follows. There should be four elementary steps in the translational process of I_2 in mixed solvents. Of these steps, the following two are responsible for the deviation from the additivity. The first step is the process of the transfer of I_2 from the vicinity of ethanol molecule to the vicinity of a solvent molecule of another kind. The other is the reverse of the above process. There exist two other steps which represent the processes of the transfer of I_2 between the solvent molecules of the same kinds. However, these steps appear to occur with a frequency proportional to x_2 and lead to an additive contribution to diffusivity. As is evident from the color of iodine in mixed solvents containing ethanol, iodine molecules are solvated preferentially by ethanol. This means that I_2 is strongly trapped by EtOH and may spend considerable time before the transfer to the vicinity of the second molecule. Therefore, the first step, which is slower than all other steps, would be a rate-determining step for the whole diffusional process. This step should become slower as the interaction of I_2 with the second solvent decreases. It is then understood that lower D_{11}° (as compared with D_{1i}°) is associated with weaker interaction of I_2 with the second solvent.

It is well known that the iodine molecule forms a charge-transfer type complex with alcohols. The enthalpy of this complex formation ΔH_f has been estimated to be 3.4 kcal/mol for I_2 + *tert*-butyl alcohol.[26] It is reasonable to assume the ΔH_f value for I_2 + EtOH complex be the same order of magnitude. Since such a value is larger than RT at room temperature, it may be

(17) R. V. Mrazek and H. C. van Ness, *A.I.Ch.E. J.*, 7, 190 (1961).
(18) S. C. P. Hwa and W. T. Ziegler, *J. Phys. Chem.*, 70, 2572 (1966).
(19) I. Brown and W. Fock, *Aust. J. Chem.*, 9, 141 (1956).
(20) J. A. Barker, I. Brown, and F. Smith, *Discuss. Faraday Soc.*, 15, 142 (1953).
(21) G. C. Paraskevopoulos and R. W. Missen, *Trans. Faraday Soc.*, 58, 869 (1962).
(22) G. Scatchard and F. G. Satkiewicz, *J. Amer. Chem. Soc.*, 86, 130 (1964).
(23) J. R. Goates, R. L. Snow, and J. B. Ott, *J. Phys. Chem.*, 66, 1301 (1962).
(24) I. Klesper, *Z. Phys. Chem. (Frankfurt am Main)*, 51, 1 (1966).
(25) J. H. Hildebrand and R. L. Scott, "Regular Solutions" Prentice-Hall, Englewood Cliff, N. J., 1962.
(26) L. J. Andrews and R. M. Keefer, "Molecular Complexes in Organic Chemistry," Holden-Day, Inc., San Francisco, Calif., 1964.

possible that iodine molecule will move partly with solvated ethanol molecule. If we can assume that the stability of I_2 + EtOH complex in the present mixed media, say, in an equimolar mixture, is larger than that in pure ethanol, such a two diffusing unit mechanism can also account for the fact that $D_{11}^{\circ}\eta_{23}/T$ is extremely small in comparison with that for pure solvents in the present mixed solvent systems.

We can thus conclude that solute–solvent interactions have a large effect on the variation of D_{11}° with the composition in the present mixed solvent systems. One may question possible inconsistency between the present interpretation and that given in P-I, as we had emphasized the importance of structural anomalies in interpreting the behavior of $D_{11}^{\circ}\eta_{23}/T$ *vs.* x_2 relation in alcohol–water solutions. Perhaps we can ascribe this difference to the facts that the hydrogen-bonded structures which prevail in aqueous alcohol solutions are three dimensional, while, in alcohol + nonpolar liquid solutions, the associations are less pronounced, the associated complex is of linear type, and there should be no structure-making effect due to the second solvents. It should also be pointed out that the modes and strength of interactions with I_2 in water and alcohol are similar to each other. This implies that alcohol + water systems are of EtOH + toluene type rather than of EtOH + *n*-hexane type, though this classification should not be taken as definitive. At the present stage, it should be indispensable for establishing a general relation to accumulate the diffusivity data for ternary systems where the interactions among three components involved are of different strength and specificity.

The Glass Transition in Amorphous Water.[1] Application of the Measurements to Problems Arising in Cryobiology

by Don H. Rasmussen and Alan P. MacKenzie*

Cryobiology Research Institute, Madison, Wisconsin 53704 *(Received April 16, 1970)*

Publication costs assisted by the U. S. Public Health Service

Values for the glass transition temperature, T_g, of aqueous solutions of glycerol, ethylene glycol, and methanol, measured by differential thermal analysis, were extrapolated to obtain values for T_g in amorphous water. For a heating rate of 5 deg min^{-1}, T_g for amorphous water is observed at $-137 \pm 1°$. The results were correlated with Jenckel's expression for the concentration dependence of T_g in binary solutions. A kinetic analysis after McMillan led to "kinetic" parameters for the glass transition that were linear functions of weight fraction and yielded a time–temperature dependence for T_g in amorphous water correlating well with previously published values.

Introduction

Thermal techniques have been applied to the study of the glass transition in pure water on several occasions. Pryde and Jones[2a] reported an approximate determination of the glass transition temperature. McMillan and Los[2b] determined, by differential thermal analysis, that, at a warming rate of 20 deg min^{-1}, the glass transition occurred at $-134°$. Sugisaki, Suga, and Seki,[3] after a calorimetric determination, reported a value of $-138°$ (though their published data suggest a maximum in dC_P/dT around $-140°$). Ghormley,[4] using thermal analysis of warming curves, could not detect a glass transition.

Several workers have examined glass transitions in aqueous solutions and estimated the glass transition temperature for water by extrapolation to zero solute concentration. Yannas[5] used a buoyancy method that determined the temperature at which the specific gravity of a solution of glycerol in water changed abruptly upon warming. Yannas' warming rates ranged from 0.5 to 2 deg min^{-1} and resulted in a glass transition temperature for water, by extrapolation, of $-146 \pm 4°$.

(1) Supported by Grant No. GM-15143 from the U. S. Public Health Service.

(2) (a) J. A. Pryde and G. O. Jones, *Nature*, **170**, 685 (1952); (b) J. A. McMillan and S. C. Los, *ibid.*, **206**, 806 (1965).

(3) M. Sugisaki, H. Suga, and S. Seki, *J. Chem. Soc. Jap.*, **41**, 2591 (1968).

(4) J. A. Ghormley, *J. Chem. Phys.*, **48**, 503 (1968).

(5) I. V. Yannas, *Science*, **160**, 298 (1968).

Angell, Sares and Bressel[6] estimated the temperature of the glass transition in water, from a study of the glass transition in concentrated salt solutions by differential thermal analysis, to be $-133 \pm 5°$.

In the course of the determination of various nonequilibrium transitions observed in several aqueous systems subjected to rapid cooling, Luyet and the present authors reported glass transition temperatures of aqueous solutions of ethylene glycol, glycerol, glucose, sucrose,[7] dimethyl sulfoxide,[8] and polyvinylpyrrolidone.[9] From these data the present authors determined the glass transition temperature for pure water to be $-140 \pm 3°$. Noting the wide divergence in values (from -133 ± 5 to $-146 \pm 4°$) we undertook a study, by differential thermal analysis, of the concentration dependence of the glass transition in aqueous solutions of several solutes at fixed heating rates and an analysis of the effect of different heating rates on the glass transition in solutions of ethylene glycol. It is our purpose here to demonstrate agreement between the several extrapolations of the glass transition temperature curves to pure water for the different solutes and to derive parameters relating to the "kinetics" of the glass transition in amorphous water from those relating to the process observed in aqueous solutions of ethylene glycol. From the nature of the concordance of our results and the temperatures for the glass transition of amorphous water previously reported[2,3,5,6] the reasons for the discrepancies among the latter values will become apparent.

Apparatus, Materials, and Methods

The apparatus for differential thermal analysis consisted of: (1) a brass block that could be precooled to $-190°$ and heated electrically at a constant rate between 1 and 21 deg min^{-1}; (2) sample tubes of 1 mm bore and 0.25 mm wall thickness made of Pyrex glass; (3) a thermocouple system made from 3-mil copper and constantan wires which measured (a) absolute reference temperature, and (b) the temperature differential between sample and reference; and (4) an amplifier–recorder system for plotting, on an X–Y basis, the differential temperature and the absolute reference temperature. The thermocouple–recorder system was calibrated at the boiling point of liquid nitrogen ($-196°$) and the freezing point of ethyl acetate ($-83.6°$). The setting of the zero point (at $-196°$) was checked before each run. Temperatures were measured always to $\pm 0.5°$ and, relative to one another, to $\pm 0.2°$. The sensitivity of the recorder to changes in the differential temperature was enhanced by preamplification *via* a Leeds and Northrup dc amplifier; the resulting sensitivity could be varied up to 0.5 μV/in. of display with minimal noise. The thermocouples were arranged to insert into the sample and reference tubes in such a way that the sample assembly, minus the block, could be cooled at a much higher rate than could the block. Higher sample cooling rates were necessary to permit the retention of the metastable amorphous state in solutions in which the water was present in higher concentrations.

For the purposes of this analysis of the glass transition behavior of aqueous solutions, we used Baker Analyzed reagent grade ethylene glycol, glycerol, and methanol. These materials contained, according to the supplier's specifications, 0.20%, 4.5%, and 0.04% water, w/w, respectively. All the solutions were prepared gravimetrically with deionized, distilled water.

After the sample and the reference tubes were filled (with 0.01-ml volumes delivered from micropipets), thermocouples were inserted. The reference (deionized distilled water) was frozen (slowly by comparison with the sample) in cold nitrogen vapor; the sample tube was immersed in liquid nitrogen (cooling rates approximated 75 deg sec^{-1} between 0 and $-150°$) or in a bath of liquid nitrogen containing frozen slushy nitrogen, at a temperature of $-210°$ (cooling rates approximated 200 deg sec^{-1} between 0 and $-150°$). The sample and reference were then transferred to the precooled block and the warming rate adjusted to the desired value between 1 and 21 deg min^{-1}. Heating rates were found to be reproducible to $\pm 5\%$ of the values desired.

Results

The curves obtained by differential thermal analysis of 50% w/w ethylene glycol solutions that were cooled by immersion in boiling nitrogen and warmed at various rates are displayed by Figure 1. These and the other glass transitions observed in this study necessarily relate to quenched glasses, the cooling rates being too high to allow a so-called "quasi-equilibrium glass"[10] to form. Without these extreme cooling rates, however, crystallization of water was invariably initiated, even in solutions of 50% w/w solute, changing the concentration of the remaining glass. A more detailed discussion of the crystallization of water during the warming of quenched solutions has been given by Luyet and Rasmussen.[7] We believe that data reported here correspond to measurements obtained with totally vitrified solutions. Continuity of behavior of the glass transition as a function of concentration as well as continuity in other transitions[7] lead us to accept the values determined from solutions above about 35% w/w solute, depending upon the solute.

The glass transition endotherm occupies an interval of 5.3–5.8 deg and exhibits a nonsymmetrical sigmoid shape (see again Figure 1). The relationship

(6) C. A. Angell, E. J. Sares, and R. D. Bressel, *J. Phys. Chem.*, **71**, 2759 (1967).

(7) B. Luyet and D. Rasmussen, *Biodynamica*, **10**, 167 (1968).

(8) D. H. Rasmussen and A. P. MacKenzie, *Nature*, **220**, 1315 (1968).

(9) B. Luyet and D. Rasmussen, *Biodynamica*, **10**, 137 (1967).

(10) G. Adam and J. H. Gibbs, *J. Chem. Phys.*, **43**, 139 (1965).

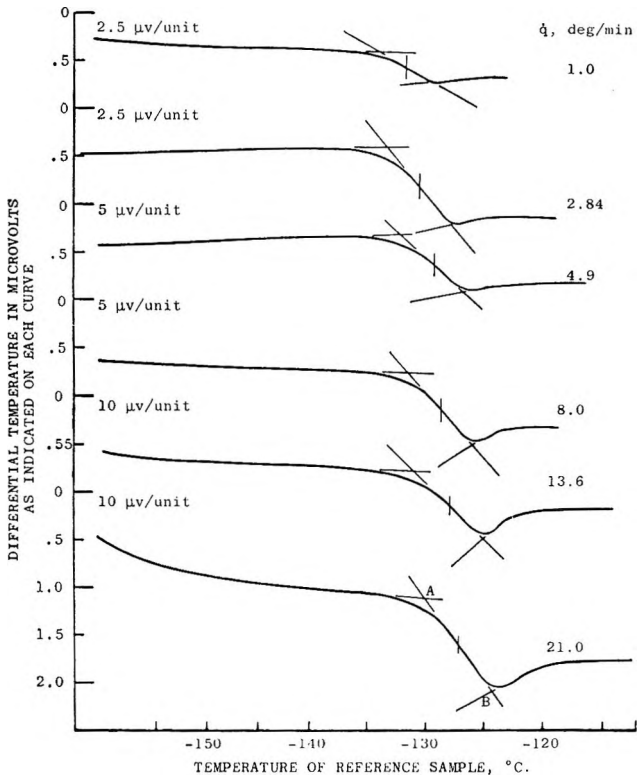

Figure 1. Thermograms for 50% ethylene glycol.

of the glass transition endotherm as observed by differential thermal analysis to the actual change in the specific heat of the sample has been discussed by McMillan.[11] According to his analysis, the rate of change of specific heat is a maximum at the point of inflexion in the thermogram. However, since the curves are asymmetric and the inflexion points difficult to determine, we adopted a technique for measuring T_g shown in Figure 1. While this method does not take direct account of the asymmetry of the transition it must be noted that, for a change in the heating rate from 1 to 21 deg min^{-1}, the temperature range which the transition spans (from point A to B in Curve 6, Figure 1) is about constant at 5.5 ± 0.3°.

The glass transition temperatures of aqueous solutions of ethylene glycol, glycerol, and methanol have been measured by this method at a heating rate of 5 deg min^{-1} in the concentration range from 35 to 100% w/w solute (95% in the case of glycerol). These data, presented in Figure 2, delimit the range of temperatures within which one would place, by extrapolation, the glass transition for amorphous water at a corresponding heating rate. We made several attempts to add other curves to Figure 2 by choosing solutes, isopropyl alcohol and 2-methoxyethanol, for example, having glass transition temperatures (−153 and −140°, respectively) different from each of the three substances first examined. Unfortunately, we were unable, with the means of rapid cooling at our disposal, to vitrify these solutions over very wide ranges of concentration.

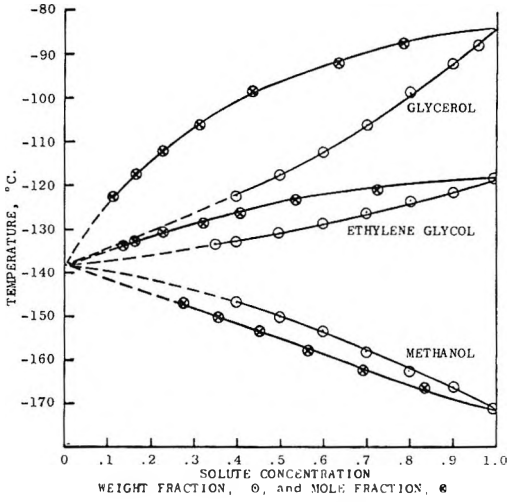

Figure 2. Glass transition temperatures for aqueous solutions of glycerol, ethylene glycol, and methanol.

Various semiempirical expressions, developed to describe the dependence of the glass transition upon composition in polymer–diluent systems, have been reviewed by Shen and Tobolsky.[12] The formula most acceptable to them, and the one used by Yannas[5] to obtain a value for the glass transition temperature of water, is that of Jenckel[13]

$$T_g = T_{g1}w_1 + T_{g2}w_2 + Kw_1w_2 \qquad (1)$$

where T_g is the glass transition temperature in deg K, w is the weight fraction of each constituent, subscripts 1 and 2 refer to water and solute, respectively, and K denotes a proportionality constant dependent on the particular compounds involved. A plot of $(T_g - T_{g2})/w_1$ *vs.* w_1 yields a slope of $-K$ and an intercept of $[T_{g1} - T_{g2} + K]$. From data that include T_{g2} and the glass transition temperature, T_g, at various concentrations, the temperature T_{g1} can be derived. The results of such an analysis on our solutions (Figure 2) at a heating rate of 5 deg min^{-1} are shown in Figure 3. The derivation yields K values of −26 ± 1 for water–glycerol, −13 ± 1 for water–ethylene glycol, and +15 ± 1 for water–methanol. The resultant values for the glass transition temperatures "T_{g1}" are in good agreement with each other and with the visual extrapolation of the curves in Figure 2. That is, a value of −137 ± 1° *at a heating rate of 5 deg* min^{-1} is found both by visual and empirical extrapolation. Though Jenckel's expression was originally intended to describe the reduction in the glass transition temperature of a polymer matrix with increased concentration of monomer or plasticizer, it appears to hold also for the concentration dependence of the glass transition in binary aqueous solutions.

(11) J. A. McMillan, *J. Chem. Phys.*, **42**, 3497 (1965).

(12) M. C. Shen and A. V. Tobolsky, *Advan. Chem. Ser.*, **No. 48**, 27 (1965).

(13) E. Jenckel and R. Heusch, *Kolloid-Z.*, **130**, 89 (1958).

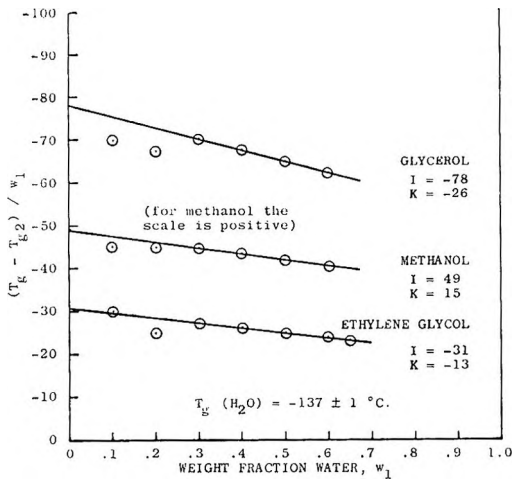

Figure 3. Analysis of the glass transition as a function of weight fraction of solute. $T_g = T_{g1}w_1 + T_{g2}w_2 + Kw_1w_2$.

In an attempt to interpret the observed variation in the glass transition temperature with heating rate, the times taken by the samples to undergo the changes in specific heat detected by dta were calculated from the temperatures spanned by the respective transitions; for example for 50% EG, the transition spanned 5.5 ± 0.3°. For a change in heating rate from 1 to 21 deg min^{-1}, the time therefore varied from 5.5 min at −131.6 ± 0.2 to 0.26 min at −127.4 ± 0.2°. These times may be considered representative of the time scales of particular experiments and the temperatures at which T_g is observed as the temperatures of the relaxation in the respective experimental time scales. Under these conditions, the time required for the observation of a T_g could be compared with relaxation times for processes such as diffusion, viscous flow, and dielectric relaxation; that is the formulas describing these processes might be used to describe the relaxation at T_g.

That there must be a lower temperature limit, T_0, above absolute zero, to the glass transition measured during an experiment of infinite time scale (zero heating rate) was pointed out by Kauzmann.[14] Below this T_0, if liquid state properties were to persist, negative entropies, volumes, etc., with respect to the crystal, would result. The use of such a lower temperature limit to liquid state properties is inherent in the Williams–Landel–Ferry[15] equation for relaxation in viscoelastic systems and in the equation due to Vogel.[16] Gibbs and DiMarzio[17] predicted a thermodynamic second-order transition at T_0 and Adam and Gibbs[10] presented the concept that the configurational entropy of the liquid disappears at T_0 and that during the glass transition the number of states available to the system is reduced to such an extent that transformation between alternative states requires prohibitively numerous cooperative rearrangements consistent with the thermal energy of the system and the time allowed for measurement; more simply, T_g is supposedly the kinetic manifestation of T_0. In the region of the glass transition, the average relaxation time follows the Vogel equation

$$\ln \tau = A + B/(T - T_0) \qquad (2)$$

where τ is the relaxation time, A and B are constants, T is the temperature of measurement of τ, and T_0 is the "zero mobility" temperature. Provided sufficient information regarding the value of T_0 is known, or sufficiently extensive experimental data relating τ to T_g, the values of constants A and B and T_0 can be evaluated. Our results, obtained by varying the heating rate from one scan by dta to another, indicate a time–temperature dependence for the glass transition, but the variation in T_g, from the highest to the lowest heating rate, was only 5 deg. These somewhat limited experimental data, indicating as they do that each individual transition spans 5.5 deg, preclude evaluation of the three-parameter equation and of the graphical tests of the usefulness of the T_0 concept. It was, consequently, not possible to test such derivations as that of Adam and Gibbs, who proposed the relationship $T_g/T_0 = 1.29$; we could not select a value for T_0 more consistent than another with the primary data.

If values for T_0 were derived for the ethylene glycol–water system from some other type of measurement, (*e.g.*, viscosity) they would suffice to permit the evaluation of the "kinetics" of the glass transition using Vogel's equation. To the authors' knowledge, however, this information is not available.

In the absence of the necessary information regarding T_0, the derivation due to McMillan, based on classical kinetic theory, was adopted in the belief that its application might provide some insight into the concentration dependence of the "kinetics" of the relaxation and allow the extrapolation of the parameters obtained to pure water. Such an analysis corresponds to the evaluation of an equation of the form of eq 2, where T_0 is set equal to 0°K, though, as previously pointed out, T_0 must in reality exceed absolute zero.

McMillan[11] derived kinetic expressions relating thermal behavior in the neighborhood of the glass transition temperature with measurements obtained by differential thermal analysis. To determine the applicability of his procedure to our data, we repeated his analysis of the effect of heating rate on the glass transition in glycerol. Though the samples we used were smaller than his by a factor of 750 and our heating rate ranged from 1 to 21 deg min^{-1}, we found, with reagent grade glycerol (95.5% glycerol) an activation energy for the glass transformation of 40.6 ± 1 kcal/mol, a value agreeing favorably with his figure of 42.4 ± 1.2

(14) W. Kauzmann, *Chem. Rev.*, **43**, 219 (1948).

(15) M. L. Williams, R. F. Landel, and J. D. Ferry, *J. Amer. Chem. Soc.*, **77**, 3701 (1955).

(16) H. Vogel, *Phys. Z.*, **22**, 645 (1921).

(17) J. H. Gibbs and E. A. DiMarzio, *J. Chem. Phys.*, **28**, 373 (1958).

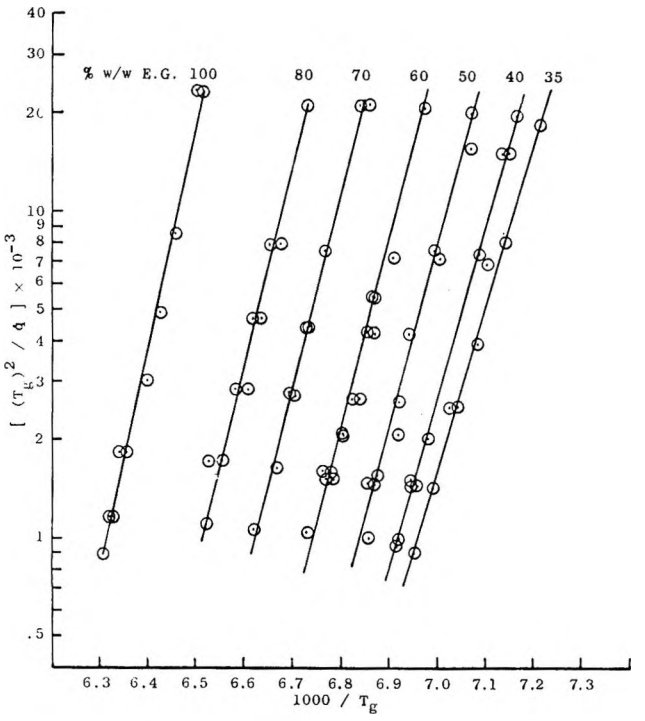

Figure 4. Effect of heating rate on the glass transition temperatures of aqueous solutions of ethylene glycol.

kcal/mol, especially so when the presence of 4.5% water by weight is considered.

An analysis of ethylene glycol and its aqueous solutions showed that McMillan's kinetic expressions were applicable since, when the heating rate was varied, the glass transition temperature varied as demonstrated in Figure 4. According to McMillan[11] the slopes of the curves in Figure 4 are related to the activation enthalpy, ΔH^*, necessary for the relaxation process by the equation

$$\Delta H^* = R\left[\frac{\mathrm{d} \ln (T_g^2/\dot{q})}{\mathrm{d}(1/T_g)}\right] \quad (3)$$

and to the activation entropy, ΔS^*, hindering the relaxation, by

$$\Delta S^* = R[\Delta H^*/RT_g + \ln (\Delta H^*/R) - \ln (T_g^2/\dot{q}) - \ln (kT_g/h)] \quad (4)$$

where R = the gas constant, T_g = the measured glass transition temperature, $\dot{q}$ = the heating rate in deg min^{-1}, k = Boltzmann's constant, and h = Planck's constant.

These parameters, ΔH^* and ΔS^*, are plotted as functions of concentration in Figure 5. The linearity of the curves is in each case strikingly apparent and is, perhaps, related to some additive property, free volume for instance, on a weight fraction basis. The extrapolated enthalpy of activation, ΔH^*, for the glass transition in water is 19.2 ± 0.5 kcal/mol; the activation entropy, ΔS^*, is 87 ± 2 cal/mol °K.

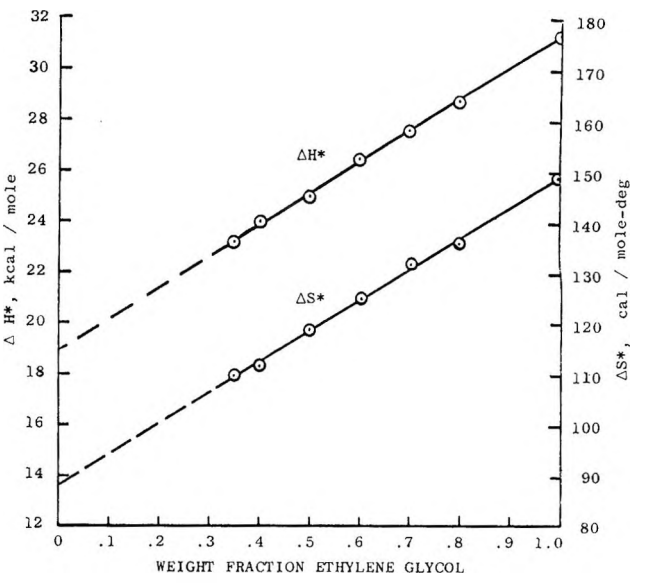

Figure 5. Activation enthalpy and activation entropy as a function of composition.

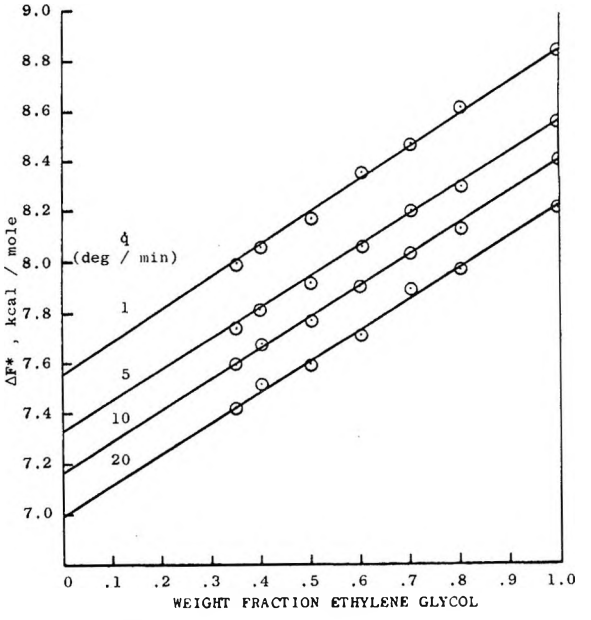

Figure 6. Activation free energy, ΔF^*, as a function of composition.

From the entropy and enthalpy of activation, the free energy of activation was calculated from the relation: $\Delta F^* = \Delta H^* - T\Delta S^*$. Thus a separate curve relating ΔF^* to the composition of the system could be obtained at each heating rate. Four such curves, presented in Figure 6, were obtained with values interpolated from the original data exhibited in Figure 4. The ΔF^* values for water range from 7.55 ± 0.1 kcal/mol at 1 deg min^{-1} to 7.0 ± 0.1 kcal/mol at 21 deg min^{-1}. Table I relates these activation parameters and the glass transition temperatures for water at 1, 5, 10, and 20 deg min^{-1} heating rate. Table II lists those pre-

Table I: Activation Parameters and Glass Transition Temperature for Water as a Function of Heating Rate

$\dot{q}$	ΔH^*, kcal/mol	ΔS^*, cal/mol °K	ΔF^*, kcal/mol	$(\Delta H - \Delta F)/\Delta S = T_g$, °K	$T_g^2/\dot{q}$	$1/T_g$
1	19.2	87	7.55	133.8	17,902	7.47×10^{-3}
5			7.33	136.5	3726	7.33
10			7.16	138.4	1915	7.23
20			7.0	140.3	984.2	7.13

Table II: Kinetic Parameters for the Glass Transition of Water as Determined from Results of Other Investigators

Research group	$\dot{q}$, deg/min	T_g, °K	$T_g^2/\dot{q}$	$1/T_g$
Angell, *et al.*	10	140	1960	7.14×10^{-3}
McMillan	20	139	966	7.19
Sugisaki, *et al.*	≈0.2	133	59,000–88,000	7.52
Yannis	0.5–2	127	8000–32,000	7.86

viously published glass transition temperatures for water associated with particular heating rates. Figure 7 compares the results of the foregoing analysis with the values for the glass transition temperature reproduced in Table II. The success of this last correlation would appear to justify the use of the method by which the activation enthalpy and entropy were each extrapolated. Other limitations to McMillan's classical analysis should not, however, be discounted.

Discussion

The foregoing analysis depends on an assumption that the initial cooling rates, which yielded quenched glasses, have not materially affected the concentration dependence or the "kinetics" of the glass transition. The cooling rates employed to achieve the glassy state were greater than those required in the pure solute and in the solutions of eutectic composition, barely great enough in 35 to 40% w/w solute and insufficient at concentrations below 35% w/w solute.

Jenckel's expression (see earlier) related the temperature, T_g, to the concentration in *equally stabilized glasses*. At present we do not know whether cooling rates exceeding those required to achieve a glassy state result in the production of less stable glasses. Were such differences demonstrated, one might further expect them to affect the "kinetic parameters," ΔH^* and ΔS^*, derived by differential thermal analysis, characteristic of the glass transitions in question. In the absence of sufficient information we have assumed that the concentration dependence is expressed adequately by Jenckel's equation and that because of the agreement between the three pairs of curves in Figure 2 with reference to T_g for water, the one cooling rate yields essentially equally stable (or unstable) glasses irrespective of the ease with which the glassy state was reached.

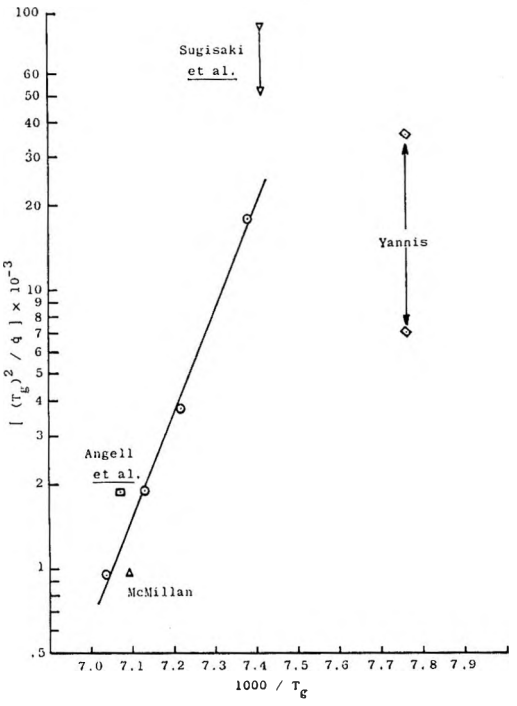

Figure 7. Effect of heating rate on the glass transition temperature for water.

The kinetic analysis after McMillan has demonstrated correlation between the glass transition temperatures in amorphous water extrapolated from measurements on solutions of ethylene glycol and the published values derived from measurements made on water. Furthermore, the predicted dependence of the glass transition on the heating rate correlated with the published results. We do not wish to imply, however, that these correlations prove the validity of the theoretical foundation of the expressions used. Rather, we suggest they demonstrate a continuity in application as a function of concentration. That is, they provide a means of relating the measurements in solution to measurements either of pure solute or pure solvent; they do not necessarily determine the choice of a model on which descriptions of the glass transition might be based.

To the cryobiologist interested in the structure of aqueous systems, both model and biological, the effects of different cooling rates, low, moderate, and very high, are of great importance. Physical transformations occurring during cooling and/or during rewarming have been implicated in various ways in attempts to explain the responses of cells and tissues to freezing and thawing.[18,19]

(18) B. Luyet in "Proceedings of the International Conference on Low-Temperature Science," Vol. II, E. Asahina, Ed., Hokkaido University, Sapporo, Japan, 1966–1967.

(19) P. Mazur and J. J. Schmidt, *Cryobiology*, **5**, 1 (1968); P. Mazur, J. Farrant, S. P. Leibo, and E. H. Y. Chu, *ibid.*, **6**, 1 (1969).

A glass transition in an amorphous portion of a frozen biological material may, at first sight, appear less important than a first-order transition, several of which have been the object of much attention. Many considerations do, however, indicate the importance, in cryobiology, of the glass transition. For example, glass transition temperatures appear to determine (1) the temperatures above which viable states deteriorate at measurable rates,[20,21] (2) the temperatures below which fracture and etching of frozen specimens must be conducted to provide surfaces suitable for electron microscopy,[22] and (3) temperatures above which freeze-drying cannot be carried out without structural collapse of the matrix.[23] It also seems that glass transition temperatures serve to indicate those somewhat higher temperatures above which devitrification proceeds in biological materials cooled at such velocities that ice formation during cooling is prevented.[24]

Since experimental measurements of the glass transition temperatures of aqueous solutions can only be made on systems of lower water content, direct measurement of the properties of greatest interest may not be possible. When such is the case, a knowledge of the variation in T_g with water content and of T_g for water and of the "kinetics" of the respective transitions should suffice to permit an estimate of the glass transition behavior in the water-rich system of interest.

Conclusion

Glass transitions in aqueous solutions of methanol, ethylene glycol, and glycerol have been examined by differential thermal analysis. The concentration dependence of the glass transition temperature appears in each case to be adequately described by an empirical expression due to Jenckel. Extrapolation of the glass transition temperature curves to zero solute concentration yielded a glass transition temperature for water of $-137 \pm 1°$ at a heating rate of 5 deg min^{-1}. In the absence of other theoretical treatments, the kinetic analysis of the glass transition according to McMillan has been applied to the water–ethylene glycol system, and the "activation energies" have been extrapolated to yield, for the glass transition in amorphous water, $\Delta H^* = 19.2 \pm 0.5$ kcal/mol, $\Delta S^* = 87 \pm 2$ cal/mol °K, and $\Delta F^* = 7.0 - 7.55$ kcal/mol. Such values indicate a time/temperature dependence sufficient to explain the wide range of previously published values for the glass transition of amorphous water.

Acknowledgment. The authors wish to express their thanks to Professor J. D. Ferry for his kindness in consenting to read and evaluate the original manuscript.

(20) A. P. MacKenzie and G. L. Rapatz, *Fed. Proc. Fed. Amer. Soc. Exp. Biol.*, 27, 700 (1968).

(21) A. P. MacKenzie in "The Frozen Cell," G. Wolstenholme and M. O'Connor, Ed., J. & A. Churchill, London, 1970.

(22) A. MacKenzie and D. Rasmussen, *Biophys. J.*, 9, A-193 (1969).

(23) A. P. MacKenzie, *Cryobiology*, 3, 387 (1967).

(24) D. Rasmussen and B. Luyet, *Biodynamica*, 10, 319 (1969).

Mass Spectra of Disilanes. Phenyl–Silicon Interaction and Silicon–Silicon Bond Strength

by J. M. Gaidis,* P. R. Briggs, and T. W. Shannon

The Dow Chemical Company, Eastern Research Laboratory, Wayland, Massachusetts 01778 *(Received September 21, 1970)*

Publication costs assisted by the Dow Chemical Company

By the use of an empirical bond-energy scheme and the assumption of negligible steric interaction across the Si–Si bond in substituted disilanes, heats of formation were determined for the species $R\cdot$, R^+, R_2, and $RSiMe_3$ ($R = Ph_nMe_{3-n}Si$). The stabilization energy of the Ph_3Si^+ cation (19.7 kcal mol^{-1} with respect to Me_3Si^+) is appreciable, but only about half that observed for Ph_3C^+. The low stabilization energy of $Ph_3Si\cdot$ (actually destabilized by 14.0 kcal with respect to $Me_3Si\cdot$) indicates very little resonance interaction between Ph and Si, and hence a probable pyramidal structure. The disilane cations undergo rearrangement before fragmentation through an intermediate related to trisubstituted alane dimers.

Recent mass spectrometric studies on organosilicon compounds have revealed interesting details about bonds between silicon and other elements.[1-4] Many workers have interpreted the results in terms of π-bonding involving acceptor 3d orbitals on silicon.[5]

For several reasons, the importance of 3d orbitals in silicon chemistry has begun to be questioned, and some workers have by experimental[6] or calculational[7] methods pointed out their inadequacies. The ease of invoking 3d orbitals, due to their uncertain energy, overlap, and orientation (in spite of theoretical efforts) has reduced their predictive potential, enabling *any* trend to be rationalized easily. If in fact 3d orbitals *are* important in bonding to second-row atoms, then 4s, 4p, and higher[8,9] orbitals should also be included in the acceptor level which is now most often called "3d".

While current thinking seems more and more to concentrate on the outer orbitals on silicon,[8,10] the valence shell 3p orbital has not been adequately characterized. From the puzzling observation that $(p\text{-}Me_2NPh)_3SiCl$ does not ionize readily [in contrast to $(p\text{-}Me_2NPh)_3CCl$],[11] one might conclude that Si 3p orbitals do not conjugate particularly well with phenyl rings. Why then, the higher energy, diffuse 3d orbitals should be so effective in back-bonding is not clear. Because there were few data regarding acceptor properties in the 3p level of silicon, we initiated a mass spectrometric study of the energetics of siliconium ions,[12] where this level is not completely filled.

Experimental Section

The mass spectra and appearance potential measurements were carried out on an AEI MS-12 mass spectrometer. The operating conditions for determination of the spectra were 75 V electron energy, 150 μA ionizing current, and 2–3 V repeller potential. The ionization efficiency curves were obtained using either xenon or carbon disulfide as the calibrating gas. The curves were treated in the semilogarithmic manner[13] using data extending to 0.01% of the 50-V value. The operating

(1) (a) D. B. Chambers, F. Glockling, and J. R. C. Light, *Q. Rev. Chem. Soc.*, **22**, 317 (1968), and their references; (b) B. G. Gowenlock and J. Stevenson, *J. Organometal. Chem.*, **15**, 503 (1968); (c) J. Silbiger, C. Lifshitz, J. Fuchs, and A. Mandelbaum, *J. Amer. Chem. Soc.*, **89**, 4308 (1967); (d) S. J. Band, I. M. T. Davidson, C. A. Lambert, and I. L. Stephenson, *Chem. Commun.*, 723 (1967).

(2) I. M. T. Davidson and I. L. Stevenson, *J. Organometal. Chem.*, **7**, 24 (1967).

(3) I. M. T. Davidson and L. I. Stephenson, *J. Chem. Soc. A*, 282 (1968).

(4) D. B. Chambers and F. Glockling, *ibid.*, 735 (1968).

(5) (a) H. Bock, H. Seidl, and M. Fochler, *Chem. Ber.*, **101**, 2815 (1968); (b) J. C. Baldwin, M. F. Lappert, J. B. Pedley, and J. A. Treverton, *J. Chem. Soc. A*, 1980 (1967); (c) S. J. Band, I. M. T. Davidson, and C. A. Lambert, *ibid.*, 2068 (1968).

(6) (a) H. Burger and U. Goetze, *J. Organometal. Chem.*, **12**, 451 (1968); (b) D. E. Fenton and J. J. Zuckerman, *Inorg. Chem.*, **7**, 1323 (1968); (c) E. W. Randall and J. J. Zuckerman, *J. Amer. Chem. Soc.*, **90**, 3167 (1968), and earlier papers; (d) A. G. Brook, D. G. Anderson, J. M. Duff, P. F. Jones, and D. M. MacRae, *ibid.*, **90**, 1076 (1968); (e) C. G. Pitt, M. S. Habercom, M. M. Bursey, and P. F. Rogerson, *J. Organometal. Chem.*, **15**, 359 (1968); (f) G. J. D. Peddle and R. W. Walsingham, *J. Amer. Chem. Soc.*, **91**, 2154 (1969).

(7) (a) F. Agolini, S. Klemenko, I. G. Csizmadia, and K. Yates, *Spectrochim. Acta, Part A*, **24**, 169 (1968); (b) R. D. Brown and J. B. Peel, *Aust. J. Chem.*, **21**, 2589, 2605, 2617 (1968).

(8) F. Bernardi and C. Zauli, *J. Chem. Soc. A*, 2633 (1968), discuss the favorable energetics of the 4s level for the case of sulfur. From their calculations and other well known approximations,[9a] one may conclude that 4p orbitals should have an acceptor function which is just as important as that of the 3d orbitals.

(9) (a) C. A. Coulson, "Valence," 2nd ed, Oxford University Press, London, 1961, pp 40–41; (b) W. Klemperer, *J. Amer. Chem. Soc.*, **83**, 3910 (1961).

(10) (a) K. A. R. Mitchell, *J. Chem. Soc. A*, 2676, 2683 (1968); (b) H. Bock and H. Seidl, *J. Amer. Chem. Soc.*, **90**, 5694 (1968).

(11) (a) A. B. Thomas and E. G. Rochow, *J. Inorg. Nucl. Chem.*, **4**, 205 (1957); (b) F. Brandmair and U. Wannagat, *Z. Anorg. Chem.*, **228**, 91 (1956).

(12) Although no siliconium ion (R_3Si^+) has been prepared in a condensed phase, J. Y. Corey and R. West, *J. Amer. Chem. Soc.*, **85**, 4034 (1964), have prepared a bipyridyl-complexed siliconium ion.

(13) F. P. Lossing, A. W. Tickner, and W. A. Bryce, *J. Chem. Phys.*, **19**, 1245 (1951).

Table I: Partial Mass Spectra of Disilanes

m/e	$(Me_3Si)_2$	$PhMe_2SiSiMe_3$	$Ph_2MeSiSiMe_3$	$(PhMe_2Si)_2$	$Ph_3SiSiMe_3$	$(Ph_2MeSi)_2$	$(Ph_3Si)_2$
45	11.8	10.9	5.5		3.2		
73	100.0	24.3	17.8	2.1	9.7		
105		9.9	17.8	10.3	14.6	11.0	16.0
107		5.7	3.2	6.3			
119		3.3	6.4	3.9		4.0	
131	29.6						
135		100.0	32.1	100.0	8.1	2.1	
146	14.7 (P)						
155					3.4		4.3
181			6.4		17.8	6.3	17.8
182			1.7		6.1		
193		13.3	2.4				
197			100.0	17.7	17.8	100.0	
208		17.6 (P)					
255			7.9	5.0	2.0		
259					100.0	8.2	100.0
270			18.5 (P)	22.2 (P)			
317					6.6		
332					27.7 (P)		
379						1.0	
394						20.8 (P)	
518							13.1 (P)

conditions for these measurements were 5 or 10 μA ionizing current, 3 V repeller potential, and 3 V trap potential.

The disilanes were a gift of W. H. Atwell, Jr., Dow Corning Corporation, except for $Me_3SiSiPh_3$, which was kindly supplied by R. West, University of Wisconsin. All the disilanes were shown to be free of isomers by vpc. The monosilanes were purchased commercially.

Results and Discussion

Mass Spectra.[14] The major peaks in the mass spectra of hexamethyl- and phenyl-substituted disilanes are presented in Table I. Intensities are expressed relative to the most abundant ion and have been corrected for isotopic contribution. The mass spectra of Ph_6Si_2 and $Ph_3SiSiMe_3$ are in good agreement with previously reported spectra.[4]

The mass spectra of hexamethyl- and hexaphenyldisilane are relatively simple and are illustrated in Scheme I. The numbers in brackets are the *m/e* ratio of the ion. Solid arrows denote transitions supported by metastable peaks. The molecule–ion undergoes fragmentation by cleavage of either the Si–Si or the Si–C bonds. The loss of a phenyl group from the molecule–ion of Ph_6Si_2 was not observed. Both the Ph_3Si^+ and Me_3Si^+ ions undergo further reaction by direct cleavage and rearrangement. Hydrocarbon elimination reactions of the type $Ph_3M^+ \rightarrow PhMC_6H_4^+ + C_6H_6$ and fragmentation of phenyl groups by successive elimination of acetylene have been observed previously[4,15] for M = Si, Ge, or Sn.

The unsymmetrical disilanes fragment at high ionizing voltage with unselective charge retention: both of the two possible siliconium ion species are formed. The fragmentation pattern of phenylpentamethyldisilane is shown in Scheme II.

The most interesting feature of the mass spectra of the disilanes is the evidence of rearrangement in the molecule–ion. The transition state shown in Scheme III is the only one which will show mixing of the groups in the mass spectra. However, for the unsymmetrical disilane two intermediates may be formed, the one illustrated and another structure involving two bridging methyl groups. If the methyl and phenyl groups possess equal ability to bridge two silicon atoms, the required transition state will form with a probability of 0.67. In the case of the symmetrical disilane, a transition state involving two bridging phenyl groups is also possible, but would not lead to mixing. The formation of a transition state with mixed bridging groups will occur with a probability of 0.44. Thus the ions resulting from formation of a bridged transition state should be more abundant by a factor of 1.5 in the spectrum of the unsymmetrical diphenyldisilane. The observed ratio is 1.62:1, close to the prediction for random bridging.

Inspection of Table I reveals similar reactions occurring in the tri- and tetraphenyl disilanes. Such exchange of organic groups across a metal–metal bond

(14) Additional mass spectral data for the hexamethyl- and phenyl-substituted disilanes will appear following these pages in the microfilm edition of this volume of the journal. Single copies may be obtained from the Reprint Department, ACS Publications, 1155 Sixteenth St., N.W., Washington, D. C. 20036, by referring to author, title of article, volume, and page number. Remit $5.00 for photocopy or $2.00 for microfiche.

(15) F. Glockling and J. R. C. Light, *J. Chem. Soc. A*, 717 (1968).

Scheme I

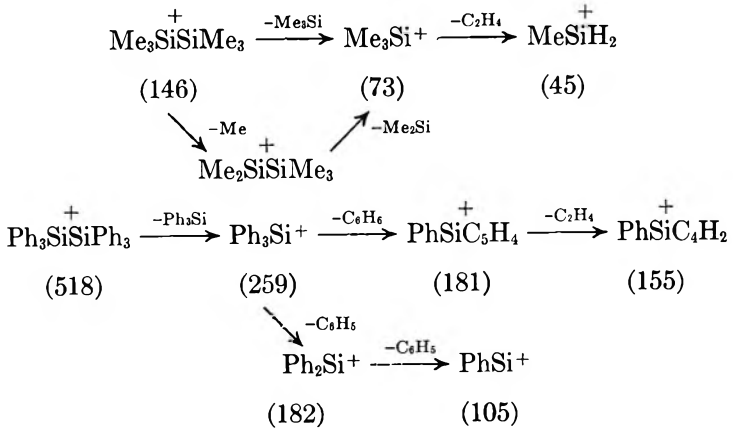

Scheme II

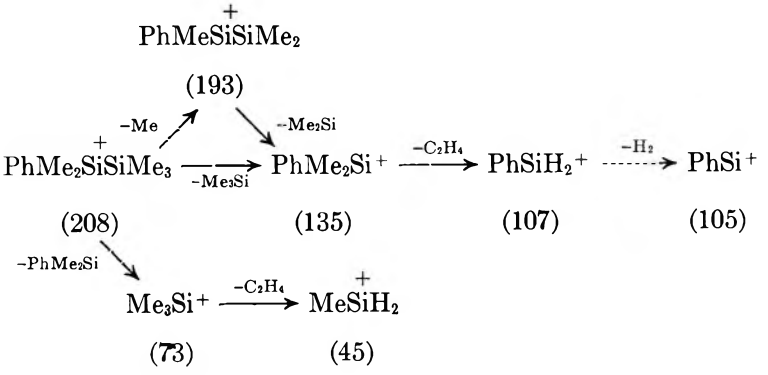

Scheme III

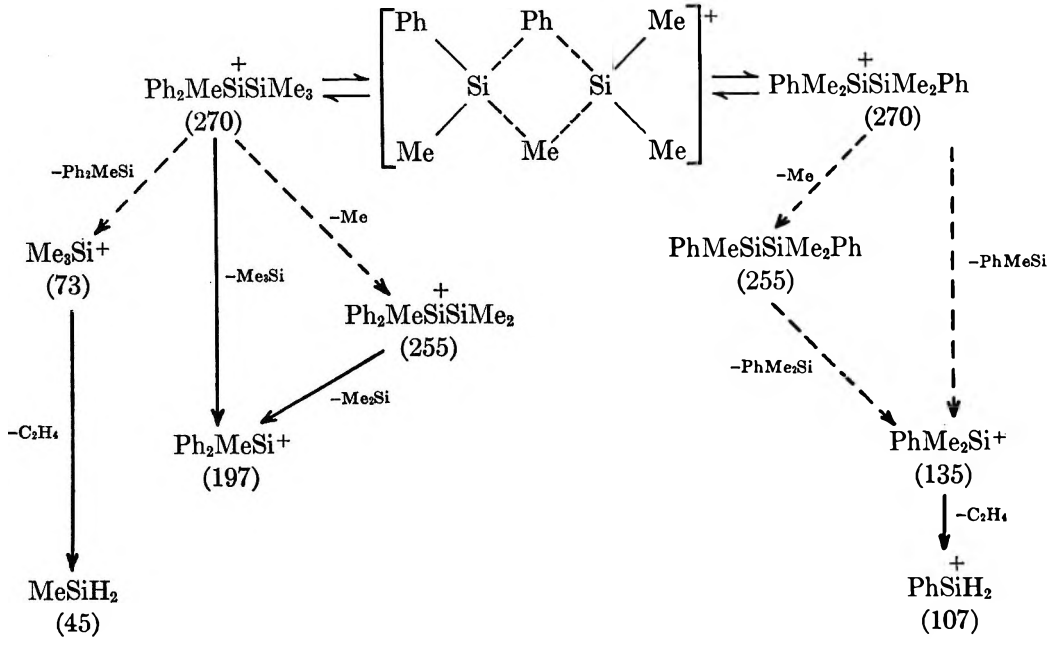

has been observed previously for compounds of the type $A_3MM'B_3$, where M,M′ = Si, Ge, or Sn,[4] and also for transition-metal compounds.[16]

A previous investigation[4] has pointed out that the fragmentation pattern does not permit a distinction between the intermediate of Scheme III and a stepwise cleavage–rearrangement–cleavage reaction

(16) (a) H. Svec and G. A. Junk, *J. Amer. Chem. Soc.*, **89**, 2836 (1967); (b) J. H. Smith, K. Mehner, and H. D. Kaesz, *ibid.*, **89**, 1759 (1967).

$$(Ph_2MeSiSiMe_3)^+ \xrightarrow{-Me} Ph_2MeSi\overset{+}{S}iMe_2 \longrightarrow$$

$$PhMeSi\overset{+}{S}iMe_2Ph \xrightarrow{-PhMeSi} PhMe_2Si^+$$

However, an examination of the metastable spectrum clearly shows rearrangement in the parent ion. In $Ph_2MeSiSiMe_3^+$, a substantial metastable peak occurs at *m/e* 67.5 for loss of $PhMe_2Si$ from the parent ion, and in $(PhMe_2Si)_2^+$, the largest metastable peak occurs at *m/e* 143.73, corresponding to loss of Me_3Si from the parent ion. Similarly, $(Ph_2MeSi)_2^+$ has two equally large metastables (the largest in the spectrum), one for symmetrical cleavage and one for loss of $PhMe_2Si$ to give Ph_3Si^+. Loss of Ph_3Si to give $PhMe_2Si^+$ occurs only $^1/_{30}$ as often. The molecule-ion $Ph_3SiSiMe_3^+$ cleaves to give Ph_2MeSi^+ and $PhMe_2Si$ with a large probability, but gives $PhMe_2Si^+$ and Ph_2MeSi only $^1/_{20}$ as often.

Molecule Heats of Formation. An important thrust of the present work is to establish the heats of formation of the ions and radicals resulting from rupture of the Si–Si bond in the disilanes investigated. These values may then be used to calculate bond dissociation energies and radical ionization potentials, which are the numbers of primary physical importance.

The appearance potential of an ion measures the heat of reaction by which the ion is formed. Thus the Me_3Si^+ ion can be formed by the process

$$Me_3SiSiR_3 + e \longrightarrow Me_3Si^+ + R_3Si\cdot + 2e \quad (1)$$

and its appearance potential equals the sum of the heats of formation of the ion and radical less that of the molecule

$$A.P.(Me_3Si^+) \geq \Delta H_f(Me_3Si^+) + \Delta H_f(Me_3Si\cdot) - \Delta H_f(MeSiSiR_3) \quad (2)$$

Similar relations can be written for the other disilanes. Then if the appearance potential can be measured and two of the other three terms obtained from another source, the third heat of formation can be calculated. We have followed the usual practice of neglecting the excess energy of the fragments. To the extent that the excess energy is nonzero, the calculated heats of formation will be upper limits.

Very little reliable thermochemical information is available even for the relatively simple alkylsilanes.[17-20] Potzinger and Lampe[21] have developed a method for calculating heats of formation of alkylsilanes and have determined parameters for the bond interaction scheme devised by Allen. Unfortunately, heats of formation are not available even for the simplest member in the series of substituted disilanes. Without this minimum information, we were unable to apply this method directly.

Our approach was to calculate the molecule heat of formation by extending Cox's bond-energy scheme[22] and correcting for interactions between next-nearest neighbor atoms. The bond contribution from Si–H in SiH_4 is simply $^1/_4$ of ΔH_f, or 1.83 kcal/mol,[23] but this value increases with increasing substitution on silicon.[24] For the methylsilanes, the terms contributing to the heat of formation are set out in the following equations

$$\Delta H_f(CH_3SiH_3) = 1.0 \text{ kcal/mol} = 3C_{sp^3}\text{–}H''' + Si\text{–}C_{sp^3} + 3Si\text{–}H''' \quad (I)$$

$$\Delta H_f((CH_3)_2SiH_2)^{20} = -7.8 \text{ kcal/mol} = 6C_{sp^3}\text{–}H''' + 2Si\text{–}C_{sp^3} + 2Si\text{–}H'' - \alpha(CSiC) \quad (II)$$

$$\Delta H_f((CH_3)_3SiH)^{20} = -18.1 \text{ kcal/mol} = 9C_{sp^3}\text{–}H''' + 3Si\text{–}C_{sp^3} + Si\text{–}H' - 3\alpha(CSiC) \quad (III)$$

$$\Delta H_f((CH_3)_4Si) = -33.0 \text{ kcal/mol} = 12C_{sp^3}\text{–}H''' + 4Si\text{–}C_{sp^3} - 6\alpha(CSiC) \quad (IV)$$

With the values for the bond contributions and next-nearest neighbor interactions (see Table II), these equations may be solved for the Si–H bond contribution as a function of substitution: Si–H'''' = Si–H''' = 1.83 kcal/mol; Si–H'' = 2.35 kcal/mol; and Si–H' = 2.9 kcal/mol. The contribution from Si–Si is $\Delta H_f(H_3Si)_2 - 6/4\ \Delta H_f(SiH_4)$. The Si–$Csp^3$ bond energy

Table II: Contributions to the Heat of Formation

Bond	Contr, kcal/mol	Interaction	Contr, kcal/mol
Csp^3–H'''	−3.48	α(CCC)	2.6
Csp^3–Csp^3	0.45		
Csp^3–Csp^2	−4.45	α(CSiC)	2.5
Phenyl group	26.80		
Si–H''' = Si–H''''	1.83	α(CCSi)	2.6
Si–H''	2.35		
Si–H'	2.90	α(CSiSi)	2.7
Si–Si	6.12		
Si–Csp^3	5.95		
Si–Csp^2	1.05		

(17) Values ranging from 46.4 to 82 kcal/mol for the Si–Si bond[18,19] have been proposed, but the best value[3,20] seems now to be 67 ± 2 kcal/mol.

(18) (a) S. R. Gunn and L. G. Green, *J. Phys. Chem.*, **65**, 779 (1961); (b) W. C. Steele and F. G. A. Stone, *J. Amer. Chem. Soc.*, **84**, 3599 (1962).

(19) J. A. Connor, G. Finney, G. J. Leigh, R. N. Haszeldine, P. J. Robinson, R. D. Sedgwick, and R. F. Simmons, *Chem. Commun.*, 178 (1966).

(20) I. M. T. Davidson and I. L. Stephenson, *ibid.*, 746 (1966).

(21) (a) P. Potzinger and F. W. Lampe, *J. Phys. Chem.*, **74**, 719 (1970); (b) Another bond energy scheme for silicon compounds was proposed by H. E. O'Neal and M. A. Ring, *Inorg. Chem.*, **5**, 435 (1966).

(22) J. D. Cox, *Tetrahedron*, **18**, 1337 (1962).

(23) F. D. Rossini, National Bureau of Standards, Circular 500, U. S. Government Printing Office, Washington, D. C.

(24) R. P. Hollandsworth and M. A. Ring, *Inorg. Chem.*, **7**, 1635 (1968).

contribution was determined from the heat of formation of methylsilane.[21] The Si–Csp^2 bond was considered to be strengthened as much relative to Si–Csp^3 as Csp^3–Csp^2 is strengthened relative to Csp^3–Csp^3.

The heats of formation of the phenyl-substituted silanes were calculated using the above scheme and setting α(PhSiPh) = α(PhSiC) = α(CSiC) and α(PhSiSi) = α(CSiSi). The values obtained are given in Table III.

Table III: Ionization Potentials, Molecule and Molecule–Ion Heats of Formation

Molecule	I_p, eV	ΔH_f(mol), kcal/mol	ΔH_f(ion), kcal/mol
$PhMe_2SiH$	8.92 ± 0.03[a]	14.2	219.9
Ph_2MeSiH	8.75 ± 0.04	46.5	248.3
$PhMe_3Si$	8.81 ± 0.03	−0.6	202.6
Ph_3SiH	8.80 ± 0.03	78.6	281.5
Ph_4Si	8.65 ± 0.01	95.8	295.3
$(Me_3Si)_2$	8.46 ± 0.01	−52.0	143.1
$PhMe_2Si_2Me_3$	8.35 ± 0.03	−19.7	172.9
$Ph_2MeSi_2Me_3$	8.38 ± 0.04	12.7	206.0
$Ph_3Si_2Me_3$	8.30 ± 0.01	45.0	236.4
$(PhMe_2Si)_2$	8.11 ± 0.03	12.7	199.7
$(Ph_2MeSi)_2$	8.05 ± 0.07	77.3	262.9
$(Ph_3Si)_2$	8.16 ± 0.14	142.0	330.2

[a] The limits of error represent the standard deviation from the mean of three or more determinations. This figure is the reproducibility of the measurements. The absolute error is probably ±0.15 eV.

Ionization and Appearance Potentials. The ionization potentials, calculated heats of formation, and molecule–ion heats of formation for all compounds examined in this work are given in Table III. The heats of formation of the disilane molecule–ions increase with increasing phenyl substitution at a rate of about 30 kcal/mol per phenyl group. The gradually decreasing ionization potential implies a similar orbital for removal of the electron in all cases.

Trimethylsilyl. For many of the disilanes investigated in this work, the determination of radical heats of formation requires a value for $\Delta H_f(SiMe_3^+)$. This particular ion has been the subject of a number of prior investigations and the available data from compounds with reliable heats of formation are summarized in Table IV. The average value of the heat of formation is 176 ± 3 kcal/mol.

The heat of formation of the trimethylsilyl radical has been determined by pyrolysis of hexamethyldisilane. The activation energy for Si–Si cleavage is 67 ± 2 kcal/mol^{-1} which is identified as the bond dissociation energy.[3] Thus

$$2\Delta H_f(SiMe_3) - \Delta H_f[(Me_3Si)_2] = D[(Me_3Si)_2] = 67 \pm 2 \text{ kcal mol}^{-1} \quad (3)$$

Table IV: Energetics of the Formation of the *m/e* 73 Ion Process $RSiMe_3 \rightarrow SiMe_3^+ + R\cdot + e$

R	$\Delta H_f(RSiMe_3)$, kcal/mol	$\Delta H_f(R\cdot)$[a]	A.P.($SiMe_3^+$), eV	$\Delta H_f(SiMe_3^+)$, kcal/mol	Ref
H	−18.1	52.1	10.78 ± 0.07	178.4	b
			10.6 ± 0.1	174.3	c
			10.72 ± 0.1	177.0	d
			10.9 ± 0.2	181.2	e
CH_3	−33.0	34.0	10.53 ± 0.2	175.8	f
			10.63 ± 0.13	178.1	b
			10.4 ± 0.1	172.8	c
			10.53 ± 0.1	175.8	d
			11.3 ± 0.15	193.6	e
			10.25 ± 0.05	169.4	g
C_2H_5	−38.0	25.7	10.53 ± 0.09	179.1	b
			10.3 ± 0.1	173.8	d
$SiMe_3$	−52.0	7.8	10.22 ± 0.18	176	d
		18.6	10.69 ± 0.04	176	b
		2.7	10.0 ± 0.1	176	c
		3.4	10.03 ± 0.1	176	d
		8.5	10.25 ± 0.08	176	h

[a] Unless otherwise noted, radical heats of formation are from J. A. Keer, D. H. Slater, and J. C. Young, *J. Chem. Soc. A*, 134 (1967). [b] G. C. Hess, F. W. Lampe, and L. H. Sommer, *J. Amer. Chem. Soc.*, **87**, 5327 (1965). [c] See ref 5c. [d] See ref 19. [e] B. G. Hobrock and R. W. Kiser, *J. Phys. Chem.*, **66**, 155 (1962). [f] M. F. Lappert, J. Simpson, and T. R. Spalding, *J. Organometal. Chem.*, **17**, P1 (1969). [g] See ref 21. [h] This work.

Using a calculated value of $\Delta H_f(Me_6Si_2)$ = −52.0 kcal in eq 3, one obtains $\Delta H_f(SiMe_3\cdot)$ = 7.5 kcal/mol. Pyrolysis of trimethylsilane[25] and measurement of the initial rates of formation of hydrogen and methane have established the Me_3Si–H bond dissociation energy as 80.3 ± 0.5 kcal/mol. Using ΔH_f(MeSiH) equal to −18.1 kcal/mol, the calculated radical heat of formation is $\Delta H_f(SiMe_3)$ = 10.1 kcal/mol. Combining these two values with the five values in Table IV, the average heat of formation of the trimethyl silyl radical is 8.4 ± 4.9 kcal/mol. Combining the ion and radical heats of formation gives an ionization potential of 7.27 ± 0.34 eV, in agreement with a published value.[2]

Phenyl-Substituted Silyl. The appearance potential data for phenyldimethylsilyl, diphenylmethylsilyl, and triphenylsilyl ions and radicals are given in Tables V, VI, and VII, respectively. The average values of the ion and radical heats of formation are collected in Table VIII. Subtracting the second value from the first leads to the ionization potential of the radical.

Bond Dissociation Energies. Bond dissociation energies calculated from the heats of formation of the radicals and molecules are given in Table VIII. For all the compounds the Si–Si bond dissociation energy increases as phenyls replace methyls. This increasing bond energy is in marked contrast to the ethane series,

(25) I. M. T. Davidson and C. A. Lambert, *Chem. Commun.*, 1276 (1969).

Table V

a. Energetics of Formation of the Phenyldimethylsilyl Ion

Molecule	Fragment	$\Delta H_f(R\cdot)$, kcal mol^{-1}	A.P., eV	$\Delta H_f(Ph\text{-}Me_2Si^+)$, kcal mol^{-1}
$PhMe_2SiSiMe_3$	$\cdot SiMe_3$	8.4	9.86 ± 0.06	199.5
$PhMe_3Si$	$\cdot Me$	34	10.26 ± 0.03	202.0
$PhMe_2SiH$	$\cdot H$	52.1	10.43 ± 0.04	202.6

b. Energetics of Formation of the Phenyldimethylsilyl Radical

Molecule	Ion	$\Delta H_f(R^+)$, kcal mol^{-1}	A.P., eV	$\Delta H_f(Ph\text{-}Me_2Si\cdot)$, kcal mol^{-1}
$PhMe_2SiSiMe_3$	$SiMe_3^+$	176	10.08 ± 0.09	36.7
$(Ph_2MeSi)_2$	$SiPh_3^+$*	250	9.35 ± 0.03	42.9
$(PhMe_2Si)_2$	$SiMe_2Ph^+$	201	9.87 ± 0.08	36.6
$Ph_2MeSiSiMe_3$	$SiMe_2Ph^+$*	201	9.75 ± 0.04	39.3

Table VI

a. Energetics of Formation of the Diphenylmethylsilyl Ion

Compd	Fragment	$\Delta H_f(R\cdot)$, kcal mol^{-1}	A.P., eV	$\Delta H_f(Ph_2\text{-}MeSi^+)$, kcal mol^{-1}
$Ph_2MeSiSiMe_3$	$\cdot SiMe_3$	8.4	9.63 ± 0.02	226.4
$(PhMe_2Si)_2$	$\cdot SiMe_3$*	8.4	9.60 ± 0.02	225.8
Ph_2MeSiH	$\cdot H$	52.1	10.97 ± 0.12	247.4

b. Energetics of Formation of the Diphenylmethylsilyl Radical

Compd	Ion	$\Delta H_f(R^+)$, kcal mol^{-1}	A.P., eV	$\Delta H_f(Ph_2\text{-}MeSi\cdot)$, kcal mol^{-1}
$Ph_2MeSiSiMe_3$	Si^+Me_3	176	10.59 ± 0.03	80.8
$(PhMe_2Si)_2$	Si^+Me_3	176	11.04 ± 0.03	91.3
$Ph_3SiSiMe_3$	Si^+Me_2Ph	201	10.13 ± 0.03	77.6
$(Ph_2MeSi)_2$	Si^+MePh_2	233	9.51 ± 0.05	63.3

where the bond dissociation energy decreases from 88 kcal/mol in ethane to 12 kcal/mol in hexaphenylethane.[26]

It should be noted that the assumption of a constant contribution to ΔH_f from the Si–Si bond does not require a constant Si–Si bond dissociation energy as a consequence. The bond dissociation energy is influenced by steric and electronic effects not only in the disilane (to which our assumption relates), but also in the product silyl radicals. The assumption appears to be a reasonable one: steric crowding in $Ph_3SiSiPh_3$ is certainly less than in Ph_3CCPh_3 (Si–Si length is 2.33 Å, Si–C is 1.90 Å;[27] C–C is 1.58 Å, C–Ph is 1.54 Å.[28]

Table VII

a. Energetics of Formation of the Triphenylsilyl Ion

Compd	Fragment (R·)	$\Delta H_f(R\cdot)$, kcal mol^{-1}	A.P., eV	$\Delta H_f(Ph_3Si^+)$, kcal mol^{-1}
Ph_4Si	$\cdot C_6H_5$	72	9.93 ± 0.08	252.8
Ph_3SiH	$\cdot H$	52.1	9.58 ± 0.08	247.4
$Ph_3SiSiMe_3$	$\cdot SiMe_3$	8.4	9.35 ± 0.03	252.2

b. Energetics of Formation of the Triphenylsilyl Radical

Compd	Ion	$\Delta H_f(R^+)$, kcal mol^{-1}	A.P., eV	$\Delta H_f(Ph_3Si\cdot)$, kcal mol^{-1}
$Ph_3SiSiMe_3$	Si^+Me_3	176	10.83 ± 0.09	118.8
$(Ph_3Si)_2$	Si^+Ph_3	250	9.61 ± 0.09	113.6

Electronic effects on the Si–Si bond might be substantial.[24] As aryl groups draw out p-character in the orbitals from silicon, they must increase the s-character in the Si–Si bond. This would be expected to lead to bond shortening and strengthening, as observed experimentally.

Only about half of the decreased bond energy in Ph_3CCPh_3 is due to steric effects;[29,30] the rest of the bond weakening is due to resonance stabilization in the product $Ph_3C\cdot$ radicals. Whereas $Ph_3C\cdot$ may gain stability by assuming a planar configuration,[29,31] the silicon atom in the $Ph_3Si\cdot$ radical probably retains a pyramidal configuration,[32] just as in the neutral disilane molecule. The stabilization energies of the radicals $Ph_3Si\cdot$ and $Ph_3C\cdot$ with respect to the trimethylated radicals may be calculated by eq 4.

$$\text{S.E. } (Ph_3M\cdot) = \Delta H_f(Ph_3MH) - \Delta H_f(Me_3MH) + \Delta H_f(Me_3M\cdot) - \Delta H_f(Ph_3M\cdot) \quad (4)$$

(26) M. Szwarc, *Chem. Rev.*, **47**, 75 (1950).

(27) (a) L. O. Brockway and J. Y. Beach, *J. Amer. Chem. Soc.*, **60**, 1836 (1938); (b) L. O. Brockway and N. R. Davidson, *ibid.*, **63**, 3287 (1941).

(28) S. H. Bauer and J. Y. Beach, *ibid.*, **64**, 1142 (1942).

(29) M. S. Newman, Ed., "Steric Effects in Organic Chemistry," Wiley, New York, N. Y., 1956, esp Chapter 7, by H. H. Wasserman.

(30) H. E. Bent, G. R. Cuthbertson, M. Dorfman, and R. E. Leary, *J. Amer. Chem. Soc.*, **58**, 165 (1936); H. E. Bent and G. R. Cuthbertson, *ibid.*, **58**, 170 (1936); H. E. Bent and E. S. Ebers, *ibid.*, **57**, 1242 (1935); H. E. Bent and J. E. Cline, *ibid.*, **58**, 1624 (1936).

(31) P. Anderson and B. Klewe, *Acta Chem. Scand.*, **21**, 2599 (1967), and R. D. Allendoerfer and A. H. Maki, *J. Amer. Chem. Soc.*, **91**, 1088 (1969).

(32) H. Sakurai, M. Murakami, and M. Kumada, *ibid.*, **91**, 519 (1969); S. W. Bennett, C. Eaborn, A. Hudson, H. A. Hussain, and R. A. Jackson, *J. Organometal. Chem.* **16**, 36 (1969); Y. Vignollet and J. C. Maire, *Chem. Commun.*, 1187 (1968); R. L. Morehouse, J. J. Christiansen, and W. Gordy, *J. Chem. Phys.*, **45**, 1751 (1966); G. S. Jackel, J. J. Christiansen, and W. Gordy, *ibid.*, **47**, 4274 (1967); A. G. Brook and J. M. Duff, *J. Amer. Chem. Soc.*, **91**, 2118 (1969); M. E. Jacox and D. E. Milligan, *J. Chem. Phys.*, **49**, 3130 (1968); D. E. Milligan, M. E. Jacox, and W. A. Guillory, *ibid.*, **49**, 5330 (1968); P. J. Krusic and J. K. Kochi, *J. Amer. Chem. Soc.*, **91**, 3938 (1969).

Table VIII: Bond Dissociation Energies (kcal/mol)

R	I.P.(R·), eV	$\Delta H_f(R^+)$	$\Delta H_f(R\cdot)$	D(Me_3Si–R)	D(R–R)
Me_3Si	7.27 ± 0.34	176 ± 3	8.4 ± 4.9	67 ± 2	67 ± 2
$PhMe_2Si$	7.03 ± 0.17	200.7 ± 1	39 ± 3	67.1 ± 8	65.3 ± 6
Ph_2MeSi	6.72 ± 0.82	233 ± 9	78 ± 10	73.7 ± 15	78.7 ± 20
Ph_3Si	5.80 ± 0.30	250.8 ± 3	116.2 ± 3	79.6 ± 8	90.4 ± 6

The calculated values of the stabilization energy are given in Table IX. The Ph_3Si radical is 14 kcal/mol less stable than $Me_3Si\cdot$. By contrast, $Ph_3C\cdot$ is 24 kcal/mol more stable than the *tert*-butyl radical. This reversal of relative stabilities on going from carbon to silicon suggests a pyramidal configuration for the Ph_3Si radical because resonance stabilization by phenyl is much less important than destabilization by inductive withdrawal of electrons.

Table IX: Radical and Ion Stabilization Energies

R·	SE(R·), kcal/mol	SE(R^+), kcal/mol
$SiMe_3$	0	0
$SiMe_2Ph$	−1.4	5.3
$SiMePh_2$	−8.1	5.6
$SiPh_3$	−14.0	19.7

The silyl cations, on the other hand, appear to be planar. The I.P. of $R_3Si\cdot$ drops stepwise a total of 1.47 eV, or 11.3 kcal/mol per phenyl, as all the R's are changed from Me to Ph. This increasing ease of ionizing $R_3Si\cdot$ must be due to resonance stabilization of the siliconium ion. It seems that whereas in $Ph_3Si\cdot$ the Si atom is approximately sp^3 hybridized, the Si atom in Ph_3Si^+ is electronegative enough to concentrate s-character in its bonds to phenyl, thereby achieving sp^2 (planar) hybridization. The stabilization energies, calculated by eq 5, are given in Table IX.

$$\text{S.E. } (Ph_3M^+) = \Delta H_f(Ph_3MH) - \Delta H_f(Me_3MH) + \Delta H_f(Me_3M^+) - \Delta H_f(Ph_3M^+) \quad (5)$$

The calculated S.E.'s show that although phenyl destabilizes a silyl radical compared to methyl (probably because of an unfavorable inductive effect), the phenyl group powerfully stabilizes a siliconium ion. The smaller stabilization of Ph_3Si^+ compared with Ph_3C^+ (which is stabilized by 38 kcal/mol over Me_3C^+) can be rationalized on the basis of smaller Si–C overlap (long Si–C bond, poorer matching between Si and C p orbitals[33]) and probably accounts for the nonionization of Ar_3SiCl compounds in solution. The stabilization energy may include some d orbital effects, but the Si 3p orbital probably plays the most important part in accepting electrons.

A positive charge on the disilane molecule evokes behavior in it reminiscent of other electron-deficient species. The bridged intermediate leading to molecular rearrangement may be structurally similar to the corresponding aluminum compounds $(PhMe_2Al)_2$.[34] Indeed, the disilane dication $R_3SiSiR_3^{2+}$ would be isoelectronic with the aluminum compounds. The aluminum dimers are bridged by aryl groups, probably through the participation of Al 3p orbitals.[35]

(33) R. S. Mulliken, C. A. Rieke, D. Orloff, and H. Orloff, *J. Chem. Phys.*, **17**, 1248 (1949).

(34) E. A. Jeffery, T. Mole, and J. K. Saunders, *Aust. J. Chem.*, 21, 137, 649 (1968); D. A. Sanders, J. P. Oliver, *J. Amer. Chem. Soc.*, **90**, 5910 (1968).

(35) G. E. Coates, M. L. H. Green, and K. Wade, "Organometallic Compounds," Methuen and Company, Ltd., London, 3rd ed, 1967, Vol. 1, p 297 ff, but for mention of d orbitals in aluminum compounds, see G. Allegra and G. Perego, *Acta Crystallogr.*, **16**, 185 (1963).

NOTES

Computation of the Statistical Complexions of Molecules and Ions[1]

by K. H. Lau and S. H. Lin*

Department of Chemistry, Arizona State University, Tempe, Arizona 85281 *(Received May 7, 1970)*

Publication costs assisted by the National Science Foundation

The rate constant[2a] for the quasiequilibrium dissociation of an isolated system can be written as[2b]

$$k(E) = \frac{W^{\ddagger}(E - \epsilon_0)}{\mathrm{d}W(E)/\mathrm{d}E} \frac{\sigma}{h} \tag{1}$$

where σ is the symmetry number of the activated complex, ϵ_0 is the activation energy, and $W^{\ddagger}(E - \epsilon_0)$ is the total number of states of the system in the activated complex configuration with the total energy $E - \epsilon_0$. The calculation of $W(E)$ by the first-order steepest-descent method has been given for a system of weakly coupled harmonic oscillators by Lin and Eyring[2b,3] and for a system of anharmonic oscillators and a system of harmonic oscillators coupled with rigid rotors by Tou and Lin.[4] Tou,[5] in a numerical comparison of the current approaches, found that the Laplace-transform technique and the steepest-descent method gave results close to the exact result for a collection of harmonic oscillators. In the present paper, the effect of including the second-order terms of the method of steepest descent is given. The calculated results for different molecules are compared with exact results, those from the first-order approximation, and those from the method of Hoare and Ruijgrok.[6]

For a collection of m harmonic oscillators of frequencies $\nu_1, \nu_2, \ldots \nu_m$, having degeneracies $g_1, g_2, \ldots, g_m$, respectively, it has been shown that the total number of quantum states $W(E)$ of energy E can be evaluated by Cauchy's residue theorem as[2b,3]

$$W_c(E) = \frac{1}{2\pi i} \int_{\gamma} \frac{\mathrm{d}z}{z} [\phi(z)]^{\langle n \rangle} \tag{2}$$

where $\langle n \rangle = E/h\langle \nu \rangle$

$$[\phi(z)]^{\langle n \rangle} = \frac{z^{-\langle n \rangle - 1} - 1}{z^{-1} - 1} \prod_{i=1}^{m} (1 - z^{\nu_i/\langle \nu \rangle})^{-g_i} \tag{3}$$

and γ is any contour lying within the circle of convergence of the power series enclosing the origin $z = 0$. The quantity $\langle \gamma \rangle$ in eq 3 and 4 is so chosen that the $\nu_i/\langle \nu \rangle$ values are integers. The result from the first-order approximation of the steepest-descent method is[3]

$$W_{c_1}(E) = \frac{\theta^{-\langle n \rangle - 1} - 1}{\theta^{-1} - 1} \prod_{i=1}^{m} (1 - \theta^{\nu_i/\langle \nu \rangle})^{-g_i} \times \left[\frac{1}{2\pi \langle n \rangle \theta^2 \phi''(\theta)/\phi(\theta)}\right]^{1/2} \tag{4}$$

where θ is the root of the equation

$$\frac{\langle n \rangle + 1}{1 - \theta^{\langle n \rangle + 1}} = \frac{\theta^{-1}}{\theta^{-1} - 1} + \sum_{i=1}^{m} \frac{g_i(\nu_i/\langle \nu \rangle)}{\theta^{-\nu_i/\langle \nu \rangle} - 1} \tag{5}$$

By applying the method of steepest descent to second-order approximations,[7] we obtain

$$W_{c_2}(E) = W_{c_1}(E) C(\theta, \langle n \rangle) \tag{6}$$

where

$$C(\theta, \langle n \rangle) = \left[1 + \frac{1}{8} \frac{B\langle n \rangle}{(\langle n \rangle \theta^2 \phi''(\theta)/\phi(\theta))^2} - \frac{5}{24} \frac{A^2 \langle n \rangle^2}{(\langle n \rangle \theta^2 \phi''(\theta)/\phi(\theta))^3}\right] \tag{7}$$

A and B are defined by

$$A = -\left[3\theta^2 \frac{\phi''(\theta)}{\phi(\theta)} + \frac{\theta^3 \phi'''(\theta)}{\phi(\theta)}\right] \tag{8}$$

and

$$B = 7\theta^2 \frac{\phi''(\theta)}{\phi(\theta)} + 6\theta^3 \frac{\phi'''(\theta)}{\phi(\theta)} + \theta^4 \frac{\phi''''(\theta)}{\phi(\theta)} - 3\theta^4 \left[\frac{\phi''(\theta)}{\phi(\theta)}\right]^2 \tag{9}$$

where $\phi''(\theta)$, $\phi'''(\theta)$ and $\phi''''(\theta)$ are the second, third, and fourth derivatives of $\phi(z)$ with respect to z, evaluated at $z = \theta$, respectively.

Substituting eq 7–9 into eq 6 and using the condition given in eq 5, the total quantum states $W_{c_2}(E)$ for a collection of harmonic oscillators can be computed. It should be noticed that the results obtained from the first-order approximation, $W_{c_1}(E)$, are greater than those of exact counting, and also greater than those from $W_{c_2}(E)$ given in eq 6, because the correction term

(1) Supported by the National Science Foundation and the Alfred P. Sloan Foundation.

(2) (a) H. M. Rosenstock, M. B. Wallenstein, A. L. Wahrhaftig, and H. Eyring, *Proc. Acad. Sci. U. S.*, **38**, 667 (1952); (b) S. H. Lin and H. Eyring, *J. Chem. Phys.*, **39**, 1577 (1963).

(3) S. H. Lin and H. Eyring, *ibid.*, **43**, 2153 (1965).

(4) J. C. Tou and S. H. Lin, *ibid.*, **49**, 4187 (1968).

(5) J. C. Tou, *J. Phys. Chem.*, **71**, 2721 (1967).

(6) M. R. Hoare and Th. W. Ruijgrok, *J. Chem. Phys.*, **52**, 113 (1970); M. R. Hoare, *ibid.*, **52**, 5695 (1970).

(7) R. H. Fowler, "Statistical Mechanics," 2nd ed, Cambridge University Press, New York, N. Y., 1965, p 16.

Table I: $W(E)$ for Artificial Harmonic Oscillator System

$\langle n \rangle$	1	2	3	4	5	6
θ	0.1862	0.2899	0.3653	0.4246	0.4716	0.7375
W_{exact}	4.00	12.00	29.0	62.0	120.00	217.00
W_{c_1}	4.4085	12.8501	30.2733	64.0720	123.7573	223.0012
W_{c_2}	3.9905	11.9917	28.9715	61.8702	120.0569	217.0916

Table II: Comparison of Calculated Values and the Exact Values of $W(E)$ for Water Molecule[a]

E (eV)	W_{exact}	W_{c_1}	W_{c_2}	θ	$C(\theta,\langle n \rangle)$	$W(E)$[b]
0.4336	3	3.234	3.014	0.99890793	0.93147	3.54
0.8672	11	10.766	10.429	0.99929048	0.96866	11.23
1.3008	23	24.828	24.275	0.99946766	0.97773	25.52
1.7435	46	47.439	46.544	0.99957238	0.98113	48.43
2.1685	78	80.625	79.229	0.99964213	0.98268	82.00
4.3361	466	474.520	467.076	0.99980181	0.98341	479.5
6.5042	1405	1432.457	1409.996	0.99986272	0.98429	1444.0

[a] Frequencies: 3652, 2595, 3756 (cm^{-1}). $\langle \nu \rangle = 2$ cm^{-1}. [b] Results of Hoare and Ruijgrok (ref 6).

$C(\theta,\langle n \rangle)$ defined in eq 7 is less than one. In order to test $W_{c_2}(E)$, we choose the artificial system of 3 oscillators, $\nu_1 = \langle \nu \rangle$, $\nu_2 = 2\langle \nu \rangle$, $\nu_3 = 3\langle \nu \rangle$ with $g_1 = 3$, $g_2 = 2$, and $g_3 = 1$, respectively. The results are shown in Table I. It can be seen that the second-order approximation gives an excellent agreement with the results from exact counting for the artificial model (Table I). This may be due to the fact that for the artificial model both $\nu_1/\langle \nu \rangle$ and $\langle n \rangle$ are integers, which is required in the application of the Cauchy's residue theorem.

A numerical comparison is made of $W_{c_1}(E)$ and $W_{c_2}(E)$ with the method of Hoare and Ruijgrok,[6] as applied to a water molecule. The results are tabulated in Table II. Table II shows that $W_{c_2}(E)$ is in good agreement with exact counting and is better than $W_{c_1}(E)$.

To compare the present method with that of Hoare and Ruijgrok,[6] we rewrite eq 2 as[3]

$$W_c(E) = \frac{1}{2\pi i} \sum_{\langle n \rangle = 0}^{\langle n \rangle} \int_\gamma \frac{dz}{z^{\langle n \rangle + 1}} \prod_{i=1}^{m} (1 - z^{\nu_i/\langle \nu \rangle})^{-g_i} \quad (10)$$

If the summation over $\langle n \rangle$ in eq 10 is carried out, we obtain eq 2. Applying the method of steepest descent to eq 10, we find

$$W_{c_1}(E) = \sum_{\langle n \rangle = 0}^{\langle n \rangle} \frac{\prod_i^m (1 - \theta^{\nu_i/\langle \nu \rangle})^{-g_i}}{\theta^{\langle n \rangle} \left[2\pi \sum_i^m \frac{g_i (\nu_i/\langle \nu \rangle)^2 \theta^{\nu_i/\langle \nu \rangle}}{(1 - \theta^{\nu_i/\langle \nu \rangle})^2} \right]^{1/2}} \quad (11)$$

where θ is determined from

$$\langle n \rangle = \sum_i^m \frac{g_i \frac{\nu_i}{\langle \nu \rangle}}{\theta^{-\nu_i/\langle \nu \rangle} - 1} \quad (12)$$

If we let $\theta = e^{-\beta h \langle \nu \rangle}$ and $\epsilon_i = h\nu_i$, eq 11 and 12 become

$$W_{c_1}(E) = \sum_{\langle n \rangle = 0}^{\langle n \rangle} h\langle \nu \rangle \frac{e^{\beta \epsilon} \prod_i^m (1 - e^{-\beta \epsilon_i})^{-g_i}}{\left[2\pi \sum_i^m \frac{g_i \epsilon_i^2 e^{-\beta \epsilon_i}}{(1 - e^{-\beta \epsilon_i})^2} \right]^{1/2}} \quad (13)$$

and

$$\epsilon = \sum_i^m \frac{g_i \epsilon_i}{e^{\beta \epsilon_i} - 1} \quad (14)$$

Comparing the general term without the factor $h\langle \nu \rangle$ in eq 13 with the expression of the density of states obtained by Hoare and Ruijgrok (*cf.* eq 5.1 of ref 6), we can see that they are identical. This is because the total number of states $W(E)$ and the density of states $\rho(E)$ are related by $\lim_{\Delta E \to 0} [W(E + \Delta E) - W(E)]/\Delta E = \rho(E)$ and $h\langle \nu \rangle$ plays the role of ΔE in this case. Thus as far as the calculation of the density of states is concerned, these two methods would give identical results. The approaches adopted in calculating the total number of states are however different in these two methods (*cf.* eq 3.1–3.3 of ref 6). Thus one may expect that the total number of states obtained from these two methods may be slightly different.

From the above numerical calculations, we can see that the correction term $C(\theta,\langle n \rangle)$ will approach unity when the internal energy E increases. According to this, the calculated results from $W_{c_1}(E)$ will be close to those from $W_{c_2}(E)$ in high energy range. In other words, the higher energy range, $W_{c_1}(E)$ is sufficient and one does not need to use the second-order approximation expression $W_{c_2}(E)$. Although in this communication, we presented the derivation of $W_{c_2}(E)$ only for a

system of harmonic oscillators, the derivation of $W_{c2}(E)$ for other cases can be easily carried out.

Acknowledgments. The authors wish to thank the referees for some helpful suggestions.

Singlet–Triplet Absorption Spectrum of *all-trans*-Retinal[1]

by Rodger A. Raubach and Anthony V. Guzzo*

Chemistry Department, University of Wyoming, Laramie, Wyoming 82070 *(Received September 2, 1970)*

Publication costs borne completely by The Journal of Physical Chemistry

Since *all-trans*-retinal does not measureably phosphoresce, the energy of the first triplet state (T_1) is known only approximately from the recent energy-transfer studies of Guzzo and Pool,[2] who estimated $E_{T(0-0)}$ = 38 kcal. This estimate required the assumption of a bandwidth for the triplet manifold of 12 kcal, the measured bandwidth of the triplet manifold in the π electron analog of retinal–dodeca-2,4,6,8,-10-pentaenal. Due to the importance of retinal as the primary photoreceptor chromophore in the visual process, it would be highly desirable to have a more direct measurement of the energy and bandwidth of its first triplet state.

The present communication describes work carried out to determine the singlet–triplet absorption spectrum of *all-trans*-retinal by means of the oxygen perturbation technique. A comparison is also made between these data and the triplet state energies found by Evans[3] for dodeca-2,4,6,8,10-pentaenal and deca-2,4,6,8-tetraenal.

Experimental Section

The solvent used for these studies was Baker reagent grade carbon tetrachloride. *all-trans*-Retinal was supplied by Sigma Chemical Company, St. Louis, Mo., and was used directly without further purification.

A high-pressure optical cell with a 5-cm path length was supplied by American Instrument Company, Silver Spring, Md., and all spectra were obtained using a Cary 14 spectrophotometer.

Two sample concentrations were necessary to accurately determine the positions of all bands. These samples were prepared immediately before use by dissolving either 1.0 or 2.0 g of retinal in carbon tetrachloride to make 10 ml of solution. The optical cell was then filled and a spectrum obtained at atmospheric pressure. The cell was then pressurized to 2150 psi oxygen, shaken intermittently for 3 hr, and a spectrum was taken. (Further shaking did not increase the intensity of the new spectral bands observed.) The pressure was then released with agitation to drive out the dissolved oxygen and the spectrum retaken. Those bands which appeared when oxygen pressure was applied and then disappeared when the pressure was released were attributed to singlet–triplet absorptions. A solvent blank in the same spectral region showed no interfering absorptions.

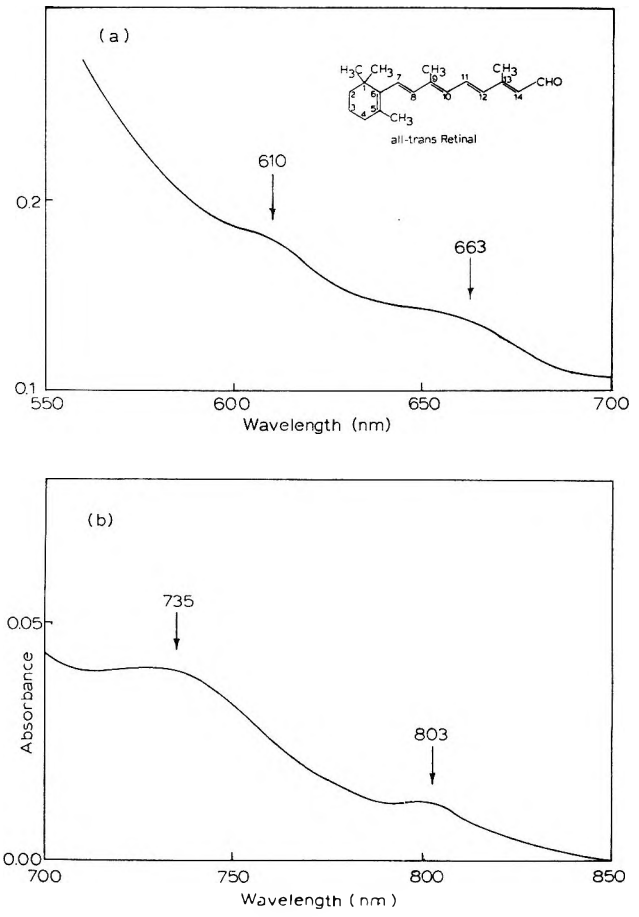

Figure 1. Singlet–triplet absorption spectrum of *all-trans*-retinal in the region 550–850 nm under 2150 psi of oxygen pressure. (a) Retinal concentration 1.0 g/10 ml. (b) Retinal concentration 2.0 g/ml. Absorption maxima are indicated by arrows. Limits of experimental error appear to be ±5 nm.

The wavelength range scanned was 900–550 nm, the Cary 14 IR-1 detector used over the range 900–750 nm and photomultiplier 750–550 nm.

Results and Discussion

The spectra obtained for *all-trans*-retinal revealed no irreversible changes due to the application of oxygen pressure, and all bands which appeared during pressurization to 2150 psi oxygen disappeared with removal of pressure.

The oxygen perturbation spectrum is presented in Figure 1. In general, the absorption observed was

(1) This work has been supported in part by the United States Atomic Energy Commission through Contract No. AT(II-I)-1627.

(2) A. V. Guzzo and G. L. Pool, *J. Phys. Chem.*, **73**, 2512 (1969).

(3) D. F. Evans, *J. Chem. Soc.*, **1960**, 1735.

very weak and the pressure-dependent extinction coefficients were not measured. We have indicated the positions of the definite shoulders in the spectrum. These were obtained reproducibly in numerous runs.

The lowest energy band that is visible is at 803 nm and we have assigned this to the (0–0) singlet–triplet transition. Progressing upwards, the energies of all observed shoulders are given in Table I. For comparison we have also listed the energies obtained by Evans for the manifold of bands in dodeca-2,4,6,8,10-pentaenal and deca-2,4,6,8-tetraenal. Evans' data were also obtained by oxygen perturbation methods.

Table I: Triplet State Energies and Total Bandwidths of Retinal, Dodeca-2,4,6,8,10-pentaenal, and Deca-2,4,6,8-tetraenal (Energies in cm^{-1})

Retinal[a]	Dodeca-2,4,6,8,10-pentaenal[b]	Deca-2,4,6,8-tetraenal[b]
16,400	14,950	16,970
15,100	13,700	15,560
13,600	12,400	14,160
12,450	11,050	12,700
	Bandwidths	
3950 cm^{-1}	3900 cm^{-1}	4270 cm^{-1}

[a] Measured in carbon tetrachloride solution. [b] Measured in chloroform solution.

It is possible that there is a change in geometry in the triplet state relative to the ground state. The most intense band observed was assigned to the 0–1 transition. The 0–0 band, on the other hand, was the weakest observed transition. If there is a geometry change, this band may be Franck–Condon forbidden.

Another important point to be emphasized is that the energy of the retinal triplet, 35 kcal, is intermediate in energy to the pentaenal and tetraenal triplets. We would expect the retinal ground-state π electron framework to be somewhat different from that found in the pentaenal compound as a result of the steric influences found near the cyclohexene ring. The interaction between the methyl groups at positions 1 and 5 and the protons on carbons 7 and 8 result in a large twisting distortion about the 6–7 bond, resulting in a net lowering of the extent of conjugation in the ground state. Although no measurement of the angle of twist has been made for retinal in solution, X-ray data have indicated an angle of twist near 45° for the carboxylic acid derivative, retinoic acid in the solid state.[4] Furthermore, Pullman, Langlet, and Berthod[5] computed an angle of twist of 40° for retinal about the 6–7 bond by means of extended Hückel calculations.

A further difference between retinal and pentaenal is, of course, the extent of methyl group substitution on the former. Work is now in progress aimed at determining which factors are important in fixing the excited-state energies of these systems.

(4) C. H. Stam and C. H. McGillavry, *Acta Crystallogr.*, **16**, 62 (1963).

(5) B. Pullman, J. Langlet, and H. Berthod, *J. Theoret. Biol.*, **23**, 492 (1969).

A Rittner Ionic Model Study of Alkali Hydride Dimers[1]

by A. Companion,* J. R. Tyndall, and A. Studencki

Department of Chemistry, Illinois Institute of Technology, Chicago, Illinois 60616 *(Received September 28, 1970)*

Publication costs assisted by the National Science Foundation

In a recent application[2a] of diatomics-in-molecules (DIM) theory[2b] a diamond-shaped dimer $(LiH)_2$ was predicted to be stable with respect to both diatomic systems $Li_2 + H_2$ and 2LiH. The similarity in shape of this species to the much studied[3] gaseous alkali metal halide dimers prompted us to compute the dimerization energy and fundamental vibrational frequencies of $(LiH)_2$ with one of the ionic models previously applied to halide analogs.

According to Varshni and Shukla,[4] the potential energy function suggested by Rittner[5] reproduces quite well the ionic binding energies (D_i) of diatomic alkali halides and, with a semiempirical value for the polarizability (α) of H^-, reproduces D_i for LiH with only a 0.3% error. The Rittner model has been applied to alkali metal halide dimers with considerable success by O'Konski and Higuchi[6] and by Berkowitz.[7]

In the calculations described here a program based on the original O'Konski formulation[6a,8] was devised to permit optimization of the dipole interaction energy at each fixed nuclear position of interest on the potential energy surface of the dimer. After a search for the optimum geometry, fundamental vibrational frequencies were computed numerically with a least-squares adapta-

(1) Supported in part by a grant from the National Science Foundation.

(2) (a) J. R. Tyndall and A. L. Companion, *J. Chem. Phys.*, **52**, 2036 (1970); (b) F. O. Ellison, *J. Amer. Chem. Soc.*, **85**, 3540 (1963).

(3) A. Snelson, *J. Phys. Chem.*, **73**, 1919 (1969), and references therein.

(4) (a) Y. P. Varshni and R. C. Shukla, *J. Chem. Phys.*, **35**, 582 (1961); (b) *Rev. Mod. Phys.*, **35**, 130 (1963).

(5) E. S. Rittner, *J. Chem. Phys.*, **19**, 1030 (1951).

(6) (a) C. T. O'Konski, *ibid.*, **23**, 1174 (1955); (b) C. T. O'Konski and W. I. Higuchi, *ibid.*, **23**, 1175 (1955).

(7) (a) J. Berkowitz, *ibid.*, **29**, 1386 (1958); (b) J. Berkowitz, *ibid.*, **32**, 1519 (1960).

(8) Since there appears to be a sign error in the dimer energy equations presented by Berkowitz[7a] and a typographical error in the similar equations of O'Konski and Higuchi,[6b] we rederived the O'Konski equations[6a] from fundamental theory as outlined by C. F. J. Böttcher, "Theory of Electric Polarization," Elsevier, Amsterdam, 1952.

tion of the mass-weighted Cartesian coordinate method described by Huff and Ellison.[9] The Rittner parameters employed for LiH were those of Varshni and Shukla[4b] with $\alpha(H^-) = 1.80$ Å^3. van der Waals attractions and Born–Mayer repulsions between like atoms were neglected, since constants appropriate to $(LiH)_2$ are not known, and our own studies of alkali halide dimers indicate that these interaction energies are quite small and generally cancel one another. The results of our calculations are presented in Table I, along with values previously computed with DIM theory.[2a] The group theoretical designations for the vibrations follow those of Berkowitz. Dimerization energies refer to the process $2LiH \rightarrow (LiH)_2$ and are quoted without zero-point energy corrections.

Table I: Comparative DIM and Rittner Model Results for $(LiH)_2$

Method	Dimerization energy, kcal/mol	R(Li–Li), Å	R(H–H), Å	Fundamental vibrational frequencies, cm^{-1} A_g	A_g'	B_{1g}	B_{1u}	B_{2u}	B_{3u}
Rittner	24.9	2.30	3.34	1630	423	872	560	885	1237
DIM	31.2	2.83	2.12	1184	438	726	371	885	1124

Despite the fact that the DIM approach includes no ionic contribution to bonding other than that intrinsic to the diatomic potential curves used and that the Rittner model permits no covalent-type electron exchange (only dipole polarization), the $(LiH)_2$ dimerization energies predicted by both these models are comparable, 24.9 and 31.2 kcal/mol. At present this prediction awaits experimental verification.

The internuclear separations predicted by the two approaches differ considerably; in particular, the H–H distance in the covalent model is much smaller. It is tempting to believe that the DIM shape is the more likely, especially since Rittner-type calculations[7] on $(LiCl)_2$ have predicted an Li–Li separation smaller than and a Cl–Cl separation larger than the experimental values.[10]

The true fundamental vibrational frequencies of the molecule are probably between the two extremes of Table I. Despite the dissimilarity in the models, these frequencies are in reasonable accord and order approximately the same. [The DIM out-of-plane bending frequency (B_{1u}) was previously[2a] considered anomalous when compared to predicted frequencies of lithium halide dimers and is probably too small.]

Since the dimerization energy prediction for $(LiH)_2$ appeared credible, the Rittner model was also applied to other possible alkali hydride dimers, none easily treated with the DIM method because of inadequate diatomic potential curve data. Results are listed in Table II, where the dimerization energies are taken as the difference between computed ionic binding energies of dimers and monomers. Note that the predicted dimerization energy of $(LiH)_2$ is lower than expected from the trend shown by others in the series, an apparent anomaly not evident in *halide* dimer series.[7a] Since the trend in dissociation energies (D_i) for the *diatomic* hydrides is monotonic,[4b] one cannot justifiably attributed the low $(LiH)_2$ value to covalent tendencies of the lithium atom; similarly, inadequacies intrinsic to the ionic model *per se* cannot be totally responsible since the Rittner D_i for diatomic LiH agrees so well with experiment. Instead, the nonmonotonic trend in dimerization energies *and* the disagreement between ionic and DIM predicted shapes of the molecule may be due to the use in the present treatment of a Born–Mayer repulsion constant for unlike atoms that was derived from *diatomic* LiH data. Rothberg[11] has suggested that the constant A in the repulsion term $A\exp(-r/\rho)$ should itself be a function of internuclear distance and has proposed two approximations describing interpolation of a dimer A from diatomic and crystal data. Unfortunately there appears to be inadequate unequivocal data on crystalline LiH to permit this approach at present. For most alkali halide dimers considered, Rothberg's total dimer energies appear to be from 4 to 20 kcal/mol lower than those computed by Berkowitz, with the larger differences occurring for dimers of *lithium* halides. Such a disproportionate shift downward in our computed alkali halide dimer energies could produce a monotonic dimerization energy trend. We are currently investigating the Hafemeister–Zahrt[12] exchange-charge-model calculations of the Born–Mayer repulsion potential in an attempt to find an appropriate description of the variation of A with r in alkali hydride clusters.

Table II: Rittner Model Predictions for Alkali Metal Hydride Dimers

Dimer	R(M–M), Å	R(H–H), Å	Dimerization energy, kcal/mol
(LiH_2)	2.30	3.34	24.9
$(NaH)_2$	2.89	3.68	26.4
$(KH)_2$	3.68	4.03	25.0
$(RbH)_2$	3.99	4.12	23.8
$(CsH)_2$	4.36	4.18	21.8

(9) N. T. Huff and F. O. Ellison, *J. Chem. Phys.*, **42**, 364 (1965).
(10) S. H. Bauer, T. Ino, and R. F. Porter, *ibid.*, **33**, 685 (1960).
(11) G. M. Rothberg, *ibid.*, **34**, 2069 (1961).
(12) D. W. Hafemeister and J. D. Zahrt, *ibid.*, **47**, 1423 (1967).

Rate of the Reaction of the Ammoniated Electron with the Ammonium Ion at −35°[1]

by J. M. Brooks and R. R. Dewald*

Department of Chemistry, Tufts University, Medford, Massachusetts 02155 *(Received December 7, 1970)*

Publication costs assisted by the National Science Foundation

Kinetic studies of the reactions of sodium with weak acids in liquid ammonia have been interpreted in terms of the following scheme

$$HA + NH_3 \underset{k_2}{\overset{k_1}{\rightleftharpoons}} NH_4^+ + A^- \qquad (1)$$

$$e_{am}^- + NH_4^+ \xrightarrow{k_3} NH_3 + {}^1/_2H_2 \qquad (2)$$

where HA represents water,[2] urea,[3] hydrazine,[4] ethanol,[5] and *tert*-butyl alcohol.[2] Analyses of the kinetic data for these reactions yield values for k_1 and k_2/k_3. If the equilibrium constants were known with certainty,[2,5-8] then one could calculate k_2 and k_3. However, estimates of k_3 have varied from 10^6 to 10^{10} M^{-1} sec^{-1}.[2,3] We have measured k_3 directly at −35° by reaction of solutions of sodium with ammonium bromide in liquid ammonia using the stopped-flow technique.

Experimental Section

The thermostated stopped-flow apparatus used in this study has been described elsewhere.[9] All operations including solution make-up, solution transfer, rapid mixing, and observation were performed *in vacuo*. The progress of the reaction was followed by monitoring the absorbance decay of the solvated electron at 1000 nm where the extinction coefficient is about 10^4.[10] The path length of the observation tube was calibrated by comparing the transmittance of acetone solutions of Kodak Q-switching dye no. 9740 as determined on a Perkin-Elmer 450 spectrophotometer and on the flow apparatus. The effective path was about 0.85 mm for a nominal diameter of 1 mm.

Ammonia was purified using procedures described elsewhere[11] and the concentration of the metal–ammonia solutions was determined conductometrically using methods and data published elsewhere.[12,13] Solutions of ammonium bromide (Fisher, reagent) were prepared by adding an appropriate amount of the aqueous salt solution to the make-up vessel followed by evaporation of the water on the vacuum line. In some experiments sodium bromide (J. T. Baker, USP, experiments 5–7; Alfa Inorganics, ultrapure, experiments 17, 18) or sodium iodide (Matheson Coleman and Bell, reagent, experiments 2–4; Alfa Inorganics, ultrapure, experiment 18) was added to the ammonium bromide solution in order to take advantage of the kinetic salt effect to slow the reaction rate.

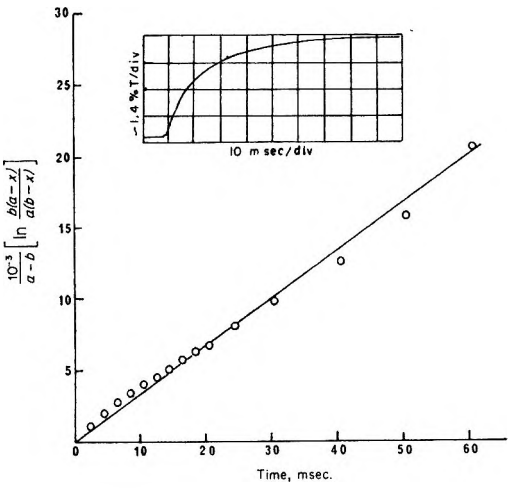

Figure 1. A typical oscilloscope trace and a plot of $[1/(a - b)] \ln [b(a - x)/a(b - x)]$ *vs.* time for experiment no. 17.

Results and Discussion

If the reaction is first order with respect to each of the reactants then a plot of $1/(a - b) \ln [b(a - x)/a(b - x)]$ *vs.* t should give a straight line with zero intercept, where a and b are the initial concentrations of ammonium ions and ammoniated electrons and x is the electron concentration at time t. The linearity of a typical second-order plot is shown in Figure 1. In experiments in which the ammonium ion concentration was sufficiently greater than the sodium concentration, the appropriate pseudo-first-order plots were also linear. In all cases the plots were linear for at least 3 half-lives or about 88% of the reaction, indicating that the reaction is second order overall. The value of the observed k_3, eq 2, was computed for each experiment. Tables I and II summarize the rate experiments.

Comparison of ammoniated electron concentration obtained from conductivity data with the concentration estimated spectrophotometrically provides a good estimate of the amount of decomposition of the sodium–ammonia solution that occurred during solution trans-

(1) Presented in part before the Physical Chemistry Division at the 160th National Meeting of the American Chemical Society, Chicago, Ill., Sept 1970.

(2) R. R. Dewald and R. V. Tsina, *J. Phys. Chem.*, **72**, 4520 (1968).

(3) W. L. Jolly and L. Prizant, *Chem. Commun.*, 1345 (1968).

(4) J. Belloni, *Int. J. Radiat. Phys. Chem.*, **1**, 411 (1969).

(5) R. R. Dewald, "Metal-Ammonia Solutions, International Conference," Butterworths, London, 1970, p 193.

(6) M. Herlem, *Bull. Soc. Chim. Fr.*, 1687 (1967).

(7) D. R. Clutter and T. J. Swift, *J. Amer. Chem. Soc.*, **90**, 601 (1968).

(8) M. Alei and A. E. Florin, *J. Phys. Chem.*, **73**, 857 (1969).

(9) R. R. Dewald and J. M. Brooks, *Rev. Sci. Instrum.*, **41**, 1612 (1970).

(10) M. Gold and W. L. Jolly, *Inorg. Chem.*, **1**, 818 (1962).

(11) R. R. Dewald and J. H. Roberts, *J. Phys. Chem.*, **72**, 4224 (1968).

(12) R. R. Dewald, *ibid.*, **73**, 2615 (1969).

(13) R. R. Dewald and K. W. Browall, *Chem. Commun.*, 1511 (1968).

Table I: Summary of the Kinetic Data for the Reaction of the Ammoniated Electron with the Ammonium Ion in Liquid Ammonia at −35° (Experiments with No or Low Concentration of Added Salt)

Expt no.	10^4[NH_4Br], M	10^6[e_{am}^-], M	10^3[salt], M	$10^{-6}k_{obsd}$ M^{-1} sec^{-1}	$10^{-6}k_{corr}$ M^{-1} sec^{-1}
6	2.7	12.0[a]	67.0[b]	1.6	1.4
12	0.38	3.4	None	11.0	1.4
15	1.6	5.0	None	9.3	1.3
16	2.0	1.8	None	6.2	0.91
17	2.0	2.0	5.3[b]	2.8	0.95
18	2.0	3.4	5.8[b]	1.5	1.2
19	2.0	3.2	6.3[c]	3.6	1.4
Av					1.2 ± 0.2[d]

[a] Cs metal; in all other experiments, Na was used. [b] NaBr. [c] NaI. [d] Standard deviation.

Table II: Summary of the Kinetic Data for the Reaction of the Ammoniated Electron with the Ammonium Ion in Liquid Ammonia at −35° (Experiments with High Concentrations of Added Salt)

Expt no.	10^4[NH_4Br], M	10^4[e_{am}^-], M	10[salt], M	$10^{-6}k_{obsd}$, M^{-1} sec^{-1}	$10^{-6}k_{corr}$, M^{-1} sec^{-1}
2	5.8	0.68	2.0[b]	3.3	5.9
3	5.6	0.77	2.1[b]	2.2	4.0
4	5.1	0.51	2.0[b]	3.1	5.6
5	5.0	2.6	3.6[c]	1.5	2.7
7	5.8	1.5[a]	4.2[c]	1.1	2.1
Av					4.1 ± 1.7[d]

[a] Cs metal; in all other experiments, Na was used. [b] NaI. [c] NaBr. [d] Standard deviation.

fer. This decomposition was found to be sufficiently small such that it did not affect the values of the observed rate constant, *i.e.*, within experimental error (±20%).

The observed rate constants (k_{obsd}) were corrected for the kinetic salt effect[13,14] according to

$$\log (k_{cor}/k_{obsd}) = 9.77\mu^{1/2}/(1 + 3.14\mu^{1/2}) \quad (3)$$

Equation 3 was derived from Brönsted–Bjerrum theory of ionic reaction combined with the extended Debye–Hückel theory assuming a mean value for the distance of closest approach of 4.5 Å, a density of 0.6825 g/ml, and a dielectric constant of 21.8 for liquid ammonia at −35°. The ionic strength was estimated by using an ion-pairing dissociation constant of 2.9×10^{-3} for NaBr[15] and 5.6×10^{-3} for NaI. The value used for NaI was estimated by using the Fuoss theory.[16]

The corrected values of the rate constant given in Table II (high added salt concentration) vary from about 2 to 6×10^6 M^{-1} sec^{-1}, while the values given in Table I (little or no added salt) are fairly consistent with an average value of about 1.2×10^6 M^{-1} sec^{-1}. We feel that the discrepancy between the values given in the two tables probably results from the fact that the equations and constants derived or measured for dilute solutions cannot be expected to yield very reliable results in the high concentration region. It should also be noted that the added salts in the experiments listed in Table II might contain sufficient impurities that could result in an increase in the observed rate. Therefore, we feel that the best value for the corrected second-order rate constant is the value given in Table I, *i.e.*, $1.2 \pm 0.2 \times 10^6$ M^{-1} sec^{-1} at −35°.

The simplest interpretation of our results assumes that the rate-limiting step is a → b in the scheme

$$\underset{a}{(e_{am}^-)} + NH_4^+ \longrightarrow \underset{b}{NH_4} \dashrightarrow \underset{c}{{}^1/_2H_2 + NH_3} \quad (4)$$

The ammonium radical might be expected to react further as

$$2NH_4 \longrightarrow 2NH_3 + H_2 \quad (5)$$

The second-order rate constant obtained in this study is in good agreement with the value reported for the reaction of the hydrated electron with the ammonium ion in aqueous solutions,[17] the value estimated by Dewald and Tsina,[2] and the value determined from pulse radiolysis studies in liquid ammonia.[18]

Acknowledgement. This research was supported by the National Science Foundation.

(14) G. V. Buxton, F. S. Dainton, and M. Hammerli, *J. Chem. Soc.*, 1191 (1967).

(15) V. F. Hnizda and C. A. Kraus, *J. Amer. Chem. Soc.*, 71, 1565 (1949).

(16) R. M. Fuoss, *ibid.*, 80, 5059 (1958).

(17) M. Anbar and P. Neta, *Int. J. Radiat. Isotopes*, 18, 493 (1967)

(18) J. L. Dye, M. G. de Backer, and L. M. Dorfman, *J. Chem. Phys.*, 52, 6251 (1970).

Kinetics and Thermochemistry of the Gas-Phase Bromination of Bromoform. The C–H Bond Dissociation Energy in $CHBr_3$ and the C–Br Bond Dissociation Energy in CBr_4[1a]

by Keith D. King,[1b] David M. Golden,* and Sidney W. Benson

Department of Thermochemistry and Chemical Kinetics, Stanford Research Institute, Menlo Park, California 94025

(Received December 9, 1970)

Publication costs borne completely by The Journal of Physical Chemistry

There are some surprising differences in the quoted values for the heat of formation of bromomethanes. According to the most recent NBS Table,[2a] $\Delta H_f°_{298}$·(CH_3Br) = −8.4, $\Delta H_f°_{298}$($CHBr_3$) = 4, and $\Delta H_f°_{298}$·

Table I: Kinetic and Equilibrium Data for the Bromination of $CHBr_3$

Temp, °C	$[Br_2]_0$, Torr	$[CHBr_3]_0$, Torr	$-10^2(d[Br_2]/dt)_i$, Torr/sec	$10^5K^{1/2}_{Br_2}$, $Torr^{1/2}$	$10^{-5}k_1$, M^{-1} sec^{-1}	$[Br_2]_e$, Torr	K_{eq}[a]
313.8	14.2	10.65	4.1	4.06	0.92	9.1	0.516
314.5	5.0	13.6	3.72	4.17	1.08		
316.5	5.25	6.64	2.1	4.45	1.14	2.8	0.508

[a] $K_{eq} = \{[CBr_4]_e[HBr]_e\}/\{[Br_2]_e[CHBr_3]_e\}$.

(CBr_4) = 19 kcal/mol. In an earlier compilation[2b] they listed $\Delta H_f°_{298}(CHBr_3)$ = 6.0 and $\Delta H_f°_{298}(CBr_4)$ = 12.0 kcal/mol. Bernstein[3] has developed an interaction scheme for predicting the thermochemical properties of halomethanes, and he estimates $\Delta H_f°_{298}(CH_3$–Br) = −8.9, $\Delta H_f°_{298}(CH_2Br_2)$ = 3, $\Delta H_f°_{298}(CHBr_3)$ = 19, and $\Delta H_f°_{298}(CBr_4)$ = 38 kcal/mol, with an estimated uncertainty of about ±2 kcal/mol.

Using Bernstein's values for the heats of formation of CH_2Br_2, $CHBr_3$, and CBr_4, combined with an estimate of $DH°(CBr_3$–Br) = 61 kcal/mol, Furuyama, Golden, and Benson[4] have calculated $DH°_{298}(CHBr_2$–H) = 103.4 and $DH°_{298}(CBr_3$–H) = 105 kcal/mol. These values seem to be too large compared with $DH°_{298}(CH_3$–H) = 104.1 and $DH°_{298}(CH_2Br$–H) = 102.0 kcal/mol, since successive halogen substitution in the chloro- and iodomethanes causes a continuous decrease in $DH°$(C–H).[4] The effect of chlorine substitution is greater than that of iodine substitution, and bromine substitution might be expected to have an intermediate effect.

In this note, we report on a brief study of the thermal bromination of $CHBr_3$, which yields values for the bond dissociation energies, $DH°(CBr_3$–H), and $DH°(CBr_3$–Br), and the heat of formation difference, $\Delta H_f°(CBr_4) - \Delta H_f°(CHBr_3)$.

Experimental Section

Reagent grade Br_2 (Allied Chemicals) was treated with KBr to remove Cl_2 and degassed at liquid nitrogen temperatures before use. Bromoform (Matheson Coleman and Bell, purified) was degassed before use.

Reaction rates were determined from the rate of disappearance of Br_2 measured spectrophotometrically with a Cary Model 15 spectrophotometer. The apparatus and procedure have been described in detail previously.[5] The pressure of Br_2 at equilibrium was measured directly, and the pressures of the other species were calculated from the stoichiometry.

Results and Discussion

The rate and equilibrium measurements are shown in Table I. The overall reaction is expected to be

$$Br_2 + CHBr_3 \rightleftarrows CBr_4 + HBr$$

No traces of noncondensable gases could be detected and there was no pressure change during the reaction. Equilibrium was established by waiting until there was no further change in Br_2 concentration. The two values obtained for K_{eq} agreed well.

Table II: Thermodynamic Data

Species	$\Delta H_f°_{298}$, kcal/mol	$S°_{298}$, gibbs/mol	$C_p°$-(298°K), gibbs/mol	$C_p°$-(600°K), gibbs/mol	Ref
Br_2	7.4	58.6	8.6	9.0	c
$CHBr_3$	[a]	79.1	17.0	21.1[b]	d
HBr	−8.7	47.4	7.0	7.1	c
CBr_4	[a]	85.6	21.8	24.5	c

[a] See text. [b] E. Gelles and K. S. Pitzer, *J. Amer. Chem. Soc.*, **75**, 5259 (1953). [c] "JANAF Interim Thermochemical Tables," D. R. Stull, Ed., Dow Chemical Co., Midland, Mich., 1961–1966. [d] Reference 2a.

Taking the mean value of K_{eq} and assigning a conservative error estimate of 20%, we calculate

$$\Delta G°(588°K) = 0.79 \pm 0.24 \text{ kcal/mol}$$

The entropies and heat capacities of all the species involved are well known and are listed in Table II. These data yield $\Delta S°(298°K) = -4.7 \pm 1.0$ gibbs/mol and $\overline{\Delta C_p} = [\Delta C_p°(298°K) + \Delta C_p°(600°K)]/2 = 2.4 \pm 1.0$ gibbs/mol which, when combined with the experimental $\Delta G°(588°K)$, yield

$$\Delta H°(298°K) = -1.7 \pm 0.7 \text{ kcal/mol}$$

From the known heats of formation of Br_2 and HBr listed in Table II, the following may be derived

$$\Delta H_f°_{222}(CBr_4) - \Delta H_f°_{298}(CHBr_3) = 14.4 \pm 0.7 \text{ kcal/mol}$$

This heat of formation difference is consistent with both Bernstein's estimates[3] for $CHBr_3$ and CBr_4 and

(1) (a) This work was supported in part by Grant No. AP-00353-07 from the National Air Pollution Control Administration, Public Health Service. (b) Post-Doctoral Research Associate.

(2) (a) "Selected Values of Chemical Thermodynamic Properties," National Bureau of Standards Technical Note, 270-3, U. S. Government Printing Office, Washington, D. C., Jan 1968. (b) "Selected Values of Chemical Thermodynamic Properties," National Bureau of Standards Circular 500, U. S. Government Printing Office, Washington, D. C., 1952.

(3) H. J. Bernstein, *J. Phys. Chem.*, **69**, 1550 (1965).

(4) S. Furuyama, D. M. Golden, and S. W. Benson, *J. Amer. Chem. Soc.*, **91**, 7564 (1969).

(5) K. D. King, D. M. Golden, and S. W. Benson, *ibid.*, **92**, 5541 (1970).

the values listed in the NBS Table.[2a] However, the NBS values were rejected by Furuyama, Golden, and Benson[4] on the basis of a large scatter in the second-order differences, $\Delta[\Delta(\Delta H_f°)]$ in the bromomethane series. Bernstein's interaction scheme appears to work fairly well, not only for estimating heats of formation, but for other molecular properties as well.[3] Nevertheless, a consideration of the bond dissociation energy[6] and heat of formation data[2b] used by Bernstein to arrive at $\Delta H_f°_{298}(CBr_4)$ = 38 kcal/mol[7] (used for calculating bond energy and interaction parameters) indicates that the estimates of the heats of formation of CH_2Br_2, $CHBr_3$, and CBr_4 could be in error by as much as ±3–4 kcal/mol.

The initial rate measurements were interpreted in accordance with the following mechanism, which is similar to that for other thermal bromination systems[5,8]

$$Br_2 \rightleftarrows 2Br; \quad K_{Br_2}$$

$$Br + CHBr_3 \underset{2}{\overset{1}{\rightleftarrows}} \dot{C}Br_3 + HBr$$

$$\dot{C}Br_3 + Br_2 \underset{4}{\overset{3}{\rightleftarrows}} CBr_4 + Br$$

A steady-state treatment gives

$$-(d[Br_2]/dt)_i = k_1 K^{1/2}_{Br_2}[Br_2]^{1/2}[CHBr_3]$$

The reproducibility of k_1 for a threefold change in Br_2 pressure and a twofold change in $CHBr_3$ pressure suggests that the mechanism is correct.

The A factors for bromine atom reactions show consistent trends with the type of hydrogen atom being abstracted and the structure of the substrate.[9] Moreover, they are well predicted by transition-state theory calculations.[5,8,10] Therefore, a consideration of the experimental A factors for similar bromine atom reactions[9,11] combined with a transition-state theory calculation leads to an assignment for A_1 of $10^{10.0\pm0.5}$ l. mol^{-1} sec^{-1}. Thus, taking the mean value of k_1 from Table I at T_m = 588°K, it may be calculated that E_1 = 10.8 ± 1.2 kcal/mol. Previous considerations[5] have shown that, in general, reactions such as (2) have E_2 = 2 ± 1 kcal/mol, and therefore, $\Delta H_{1,2}(588°K)$ = 8.7 ± 1.5 kcal/mol. Combined with an estimated $\overline{\Delta C_p}$ = 1.0 ± 1 gibbs/mol, this leads to

$$\Delta H_{1,2}(298°K) = 8.5 \pm 1.6 \text{ kcal/mol}$$

Consequently

$$DH°_{298}(CBr_3\text{–}H) = \Delta H_{1,2}(298°K) + DH°_{298}(H\text{–}Br)$$
$$= 96.0 \pm 1.6 \text{ kcal/mol}$$

Also, from the relation

$$DH°(CBr_3\text{–}H) - DH°(CBr_3\text{–}Br) = \Delta H_f°(CBr_4) - \Delta H_f°(CHBr_3) + \Delta H_f°(H) - \Delta H_f°(Br)$$

we obtain $DH°_{298}(CBr_3\text{–}Br)$ = 56.2 ± 1.8 kcal/mol. These values are less than the estimates of $DH°_{298}(CBr_3\text{–}H)$ = 105 and $DH°_{298}(CBr_3\text{–}Br)$ = 61 kcal/mol obtained by Furuyama, Golden, and Benson,[4] and they seem to be more in line with the periodicity of halogen substitution effects.

(6) E. W. R. Steacie, "Atomic and Free Radical Reactions," Vol. I, 2nd ed., Reinhold, New York, N. Y., 1954, pp 95, 96.

(7) See ref 3, p 1557, for further details.

(8) K. D. King, D. M. Golden, and S. W. Benson, *Trans. Faraday Soc.*, **66**, 2794 (1970).

(9) G. C. Fettis, J. H. Knox, and A. F. Trotman-Dickenson, *J. Chem. Soc.*, 4177 (1960).

(10) G. C. Fettis and J. H. Knox, *Progr. React. Kinet.*, **2**, 2 (1964).

(11) J. C. Amphlett and E. Whittle, *Trans. Faraday Soc.*, **64**, 2130 (1968).

COMMUNICATIONS TO THE EDITOR

Fluorescence Decay Times of Cyclic Ketones, Acetone, and Butanal in the Gas Phase[1]

Publication costs assisted by the National Science Foundation

Sir: Primary unimolecular processes which govern the fate of the photoexcited carbonyl compounds in the gas phase are fluorescence emission, singlet–triplet intersystem crossing, internal conversion, and chemical decomposition (and/or isomerization) resulting from the first excited singlet state (S_1) as shown below[2]

$$S_1 \begin{cases} \longrightarrow S_0 + h\nu & k_F \\ \longrightarrow T_1 & k_{ISC} \\ \longrightarrow S_0 & k_{IC} \\ \longrightarrow \text{products} & k_d \end{cases}$$

According to recent measurements of fluorescence decay times ($\tau_F = 1/[k_F + k_{ISC} + k_{IC} + k_d]$), the radiative rate ($k_F$) is nearly insensitive to the increase in the excess vibrational energy content in S_1, while the rates of the radiationless processes increase appreciably with the increasing vibrational energy.[3] Also, recent studies suggest that the single most important primary process in the gas-phase photochemistry of cyclic ketones is

(1) This research has been supported by National Science Foundation Grant GP-11390.

(2) See for a review, R. B. Cundall and A. S. Davies, *Progr. React. Kinet.*, **4**, 149 (1967).

(3) (a) A. M. Halpern and W. R. Ware, *J. Chem, Phys.*, **53**, 1969 (1970); (b) E. W. Schlag and H. von Weyssenhoff, *ibid*,. **51**, 2508 (1969).

the $S_1 \rightsquigarrow T_1$ intersystem crossing.[4,5] If this is true, a direct measurement of the singlet lifetime, previously unavailable, would enable calculation of the intersystem crossing rate ($k_{ISC} = \Phi_{ISC}/\tau_F$). Such a measurement requires a highly sensitive and fast response, decay fluorometer using a single-photon time correlation technique,[6] because of the inherently low fluorescence quantum yield ($\Phi_F \leq 0.002$), the low molar absorptivity ($\epsilon < 20$), and the low gas density where the lifetimes of cyclic ketones must be measured. We now wish to present the results obtained by such an apparatus.

We have modified the TRW decay fluorometer used in our early experiments[7] for single-photon counting.[6] A small Bausch and Lomb monochromator was used for selecting the excitation wavelength, while a Corning O-52 filter was used to observe the fluorescence emission from the carbonyl compounds. The performance of the apparatus was checked by observing the fluorescence decay from benzene[7] and the timing was calibrated with a variable delay line (ADYU 20B1). The values of τ_F obtained from the exponential decay plots are shown in Table I. It was not necessary to deconvolute the decay curve due to a short lamp decay time (≤ 1.1 nsec).

The most striking observations are that (1) all of the aliphatic ketones and butanal have about the same value of τ_F in the gas phase, 2.4–4.7 nsec, near the onset of the $S_0 \rightarrow S_1$ absorptions; (2) deuteration of cyclopentanone increases the value of τ_F by ~1.7, somewhat more than the increase observed with deuterated acetone;[8] and (3) substitution at the α position increases significantly the value of τ_F in *cis*- and *trans*-DMCP. The values of $k_F = \Phi_F/\tau_F$ obtained from the data listed in Table I are 4×10^5, 6×10^5, 8×10^5, and 8×10^5 sec^{-1} for cyclobutanone, cyclopentanone, cyclohexanone, and acetone, respectively, indicating a factor of 2 variation among them. Furthermore, variation of k_F is only slight with the wavelength variation as observed in the cases of the excited singlet hexafluoroacetone[3a] and β-naphthylamine.[3b]

Our values of τ_F obtained in the gas phase are 1.2–1.3 times the values of τ_F recently measured in solution for cyclopentanone (1.9 nsec),[9a] cyclohexanone (2.5 nsec),[9b] and acetone (2.0 nsec).[9c] This indicates that rates of the radiationless relaxation of these carbonyl $S_1(n,\pi^*)$ states, $(3 \sim 4) \times 10^8$ sec^{-1}, are intrinsic and are virtually not affected by the medium. The quantum yields of the $S_1 \rightsquigarrow T_1$ intersystem crossing are close to unity in cyclohexanone[4c] and acetone,[2,9c,10] and thus k_{ISC}'s for these ketones are close to 3×10^8 sec^{-1}. Thus, it is likely that the similarity of the τ_F values for all of the carbonyl compounds studied here near the $S_0 \rightarrow S_1$ absorption threshold is mainly due to the similarity in their k_{ISC} values. It is interesting to note that deuteration and methylation at the α position reduce appreciably the value of k_{ISC}. Furthermore, shortening of the τ_F values observed at short wavelengths, a measure of the increasing values of k_d and k_{ISC} (in competition with k_{ISC}) with increasing vibrational excitation energy, is particularly noticeable with cyclobutanone.[5] A more detailed analysis shall be reported later.

Table I: Fluorescence Decay Times (τ_F) and Quantum Yields (Φ_F) of Cyclobutanone (CB), Cyclopentanone (CP), 2,5-Dimethylcyclopentanones (DMCP), Cyclohexanone (CH), Acetone (AC), and Butanal in the Gas Phase at 23°

Gas	Pressure, Torr	Exciting wavelength, nm[a]	τ_F, nsec	Φ_F
CB	11;30	<310	≪1	<0.0001[c]
		320	4.7 ± 0.3	~0.0019[c]
CP(CP-d_8)	6.0	260	<1.8 (3.2)	~0.001[c]
		280	2.1 ± 0.3 (3.5)	~0.0014[c]
		300	2.2 ± 0.3 (3.6)	~0.0014[c]
		320	2.4 ± 0.3 (4.1)	~0.0014[c]
cis-DMCP	3.1	320	3.7 ± 0.3	
trans-DMCP	4.8	320	4.2 ± 0.3	
CH	3	270	2.9 ± 0.3	~0.0018[c]
		295	2.9 ± 0.3	~0.0018[c]
		320	3.2 ± 0.3	~0.0018[c]
AC(AC-d_6)	20[b]	260	<1.6 ± 0.3 (2.2)	
		280	1.7 ± 0.3 (2.3)	~0.0017[d]
		295	2.1 ± 0.3 (2.7)	~0.0019[d]
		313	2.7 ± 0.3 (3.2)	~0.0021[d]
Butanal	18	320	4.2 ± 0.3	

[a] Spectral bandwidth was ~20 nm. [b] 1.5 Torr of O_2 added. [c] Reference 5. [d] J. Heicklen, *J. Amer. Chem. Soc.*, **81**, 3863 (1959).

Acknowledgment. The advice given by Professor W. R. Ware at University of Minnesota on the instrumentation is greatly appreciated.

(4) (a) E. K. C. Lee, *J. Phys. Chem.*, **71**, 2804 (1967); (b) H. O. Denschlag and E. K. C. Lee, *J. Amer. Chem. Soc.*, **90**, 3628 (1968); (c) R. G. Shortridge, Jr., and E. K. C. Lee, *ibid.*, **92**, 2228 (1970).

(5) R. G. Shortridge, Jr., C. F. Rusbult, and E. K. C. Lee *ibid.*, in press.

(6) (a) J. B. Birks, *Progr. React. Kinet.*, **4**, 239 (1967); (b) W. R. Ware in "Creation and Detection of the Excited State," A. Lamola, Ed., Marcel Dekker, New York, N. Y., in press.

(7) G. M. Breuer and E. K. C. Lee, *J. Chem. Phys.*, **51**, 3130 (1969).

(8) A. M. Halpern and W. R. Ware, private communication; our τ_F values for acetone and theirs agree within the accuracy of the measurement.

(9) (a) J. C. Dalton, D. M. Pond, D. S. Weiss, F. D. Lewis, and N. J. Turro, *J. Amer Chem. Soc.*, **92**, 2564 (1970); (b) J. C. Dalton, D. M. Pond, and N. J. Turro, *ibid.*, **92**, 2173 (1970); (c) N. C. Yang, E. D. Feit, M. H. Hui, N. J. Turro, and J. C. Dalton, *ibid.*, **92**, 6974 (1970).

(10) R. F. Borkman and D. R. Kearns, *J. Chem. Phys.*, **44**, 945 (1966).

(11) National Science Foundation Predoctoral Fellow, 1966–1970.

DEPARTMENT OF CHEMISTRY
UNIVERSITY OF CALIFORNIA
IRVINE, CALIFORNIA 92664

GEORGE M. BREUER[11]
EDWARD K. C. LEE*

RECEIVED JULY 31, 1970

ISOTOPE EFFECTS IN CHEMICAL PROCESSES
ADVANCES IN CHEMISTRY SERIES NO. 89

Thirteen papers from a symposium by the Division of Nuclear Chemistry and Technology of the American Chemical Society, chaired by William Spindel. Includes:

- Separating isotopes by chemical exchange, distillation, gas chromatography, electromigration, and photochemical processes
- Methods for fractionating isotopes of hydrogen, lithium, boron, carbon, and nitrogen
- Thermotransport in monatomic and ionic liquids
- Statistical-mechanical theory determining isotope effects

278 pages with index Clothbound (1969) $13.00

Set of L.C. cards free with library orders upon request

Other books in the ADVANCES IN CHEMISTRY SERIES in physical and colloid chemistry include:

No. 87 Interaction of Liquids at Solid Substrates. Twelve papers survey recent research on solid/liquid interaction, including work on "coupling agents," adhesion of polymers, organic/inorganic interfaces, ultrasonic impedometry. Four more papers are concerned with heparinized surfaces at the blood/material interface. 212 pages
Cloth (1968) $9.50

No. 84 Molecular Association in Biological and Related Systems. Nineteen articles survey and report new work on molecular association in fat digestion, in soap systems, in membrane constituents, and in mixed monolayers. Other topics include bile salt micelles, lipid monolayers and membranes, and a definitive review of biological membrane structure. 308 pages
Cloth (1968) $10.50

No. 82 Radiation Chemistry—II. Thirty-six papers and 17 abstracts on radiation chemistry in gases, solids, and organic liquids. Includes three plenary lectures. 558 pages
Cloth (1968) $16.00

No. 81 Radiation Chemistry—I. Forty-one papers and 17 abstracts on radiation chemistry in aqueous media, biology, and dosimetry. From the international conference at Argonne National Laboratory. 616 pages
Cloth (1968) $16.00
No. 81 and No. 82 ordered together $30.00.

No. 79 Adsorption from Aqueous Solution. Fifteen papers discuss thermodynamic and kinetic aspects of adsorption phenomena and the results of studies on a variety of adsorbate-adsorbent systems. 212 pages
Cloth (1968) $10.00

No. 68 Mössbauer Effect and its Application in Chemistry. Ten papers that will familiarize chemists with Mössbauer spectroscopy as an analytical tool, for studying chemical bonding, crystal structure, electron density, magnetism, and other properties. 178 pages
Cloth (1967) $8.00

No. 67 Equilibrium Concepts in Natural Water Systems. Sixteen papers represent the collaboration of aquatic chemists, analytical chemists, geologists, oceanographers, limnologists, and sanitary engineers, working with simplified models to produce fruitful generalizations and valuable insights into the factors that control the chemistry of natural systems. 344 pages
Cloth (1967) $11.00

No. 64 Regenerative EMF Cells. Seventeen papers survey current progress and research on regenerative systems for converting and storing electrical energy. Principal emphasis is on thermally regenerative systems, but chemical and photochemical systems are considered. 309 pages
Cloth (1967) $11.00

No. 63 Ordered Fluids and Liquid Crystals. Twenty-two studies on characterization, properties, and occurrence of these phenomena in many substances such as tristearin, p-azoxyanisole, mono-and di-hydric alcohols, phospholipids and polypeptides. 332 pages
Cloth (1967) $11.50

No. 58 Ion-Molecule Reactions in the Gas Phase. Eighteen papers survey spectrometric and other methods for producing and studying ion-molecule reactions, such as pulsed sources for studying thermal ions, reactions in flames and electrical discharges. 336 pages
Cloth (1966) $10.50

No. 54 Advanced Propellant Chemistry. Primarily directed to the search for new oxidizers; 26 papers survey oxygen-containing oxidizers, fuels and binders, fluorine systems including oxygen difluoride and difluoramines and liquid systems. 290 pages
Cloth (1966) $10.50

No. 50 Solvated Electron. Reviews of theory, structure, reactions of solvated and hydrated electrons; detailed papers on electrical transport properties, photochemistry, theory of electron transfer reactions, structure of solvated electrons, hydrated electron research. 304 pages
Cloth (1965) $10.50

No. 47 Fuel Cell Systems. Developments in theory, performance, construction, and new systems for the energy converter that is proving itself in military and space uses. 360 pages
Cloth (1965) $10.50

No. 43 Contact Angle, Wettability, and Adhesion. Twenty-six papers on theoretical and practical approaches to wettability and adhesion; with summary of the surface chemical studies of W. A. Zisman, the 1963 Kendall Award winner. 389 pages
Cloth (1964) $10.50

No. 40 Mass Spectral Correlations. By Fred W. McLafferty. Over 4000 spectra listed by mass/charge ratios of fragment ions with the most probable original structures for each. 117 pages
Paper (1963) $6.00

No. 33 Solid Surfaces and the Gas-Solid Interface. Thirty-seven papers from the Kendall Award Symposium honoring Stephen Brunauer. Theory and techniques for studying surface phenomena.
Cloth (1961) $12.00

No. 31 Critical Solution Temperatures. By Alfred W. Francis. CST answers the question, "Do two liquids mix?" and is widely used for screening solvents. Over 6000 systems are included, 70% with a hydrocarbon as one component; nearly 1100 non-hydrocarbon solvents are listed. 246 pages
Cloth (1961) $8.00

All books postpaid in U.S. and Canada; plus 30 cents in PUAS and elsewhere.

Order from: SPECIAL ISSUES SALES
AMERICAN CHEMICAL SOCIETY
1155 SIXTEENTH ST., N.W.
WASHINGTON, D.C. 20036

for your courses . . .
texts that set
standards of
excellence

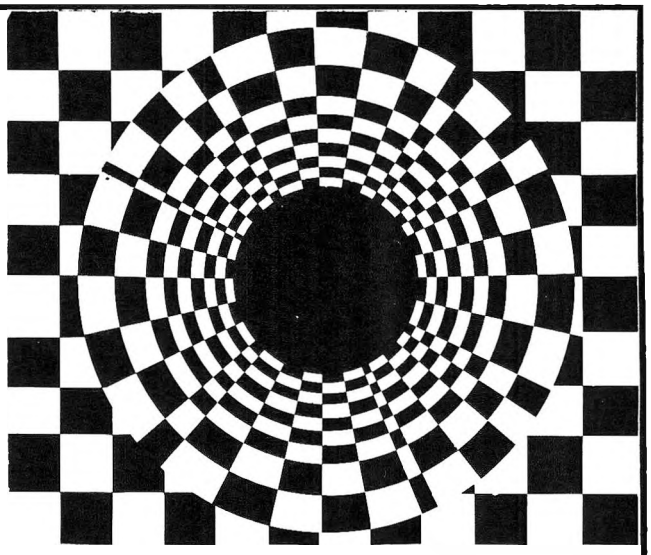

Second Edition
Physical Chemistry

William F. Sheehan, Jr., University of Santa Clara

1970, 1017 pp.

". . . *a very modern, advanced book. For the good, motivated student it should be a good text.*"—Paul Simpson, Stanford University.

"*This is an excellent text for general physical chemistry . . . I especially like the example problems.*"—R. Shigeishi, Carleton University.

Since the second edition of this distinguished text was published in 1970, over 50 class-size orders have been received from colleges and universities across the country. Among the schools—Louisiana State University, Baton Rouge and New Orleans • Boston University • Northern Illinois University • Lamar State College • University of Minnesota • Rensselaer Polytechnic Institute • University of Iowa • Yale University • Colorado State University • University of Texas, El Paso • State University of New York, Albany • Tulane University.

Quantum Chemistry

Ira N. Levine, Brooklyn College

Volume I: Quantum Mechanics and Molecular Electronic Structure. 1970, 591 pp.

Volume II: Molecular Spectroscopy. 1970, 477 pp.

"*This is a rare treat, a rigorous textbook that is sufficiently elementary for the general student.*"—from CHOICE on Volume I. "*This volume, along with Volume II, is one of the best treatments of Quantum Chemistry for first year graduate students that I have seen.*"—John R. Sabin, University of Missouri.

Volume I of this comprehensive two-volume introduction deals with quantum mechanics, atomic structure, and molecular electronic structure. Volume II covers electronic, vibrational and rotational spectra of molecules, NMR and ESR spectroscopy, group theory and matrix algebra.

ALLYN AND BACON, INC.

College Div., Dept. 893 / 470 Atlantic Ave., Boston, MA 02210